AFIT/ENP/DSP/97-09.

HYBRID QUANTUM AND MOLECULAR MECHANICS EMBEDDED CLUSTER MODELS FOR CHEMISTRY ON SILICON AND SILICON CARBIDE SURFACES

DISSERTATION

James Richard Shoemaker
Major, USAF

AFIT/ENP/DSP/97-09.

DTIC QUALITY INSPECTED 2

19971203 046

Approved for public release; distribution unlimited

The views expressed in this dissertation are those of the author and do not reflect the official policy or position of the Department of Defense or the U. S. Government.

AFIT/ENP/DSP/97-09.

HYBRID QUANTUM AND MOLECULAR MECHANICS EMBEDDED CLUSTER MODELS FOR CHEMISTRY ON SILICON AND SILICON CARBIDE SURFACES

DISSERTATION

Presented to the Faculty of the School of Engineering

of the Air Force Institute of Technology

Air University

In Partial Fulfillment of the

Requirements for the Degree of

Doctor of Philosophy

James Richard Shoemaker, B.S., M.S.

Major, USAF

December, 1997

Approved for public release; distribution unlimited

AFIT/ENP/DSP/97-09.

HYBRID QUANTUM AND MOLECULAR MECHANICS EMBEDDED CLUSTER MODELS FOR CHEMISTRY ON SILICON AND SILICON CARBIDE SURFACES

James Richard Shoemaker, B.S., M.S.

Major, USAF

Approved:

Larry W. Burggraf 31 Oct 97

Dr. Larry W. Burggraf, Chairman

Philip S. Beran 3 NOV 97

Dr. Philip S. Beran

Mark S. Gordon 10/24/97

Dr. Mark S. Gordon

R Pachter 10/31/97

Dr. Ruth R. Pachter

10/31/97

Dr. Glen P. Perram

Dennis W Quinn 31 OCT 97

Dr. Dennis W. Quinn

30 Oct 91

Dr. David E. Weeks

Robert A. Calico, Jr

Dean

I'd like to acknowledge the guidance from my committee, the folks at the help desk at the ASC MSRC for putting up with my frequent calls, the Theresa Windus for showing me the 10 crucial lines of code that got my code running on parallel machines, Brett Bode for his upgrades to MacMolplot that made making a lot of figures a deal easier, Mike Schmidt for his advice on GAMESS, and the rest of the Gordon Group who put up with me when I came out to visit. I'd also like to thank my parents for letting me stay up past my bedtime to watch all the Apollo launches, and in general for putting up with my long held belief that coloring serves no purpose in life.

This work was supported in part by a grant of HPC time from the DoD HPC Center ASC Major Shared Resource Center IBM SP2 and SGI/Cray Origin 2000.

Table of Contents

Page

List of Figures xii

List of Tables xviii

Abstract xxiii

I. Methods for modeling chemistry on surfaces 1-1

1.1 Motivation 1-1

1.2 Background 1-2

1.3 Problem Statement 1-5

1.4 Overview 1-5

1.5 Approach 1-8

1.6 Application 1-9

II. An Overview of Computational Methods for Determining Molecular Properties 2-1

2.1 *Ab Initio* Hartree-Fock Self Consistent Field Technique . . . 2-1

2.1.1 Born-Oppenheimer Approximation 2-1

2.1.2 Approximate Electronic Wavefunctions 2-5

2.1.3 Optimization of the Approximate Wavefunction: The Hartree-Fock-Roothaan Procedure 2-9

2.1.4 Basis Functions and Matrix Elements 2-12

2.1.5 A Simple HF-SCF Example: H_2 2-16

2.1.6 Effects of Electron Correlation: The Hartree Fock Limit 2-17

2.1.7 Beyond the Hartree-Fock Limit 2-19

2.1.8 Optimized Approximate Wavefunctions: Metrics and Accuracy 2-25

Page

2.2 Other Computational Approaches 2-29

2.2.1 Semi-Empirical HF-SCF 2-29

2.2.2 Molecular Mechanics 2-31

2.2.3 Density Functional Theory 2-36

2.3 Discussion 2-40

III. Merging Molecular Mechanics with Quantum Mechanics 3-1

3.1 Introduction 3-1

3.2 Construction of the Hybrid System 3-2

3.3 The Hybrid Optimization Procedure 3-7

3.3.1 Formal Derivation of Hybrid Energy and Gradient Equations 3-7

3.3.2 Energy and Gradient Equations using Region 5 . . . 3-8

3.3.3 Double Counting 3-9

3.3.4 An alternate embedding approach: Weiner's method 3-9

3.4 Internal Coordinates for Cages 3-10

3.5 Summary of GAMESS/MM3 implementation 3-13

3.5.1 Program flow 3-13

3.5.2 An example: the Si_6H_{12}/Si_9H_{12} hybrid system 3-15

3.6 Comparison of methods 3-17

3.7 Models of the Dimerized Si(001) Surface 3-22

3.7.1 Low Index Surfaces of a Cubic Lattice 3-22

3.7.2 Previous Cluster Models of the dimerized Si(001) surface 3-23

3.7.3 New Cluster Model of the Dimerized Si(001) Surface 3-30

3.7.4 Cluster Model of Two Surface Dimers 3-40

3.8 MIMOMM Optimization of Si_9H_{12} 3-44

3.8.1 Hybrid Cluster Model of Si(001) Surface 3-44

Page

3.9 Discussion 3-44

3.9.1 Guidance on Embedded Cluster Design 3-44

3.9.2 Molecular Mechanics Potentials 3-46

3.10 Recommendations 3-46

IV. Modifying the electronic environment of finite cluster models of surface reaction sites 4-1

4.1 Introduction: The Problem of Cluster Termination 4-1

4.2 The Electronic Environment of a Molecule 4-4

4.3 Altering the Electronegativity of a Hydrogen Atom 4-6

4.4 Creation of $\overline{H}$s: Three Approaches 4-10

4.4.1 Previous Work 4-10

4.4.2 Creation of $\overline{H}$ Atoms Using Si_5H_{12} Model System . 4-11

4.4.3 Mulliken Charge Mirror Model 4-14

4.4.4 Optimum Si-$\overline{H}$ separation 4-17

4.4.5 Bulk Molecular Orbital Model of $\overline{H}$ 4-18

4.5 Evaluation of Procedures used to make $\overline{H}$ 4-22

4.5.1 Comparison of Model Systems 4-22

4.5.2 Effect of Si-$\overline{H}$ Separation 4-25

4.5.3 Discussion on $\overline{H}$s 4-27

4.6 Detailed Evaluation of MC Mirror $\overline{H}$ 4-27

4.6.1 Mulliken Charges 4-28

4.6.2 Structure 4-30

4.6.3 Energetics 4-36

4.6.4 Ionization Potential 4-37

4.6.5 Discussion of Silicon $\overline{H}$s 4-40

4.7 Terminating Silicon Carbide 4-41

4.7.1 Mulliken Population of SiC 4-41

Page

4.7.2 Creating $\overline{H}$ Atoms for SiC: Equivalence 4-42

4.8 Recommendations 4-47

V. Silicon Carbide and Silicon Surface Chemistry Studies 5-1

5.1 Introduction 5-1

5.2 SiC(111) Structure: Polytypes 5-1

5.3 Previous research on SiC Surfaces 5-2

5.4 Designing an SiC(111) Surface Model 5-8

5.4.1 SiC(111) Embedded Cluster Design Considerations . 5-8

5.4.2 Bulk Cluster Design Considerations 5-9

5.5 SiC(111) Surface Reconstruction 5-14

5.5.1 Energetics 5-14

5.5.2 Quartet Surface Reconstruction: Structures 5-16

5.5.3 Doublet Surface Reconstruction: Structures 5-16

5.6 Hydrogenation of SiC(111) Surface 5-21

5.6.1 Si-terminated SiC(111) Surface 5-21

5.6.2 C-terminated SiC(111) Surface 5-27

5.7 Oxidation of SiC 5-31

5.7.1 Background 5-31

5.7.2 Methodology for Simulating Oxidation 5-31

5.8 Oxidation of the Si-terminated SiC(111) Surface 5-33

5.8.1 O-Si Ontop Site Adsorption: Structure 5-33

5.8.2 Si-O-Si Bridge Site Adsorption 5-34

5.8.3 Si-O-C Ring Insertion: Structure 5-41

5.8.4 O-Si-O-Si Ontop and Ring Insertion: Structure . . . 5-44

5.8.5 Comparison of Adsorption Site Energetics 5-44

5.9 Oxidation of the C-terminated SiC(111) Surface 5-46

5.9.1 O-C Ontop Site Adsorption: Structure 5-46

Page

5.9.2 C-O-C Bridge Site Adsorption 5-48

5.9.3 C-O-Si Ring Insertion: Structure 5-54

5.9.4 O-C-O-Si Ontop and Ring Insertion: Structure . . . 5-57

5.9.5 Comparison of Adsorption Site Energetics 5-59

5.10 Surface Vacancies 5-61

5.10.1 Si Vacancy at the Si-terminated SiC(111) Surface: Structure 5-61

5.10.2 C Vacancy in the C-terminated SiC(111) Surface . . 5-62

5.10.3 Comparison of Surface Vacancy Energetics 5-68

5.11 Silicon (111) Surface Calculations 5-68

5.11.1 Hybrid Cluster for Si(111) 5-70

5.11.2 Reconstruction of the Si(111) Surface 5-73

5.11.3 Si(111) Hydrogenation Energetics 5-73

5.11.4 Si(111) O-Si Ontop Site Adsorption: Structure . . . 5-73

5.11.5 Si(111) Si-O-Si Bridge Site Adsorption: Structure . 5-76

5.11.6 Si(111) Si-O-Si Ring Insertion: Structure 5-79

5.11.7 Si(111) O-Si-O-Si Ontop and Ring Insertion: Structure 5-82

5.11.8 Comparison of Si(111) Oxygen Adsorption Site Energetics 5-84

5.11.9 Si Vacancy in the Si(111) Surface 5-84

5.12 Discussion 5-91

5.12.1 Steric Effects on O Atom Bridge Site Formation . . 5-91

5.12.2 Etching of the C-terminated SiC(111) Surface 5-95

5.13 Summary of Oxidation Energetics 5-97

5.14 Conclusions 5-97

5.15 Recommendations 5-98

5.15.1 SiC Oxidation 5-98

5.15.2 MIMOMM 5-98

Page

VI. Conclusions and Recommendations 6-1

6.1 Summary 6-1

6.2 Conclusions 6-2

6.3 Recommended Future Work 6-4

6.3.1 Code development 6-4

6.3.2 Silicon and SiC surface chemistry models 6-4

Appendix A. Definition of terms A-1

Appendix B. List of Symbols B-1

Appendix C. SiC Model System Energies C-1

Appendix D. Generation and use of Delocalized Coordinates D-1

D.1 Generation of DLCs D-1

D.1.1 Source Code Description D-1

D.1.2 Using Delocal.x D-2

D.2 Frozen Primitive Coordinates in DLCs D-3

D.3 Modifications to GAMESS to enable the use of DLCs D-6

D.3.1 Reading the $ZMAT deck D-6

D.4 Modifications to the iterative process to convert internals to cartesians D-7

D.5 delocal.f Source Code D-9

Appendix E. Program Modifications for the IMMOM: GAMESS and MM3 E-1

E.1 Overview E-1

E.2 GAMESS Source Code Modifications E-2

E.2.1 MAIN Module gamess.S.f E-2

E.2.2 Deck START Module Sinputa.S.f E-2

E.2.3 Deck MBLDR Module inputc.S.f E-2

Page

E.2.4 Deck SIGINI Module statpt.S.f E-3

E.2.5 Deck SIGVAL Module statpt.S.f E-3

E.3 MM3 Source Code Modifications E-4

E.3.1 COMMON.PAR E-4

E.3.2 Module mm3_aix.f E-6

E.3.3 Module mm31.S.f SUBMM3 . . . . . E-6

E.3.4 Module mm31.S.f subroutine part1 . . . . . E-7

E.3.5 Module mm31.S.f subroutine part2 . . . . . E-8

E.3.6 Module mm31.S.f subroutine part3 . . . . . E-8

E.3.7 Module mm31.S.f subroutine Davejr E-9

E.3.8 Module mvib31.S.f subroutine fmin E-9

E.3.9 Module mvib31.S.f subroutine fd_estr E-10

E.3.10 Module mvib31.S.f subroutine fmove E-10

E.3.11 Module mvib31.S.f subroutine fd_ebend E-10

E.3.12 Module mvib31.S.f subroutine fd_ebbnd E-12

E.3.13 Module mvib32.S.f subroutine fd_vdwbd E-13

E.3.14 Module mvib32.S.f subroutine fd_vdwod E-14

E.3.15 Module mvib32.S.f subroutine fd_chgchg E-14

E.3.16 Module mvib32.S.f subroutine fd_dipole E-15

E.3.17 Module mvib32.S.f subroutine fd_chgdip E-16

E.3.18 Module mvib32.S.f subroutine fd_dipchg E-16

E.3.19 Module mvib32.S.f subroutine fd_etors E-16

E.4 New Modules:ghmm2.f E-17

E.5 Resolution of GAMESS-MM3 Name Conflicts E-17

Bibliography BIB-1

Vita VITA-1

List of Figures

Figure		Page
1.1.	$Si_{73}C_{69}H_{109}$ cluster model of a Si-terminated SiC(111) surface.	1-3
1.2.	$Si_{70}C_{70}H_{87}$ cluster model of a Si-terminated SiC(111) surface.	1-3
1.3.	$Si_9C_{13}H_{25}$ model of a Si-terminated SiC(111) surface, 416 basis functions.	1-6
1.4.	$C_9Si_{13}H_{25}$ model of a C-terminated SiC(111) surface, 432 basis functions.	1-6
1.5.	Clean Si-terminated SiC(111) embedded cluster, xz view, *ab initio* optimized geometry.	1-7
1.6.	*Ab initio* optimized Si-terminated SiC(111) EC with O atom adsorbed in a bridge site. Directions of atom displacements from lattice positions are shown by arrows.	1-7
2.1.	H_2 Total Energy PES Components	2-4
2.2.	H_2 STO-3G Virial Ratio	2-27
2.3.	Molecular Mechanics Potential Energy Modes	2-33
2.4.	Two Body Bond Potential Energy Surfaces	2-34
3.1.	Hybrid system partitioning, IMOMM	3-3
3.2.	Embedded cluster partitioning, IMOMM	3-3
3.3.	Hybrid system partitioning, modified IMOMM (MIMOMM).	3-5
3.4.	Embedded cluster partitioning, modified IMOMM (MIMOMM).	3-5
3.5.	Limitation of IMOMM Region 2-3 linking	3-6
3.6.	Si_6H_{12}/Si_9H_{12} embedded and hybrid clusters	3-16
3.7.	Si_6H_{12} *ab initio* optimized geometry	3-17
3.8.	Si_6H_{12} MIMOMM optimized geometry	3-17
3.9.	$Si_6H_{12}/Si_{38}H_{36}$ hybrid cluster	3-20
3.10.	Determination of the indices of a lattice surface plane.	3-24
3.11.	The (001), (110), and (111) planes of a cubic lattice.	3-24
3.12.	Low index surfaces of an ideal tetrahedrally bonded cubic lattice. . . .	3-25

Figure Page

3.13. Dimerization of a silicon (001) surface. 3-26

3.14. Si_9H_{12} model of a single dimer on a Si(001) surface 3-27

3.15. Comparison of *ab initio* optimized geometries of $Si_{10}H_{16}$ and Si_9H_{12}. . 3-31

3.16. Atom displacements induced by symmetric dimer formation in the Si_9H_{12} model of the Si(001) surface. 3-32

3.17. *Ab initio* GVB-PP(1) optimized geometry of $Si_{66}H_{52}$, HW ECP(d) basis set, interior view. 3-35

3.18. *Ab initio* GVB-PP(1) optimized geometry of $Si_{66}H_{52}$, HW ECP(d) basis set, surface view. 3-36

3.19. *Ab initio* GVB-PP(1) optimized geometry of $Si_{66}H_{52}$, HW ECP(d) basis set, subsurface view. 3-37

3.20. GVB-PP(2) 6-31G* optimized geometry of the $Si_{15}H_{16}$ cluster model of two adjacent dimers on the Si(001) surface. 3-42

4.1. ζ dependence of the STO-3G basis set 4-8

4.2. ζ dependence of hydrogen electronegativity 4-9

4.3. Si_5H_{12} model system used to create $\overline{H}$ atoms 4-10

4.4. Mulliken charge mirror model system 4-15

4.5. $Si_4H_9^{\bullet}$ model system 4-19

4.6. $Si_4H_9^{\bullet}$ single electron MO contours. 4-19

4.7. Fitting procedure applied to GAMESS STO-3G hydrogen atom MO. . 4-20

4.8. Si_4H_9 single electron MO. 4-21

4.9. Si_9 cage with atom number labeled 4-23

4.10. $Si_9\overline{H}_{12}$ 6-31G* optimized geometry 4-33

4.11. $Si_9\overline{H}_{12}$ 6-31G* optimized geometry 4-33

4.12. $Si_9H_{12}H$ optimized geometry, C_s symmetry. 4-38

4.13. $Si_9\overline{H}_{12}H$ optimized geometry, C_s symmetry. 4-38

4.14. $Si_{18}C_{18}H_{42}$ molecule evaluated as a model system for creation of $\overline{H}$s. . 4-43

4.15. $SiC_4Si_{12}H_{36}$ tetrahedral model for bulk SiC. 4-45

Figure Page

5.1. Wurtzite (hexagonal) bonding between Si and C atoms in adjacent bilayers. 5-2

5.2. Zinc-blende (cubic) bonding between Si and C atoms in adjacent bilayers. 5-2

5.3. SiC 3C polytype crystal structure. 5-3

5.4. SiC 2H polytype crystal structure. 5-4

5.5. SiC 4H polytype crystal structure. 5-5

5.6. SiC(001) Si-terminated surface reconstruction. 5-6

5.7. $Si_9C_{13}H_{25}$ (unreconstructed) EC used to model the Si-terminated SiC(111) surface. 5-10

5.8. $C_9Si_{13}H_{25}$ (unreconstructed) EC used to model the Si-terminated SiC(111) surface. 5-10

5.9. SiC 4 layer bulk cluster, Si-terminated (111) surface 5-12

5.10. Si-terminated (111) surface of SiC 4 layer bulk cluster. 5-12

5.11. SiC 2 layer bulk cluster, Si-terminated (111) surface. 5-13

5.12. Si-terminated (111) surface of SiC 2 layer bulk cluster. 5-13

5.13. Reconstruction of Si and C-terminated embedded cluster models of SiC(111) surfaces. 5-17

5.14. *Ab initio* ^{2}ROHF (6-31G*) optimized Si-terminated SiC(111) cluster. . 5-20

5.15. *Ab initio* ^{2}GVB-PP(1) (6-31G*) optimized Si-terminated SiC(111) cluster. 5-20

5.16. H atom adsorption onto the Si-terminated SiC(111) cluster. 5-22

5.17. Comparison of *ab initio* and MIMOMM optimized Si-terminated SiC(111) cluster geometry with 1 H atom adsorbed. 5-23

5.18. Comparison of *ab initio* and MIMOMM optimized Si-terminated SiC(111) cluster geometry with 2 H atoms adsorbed. 5-24

5.19. Comparison of *ab initio* and MIMOMM optimized Si-terminated SiC(111) cluster geometry with 3 H atoms adsorbed. 5-25

5.20. H atom adsorption on the C-terminated SiC(111) cluster. 5-28

5.21. Starting points for O atom reactions with SiC. 5-32

Figure Page

5.22. Comparison of Si-terminated SiC(111) cluster geometry with 1 O atom adsorbed onto an ontop site, without and with MM3 steric forces. . . . 5-35

5.23. Clean Si-terminated SiC(111) embedded cluster, xz view 5-38

5.24. *Ab initio* optimized Si-terminated SiC(111) embedded cluster with O atom adsorbed in a bridge site. 5-38

5.25. IMOMM optimized Si-terminated SiC(111) embedded cluster with O atom adsorbed in a bridge site, 2 bilayer bulk cluster 5-39

5.26. MIMOMM optimized Si-terminated SiC(111) embedded cluster with O atom adsorbed in a bridge site, 4 bilayer bulk cluster 5-39

5.27. *Ab initio* optimized ^{4}ROHF (6-31G*) geometry of Si-O-C ring insertion, Si-terminated SiC(111) surface. 5-42

5.28. MIMOMM optimized ^{4}ROHF (6-31G*/4 bilayer BC) geometry of Si-O-C ring insertion, Si-terminated SiC(111) surface. 5-42

5.29. *Ab initio* optimized ^{4}ROHF (6-31G*) geometry of Si-O-C ring insertion bridge, Si-terminated SiC(111) surface. 5-43

5.30. MIMOMM optimized ^{4}ROHF (6-31G*/4 bilayer BC) geometry of Si-O-C subsurface bridge, Si-terminated SiC(111) surface. 5-43

5.31. *Ab initio* optimized ^{4}ROHF (6-31G*) geometry of Si-terminated SiC(111) cluster with two O atoms adsorbed, O_{ontop}Si-O_{ring}-Si. 5-45

5.32. Clean C-terminated SiC(111) embedded cluster, *ab initio* optimized geometry. 5-48

5.33. C-terminated SiC(111) embedded cluster with one O atom adsorbed in an ontop site, 6-31G* optimized geometry. 5-49

5.34. C-terminated SiC(111) *ab initio* optimized EC with 1 O atom adsorbed in a bridge site. 5-50

5.35. C-terminated SiC(111) surface with O atom adsorbed in a bridge site, IMOMM optimized geometry, 2 bilayer bulk cluster. 5-50

5.36. C-terminated SiC(111) surface with O atom adsorbed in a bridge site, IMOMM optimized geometry, 4 bilayer bulk cluster. 5-52

5.37. *Ab initio* optimized ^{4}ROHF (6-31G*) geometry of C-O-Si ring insertion site, C-terminated SiC(111) surface, XZ view 5-55

Figure Page

5.38. IMOMM optimized ^{4}ROHF (6-31G*/4 bilayer BC) geometry of C-O-Si ring insertion site, C-terminated SiC(111) surface, XZ view 5-55

5.39. *Ab initio* optimized ^{4}ROHF (6-31G*) geometry of C-O-Si ring insertion site, C-terminated SiC(111) surface, YZ view 5-56

5.40. IMOMM optimized ^{4}ROHF (6-31G*/4 bilayer BC) geometry of C-O-Si ring insertion site, C-terminated SiC(111) surface, YZ view 5-56

5.41. *Ab initio* optimized (^{4}ROHF 6-31G*) geometry of C-terminated SiC(111) cluster with two O atoms adsorbed, ontop and ring insertion. 5-58

5.42. Si-terminated SiC(111) EC with a Si vacancy, *ab initio* ^{4}ROHF optimized geometry. 5-63

5.43. Si-terminated SiC(111) EC with a Si vacancy, MIMOMM ^{4}ROHF optimized geometry, 4 bilayer bulk cluster. 5-63

5.44. Si-terminated SiC(111) EC with a Si vacancy, ^{2}ROHF *ab initio* optimized geometry. 5-65

5.45. C-terminated SiC(111) EC with a C vacancy, *ab initio* optimized geometry (6-31G* basis set). 5-66

5.46. C-terminated SiC(111) EC with a C vacancy, MIMOMM optimized geometry, 4 bilayer bulk cluster (6-31G* basis set). 5-66

5.47. Hybrid cluster for Si(111) surface studies. 5-71

5.48. Comparison of Si-terminated SiC(111) and Si(111) embedded clusters. 5-72

5.49. Comparison of *ab initio* (6-31G* basis set) optimized Si(111) cluster geometry, bare and with 1 O atom adsorbed at an ontop site. 5-75

5.50. *Ab initio* optimized ^{4}ROHF (6-31G*) geometry of Si-O-Si bridge, Si(111) surface. 5-77

5.51. MIMOMM optimized ^{4}ROHF (6-31G*/3BL) geometry of Si-O-Si bridge, Si(111) surface. 5-77

5.52. *Ab initio* optimized ^{4}ROHF (6-31G*/3BL) geometry of Si-O-Si ring insertion, Si(111) surface. 5-80

5.53. IMOMM optimized ^{4}ROHF (6-31G*/3BL) geometry of Si-O-Si ring insertion, Si(111) surface. 5-80

Figure Page

5.54. *Ab initio* optimized ^{4}ROHF (6-31G*/3BL) geometry of Si-O-Si ring insertion, Si(111) surface. 5-81

5.55. IMOMM optimized ^{4}ROHF (6-31G*/3BL) geometry of Si-O-Si ring insertion, Si(111) surface. 5-81

5.56. *Ab initio* optimized ^{4}ROHF (6-31G*) geometry of Si(111) cluster with two O atoms adsorbed, O_{ontop}Si-O_{ring}-Si. 5-83

5.57. *Ab initio* optimized ^{4}ROHF (6-31G*) geometry of Si(111) cluster. . . . 5-86

5.58. *Ab initio* optimized ^{4}ROHF (6-31G*) geometry of Si(111) cluster with a surface vacancy. 5-86

5.59. *Ab initio* optimized ^{4}ROHF (6-31G*) geometry of Si(111) cluster. . . . 5-87

5.60. MIMOMM optimized ^{4}ROHF (6-31G*) geometry of Si(111) cluster with a surface vacancy. Distortion of cluster much larger than in SiC 5-87

5.61. *Ab initio* optimized ^{4}ROHF (6-31G*) geometry of Si(111) cluster with a surface vacancy. Atoms 4 and 8 have bonded in the reconstruction following creation of the vacancy. 5-88

5.62. IMOMM optimized ^{4}ROHF (6-31G*) geometry of Si(111) cluster with a surface vacancy. 5-88

5.63. Optimized geometry of H_3Si-O-SiH_3 5-92

5.64. Boys localized singly occupied molecular orbitals for Si and C-terminated SiC(111) surfaces. 5-95

D.1. Fluorethylene input file for program Delocal.x D-3

D.2. Screen dump from DLC generation for fluoroethylene D-4

D.3. $ZMAT deck for fluoroethylene DLCs D-5

List of Tables

Table		Page
2.1.	H_2 Total Energy and Equilibrium Bond Lengths	2-28
2.2.	Computational Accuracy Limits	2-28
3.1.	Comparison of constraints on different regions of a hybrid optimization	3-10
3.2.	MM3 Cartesian Gradient on frozen Region 1 atoms and optimized Region 4 atoms taken from a GAMESS .log file for an MIMOMM optimization of Si_6H_{12} embedded in Si_9H_{12}.	3-18
3.3.	Converged hybrid gradient from a MIMOMM optimization of Si_6H_{12} embedded in Si_9H_{12}.	3-18
3.4.	Comparison of embedding schemes on Si_6H_{12} embedded cluster.	3-19
3.5.	Comparison of embedding schemes on $Si_6H_{12}/Si_{38}H_{36}$ hybrid cluster.	3-21
3.6.	Comparison of symmetric dimer length in Si_9H_{12}	3-28
3.7.	Atom displacements induced by symmetric dimer formation in the $Si_{66}H_{52}$ model of the Si(001) surface, HW ECP(d) optimized geometry.	3-38
3.8.	Comparison of atom displacements caused by dimer formation on the Si(001) surface.	3-39
3.9.	Comparison of $Si_{15}H_{16}$ optimized geometry, RHF and GVB-PP(2) models.	3-43
3.10.	Atom displacements induced by dimer formation in $Si_{15}H_{16}$	3-43
3.11.	Effect of bulk cluster on Si_9H_{12} structure	3-45
4.1.	Mulliken charges on the $Si_5\overline{H}_{12}$ molecule, HW ECP basis set.	4-13
4.2.	Mulliken Charges on the $Si_5\overline{H}_{12}$ molecule, HW ECP(d).	4-13
4.3.	Mulliken Charges on the $\overline{H}$-$Si(SiH_3)_3$ molecule, HW ECP basis set.	4-16
4.4.	Mulliken Charges on the $\overline{H}$-$Si(SiH_3)_3$ molecule, 6-31G* basis set.	4-17
4.5.	Optimum distance for $\overline{H}$ creation	4-17
4.6.	Mulliken charges in Si_9H_{12} obtained using a number of different $\overline{H}$ atoms for termination in place of hydrogen	4-24

Table Page

4.7. Mulliken charges in $Si_9\overline{H}_{12}$ for $\overline{H}$s created at different Si-$\overline{H}$ separations in the model system 4-25

4.8. Mulliken charges in $Si_9\overline{H}_{12}$ using $\overline{H}_{Si3s}$ at fixed and optimized Si-$\overline{H}$ separations. 4-27

4.9. Test cases used to evaluate the effect of effect of $\overline{H}$ termination on small silicon clusters 4-28

4.10. Comparison of Mulliken Charges, Bare Dimer (HW ECP basis set), in *ab initio* and MIMOMM optimized systems. 4-29

4.11. Comparison of Mulliken Charges, hydrogenated Dimer (HW ECP basis set), in *ab initio* and MIMOMM optimized systems. 4-29

4.12. Comparison of Mulliken Charges, bare dimer, for $\overline{H}$ atoms created to be used with the 6-31G* basis set. 4-30

4.13. Comparison of Si_9 structure, bare dimer, HW ECP basis set. 4-32

4.14. Atom displacements induced by symmetric dimer formation in the Si_9H_{12} model of the Si(001) surface. 4-32

4.15. Comparison of Si_9 structure with two H atoms adsorbed on the dimer 4-34

4.16. Comparison of Si_9 structure, unsaturated dimer using $\overline{H}$s created at different Si-$\overline{H}$ separations in the model system 4-34

4.17. Effect of $\overline{H}$ termination on Si_9H_{12} *ab initio* optimized geometry, 6-31G* basis set. 4-35

4.18. Atom displacements induced by symmetric dimer formation in the Si_9H_{12} model of the Si(001) surface. 4-35

4.19. State energies used to calculate energy of hydrogenation, H and $\overline{H}$ terminated molecules. 4-37

4.20. Comparison of energy of hydrogenation, H and $\overline{H}$ terminated molecules. 4-37

4.21. Ionization potential of a silicon dangling bond as a function of radial scaling parameter, HW ECP + d basis set 4-39

4.22. Mulliken Charges in the $\overline{H}Si(CH_3)_3$ molecule, HW ECP basis set. . . . 4-44

4.23. Mulliken charges on the $C_5\overline{H}_{12}$ molecule, HW ECP basis set. 4-46

Table | Page

4.24. Mulliken Charges in the $Si_{18}C_{18}\overline{H}_{42}$ molecule, HW ECP and HW ECP(d) basis sets. 4-47

5.1. Structural parameters for Si-terminated SiC(001)-(2X1) surface. 5-6

5.2. 6-31G* energies of SiC clusters, quarter and doublet surface reconstruction. 5-15

5.3. Comparison of reconstruction of Si and C-terminated embedded clusters, conventional *ab initio* optimization 5-18

5.4. Comparison of *ab initio* (6-31G*) and MIMOMM optimized geometries of the silicon terminated SiC(111) embedded cluster. 5-18

5.5. Effect of bulk cluster on Si-terminated SiC(111) surface energies of hydrogenation 5-26

5.6. Comparison of energies of hydrogenation, Si-terminated SiC(111) surface 5-26

5.7. Structural changes caused by H atom adsorption on the C-terminated SiC(111) cluster. 5-29

5.8. Effect of bulk cluster on C-terminated SiC(111) surface energies of hydrogenation 5-30

5.9. Comparison of energy of hydrogenation, C-terminated SiC(111) surface 5-30

5.10. Atom displacements induced by O atom adsorption onto a bridging site of an Si-terminated SiC(111) surface. 5-37

5.11. Comparison of *ab initio* and MIMOMM optimized Si-terminated SiC(111) cluster geometry with 1 O atom adsorbed onto a *bridge* site. 5-40

5.12. Comparison of *ab initio* and MIMOMM (4 bilayer) optimized (6-31G*) Si-terminated SiC(111) cluster geometry with an O atom adsorbed at a Si-O-C ring insertion site. 5-41

5.13. Comparison of Si-terminated SiC(111) cluster *ab initio* optimized geometry (6-31G*) with 0, 1, and 2 O atoms adsorbed. 5-44

5.14. 6-31G* energies of SiC clusters used in calculating energy of oxidation. 5-47

5.15. Comparison of energy of oxidation, Si-terminated SiC(111) surface. . . 5-47

5.16. Atom displacements induced by O atom adsorption onto a bridging site of a C-terminated SiC(111) surface. 5-51

Table Page

5.17. Comparison of *ab initio* and MIMOMM optimized C-terminated SiC(111) cluster geometry with 1 O atom adsorbed onto an *bridge* site. 5-53

5.18. Comparison of *ab initio* and MIMOMM (4 bilayer) optimized (6-31G*) C-terminated SiC(111) cluster geometry with an O atom adsorbed at a C-O-Si ring insertion site. 5-54

5.19. Comparison of C-terminated SiC(111) cluster *ab initio* optimized geometry (6-31G*) with 0, 1, and 2 O atoms adsorbed. 5-57

5.20. 6-31G* energies of C-terminated SiC clusters used in calculating energy of oxidation. 5-60

5.21. Comparison of energy of oxidation, C-terminated SiC(111) surface . . 5-60

5.22. Atom displacements induced by a Si atom vacancy at the Si-terminated SiC(111) surface. 5-64

5.23. Comparison of *ab initio* and MIMOMM optimized geometries of Si-terminated cluster with a Si surface vacancy 5-64

5.24. Atom displacements induced by a C atom vacancy at the C-terminated SiC(111) surface. 5-67

5.25. Comparison of *ab initio* and MIMOMM optimized geometries of C-terminated cluster with a C surface vacancy, (6-31G* basis set). 5-67

5.26. Surface vacancy energies, Si and C-terminated SiC(111) clusters. . . . 5-69

5.27. Comparison of ^{4}ROHF energy of vacancy creation, Si and C-terminated SiC(111) clusters. 5-69

5.28. Comparison of bulk silicon lattice and reconstructed Si(111) cluster (6-31G* basis set). 5-73

5.29. Hydrogenation energetics of silicon(111) cluster. 5-74

5.30. Comparison of *ab initio* and MIMOMM optimized Si(111) cluster geometry with 1 O atom adsorbed onto a *bridge* site. 5-76

5.31. Atom displacements induced by an O atom Si-O-Si bridge adsorption site on the Si(111) surface. 5-78

5.32. Comparison of *ab initio* and MIMOMM (3 bilayer) optimized (6-31G*) Si(111) cluster geometry with an O atom adsorbed at a Si-O-Si ring insertion site. 5-79

Table | Page

5.33. Comparison of Si(111) cluster *ab initio* optimized geometry (6-31G*) with 0, 1, and 2 O atoms adsorbed. 5-82

5.34. Oxidation energetics of Si(111) cluster. 5-85

5.35. Si(111) surface vacancy energetics 5-89

5.36. Atom displacements induced by a Si vacancy on the Si(111) surface. . 5-89

5.37. Internal coordinates of an *ab initio* and MIMOMM optimized (6-31G* basis set) geometries of Si(111) cluster with a Si surface vacancy. . . . 5-90

5.38. Small molecule models for Si-O bond energies. 5-93

5.39. Si-O bond energies in SiC cluster models (6-31G* basis set). 5-93

5.40. Comparison of bond angles in $H_3SiOSiH_3$ with O atom ontop and bridge adsorption sites on the Si-terminated SiC(111) surface. 5-93

5.41. Small molecule models for C-O bond energies. 5-94

5.42. C-O bond energies in SiC cluster models (6-31G* basis set). 5-94

5.43. Comparison of bond angles in H_3COCH_3 with O atom ontop and bridge adsorption sites on the C-terminated SiC(111) surface. 5-94

5.44. Energetics of CO_2 desorption from C-terminated SiC(111) cluster. . . . 5-97

5.45. Summary of O atom adsorption energies on SiC(111) and Si(111). . . . 5-100

C.1. 6-31G* energies of small molecules used in reaction caculations. C-1

C.2. Hartree-Fock (6-31G*) energetics of Si-terminated SiC(111) clusters used in this work C-2

C.3. MP2 (6-31G*) energetics of Si-terminated SiC(111) clusters used in this work C-3

C.4. Hartree-Fock (6-31G*) energies of C-terminated SiC(111) clusters used in this work C-4

C.5. MP2 (6-31G*) energies of C-terminated SiC(111) clusters used in this work C-5

C.6. Hartree-Fock (6-31G*) energies of silicon(111) cluster used in this work C-6

AFIT/ENP/DSP/97-09.

Abstract

Fabrication of silicon carbide (SiC) semiconductor devices are of interest for aerospace applications because of their high-temperature tolerance. Growth of an insulating SiO_2 layer on SiC by oxidation is a poorly understood process, and sometimes produces interface defects that degrade device performance. Accurate theoretical models of surface chemistry, using quantum mechanics (QM), do not exist because of the huge computational cost of solving Schrödinger's equation for a molecular cluster large enough to represent a surface. Molecular mechanics (MM), which describes a molecule as a collection of atoms interacting through classical potentials, is a fast computational method, good at predicting molecular structure, but cannot accurately model chemical reactions.

A new hybrid QM/MM computational method for surface chemistry was developed and applied to silicon and SiC surfaces. The addition of MM steric constraints was shown to have a large effect on the energetics of O atom adsorption on SiC. Adsorption of O atoms on Si-terminated SiC(111) favors above surface sites, in contrast to Si(111), but favors subsurface adsorption sites on C-terminated SiC(111). This difference, and the energetics of C atom etching via CO_2 desorption, can explain the observed poor performance of SiC devices in which insulating layers were grown on C-terminated surfaces.

HYBRID QUANTUM AND MOLECULAR MECHANICS EMBEDDED CLUSTER MODELS FOR CHEMISTRY ON SILICON AND SILICON CARBIDE SURFACES

I. Methods for modeling chemistry on surfaces

1.1 Motivation

Chemical reactions on surfaces play a key role in many processes of technological importance, for example, surface catalyzed reactions such as NO and CO conversion in automobile catalytic converters, semiconductor processing and fabrication, and surface corrosion and rust. Fabrication of silicon carbide (SiC) Metal Oxide Semiconductor Field Effect Transistor (MOSFET) devices are of high interest to the Air Force because their high operating temperature makes them appealing for aerospace applications [1]. (SiC devices could operate uncooled, unlike silicon devices which must be cooled.) One of the integral steps in the fabrication of a SiC MOSFET device is the deposition of an insulating oxide layer (SiO_2 in both silicon and SiC) on the semiconductor material. The oxide layer is grown by exposing the SiC surface to an oxygen plasma, in which the reactive O atoms are thought to be the dominant species involved in oxide layer growth. Significant differences in SiC MOSFET device performance have been observed if the oxide layer is grown on a Si or C terminated SiC surface. Based on related experience from silicon MOSFET fabrication [2], it is thought that O atom exposure to the C terminated surface etches the C atoms, creating defects at the SiC surface. Creation of surface defects causes reconstruction of the lattice several layers down, so the effect of these surface defects propagate on the order of $10\mathring{A}$ into the SiC. As fabrication proceeds, the SiC surface becomes the interface between the semiconductor and the insulator. Since much of the current in MOSFET devices is carried in a thin layer adjacent to this interface, the defects created during oxide layer deposition significantly degrade device performance.

The surface chemistry of SiC is poorly understood. Very little experimental characterization of oxygen chemisorbed on SiC has been performed [3], and very few theoretical and experimental investigations have been described in the literature. The purpose of this study is to provide an understanding of this problem by developing a computational approach that will allow the simulation of surfaces of bulk materials.

1.2 Background

Ab initio quantum mechanical calculations of the electronic wavefunction for molecules have been shown to predict energetics for chemical reactions that agree well with experiment, with a typical "chemical" accuracy of $\pm 5 \frac{kcal}{mol}$. Unfortunately, *ab initio* approaches cannot currently be used to model surface chemistry. Since one needs to use a molecular system in an *ab initio* approach, the surface of a real material is simulated by designing a large molecular cluster (model system) that matches the lattice geometry of the real system, and has one face that matches the surface structure of the real system. This molecular cluster must be large enough to provide a realistic representation of the steric (mechanical) and electronic environments of a bulk material. *The problem with using ab initio calculations for modeling surface chemistry is that the minimum size for a molecular cluster that provides an adequate representation of the surface of a bulk material greatly exceeds the maximum size of a practical ab initio calculation.*

A concrete example to illustrate this problem is shown in Figure 1.1 with the molecule $Si_{73}C_{69}H_{109}$, which is a model of a Si-terminated SiC surface in the (111) orientation (surface notation is defined in Section 3.7.1). This cluster has 3 unsaturated Si atoms (the white atoms in the top layer) which serve as reactive sites for H and O atom adsorption. Figure 1.2 shows a similar example, the molecule $Si_{70}C_{70}H_{87}$, which is another model of a Si-terminated SiC surface in the (111) orientation. This cluster also has 3 unsaturated Si atoms in the top layer to serve as reactive sites. Both clusters contain roughly the same number of atoms, with similar computational cost. Note that it is still unclear which cluster would provide a better model of the SiC(111) surface; this question is addressed in Chapter V.

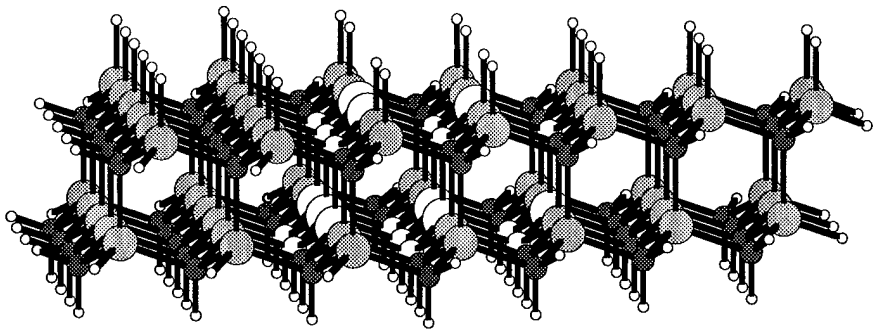

Figure 1.1 $Si_{73}C_{69}H_{109}$ cluster model of a Si-terminated SiC(111) surface.

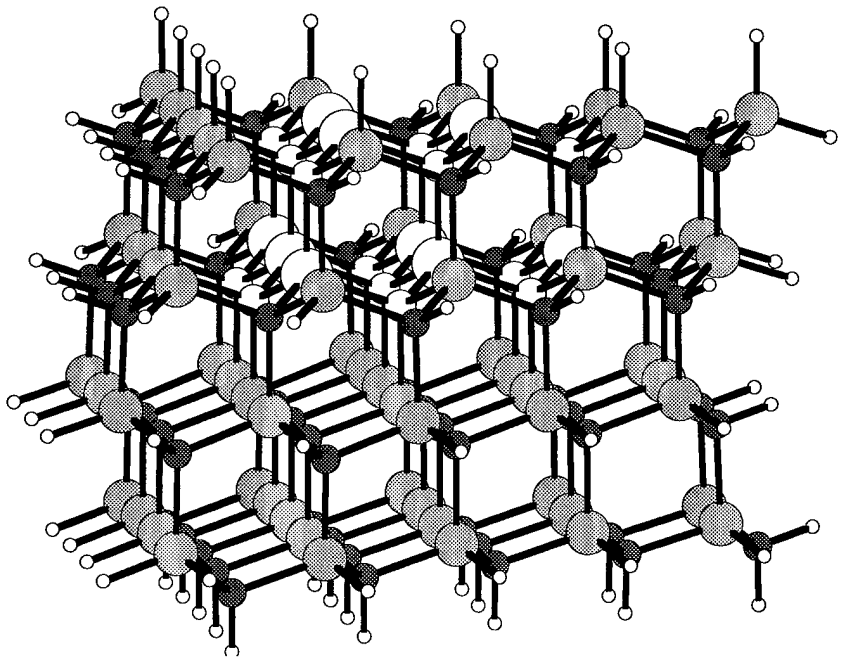

Figure 1.2 $Si_{70}C_{70}H_{87}$ cluster model of a Si-terminated SiC(111) surface.

In an *ab initio* calculation, one solves for the (approximate) electronic wavefunction using quantum mechanics (QM). Thus, the size of the problem depends on the total number of electrons in the molecule. A functional expansion is used to represent the wavefunction, so the exact computational cost is determined by the number of basis functions used to represent the wavefunction. (The number of basis functions per electron is a user selected parameter. The more basis functions per electron, the higher the accuracy of the result.) Using a basis set (specific functional expansion, see Section 2.1.4 for details) that provides good predictions of molecular structure, $Si_{73}C_{69}H_{109}$ contains 2640 basis functions, and $Si_{70}C_{70}H_{87}$ contains 2554 basis functions. The largest *ab initio* calculation performed in this research contained 686 basis functions, and had a computation time of 100 hours on 32 nodes of an IBM SP2 supercomputer. *Ab initio* calculations formally scale as the number of basis functions raised to the fourth power; for large clusters such as these, the power scaling is somewhere between 3 and 4. *Using a scaling of 3.5, the estimated calculation time for a single geometry optimization calculation on these clusters is over over one year.* As one would need to do tens of such calculations to investigate the initial oxidation of SiC, it is clearly impractical to use clusters of this size in *ab initio* modeling.

Thus, the size of the cluster must be reduced in order to use *ab initio* quantum mechanical techniques. Figures 1.3 and 1.4 show Si and C-terminated SiC clusters that are computationally tractable. The Si-terminated cluster contains 416 basis functions, and the C-terminated cluster contains 432 basis functions. The computation time for each is roughly 24 hours on 32 IBM SP2 nodes, which is quite reasonable. However, since these clusters are so much smaller than the clusters described above, their reliability is questionable. Indeed, these clusters provide a very poor model of the SiC(111) surface. Figure 1.6 shows this Si-terminated cluster with one O atom adsorbed to two adjacent Si surface atoms. (This cluster without an O atom adsorbed is shown in Figure 1.5 for comparison.) The two Si atoms have displaced roughly 0.7$\AA$ from their lattice positions to bond with the O atom, and in the process have changed the positions of their neighboring atoms as well. The cluster has curled up because its edges are so close to the reaction site, which is clearly a poor model of real SiC surface where the edges would be on the

order of 10^{23} atoms away from the reaction site. Clearly, an approximate approach must be developed to address these limitations.

1.3 Problem Statement

The problems addressed in this research are the development of a hybrid QM/MM computational technique that will enable relatively small molecular clusters to simulate surfaces of bulk materials, and its application to the study of the surface chemistry of silicon carbide, with emphasis on the oxidation of SiC(111) surfaces.

1.4 Overview

In order to simulate a bulk material with a small molecular cluster (cluster), the mechanical and electronic environment of a bulk material must be accounted for. Molecular structure computational methods based on classical mechanics have been shown to work well for molecular structure. In the technique known as molecular mechanics (MM), a molecule is described as a collection of atoms interacting through various classical 2-body (bond stretch), 3-body (angle bend), and 4-body (torsion angle rotation) potentials. These potentials are derived from experimental data and *ab initio* calculations of small model compounds. MM calculations are appropriate for predicting molecular structure, but cannot predict the chemistry since MM lacks an explicit description of electronic behavior. However, an advantage of MM calculations is that they are much faster than corresponding *ab initio* calculations. For example, the *ab initio* geometry optimization of $Si_{70}C_{70}H_{87}$, which was predicted to take one year on 32 nodes of an IBM SP2, *only took 15 minutes on one IBM SP2 node using MM.*

A number of researchers have devised hybrid *ab initio*/MM (QM/MM) computational schemes that use MM to simulate the mechanical environment of large molecules by embedding a small piece of the molecule modeled with QM *embedded* within the rest of the molecule modeled with MM. Maseras et al. [4] have developed an interesting method to merge MM and *ab initio* calculations, the so-called Integrated Molecular Orbital Molecular Mechanics (IMOMM). In IMOMM, forces (energy gradients) from MM are used to modify an *ab initio* geometry. *However, the method used to link embedded and bulk clus-*

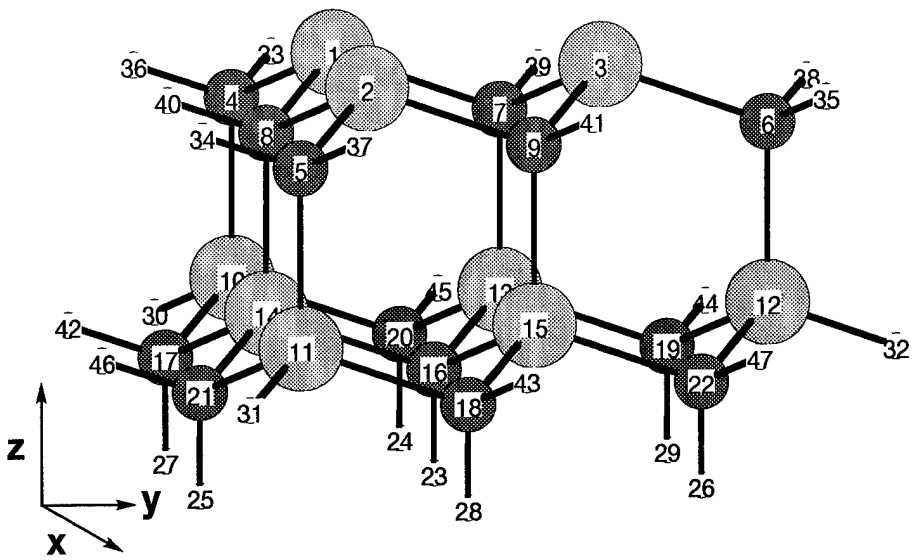

Figure 1.3 $Si_9C_{13}H_{25}$ model of a Si-terminated SiC(111) surface, 416 basis functions.

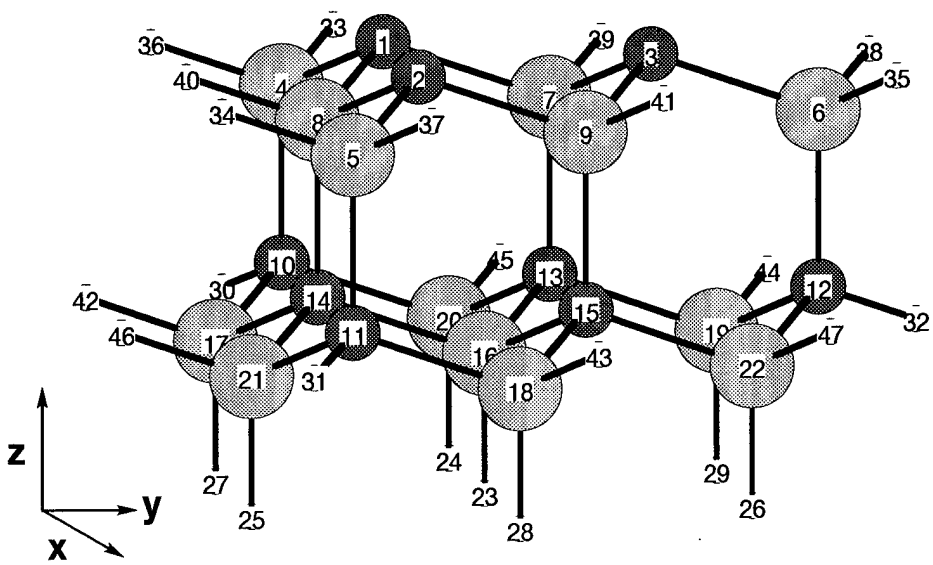

Figure 1.4 $C_9Si_{13}H_{25}$ model of a C-terminated SiC(111) surface, 432 basis functions.

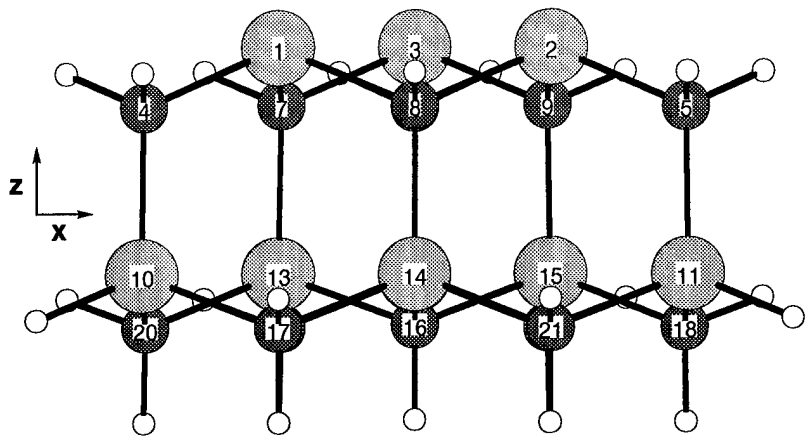

Figure 1.5 Clean Si-terminated SiC(111) embedded cluster, xz view, *ab initio* optimized geometry.

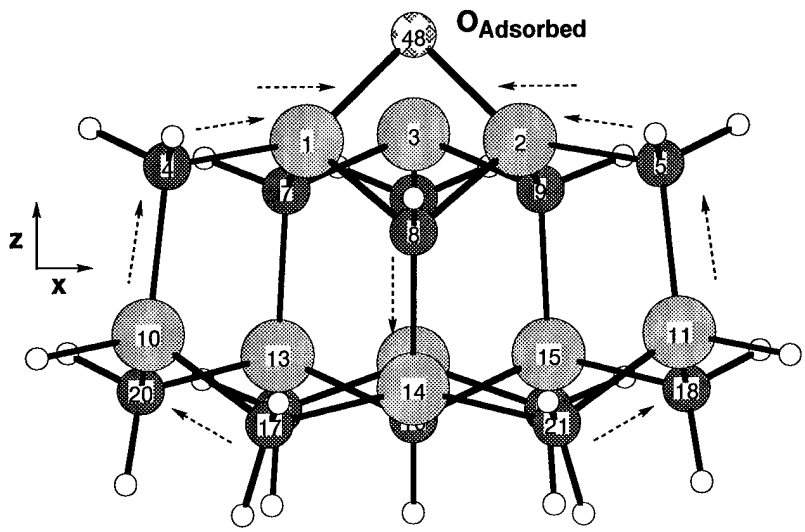

Figure 1.6 *Ab initio* optimized Si-terminated SiC(111) EC with O atom adsorbed in a bridge site. Directions of atom displacements from lattice positions are shown by arrows.

ters in IMOMM is unsuitable for surface calculations. IMOMM was initially implemented using commercial computer programs, the *ab initio* code Gaussian92 [5] and the MM code MM3 [6] [4]; however, IMOMM is not yet available to the public.

Now, one must address the problem of simulating the electronic environment of a bulk material in a molecular cluster. The atoms at the faces of a small cluster would be bonded to lattice atoms if the cluster were part of a bulk material. These boundary atoms in small clusters are generally bonded to H atoms instead of lattice atoms to eliminate unbonded electrons at the boundary, i.e., saturate the "dangling" bonds. The H atoms used to saturate the dangling bonds produce a mismatch in electronegativity with the bulk material. The electronic environment in the small cluster is different than in the bulk material, hence the chemical reactivity of the cluster will be different than the bulk material. In an attempt to modify the electronic environment of small clusters to make them more bulk-like, several researchers have created artificial one-electron "atoms", $\overline{H}$s, that mimic the electronic behavior of bulk silicon atoms, and used them to terminate small silicon clusters [7, 8]. This previous work has only explored the use of $\overline{H}$s under very limited conditions, so the generic utility of $\overline{H}$s for terminating silicon is not known. The possibility of terminating SiC clusters with similar $\overline{H}$s has not been previously explored.

1.5 Approach

A hybrid MM/*ab initio* technique is promising for surface calculations. In this work, the IMOMM approach of Maseras and Morokuma was modified for use in surface calculations. This Modified IMOMM (MIMOMM) approach was implemented in the public domain *ab initio* quantum mechanics code GAMESS [9] (General Atomic and Molecular Electronic Structure System) with the molecular mechanics code MM3. The initial implementation will use MM3 to enable direct comparisons with the original IMOMM. MM3 is a commercial code, so a search for a public domain MM code will also be conducted. In addition to a new method used to link the quantum and molecular mechanics regions of the hybrid system, a new type of internal coordinates, delocalized coordinates [10] was also implemented in GAMESS to enable the application of MIMOMM to surface (and other highly coupled) clusters. In addition to MIMOMM, an alternate method to merge *ab initio*

and MM calculations as described by Weiner et al. [11] was also implemented, and the two methods compared on cluster models of the dimerized silicon(001) surface. The hybrid methods were benchmarked against an *ab initio* optimized geometry of a very large silicon surface cluster model. For this particular system, *ab initio* calculations on small cluster models, MIMOMM calculations on a large hybrid cluster, and the *ab initio* calculation on the large silicon cluster were all found to agree well with experiment.

1.6 Application

The newly developed MIMOMM method was used to predict structures and energies for O atoms adsorbed onto Si and C-terminated SiC(111) surfaces, which is a poorly understood problem that has not been well characterized. The relative energies of several O atom adsorptions sites on the Si-terminated SiC(111) surface favored above surface sites, while a subsurface adsorption site was energetically favored for the C-terminated SiC(111) surface. This difference, along with relative energetics for adsorbed O atoms and gas phase CO and CO_2 may favor etching of C-terminated SiC(111) by O atoms, and favor passivation of the Si-terminated SiC(111) surface. MIMOMM predicted structures and energies for O atoms adsorbed on a similar Si(111) surface show how differences in lattice size can explain the observed differences between the Si and C-terminated SiC(111) surfaces.

In summary, the key element for success of a hybrid *ab initio*/MM model is the design of the hybrid model system, the *ab initio* optimized small cluster and the MM optimized large cluster in which the *ab initio* cluster is embedded. This is not just a matter of designing for computational efficiency, but more importantly, requires an understanding of how a bulk material affects reactivity on the surface. While the bulk effects on surface chemistry are known to be important, the specific influence of the bulk has not yet been quantified. With a MIMOMM, bulk mechanical effects can be separated by comparing conventional *ab initio* calculations on the small cluster with hybrid calculations using this same *ab initio* piece.

II. An Overview of Computational Methods for Determining Molecular Properties

A description of the methods currently used to calculate molecular properties and chemical behavior is presented in this chapter The reader will be directed to more detailed references on each technique. The goal of this chapter is to provide enough information to understand the limitations of each technique and the applications where each is most appropriate.

2.1 Ab Initio Hartree-Fock Self Consistent Field Technique

The Hartree-Fock Self Consistent Field (HF-SCF or simply SCF) is used to calculate the approximate electronic wavefunction of an atom or molecule by solving Schrödinger's wave equation. Solution of the Schrödinger equation for systems with more than one electron is very difficult, so several approximations must be made in order to find numerical solutions. The HFSCF procedure is at the core of every *ab initio* quantum chemistry code. To understand the accuracy and applicability of the answers these codes provide, it is important to understand the approximations that had to be made along the way.

2.1.1 Born-Oppenheimer Approximation. Born and Oppenheimer originated the central approximation used in calculating the electronic wavefunction of molecules in 1927 [12]. The general time-independent Schrödinger wave equation (in atomic units) for a collection of N electrons and M nuclei, neglecting spin and relativistic effects is [13]

$$\left[\hat{T}_n + \hat{T}_e + \hat{V}_{nn} + \hat{V}_{ee} + \hat{V}_{en}\right] \Psi(\vec{R}, \vec{r}) = E\Psi(\vec{R}, \vec{r}). \tag{2.1}$$

The terms in this Hamiltonian, in atomic units, are

$\hat{T}_n \implies \sum_{i=1}^{M} -\frac{1}{2M_A}\nabla_A^2$ Nuclear Kinetic Energy Operator

M_A *mass of nuclei A*

∇_A^2 *second derivative with respect to coordinates of nuclei A*

$\hat{T}_e \implies \sum_{i=1}^{N} -\frac{1}{2}\nabla_i^2$ Electron Kinetic Energy Operator

∇_i^2 *second derivative with respect to coordinates of electron i*

$\hat{V}_{nn} \implies \sum_{A=1}^{M} \sum_{B>A}^{M} \frac{Z_A Z_B}{R_{AB}}$ Nuclear-Nuclear Potential Energy Operator

Z_A *charge of nuclei A*

R_{AB} *separation between nuclei A and B*

$\hat{V}_{ee} \implies \sum_{i=1}^{N} \sum_{i>j}^{N} \frac{1}{r_{ij}}$ Electron-Electron Potential Energy Operator

r_{ij} *separation between electrons i and j*

$\hat{V}_{en} \implies \sum_{i=1}^{N} \sum_{A=1}^{M} \frac{Z_A}{r_{iA}}$ Electron-Nuclear Potential Energy Operator

Z_A *charge of nuclei A*

r_{iA} *separation between electron i and nuclei A*

The solution to this Partial Differential Equation (PDE) is a wavefunction in which nuclear and electronic motion is coupled. However, Born and Oppenheimer suggested that because of the great difference in the electron and nuclear masses, on the timescale of electronic motion the nuclei will appear nearly stationary. Thus, to an approximation, one can decouple the nuclear and electronic motion and express the total wavefunction as a product of a function of nuclear coordinates only and a function of electronic coordinates at a specific nuclear geometry. That is, the electronic wavefunction depends explicitly on the electron coordinates and parametrically on the nuclear coordinates.

$$\Psi(\vec{R};\vec{r}) = \phi(\vec{R})\psi(\vec{r};\vec{R}) \tag{2.2}$$

where $\vec{R}$ denotes nuclear coordinates, and $\vec{r}$ denotes electron coordinates. The nuclear kinetic energy operator $\hat{T}_n$ only acts on nuclear coordinates, and the electronic kinetic energy operator $\hat{T}_e$ only acts on electronic coordinates.

$$\begin{aligned}
\hat{T}_n[\phi(\vec{R})\psi(\vec{r};\vec{R})] &= [\hat{T}_n\phi(\vec{R})]\psi(\vec{r};\vec{R}) + \phi(\vec{R})[\hat{T}_n\psi(\vec{r};\vec{R})] &= [\hat{T}_n\phi(\vec{R})]\psi(\vec{r};\vec{R}) + 0 \\
\hat{T}_e[\phi(\vec{R})\psi(\vec{r};\vec{R})] &= [\hat{T}_e\phi(\vec{R})]\psi(\vec{r};\vec{R}) + \phi(\vec{R})[\hat{T}_e\psi(\vec{r};\vec{R})] &= 0 + \phi(\vec{R})[\hat{T}_e\psi(\vec{r};\vec{R})]
\end{aligned} \tag{2.3}$$

Within this approximation, Schrödinger's equation becomes

$$\phi(\vec{R})[\hat{T}_e\psi(\vec{r};\vec{R})] + [\hat{T}_n\phi(\vec{r})]\psi(\vec{r};\vec{R}) + \phi(\vec{R})\psi(\vec{r};\vec{R})[\hat{V}_{nn} + \hat{V}_{ee} + \hat{V}_{en} - E] = 0. \tag{2.4}$$

Rearranging terms in Eq 2.4, we obtain

$$\phi(R)[\hat{T}_e + \hat{V}_{ee} + \hat{V}_{en}]\psi(\vec{r};\vec{R}) + \psi(\vec{r};\vec{R})[\hat{T}_n + \hat{V}_{nn} - E] = 0. \tag{2.5}$$

Since $\psi(\vec{r};\vec{R})$ only has parametric dependence on $\vec{R}$, we can define a separate eigenvalue problem for the electronic piece of the wavefunction, which is

$$[\hat{T}_e + \hat{V}_{ee} + \hat{V}_{en}]\psi(\vec{r};\vec{R}) = \varepsilon_e\left\{\vec{R}\right\}\psi(\vec{r};\vec{R}). \tag{2.6}$$

Replacing the appropriate terms in Eq 2.5 with the definition of the eigenvalue problem for the electronic part of the total wavefunction, Eq 2.6, we obtain

$$\psi(\vec{r};\vec{R})\left[[\hat{T}_n + (\hat{V}_{nn} + \varepsilon_e\left\{\vec{R}\right\}) - E]\phi(\vec{R})\right] = 0. \tag{2.7}$$

The combination of $\hat{V}_{nn} + \varepsilon_e$ defines an effective potential for molecular vibrations. It is the potential energy for the nuclei in the field created by the electrons. In general, the electronic energy becomes more negative as the nuclei are moved closer together. The internuclear potential energy becomes more positive as the nuclei are moved closer together. Thus, the minimum energy configuration of a molecule is a compromise between these two factors. This is illustrated in the sample calculation for H_2 shown in Figure 2.1.

The Born-Oppenheimer approximation is one of the best approximations made in chemical physics because it is valid in a very wide range of situations. However, the product form of the wavefunction is still useful in those situations where the Born-Oppenheimer approximation breaks down. We know that any function of one variable can be expressed as an infinite sum of orthogonal functions, a generalized Fourier series. Similarly, a function of two variables can be expressed exactly as an infinite sum of products of single variable

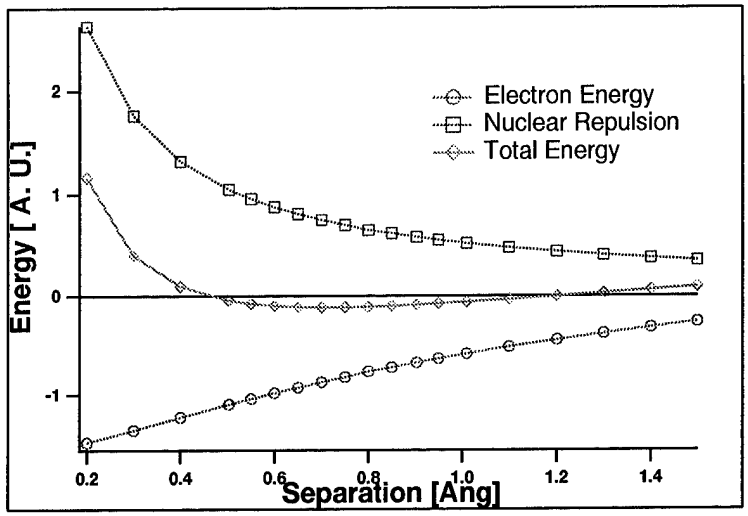

Figure 2.1 H_2 Molecule Total Energy as the Sum of Electronic and Nuclear Repulsion Components.

functions,

$$F(x,y) = \sum_{i=1}^{\infty}\sum_{j=1}^{\infty} c_{ij} f_i(x) g_j(y). \tag{2.8}$$

The Born-Oppenheimer approximation makes the assumption that

$$\begin{aligned} c_{ij} &= 1; \quad i,j = 1 \\ &= 0; \quad i,j \neq 1. \end{aligned} \tag{2.9}$$

Approximate nuclear-electronic wavefunctions would be obtained by a finite number of terms. Calculations that do not use the Born-Oppenheimer approximation are exceptionally challenging, and at the present time are limited to very simple systems. We are primarily concerned with solutions for the electronic wavefunction since the electronic wavefunction determines the effective potential in which the nuclei move (under the BO approximation), thus it drives the solution for the nuclear wavefunction (molecular geometry) as well.

2.1.2 Approximate Electronic Wavefunctions. The time-independent Schrödinger equation for the electronic wavefunction is

$$\left(\left(\sum_{i=1}^{N} -\frac{1}{2}\nabla_i^2 + \sum_{i=1}^{N}\sum_{A=1}^{M} -\frac{Z_A}{r_{iA}}\right) + \sum_{i=1}^{N}\sum_{j>i}^{N} \frac{1}{r_{ij}}\right) \psi(\vec{r};\vec{R}) = \varepsilon_e \left\{\vec{R}\right\} \psi(\vec{r};\vec{R}). \tag{2.10}$$

We see that the first two operators on the left hand side of Eq 2.10 involve coordinates of only one electron at a time. One could obtain an exact solution as a simple product of functions of individual electron coordinates if we only had to worry about these two operators. The third operator, describing electron-electron interactions, is more troublesome because coupling pairs of electrons eliminates the separability in the problem. The fundamental difficulty one encounters in finding an electronic wavefunction is trying to solve a nonseparable PDE.

The most common method for solving a nonseparable PDE is to represent the PDE on a basis of orthogonal functions, i.e., a generalized Fourier series solution. One then uses the PDE to determine the coefficients for each term in the series. The accuracy of the solution depends on the number of terms in the series (number of basis functions), with an exact solution requiring an infinite number of terms. As the electronic wavefunction is a function of 3n variables, where n is the number of electrons, the generalized Fourier series solution method is computationally demanding. (The solution for a multi-electron atom is somewhat simpler than a molecule because all the electrons are centered at the same point in space, facilitating the construction of an orthogonal basis [14].) Since solutions for multi-electron wavefunctions were originally sought before the invention of digital computers, compromises in the accuracy of the solution were necessary. A logical first step was to include just one term in the series, but apply physical insight to develop a scheme to find the best single-term solution for the approximate wavefunction. This is the essence of the Hartree Fock Self Consistent Field (HF-SCF) procedure. [15, 16].

The choice of the initial trial wavefunction is crucial to the success of the HF-SCF procedure. The postulates of quantum mechanics help guide the selection of the trial function. First, we know that electrons moving about in an atom or molecule are indistinguishable particles. This means that the probability density derived from an electronic

wavefunction must be invariant with respect to labeling of the electron coordinates. For the probability to be invariant, the following relationship must hold for any pair of electrons:

$$\Psi^2\left(r_1, r_2, ...\mathbf{r_i}, \mathbf{r_j}, ...r_N\right) = \Psi^2\left(r_1, r_2, ...\mathbf{r_j}, \mathbf{r_i}, ...r_N\right). \tag{2.11}$$

(Note: The parametric dependence on the nuclear positions $\vec{R}$ is always implied even if it is not explicitly written.) For the wavefunction itself, this means that the interchange of a pair of electron coordinates can change the wavefunction by a factor of $\exp(i\phi)$. For electrons and other half-integer spin particles (fermions), $\phi = \pi$, so the electronic wavefunction is antisymmetric, changes sign, with respect to interchange of electron labels. This is a statement of the Pauli exclusion principle as applied to electronic wavefunctions. In order to satisfy the Pauli exclusion principle, we need to seek antisymmetric approximate solutions for the electronic wavefunction.

There are a number of ways to construct antisymmetric approximate wavefunctions; however, the determinant form of the wavefunction originated by Slater is perhaps the easiest to understand. This can be illustrated by investigating a two electron system. The simplest product form of our approximate wavefunction would be

$$\Phi\left(r_1, r_2\right) \approx \chi_1(r_1)\chi_2(r_2). \tag{2.12}$$

The product form in Eq 2.12, the Hartree product [15], is clearly not antisymmetric with respect to exchange of labels. However, an antisymmetric form is given by

$$\Psi\left(r_1, r_2\right) \approx \chi_1(r_1)\chi_2(r_2) - \chi_1(r_2)\chi_2(r_1). \tag{2.13}$$

It is clear that

$$\Psi\left(r_1, r_2\right) = -\Psi\left(r_2, r_1\right). \tag{2.14}$$

It is easy to see that Eq 2.13 could be obtained from the determinant of a matrix

$$\mathrm{Det}\begin{vmatrix} \chi_1(r_1) & \chi_2(r_1) \\ \chi_1(r_2) & \chi_2(r_2) \end{vmatrix} = \chi_1(r_1)\chi_2(r_2) - \chi_1(r_2)\chi_2(r_1). \tag{2.15}$$

For normalization, one would have to multiply Eq 2.15 by $\frac{1}{\sqrt{2}}$. Slater originated this form of the wavefunction, which is called the Slater determinant [17]. The general pattern for a Slater determinant wavefunction is

$$\Psi\left(r_1 ..., r_N\right) = \frac{1}{\sqrt{N!}} \mathrm{Det} \begin{vmatrix} \chi_1(1) & \chi_2(1) & \chi_3(1) & \cdots & \chi_N(1) \\ \chi_1(2) & \chi_2(2) & \chi_3(2) & \cdots & \chi_N(2) \\ \chi_1(3) & \chi_2(3) & \chi_3(3) & \cdots & \chi_N(3) \\ \cdots & \cdots & \cdots & \cdots & \cdots \\ \chi_1(N) & \chi_2(N) & \chi_3(N) & \cdots & \chi_N(N) \end{vmatrix} \tag{2.16}$$

The Slater determinant wavefunction is commonly abbreviated as $\mathrm{Det}\,|\Psi\left(r_1 ..., r_N\right)\rangle$. Exchange of electrons would correspond to swapping two rows in the matrix, which will change the sign of the determinant satisfying the antisymmetry requirement. If two columns in the matrix are identical, i.e., two electrons of the same spin are placed in the same orbital, the determinant is 0, as required by the Pauli exclusion principle.

The functions used in the Slater determinant must describe both the spatial behavior and the spin of the electron. Thus,

$$\begin{aligned} \chi_1 &= \psi_1 \alpha \\ \chi_2 &= \psi_1 \beta. \end{aligned} \tag{2.17}$$

where α is a spin eigenfunction with eigenvalue of the $\hat{S}_z$ operator of +1/2 (spin up), and β is a spin eigenfunction with $\hat{S}_z$ eigenvalue -1/2 (spin down). A molecule usually has an even number of electrons, i.e., a "closed shell", so one can assume that each pair of alpha and beta electrons reside in the same spatial wavefunction. This assumption enables one to eliminate an explicit consideration of spin from the problem. This assumption is used in the Restricted Hartree Fock (RHF) procedure, where restricted refers to the restriction that pairs of electrons reside in the same spatial wavefunction. In the Unrestricted Hartree Fock (UHF) procedure, each electron is taken to reside in a different spatial wavefunction. This increases the size of the calculation, but may provide a lower energy approximate wavefunction. However, one is not guaranteed that the approximate wavefunction produced using the UHF procedure will be an eigenfunction of the $\hat{S}^2$ operator. (This topic will be discussed in greater detail in Section 2.1.8.) Spin contamination problems can be

avoided by using the Restricted open shell Hartree Fock (ROHF) procedure. In the ROHF approach, doubly occupied molecular orbitals are restricted to be identical for both α and β spins, while the unpaired electrons are taken to reside in different orbitals.

In quantum chemistry calculations, the spatial wavefunctions that build up the Slater determinant wavefunction are typically molecular orbitals (MOs) generated from the linear combination of atomic orbitals (LCAO) procedure. That is,

$$\psi_j = \sum_j c_j \phi_j . \tag{2.18}$$

The functions used for the spatial wavefunctions are crucial for the accuracy and computational time required for the calculation of approximate wavefunctions, and will be discussed in greater detail in Section 2.1.4.

Finally, it is instructive to look at the expectation value of the electronic Hamiltonian calculated with Slater determinant wavefunction. We see that the terms $\hat{T}_e$ and $\hat{V}_{en}$ depend on only the coordinates of a single electron, and will be equal for all the electrons. These two terms are also present in the single electron case, and are generally lumped together under the designation h(1). The electron-electron interaction term is not present in the one electron case, and gives rise to interesting matrix elements. For a two electron Slater wavefunction,

$$\left\langle \chi_a(1)\chi_b(2) - \chi_a(2)\chi_b(1) \left| \frac{1}{r_{12}} \right| \chi_a(1)\chi_b(2) - \chi_a(2)\chi_b(1) \right\rangle =$$

$$\begin{aligned} \left\langle \chi_a(1)\chi_b(2) \left| \tfrac{1}{r_{12}} \right| \chi_a(1)\chi_b(2) \right\rangle &- \left\langle \chi_a(1)\chi_b(2) \left| \tfrac{1}{r_{12}} \right| \chi_a(2)\chi_b(1) \right\rangle - \\ \left\langle \chi_a(2)\chi_b(1) \left| \tfrac{1}{r_{12}} \right| \chi_a(1)\chi_b(2) \right\rangle &+ \left\langle \chi_a(2)\chi_b(1) \left| \tfrac{1}{r_{12}} \right| \chi_a(2)\chi_b(1) \right\rangle . \end{aligned} \tag{2.19}$$

An alternate notation for these integrals is

$$[aa|bb] - [ab|ba] - [ba|ab] + [bb|aa]. \tag{2.20}$$

The first and last integrals in 2.19 look like the charge density of electron 1 (2) in orbital χ_a (χ_b) interacting with the charge density of electron 2 (1) in orbital χ_b (χ_a) over the distance

r_{12}^{-1}. These resemble classical Coulombic interactions, hence these terms are referred to as Coulomb integrals. However, the second and third integrals arise from the antisymmetry of the wavefunction and have no classical interpretation. They look as though electron labels have been "exchanged" between the two orbitals, and are referred to as exchange integrals. Unlike the Coulomb terms where the charge density can be localized to specific areas of the molecule, the exchange terms cannot be localized. In Eq 2.20, the Coulomb terms have positive signs, adding to total energy, hence are "repulsive", as one expects for Coulombic interactions of two particles with the same charge. The exchange terms have negative signs in Equation 2.20, reducing the total energy, and thus are "attractive".

We also note that the Coulomb integrals are positive ("repulsive"), while the exchange integrals are negative ("attractive").

2.1.3 Optimization of the Approximate Wavefunction: The Hartree-Fock-Roothaan Procedure. Now that we have established a form for the Hartree-Fock trial wavefunction, we need to develop a systematic procedure to calculate the best single determinant wavefunction approximation to the right answer. The energy, the expectation value of the electronic Hamiltonian, is a functional of the spin (molecular) orbitals. Thus, functional minimization of energy subject to the constraint that the spin orbitals remain orthonormal will provide equations for the solution of the best approximate wavefunction. This procedure was performed by Hartree and Fock, and led to the canonical Hartree-Fock equations for the spin orbitals:

$$\hat{f}\,|\chi_i\rangle = \epsilon_i\,|\chi_i\rangle\,. \tag{2.21}$$

Here, $\hat{f}$ is the Fock operator, which is the electronic Hamiltonian operator represented in a Slater determinant wavefunction basis. This canonical Hartree Fock procedure results in a set of N coupled PDE's, which, as discussed earlier, cannot be efficiently solved by numerical integration.

In a seminal development, Roothaan [18] showed for the RHF case that by representing the Hartree Fock equations on an explicit set of spatial basis functions, one could obtain a set of algebraic equations that could be solved by straightforward matrix techniques. In this derivation, each pair of electrons is represented by a molecular orbital (spatial part

of the spin orbitals) that are built from linear combinations of atomic orbitals (LCAO). In the minimal basis set, each electron contributes one AO to the MO. Thus, the minimal basis set for molecular hydrogen is

$$\begin{aligned}
\psi_1(r_i) &= c_{11}\phi_a(r_i) + c_{21}\phi_b(r_i) && \text{Molecular Orbital 1} \\
\psi_2(r_i) &= c_{11}\phi_a(r_i) + c_{21}\phi_b(r_i) && \text{Molecular Orbital 2} \\
\Psi(r_1, r_2) &\approx \psi_1(r_1)\psi_2(r_1) - \psi_1(r_2)\psi_2(r_2) && \text{Antisymmetrized Wavefunction.}
\end{aligned} \tag{2.22}$$

Applying functional minimization to the expectation value of the energy, Roothaan obtained the following nonlinear matrix equation:

$$\overline{\overline{\mathbf{F}}}\left(\overline{\overline{\mathbf{C}}}\right)\overline{\overline{\mathbf{C}}} = \overline{\overline{\mathbf{S}}}\,\overline{\overline{\mathbf{C}}}\,\vec{\varepsilon}. \tag{2.23}$$

$\overline{\overline{\mathbf{F}}}$ is the matrix representation of the Fock Hamiltonian. $\overline{\overline{\mathbf{C}}}$ is the matrix of coefficients of the AO's. $\overline{\overline{\mathbf{S}}}$ is the overlap matrix of the AO's. Because the AO's are not centered on the same point in space, the overlap matrix is not the identity matrix and must be carried along in the solution. $\vec{\varepsilon}$ is the matrix of eigenvalues, which can be taken to be diagonal and treated as a vector without loss of generality. The dependence of the Fock matrix on the molecular orbitals introduces the nonlinearity in the problem.

Two factors complicate the solution of the Roothaan equation. The Roothaan equation is not in the canonical form of a matrix eigenvalue equation because the basis of AOs is not orthogonal. One must transform to an orthogonal basis, solve the resulting matrix eigenvalue equation, and then transform back to the original nonorthogonal basis. Second, $\overline{\overline{\mathbf{F}}}$ depends on $\overline{\overline{\mathbf{C}}}$, making the Roothaan equation nonlinear. Thus, one is forced to use an iterative method to obtain a solution.

Roothaan used the following procedure to solve Eq 2.23. First, one makes an initial guess at the coefficient matrix $\overline{\overline{\mathbf{C}}}_0$ (the electronic wavefunction) and calculates an initial value for $\overline{\overline{\mathbf{F}}}$. The problem is then transformed to an orthogonal basis. The resulting matrix equation is solved, producing the first approximation to the coefficients of the wavefunction $\overline{\overline{\mathbf{C}}}_1'$. This solution is transformed back to the original nonorthogonal basis and compared to $\overline{\overline{\mathbf{C}}}_0$. If $\overline{\overline{\mathbf{C}}}_0$ and $\overline{\overline{\mathbf{C}}}_1$ differ by more than some user-determined limit, a second iteration

is started using $\overline{\overline{\mathbf{C}}}_1$. This process is repeated until the difference between a solution $\overline{\overline{\mathbf{C}}}_n$ differs by less than the user-determined limit from the previous solution, $\overline{\overline{\mathbf{C}}}_{n-1}$. When this condition is satisfied, the solution is said to be self consistent, hence the origin of the name Self Consistent Field. Because the Roothaan equations are nonlinear, the simple iteration procedure described above is not guaranteed to converge [19]. Convergence problems are not unusual, but more sophisticated iteration schemes generally achieve convergence except when the initial geometry specification contains significant errors.

Pople and Nesbit subsequently extended Roothaan's work to the Unrestricted Hartree Fock (UHF) case, in which pairs of spin α and β electrons are not restricted to reside in the same spatial wavefunction [20]. In analogy with the RHF case, they obtained two coupled matrix eigenvalue problems

$$\begin{aligned} \overline{\overline{\mathbf{F}}}_\alpha \left(\overline{\overline{\mathbf{C}}}_\alpha, \overline{\overline{\mathbf{C}}}_\beta\right) \overline{\overline{\mathbf{C}}}_\alpha &= \overline{\overline{\mathbf{S}}}\, \overline{\overline{\mathbf{C}}}_\alpha\, \vec{\varepsilon}_\alpha \\ \overline{\overline{\mathbf{F}}}_\beta \left(\overline{\overline{\mathbf{C}}}_\alpha, \overline{\overline{\mathbf{C}}}_\beta\right) \overline{\overline{\mathbf{C}}}_\beta &= \overline{\overline{\mathbf{S}}}\, \overline{\overline{\mathbf{C}}}_\beta\, \vec{\varepsilon}_\beta . \end{aligned} \tag{2.24}$$

These matrix equations can be solved independently at each step in the iterative process, though they are coupled through the formation of the Fock matrices. The UHF procedure may be used for closed and open shell systems. The Restricted Open shell Hartree Fock procedure (ROHF) avoids the spin contamination problem of the UHF approach by restricting doubly occupied molecular orbitals to be identical for both α and β spins, while the unpaired electrons are taken to reside in different orbitals.

The HF-SCF procedure produces a set of eigenvalues and eigenvectors of a matrix equation. The eigenvalues are the orbital energies; the eigenfunctions are the molecular orbitals that minimize the energy. For a closed shell system, a single determinant wavefunction is invariant to an arbitrary unitary transform (of the coefficient matrix). Thus, the spin orbitals that make the total energy stationary are not unique, and no particular physical significance can be given to a set of spin orbitals. However, a specific set of spin orbitals may have properties that make them preferred. The spin orbitals defined in the energy eigenbasis of the Hamiltonian produce a diagonal set of orbital energies and will form a basis for an irreducible representation of the point group of the molecule. Having *a*

priori knowledge about the symmetry of the solution can enable one to use this symmetry to simplify the calculation. One can use a criterion such as minimization of the exchange interaction between spin orbitals to transform to a set of "localized" spin orbitals which better match the qualitative interpretation of chemical bonding [21].

2.1.4 Basis Functions and Matrix Elements. The choice of spatial basis functions for use in the HF-SCF procedure is driven by several sometimes conflicting considerations: accuracy of the answer (energy, geometry), ease of calculating the matrix elements, and the desire for a clear physical interpretation. Building on the qualitative linear combination of atomic orbitals molecular orbital (LCAO-MO) picture of molecular electronic structure, the logical first choice for HF-SCF basis functions was hydrogen atom wavefunctions. The hydrogen atom electronic wavefunctions are of the form

$$\Phi(r,\theta,\phi) = R_{nl}(r)Y_{lm}(\theta,\phi). \tag{2.25}$$

The radial dependence is given by

$$\mathrm{R}_{n\ell}(r) = -2\left(\frac{Z}{na_0}\right)^{\frac{3}{2}}\sqrt{\frac{(n-\ell-1)!}{n((n+\ell))^3!}}\left(\frac{2Zr}{na_0}\right)^{\ell} Exp\left[-\frac{Zr}{na_0}\right] L_{n+\ell}^{2\ell+1}\left(\frac{2Zr}{na_0}\right), \tag{2.26}$$

where $L_{n+\ell}^{2\ell+1}\left(\frac{2Zr}{na_0}\right)$ are the associated Laguerre polynomials and the angular dependence is given by $Y_{lm}(\theta,\phi)$, the spherical harmonics [22]. Three-dimensional plots of these functions can be found in almost all texts on quantum mechanics.

The complicated form of the associated Laguerre polynomials gives rise to the familiar radial nodes in electron density in the hydrogen atom. This complicated form is difficult to integrate in matrix element calculations. Slater proposed a much simpler analytic form for the radial part of the wavefunction:

$$R_{n\ell}(r) = (2\zeta)^{n+\frac{1}{2}}[(2n)!]^{-\frac{1}{2}}r^{n-1}Exp[-\zeta r]. \tag{2.27}$$

The orbital exponent ζ is given by

$$\zeta = \frac{Z-s}{n^*}. \tag{2.28}$$

Here, s is a screening constant and n^* is an effective quantum number. Slater also developed some empirical rules for choosing s and n^* for different elements. Optimized values for orbital exponents in Slater functions currently in use have been obtained by numerical fits of HF-SCF on atoms calculations to experimental data. These optimized parameters do not differ greatly from those obtained using Slater's rules.

An important feature of the Slater radial functions is that with their simpler dependence on r, they do not produce radial nodes in the electron density. This lack of radial nodes has two consequences. First, Slater functions centered on the same origin are not orthogonal. This is not a problem since a molecular HF-SCF calculation necessarily involves nonorthogonal sets of functions because each set is centered on a different point in space, i.e., the various nuclei in the molecule. One can construct an orthogonal set of single-center Slater functions using the Gramm-Schmidt process, for example. However, this doesn't eliminate the need to orthogonalize the atomic basis in order to solve the Roothaan equations, and thus offers no computational advantage.

A more important concern about the lack of radial nodes is its poor physical description of electronic behavior. This is very important in an HF-SCF calculation on an atom. However, molecular behavior has been found to be predominantly driven by the atoms' outer-shell electrons, whose electron density is modeled well by a decaying exponential. The poor description of electron density near the nuclei has been found in general to have a minor effect in calculations of molecular behavior, though this effect is larger in calculations involving light elements. This poor description of the electronic behavior in the vicinity of the nuclei also produces large errors in the prediction of properties such as nuclear magnetic resonance (NMR) coupling constants and electron spin resonance (ESR) hyperfine constants [19].

Slater functions have been shown to work well in HF-SCF calculations. That is, to obtain given level of required accuracy, fewer Slater functions can be used than other types of functions. Unfortunately, the good physical description of atomic electron density provided by Slater functions is overwhelmed by the computational difficulty of evaluating matrix elements using Slater functions. This is easily illustrated by looking at an electron-electron matrix element between electrons centered on two different atoms, A and B.

Neglecting the angular part, we have

$$\langle A|B\rangle = \int d\vec{r}_1 Exp[-\alpha|\vec{r}_1 - \vec{R}_A|] \times Exp[-\alpha|\vec{r}_1 - \vec{R}_B|]. \tag{2.29}$$

Evaluation of this integral is difficult and computationally expensive because the two exponentials are not centered at the same point in space. Boys [23] introduced the use of Gaussian functions to address the computational difficulties involved with integrating products of Slater functions. Products of Gaussian functions possess a very useful property:

$$Exp[-\alpha|\vec{r}_1 - \vec{R}_A|^2] \times Exp[-\beta|\vec{r}_1 - \vec{R}_B|^2] = KxExp[-p|\vec{r}_1 - \vec{R}_B|^2], \tag{2.30}$$

where

$$\begin{aligned} p &= \alpha + \beta \\ K &= Exp[-\tfrac{\alpha\beta}{\alpha+\beta}|\vec{R}_A - \vec{R}_B|^2] \\ \vec{R}_p &= \tfrac{\alpha\vec{R}_A + \beta\vec{R}_B}{\alpha+\beta}. \end{aligned} \tag{2.31}$$

Here we see that the product two Gaussians centered on different points is a third Gaussian centered at a single point in space, which can be integrated very rapidly. Gaussians might be a very efficient choice for basis functions.

Unfortunately, Gaussians do not model electronic behavior nearly as well as an exponential. Compared with the exact solution for electron density of atomic hydrogen as a function of distance from the nucleus, a Gaussian description of falls off much too rapidly as a function of distance (R) from the nucleus, and the spatial derivative of a Gaussian is non-zero at $R = 0$, while the exact solution has a derivative equal to zero at $R = 0$. Pople et al. [24] suggested a very useful alternative, representing a Slater function with an expansion of Gaussian functions. Pople and others have found that one needs approximately three times as many Gaussian Type Orbitals (GTOs) than STOs to obtain the same level of accuracy, increasing the size (memory requirements) of the calculation. However, the computation time using the larger number of Gaussians is more than an order of magnitude faster than the smaller calculation using exponentials. With the exception of periodic crystal calculations that use Bloch orbitals, nearly all contemporary computational chemistry codes use Gaussians, with a small minority using pure STOs.

A specific vocabulary has evolved to describe the various types of basis set expansion commonly in use. A minimal basis set (MBS) contains only as many orbitals as are needed to accommodate the electrons of the neutral atom. Thus, the minimal basis set description of both oxygen (8 electrons) and carbon (6 electrons) contains 5 basis functions since oxygen and carbon are both second row elements. The MBS for each contains terms for 1s, 2s, $2p_x$, $2p_y$, and $2p_z$ atomic orbitals. The differences between oxygen and carbon are reflected in the parameters used in these atomic orbitals. A typical MBS using a Gaussian fit to a Slater Type Orbital (STO) is termed a STO-nG basis set, where n is the number of Gaussians used to approximate the Slater function. While an MBS calculation yields energies significantly above the HF limit, an MBS result maps directly to qualitative LCAO descriptions commonly used in chemistry and thus can be readily interpreted.

One reason why an MBS calculation provides poor results is that an MBS description does not have the capability to expand or contract the orbital in response to different bonding environments. One solution to this problem is to use a *split-valence* or *double* ζ (DZ) basis set. In these basis sets, the atomic orbitals are split into two parts: an inner, compact orbital and an outer, more diffuse orbital. The coefficients of these two types of orbitals can be varied independently in the SCF procedure. Thus, the radial extent of the atomic orbital that contributes to the molecular orbital can be varied within the limits set by the inner and outer basis functions. A split valence basis set only splits the valence orbitals this way, while a DZ basis set also splits the core atomic orbitals. The *triple* ζ (TZ) splits each orbital into three pieces [25].

The effect of core electrons in molecular electronic structure is minimal in most situations, so split valence basis sets are used more often than DZ or TZ basis sets. A popular family of split valence basis sets is the 6-31G basis set, which uses a 6 term Gaussian expansion to represent the core electrons three Gaussians for the inner valence electrons, and a single Gaussian for the outer valence electrons. The 6-31G* (6-31G(d)) adds a spatial function that resembles an atomic hydrogen d orbital on valence electrons of second and third row elements. The 6-31G** (6-31G(d,p)) also adds p type orbitals on the valence electrons of hydrogen atoms. The additional orbitals in these basis sets are referred to as polarization functions [26].

Basis sets used in commercial computational chemistry codes are a compendium of the work of a large number of researchers who have generated optimized basis sets for almost every element in the periodic table. A comprehensive reference of optimized basis sets can in the manual of a "production" computational chemistry code such as Gaussian92 [5] or GAMESS [9]. Variations of the 6-31G(d) basis set are generally considered the minimum needed for reliable accuracy in geometry optimization.

While the accuracy of the answer of an HF-SCF calculation improves with increasing basis set size, the computational cost increases even faster. The computational cost of an HF-SCF calculation scales roughly as n^4, where n is the total number of basis functions in the molecule. The total energy asymptotically approaches the Hartree-Fock limit as the number of basis functions increases.

2.1.5 A Simple HF-SCF Example: H_2 . As a concrete example, here are some illustrative results (in atomic units) for a minimal STO-3G basis set RHF calculation for molecular hydrogen. These values are calculated at a fixed internuclear separation of 1.4206 atomic units.

$$\begin{array}{ccccc} \text{One Electron Terms} & & \text{Two Electron Terms} & & \text{Initial Guess of Coefficients} \\ \left(\begin{vmatrix} -1.1139 & -0.954 \\ -0.9546 & -1.113 \end{vmatrix} \right. & + & \left. \begin{vmatrix} 0.7541 & 0.3571 \\ 0.3571 & 0.7541 \end{vmatrix} \right) & \times & \begin{vmatrix} c_{11}^0 & c_{12}^0 \\ c_{21}^0 & c_{22}^0 \end{vmatrix} = \\ \begin{vmatrix} 1.0 & 0.6522 \\ 0.6522 & 1.0 \end{vmatrix} & \times & \begin{vmatrix} c_{11}^0 & c_{12}^0 \\ c_{21}^0 & c_{22}^0 \end{vmatrix} & \times & \begin{vmatrix} \varepsilon_1 \\ \varepsilon_1 \end{vmatrix} \\ \text{Overlap Matrix} & & \text{Initial Guess of Coefficients} & & \text{Energy Eigenvalues} \end{array} \tag{2.32}$$

The eigenvectors of the one electron terms are often used as the initial guess of the coefficients. A different initial guess will converge to the same result with a simple iteration scheme for this problem.

An HF-SCF calculation gives the following results for H_2:

$$\begin{array}{lrr} & MO_1 & MO_2 \\ AO_a & 0.7071 & 0.7071 \\ AO_b & 0.7071 & -0.7071 \\ \text{Orbital} & -0.5737 & 0.6591 \\ \text{Energy} & & \end{array} \tag{2.33}$$

These results are consistent with what one expects. There are two molecular orbitals, one bonding (negative energy) and one antibonding (positive energy). The lower energy MO has two positive coefficients in its approximate wavefunction, thus has no nodes in the electron density (square of the wave function). The higher energy MO has one positive and one negative coefficient, thus has one node in its electron density. Since we are using the RHF approximation, one spin alpha and one spin beta electron would fill the bonding MO. The total energy of the configuration, electronic energy plus nuclear repulsion, is -1.116 Hartrees. The dissociation energy, the difference between the total energy of the H_2 molecule and two separated H atoms, is predicted to be 3.155 eV, roughly a 33% error from the experimental value of 4.74 eV.

2.1.6 Effects of Electron Correlation: The Hartree Fock Limit. Seeking the solution to a PDE as a product of single variable functions is only correct when the PD operator does not couple any of the variables. When one seeks a solution to the molecular Schrödinger equation in the form of a Hartree-Fock product wavefunction, the wavefunction does not account for the fact that the motion of the electrons is coupled, although the electrons are coupled in the Hamiltonian. The Born-Oppeinheimer approximation is based on the fact that the mass of an electron is so much smaller than the mass of a nucleus to say that nuclear and electronic motion is independent, i.e., that nuclear and electronic motions are uncorrelated. There is no similar physical justification for decoupling the motion of one electron from another. One expects electron-electron motion to be highly correlated. Thus, the Born-Oppeinheimer approximation is a much better approximation than the Hartree-Fock approximation.

There are three factors involved in correlation of electron motion within a molecule. First, there is Coulomb repulsion, $\frac{1}{ij}$, which becomes infinite when r_{ij} is zero, which makes

it energetically unfavorable for two electrons to be close to each other. A two-electron density function is always smaller in regions where the electrons are close to each other than corresponding density from two one-electron density functions. A second source of correlation effects is associated with the Pauli principle. In a single determinant wavefunction, interactions between electrons of different spin are smaller since that is a Coulombic but not an exchange interaction between electrons that have different spins. A correlated description of the motion of two electrons keeps their time-averaged separation from becoming too close. The third factor which influences electron correlation is the spatial symmetry of the molecule.

The effect of electron correlation is primarily described in terms of energy. One of the most widely used definitions of the correlation energy is given by Löwden [27]:

> *The correlation energy for a certain state with respect to a specified Hamiltonian is the difference between the exact eigenvalue of the Hamiltonian and its expectation value in the Hartree-Fock approximation for the state under consideration.*

An HF-SCF answer improves (becomes lower in energy) as one increases the size of the basis set, and converges to a limit. The limit to which the HF-SCF procedure converges is known as the Hartree-Fock limit. The correlation energy at equilibrium is typically 20-30% of the dissociation energy, i.e., correlation errors are large. Correlation error often increases with increasing internuclear separation. Thus, the use of the uncorrelated electronic wavefunction in the HF-SCF model will produce larger errors for chemical reactions that involve bond making and breaking than the calculation of equilibrium properties. HF-SCF will be quantitatively wrong for the simulation of chemical reactions, and may also predict qualitatively wrong behavior.

In spite of the limitations of the HF-SCF procedure, there are a number of reasons why HF-SCF is so widely used. Historically, molecular problems were investigated before the advent of digital computers, and the Hartree Fock approximation was the only computationally tractable model available. Because HF-SCF calculations have been performed for a long time, they're limitations are well understood, so one can judge whether an unexpected result was caused by a limitation in the calculation or a new physical mech-

anism. On current computers, a wide range of problems can be solved relatively quickly, so within the limitations of HF-SCF, qualitative behavior can be mapped out before turning to more accurate and computationally intensive methods. Failures of this approximation provide guidance on what kinds of improvements are needed to improve the accuracy of the calculations. (Bond breaking is one important process for which HF-SCF description is inadequate.) Finally, the single term wavefunction often provides a good starting point for methods that can go beyond the Hartree-Fock limit.

2.1.7 Beyond the Hartree-Fock Limit.

2.1.7.1 Configuration Interaction. As discussed earlier, a function of more than one variable can be expressed exactly as an infinite series of products of single variable functions. The Hartree-Fock optimized wavefunction is the best leading term in the exact infinite series expansion of this the multi-electron wavefunction (to the accuracy of the basis set used). An obvious method to improve on this approximation would be to include more terms in the series. This method is called configuration interaction (CI).

A CI calculation essentially consists of representing the molecular Hamiltonian on a basis of a set of Slater determinant spin orbitals (configurations) and diagonalizing the resulting matrix. The lowest energy eigenvalue is the approximate ground state energy. The lowest energy eigenvector provides the coefficients for the series expansion of the ground state wavefunction in terms of the Slater determinant spin orbital basis. In CI, correlation of electron motion is accounted for by including configurations in the basis set that possess different spatial distributions to enable the electrons to find ways to stay away from each other as needed to reduce the energy. The Hartree-Fock approximation only provides the electrons with a single configuration.

The price paid for recovering the correlation energy is a greatly increased computational cost. In a minimal basis set, for N electrons one has a total of 2N spin orbitals. From these spin orbitals, one can create $\binom{2N}{N}$ unique determinant wavefunctions. For H_2, one can create 6 unique determinants. For H_2O with 8 valence electrons, the number of unique determinants grows to 12,870. In practice, one can use symmetry arguments and

other tricks to arrange the eigenbasis so that the matrix representation of the Hamiltonian pops out in block form; however, almost always, one must truncate a CI expansion.

One needs to obtain set of spin orbitals before setting up a CI expansion. A common way to obtain a reasonable set of spin orbitals is to first perform an HF-SCF calculation. However, the spatially delocalized, energy eigenbasis MOs produced by the HF-SCF procedure have proven to give poor convergence behavior in CI. The set of natural orbitals, introduced by Löwdin, performs better in CI calculations (fewer configurations required for the same level of accuracy) than HF-SCF orbitals; however, the solution for the CI wavefunction is required before natural orbitals can be calculated [28]. Various schemes for obtaining approximate natural orbitals that can be used in CI calculations have been developed [29].

To summarize, in HF-SCF one uses a single determinant wavefunction to approximate the ground state wavefunction, but optimizes the orbitals that construct the wavefunction to minimize the energy. In CI, one uses many single determinant wavefunctions to approximate the ground state wavefunction, but optimizes the coefficients of each single determinant wavefunction to minimize the energy. An alternate, hybrid approach, the multi configuration self consistent field (MCSCF) procedure, has also been developed. In MCSCF, a number of single determinant wavefunctions are used in a series expansion of the ground state wavefunction; however, both the coefficients of these terms as well as the orbitals that construct the determinant wavefunctions are optimized.

2.1.7.2 Generalized Valence Bond. The Generalized Valence Bond (GVB) wavefunction developed by Goddard et al. can be regarded as a special form of an MCSCF wavefunction [30, 31]. GVB is the simplest method that correctly models the configuration of diradicals. Since diradicals arise in the surface models considered in this research, and GVB calculations are performed, a brief description of the GVB method is presented here.

As its name suggests, GVB is an extension of the Valence Bond (VB) concept of Heitler and London. Again, the concept is most clearly demonstrated for the simple case

of H_2. For H_2, the VB spatial wavefunction (neglecting normalization) is

$$\psi^{VB}(1,2) = \phi_a(1)\phi_b(2) + \phi_a(2)\phi_b(1), \tag{2.34}$$

where ϕ_a, ϕ_a are AOs centered on nuclei a and b. The total VB wavefunction is

$$\Psi^{VB}(1,2) = \psi^{VB}(1,2)\left[\alpha(1)\beta(2) - \beta(1)\alpha(2)\right]. \tag{2.35}$$

In both terms of the RHS of Equation 2.34, one electron is centered on each nuclei, i.e., the electrons are equally shared in the VB wavefunction. This corresponds to the concept of a covalent bond. The VB wavefunction is exact for infinite internuclear separation, but only approximate for finite separations. The errors in calculated equilibrium bond lengths and bonding energies are too large for quantitative purposes.

Recalling the minimal basis set RHF solution for H_2 (Equation 2.33), we obtained two spatial MOs (neglecting normalization)

$$\begin{aligned} \psi_1(r_i) &= \phi_a(r_i) + \phi_b(r_i) \\ \psi_2(r_i) &= \phi_a(r_i) - \phi_b(r_i). \end{aligned} \tag{2.36}$$

Since each MO can hold 2 electrons in the RHF model, only $\psi_1()$ is occupied. The Hartree-Fock wavefunction is

$$\Psi^{HF}(1,2) = \psi_1(1)\psi_1(2)\left[\alpha(1)\beta(2) - \beta(1)\alpha(2)\right]. \tag{2.37}$$

The spatial part of the HF wavefunction is

$$\begin{aligned} \Psi_s^{HF}(1,2) &= \psi_1(1)\psi_1(2) = \left[\phi_a(1) + \phi_b(1)\right]\left[\phi_a(2) + \phi_b(2)\right] \\ &= \left[\phi_a(1)\phi_b(2) + \phi_a(2)\phi_b(1)\right] + \left[\phi_a(1)\phi_a(2) + \phi_b(1)\phi_b(2)\right] \\ &= \psi_{Covalent} + \psi_{Ionic} \end{aligned} \tag{2.38}$$

We see the HF wavefunction includes the covalent term found in the VB wavefuction, but adds a new term. Since this new term has both electrons simultaneously residing on either

nuclei a or b, it corresponds to an ionic description. *The HF description forces an equal amount of covalent and ionic character into the wavefunction.*

In the case of strong bonding (equilibrium internuclear separation for H_2), the overlap between ϕ_a and ϕ_b is large, the value of 0.65 seen in the off-diagonal terms in the overlap matrix in Equation 2.32. This leads to an overlap between the normalized $\phi_{Covalent}$ and ϕ_{Ionic} of $\frac{2S}{1+s^2} = 0.91$. For this case, the restriction of fixed ratio between $\phi_{Covalent}$ and ϕ_{Ionic} is not of major importance. However, for small overlaps, the restriction of a fixed ratio can cause severe problems. Small overlaps occur as bonds are broken, and in other systems that have weakly overlapping orbitals, such as diradicals.

The GVB wavefunction for H_2 is of the form

$$\Psi^{GVB}(1,2) = \left[\tilde{\phi}_a(1)\tilde{\phi}_a(2) + \tilde{\phi}_b(1)\tilde{\phi}_b(2)\right] \tag{2.39}$$

where

$$\begin{aligned} \tilde{\phi}_a &= \phi_a + \lambda\phi_b \\ \tilde{\phi}_b &= \lambda\phi_a + \phi_b. \end{aligned} \tag{2.40}$$

The coefficient λ is determined from optimization of the energy. Substituting Equation 2.40 into Equation 2.39, we obtain

$$\Psi^{GVB} = (1+\lambda^2)\psi_{Covalent} + 2\lambda\psi_{Ionic}. \tag{2.41}$$

Thus, in GVB, the ratio of covalent to ionic character of the wavefuntion is determined from energy optimization. For cases of small overlap, the optimum value of λ is very small, leading to a simple VB wavefunction. For cases with large overlap, $\lambda \approx 0.1$, and both terms are important.

An alternate form of the GVB wavefunction may be obtained by using MOs instead of AOs in Equation 2.39. The resulting GVB wavefunction expressed in MOs is

$$\Psi^{GVB}(1,2) = c_1\psi_1(1)\psi_2(2) + c_2\psi_1(1)\psi_2(2). \tag{2.42}$$

In molecular orbital language ψ_2, the unoccupied orbital, enables correlation between the electrons in the occupied orbital. This result emphasizes a fundamental limitation of the HF wavefunction. One can obtain a better energy, hence better approximation to the total wavefunction, by including an MO that HF theory says is unoccupied! For the case in which a single pair of (orthogonal) MOs is used, the GVB and MCSCF wavefunctions are identical.

Evaluation of the total energy of the GVB wavefunction and application of the variational principle to obtain the optimum GVB orbitals leads to a set of equations very similar to the HF equations except there is now a separate equation for each GVB MO.

For a multi-electron system, the GVB wavefunction can be obtained from HF by replacing each electron pair

$$\psi_i(2i-1)\psi_i(2i) \tag{2.43}$$

of the HF wavefunction with the electron pair

$$\psi_{ia}(2i-1)\psi_{ib}(2i) + \psi_{ib}(2i-1)\psi_{ia}(2i) \tag{2.44}$$

resulting in a product wavefunction of the form

$$(\psi_{1a}\psi_{1b} + \psi_{1b}\psi_{1a})(\psi_{2a}\psi_{2b} + \psi_{2b}\psi_{2a})...(\psi_{Na}\psi_{Nb} + \psi_{Nb}\psi_{Na}). \tag{2.45}$$

The total wavefunction, obtained antisymmetric combinations of Equation 2.41 and spin, is composed of a large number of Slater determinants.

In many situations, one is interested in a correlated description of only a single bond in a molecule. In cases like this, the total wavefunction consists of two Slater determinants: a small one for the pair of GVB orbitals, and a large one for the rest of the molecule. I.e., many GVB calculations look like RHF calculations plus a little bit more. Because of this, the computational cost of GVB calculations scales as n^4. GVB calculations are useful because one can recover a a good chunk of the correlation energy for a relatively low (compared to other methods that include correlation) computational cost.

2.1.7.3 Perturbation Expansion of the Correlation Energy. Perturbation theory is commonly used in quantum mechanics to obtain solutions to problems which do not have exact (in a finite number of terms) solutions. The Hamiltonian is partitioned into two pieces: a zeroth-order part which has known eigenvalues and functions and a perturbation term.

$$\hat{\mathcal{H}} = \hat{\mathcal{H}}_0 + \hat{\mathcal{V}} \tag{2.46}$$

One can derive a power series expansion for the perturbation term. In order to obtain the first-order correction to the energy (eigenfunction), one needs the zeroth-order wavefunction (eigenfunction). By definition, the perturbation must be smaller than the zeroth order term in the Hamiltonian. The smaller the size of the perturbation compared to the zeroth order term, the fewer terms will be needed in the series expansion to obtain a desired level of accuracy.

The perturbation approach described above is known as Rayleigh-Schrödinger Perturbation Theory [32]. A perturbation approach seems ideal for HF-SCF since the electronic Hamiltonian, Eq. 2.10, naturally partitions itself into a one-electron piece with exact eigenfunctions and eigenvalues and the two-electron piece that causes all the trouble. Unfortunately, the two-electron energy is not small compared to the one electron energy, so a perturbation expansion of the two-electron energy is inappropriate. However, the correlation energy is small compared to the Hartree-Fock energy, so we can devise a perturbation expansion in terms of the correlation energy.

First, we partition the electronic Hamiltonian as in Eq. 2.46. Here, $\hat{\mathcal{H}}_0$ is the Hartree Fock Hamiltonian,

$$\hat{\mathcal{H}}_0 = \sum_i \left[h(i) + v^{\mathrm{HF}}(i)\right], \tag{2.47}$$

where $v^{\mathrm{HF}}(i)$ is the sum of the Coulomb and Exchange terms, and

$$\hat{\mathcal{V}} = \sum_{i<j} r_{ij}^{-}1 - \sum_i v^{\mathrm{HF}}(i). \tag{2.48}$$

The perturbation term is the difference between the Hartree-Fock representation for the two electron interactions and the exact representation of the two electron interactions. The

use of this partitioning of the Hamiltonian and the Rayleigh Schrödinger perturbation expansion is known as Moeller-Plesset Perturbation Theory [19, 33]. Using this partitioning, one can show that the factor of $\frac{1}{2}$ added to the two electron terms in the Hartree-Fock Hamiltonian to avoid double counting of electron-electron interactions is actually the first order correction to the energy. Moeller-Plesset (MP) perturbation corrections for the correlation energy start at second order, MP2.

MP2 and MP4 perturbation expansions are available in many commercial computational chemistry codes. Perturbation approaches provide comparable recovery of the correlation energy for a lower computational cost than a CI calculation. However, it is important to note that perturbation expansion techniques operate on single configuration wavefunctions. Thus, a CI (MCSCF) calculation may be required in situations (dissociation) poorly described by single configuration wavefunctions.

2.1.8 Optimized Approximate Wavefunctions: Metrics and Accuracy.

2.1.8.1 Metrics. The HF-SCF procedure produces an optimized, approximate electronic wavefunction. However, the wavefunction itself is not a directly observable entity, so we must judge the quality of the result of the HF-SCF by comparing predicted observable properties (expectation values of Hermitian operators on the approximate wavefunction) with experimental results. Useful metrics are the total energy, the geometry, the spin eigenvalue, and the virial of the wavefunction. These parameters are not all equally sensitive to small changes in the wavefunction.

The variational approach used to derive the HF-SCF procedure guarantees that the expectation value of the energy of the approximate wavefunction will monotonically approach the true ground state energy from above as a limiting value. Thus, if you have two approximate HF-SCF wavefunctions, the one that has the lower energy is a better approximation to the true ground state wavefunction. The energy is sensitive to small variations of the wavefunction, and is the primary metric of the approximate wavefunction. Comparisons with experiment are not always as straightforward because experiments measure energy differences rather than absolute energies. The dissociation energy of H_2 is

defined as the difference in energy between the molecule and two separated H atoms. The STO-3G calculated dissociation energy of H_2 is 5.0 eV, greater than the experimental value of 4.74 eV. This is primarily a reflection of the problems with the accuracy of a STO-3G calculation on the H atom, as is seen below:

H atom STO 3		H_2 STO-3G		
$2 \times (-12.690)$	$-$	30.399	$=$	5.019 eV
H atom Exact		H_2 STO-3G		
$2 \times (-13.607)$	$-$	30.399	$=$	3.185 eV.

The calculated geometry of a molecule, bond lengths, bond angles, etc is often used as a metric of the approximate wavefunction. However, these properties are not very sensitive to small changes in the wavefunction.

We know from quantum mechanics that the $\hat{S}^2$ operator has exact eigenvalues when operating on the electronic wavefunction. A RHF calculation places pairs of opposite spin electrons in the same spatial molecular orbital, so the spin exactly cancels out and the spin eigenvalue is exactly zero. A UHF calculation places each electron into a different spatial orbital. This added flexibility means that while a UHF calculation will in general produce a lower energy than an RHF calculation on the same molecule, it is not guaranteed to produce an exact spin eigenvalue. This phenomenon is called spin contamination. A UHF answer with a good energy value but with a spin eigenvalue significantly different from the correct value is most likely a poorer approximation than a slightly higher energy answer with smaller spin contamination. Pulay [25] recommends that a result with spin contamination less than 10% greater than the exact value for $\left\langle \hat{S}^2 \right\rangle$ can be considered reliable.

One can show that the minimum energy solution for the electronic wavefunction satisfies the virial theorem [34], i.e.,

$$\left\langle \Psi\left(\vec{r}_1, \vec{r}_2, ..., \vec{r}_N\right) \middle| \hat{T} \middle| \Psi\left(\vec{r}_1, \vec{r}_2, ..., \vec{r}_N\right) \right\rangle = -\frac{1}{2} \left\langle \Psi\left(\vec{r}_1, \vec{r}_2, ..., \vec{r}_N\right) \middle| \hat{V} \middle| \Psi\left(\vec{r}_1, \vec{r}_2, ..., \vec{r}_N\right) \right\rangle . \tag{2.49}$$

The virial theorem provides another check on the approximate answer. Large deviations from a virial ratio, $-\frac{\langle V \rangle}{\langle T \rangle}$ of 2 indicate problems with the results. Figure 2.2 shows the

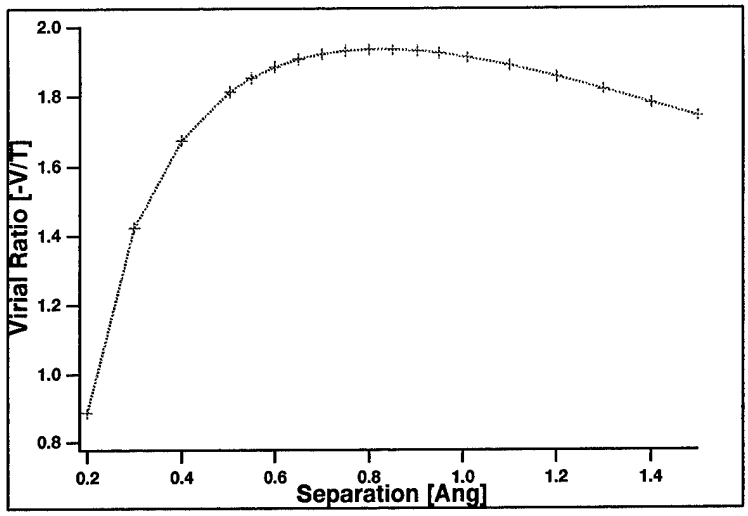

Figure 2.2 H_2 STO-3G Virial Ratio

values of the virial ration for H_2 for a range of separations. (The energy components of these calculations were shown in Figure 2.1.) The STO-3G optimized wavefunction gives a virial ratio of 1.9247, while the 6-31G optimized wavefunctions result in a virial ratio of 1.9925.

2.1.8.2 Accuracy: Equilibrium Properties. The issue of accuracy in an HF-SCF calculation is complicated because all the molecular properties are not equally sensitive to changes in the electronic wavefunction. Compounding the issue is the fact that HF-SCF accuracy is a function of internuclear separation; the accuracy of an HF-SCF result degrades as one moves away from the equilibrium configuration. Table 2.1 shows the calculated total energies for H_2 with several basis sets. The percentage change of the total energy from STO-3G to the Hartree-Fock limit is only 1.5%. However, the predicted dissociation energy changes by 13%. The bond length is seen to change by 3% for this range of basis sets.

This simple example illustrates a fundamental challenge in computational chemistry: the observable properties of interest must be calculated from small differences of very large quantities. Improvements in these small differences are not proportional to improvements in the quantities you can calculate.

Basis Set	Energy (eV)	Bond Length (Ang)
STO-3G	−30.398	0.7122
4-31G	−30.671	0.7303
6-31G**	−30.780	0.7329
HF Limit	−30.862[35]	
Experiment	−31.94	0.7414

Table 2.1 H_2 Total Energy and Equilibrium Bond Lengths

Typical accuracies that can be achieved in HF-SCF plus correlation correction calculations are listed below. Is this accuracy good or bad? It depends on what kind of data one

Parameter	Accuracy Limit
Bond Length	0.01 − 0.02 Angstroms
Bond Angle	1 − 2 Degrees
Reaction Barrier	10 $\frac{kcal}{mole}$

Table 2.2 Computational Accuracy Limits

is comparing. For spectroscopy, where one can measure energy differences down to parts per billion, this accuracy is atrocious. For a materials science, where the primary interest is in ground state geometries, this level of accuracy good enough for almost all cases. For chemistry, where one is attempting to explain a reaction mechanism, this accuracy is good enough most of the time. However, some pathological reactions, like $F + H_2 \rightarrow HF + H$ have reaction barriers approximately equal to the ultimate uncertainty of the best calculations. For reactions such as these, it's very difficult to obtain reliable theoretical estimates of reaction rates.

2.1.8.3 Dissociation Limit. Most electronic structure calculations are concerned with finding equilibrium molecular properties such as structures and energies. However, to model chemical reactions, one also needs to insure that the wavefunction used to describe the equilibrium behavior of the molecule also has the correct dissociation limits. This issue is commonly illustrated by the example of the H_2 molecule. At the minimum energy equilibrium separation, we know from spectroscopic measurements that H_2 is a pure singlet state. In order to insure the correct solution, the ground state of H_2 must be described using the RHF approximation. Unfortunately, the RHF approximation forces both

electrons into the same spatial orbital, so that if one increases the internuclear separation to beyond the dissociation limit and calculates the minimum energy solution, one finds that the predicted dissociation limit is $H^- + H^+$, clearly at odds with the correct limit of 2 neutral hydrogen atoms. Using the UHF approximation corrects this discrepancy in the dissociation limit. Unfortunately, the ground state of H_2 in the UHF approximation is no longer a pure singlet. Thus a single configuration cannot adequately describe the behavior of H_2 over the full range of internuclear separations. Only a multi-configuration approach can correctly describe this behavior.

A simple way to correct this problem is to describe H_2 using two configurations, a pure singlet for the ground state, and two separated hydrogen atoms to match the dissociation limit, with adjustable coefficients. At equilibrium, the coefficient of the separated hydrogen atom configuration is zero. At the dissociation limit, the coefficient of the singlet configuration is zero. At intermediate separations, the coefficients vary to provide the minimum energy solution.

2.2 Other Computational Approaches

2.2.1 Semi-Empirical HF-SCF. Semi-empirical (SE) HF-SCF techniques originated in the 1960's when it became obvious that *ab initio* HF-SCF techniques would be impractical for the study of large polyatomic systems with the computers available at that time. SE techniques derive their name from the fact that they are based on a Hamiltonian operator-electronic wavefunction (quantum mechanical) framework. However, unlike *ab initio* techniques which calculate all the matrix elements in the representation of the electronic Hamiltonian, SE techniques make extensive use of approximations to these terms avoiding the time consuming integrations involved. The use of experimental (empirical) data to determine the parameters in these approximations results in chemically useful accuracy, in significantly (orders of magnitude) less time than a corresponding *ab initio* calculation. However, as more terms are added to the approximation to improve the agreement of the calculated answer with the experimental result, the physical meaning of each term becomes more poorly defined and the SE technique may become more of a curve fit than a physical model.

As SE techniques have evolved, more and more variable parameters have been included in the approximate Hamiltonian to correct deficiencies identified with previous techniques. The underlying source of error is the incomplete functional approximations of the (crucial) neglected two electron matrix elements, referred to as differential overlap integrals. For example, the approximations made in Complete Neglect of Differential Overlap (CNDO) [36, 37] did not balance electron-nuclei attraction and electron-electron repulsion, which led to the spurious result that two neutral atoms several angstroms apart would still be attracted to each other. This deficiency was corrected in CNDO/2 by adding a parameter to reduce electron-nuclei attraction. This correction had the unfortunate side effect of making the interaction between two hydrogen atoms in molecular hydrogen repulsive at all distances, but was retained because of its improvement on the majority of data in the parameterization set. Overall, CNDO left out too many matrix elements to give good results for many molecules of interest, so Intermediate NDO (INDO), in which fewer two electron integrals were set to zero, followed [38]. Neglect of Diatomic DI (NDDO)[36] neglected the differential overlap only for atomic orbitals on different atoms (hence the term Diatomic overlap). Modified INDO (MINDO 3)[39] modified the nuclei-nuclei interaction term and made the orbital exponents in the Slater functions variable instead of fixing them at the values suggested by Slater's rules. MINDO 3 was also the first attempt to develop a "generic tool" by including parameters for a large number of elements. Modified Neglect of Diatomic Overlap (MNDO) incorporated a correction term for interactions between lone pairs of electrons [40]. MNDO's main deficiency was its inability to reproduce hydrogen bonding, which precluded its application for many biological systems. The Austin Model 1 (AM1) version of MNDO attempted to correct this deficiency by assigning a number of spherical Gaussian functions to each atom to mimic correlation effects [41]. The third parameterization of MNDO, MNDO-PM3 [42], uses the same terms as AM1 but with a more sophisticated fitting algorithm for the parameters and is based on a much larger set of molecular reference data set than previous methods.

For a more complete discussion, the reader is referred to Stewart's [43] review of SE techniques. Pople and Beveridge [44] present a more detailed discussion of approximate

molecular orbital theory than is contained in Stewart's article, but it only considers Pople's methods and is older.

Advances in computers have meant that many "large" polyatomic system as defined in the 1960's can now be calculated using *ab initio* techniques, but SE techniques are still widely used. SE techniques can still handle much larger polyatomic systems than *ab initio* techniques. In addition, SE techniques are so much faster than *ab initio*, one can save a considerable amount of time by first performing a SE calculation to obtain a better initial guess for an *ab initio* calculation. However, one source of the speed of SE techniques is also the source of the its primary limitation. SE techniques will give good results for conditions that match the data upon which the particular SE technique was parameterized. For example, equilibrium heat of formation is commonly used to parameterize SE techniques. Away from the equilibrium structure, the predicted heat of formation is suspect. Building up a potential energy surface (PES) for a reaction involves deformations far away from equilibrium, therefore a SE calculated PES is may not even be qualitatively reliable. Other equilibrium molecular properties not included in the parameterization, such as dipole moments, may also be suspect.

2.2.2 Molecular Mechanics. Molecular Mechanics (MM) is based on a classical description of molecules rather than a quantum description. Basically, molecular mechanics approximates the N electron M nuclei interaction in the quantum mechanical description of a molecule with a sum of effective two, three, and, and four atom interaction within the M atom molecule. In MM, the potential energy (PE) of a molecule is thus given by

$$V\left(\vec{R}_1, ..., \vec{R}_M\right) = \sum_{i=1}^{M-1} V_b + \sum_{i=1}^{M-2} V_\theta + \sum_{i=1}^{M-3} V_\tau + \sum_{i=1}^{M-3} V_\chi + \sum_{i=1}^{M} V_{nb} + \sum_{i=1}^{M} \sum_{j>i}^{M} \frac{q_i q_j}{\vec{R}_{ij}}.$$

$\sum_{i=1}^{M-1} V_b$	PE due to deviations from equilibrium bond lengths
$\sum_{i=1}^{M-2} V_\theta$	PE due to deviations from equilibrium bond angles
$\sum_{i=1}^{M-3} V_\tau$	PE due to deviations from equilibrium dihedral angles
$\sum_{i=1}^{M-3} V_\chi$	PE due to deviations from equilibrium out of plane bends
$\sum_{i=1}^{M} V_{nb}$	PE due to Van der Waals Interactions
$\sum_{i=1}^{M} \sum_{j>i}^{N} \frac{q_i q_j}{\vec{R}_{ij}}$	PE due to Coulomb interactions

(2.50)

These potential energy terms are uncoupled in that they assume a change in one parameter has no effect on another. Coupled potential terms, such as bond-angle and angle-angle deviations, may also be added. These potential terms are illustrated in Fig 2.3. As is seen in this figure, MM is essentially a "ball and spring" model of molecules, which is much easier to understand than the underlying quantum mechanics. The accuracy of a MM depends critically on the potentials used to describe the interactions.

A two atom bonding PES is commonly approximated with the Morse [45] potential, which is of the form:

$$V_b(r_{ij}) = D_e\left[1 - Exp\left[-\alpha\left(r_{ij} - r_{ij}^{eq}\right)\right]\right]^2. \tag{2.51}$$

D_e is the well depth (dissociation energy plus zero point vibrational energy), r_{ij}^{eq} is the equilibrium separation, and α is the zero crossing point. These parameters are determined from spectroscopic data. The Morse potential qualitatively models the interaction of two atoms quite well: it's stiffer in compression than extension, it softens out with extension, and approaches zero as the separation goes to infinity. Quantitative predictions of a Morse potential can be quite good for moderate deviations from the equilibrium separation; how-

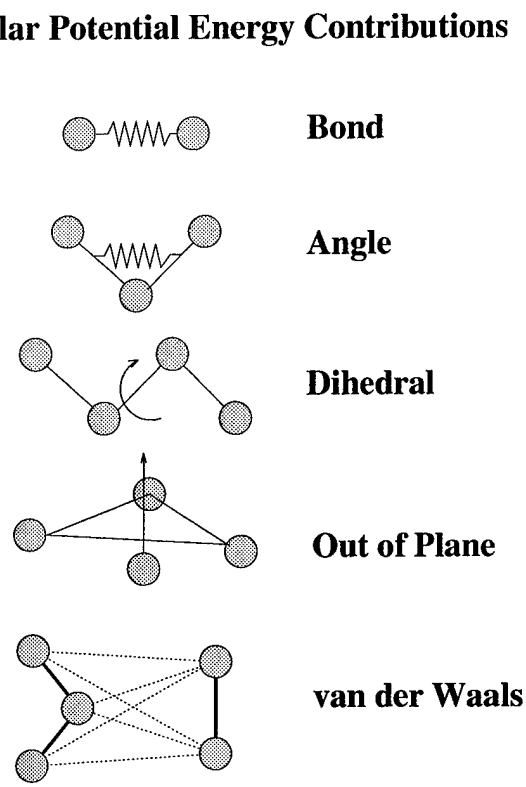

Figure 2.3 Molecular Mechanics Potential Energy Modes

ever, quantitative agreement with experiment near the dissociation limit is not as good for two main reasons. First, the Morse potential parameters are based on equilibrium data, i.e., there isn't enough mathematical flexibility in the Morse potential form to accurately describe the whole range of atom separations. Second, experimental spectroscopic data for extreme atom separations is exceptionally difficult to obtain. Unfortunately, this poor behavior near dissociation limits the utility of a Morse potential to describe chemical reactions. This behavior can be improved by using a linear combination of Morse functions.

Another common two body potential is the familiar Hooke's law expression for a harmonic oscillator:

$$V_b(r_{ij}) = \frac{1}{2}K_b(r_{ij} - r_{ij}^{eq})^2 \tag{2.52}$$

where r_{ij}^{eq} is the equilibrium separation for bodies i and j. A comparison of a Morse and Harmonic potentials is shown in Figure 2.4. For small deviations from equilibrium, the Morse and Harmonic potentials agree quite well. However, the dissociation behavior of

the Harmonic potential is qualitatively wrong, as a harmonic oscillator never dissociates. While the Morse potential is a much better model of two atom interactions, harmonic potentials are more commonly used in MM because they can be evaluated much faster, significantly decreasing computation times.

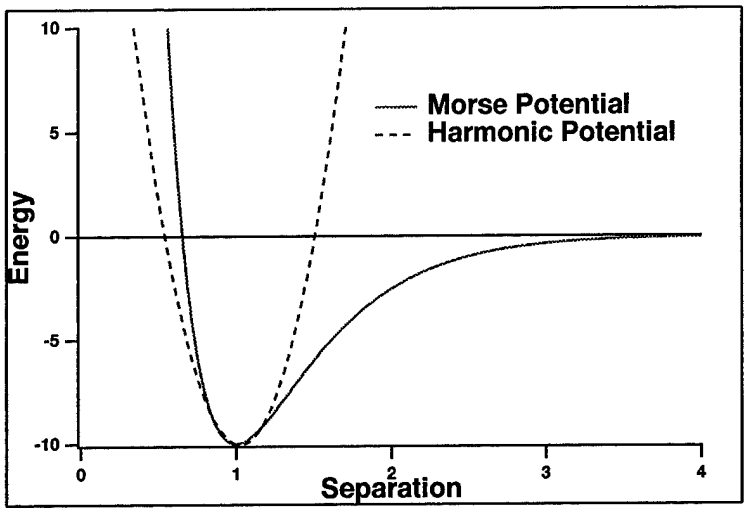

Figure 2.4 Comparison of Morse and Harmonic Potentials.

Harmonic potentials are also generally used for bond angle changes and out-of-plane bends. Changes in dihedral angle are commonly represented by a Fourier series of the form:

$$V_\tau = \sum_j \frac{1}{2} V_j \left[1 + (-1)^{j+1} \cos(j\tau)\right]. \tag{2.53}$$

Here V_τ is the rotation barrier height, τ is the dihedral angle, and j is the periodicity. The nonbonding interactions between atoms, i.e. van der Waals interactions, are commonly represented by a Lennard-Jones PES,

$$V_{nb}(r_{ij}) = 4\varepsilon_{ij} \left[\left(\frac{\sigma_{ij}}{r_{ij}}\right)^{12} - \left(\frac{\sigma_{ij}}{r_{ij}}\right)^{6} \right], \tag{2.54}$$

where ε_{ij} is the potential well depth, σ_{ij} is the Lennard-Jones diameter, and r_{ij} is the separation between atoms i and j. The coulombic potential energy can be used to represent the interaction between the effective charges on the nuclei (ionic bonding) or the interactions

between bond dipoles. Coulomb potentials are of the form

$$V_c = \sum_{i=1}^{N} \sum_{j>i}^{N} \frac{q_i q_j}{\varepsilon |\vec{R}_{ij}|}, \tag{2.55}$$

q_i is the net charge on atom i (not the nuclear charge), R_{ij} is the separation between atoms i and j which are not also described by an atom pair bonding potential, and ε is the dielectric constant of the medium in question

The minimum energy configuration of a collection of molecules or atoms is determined by minimizing the gradient of the system with respect to the atomic positions. Numerous schemes exist to perform this minimization. A good review of current methods is given by Schlick [46].

MM techniques have a number of significant limitations. First, the "bonded" potentials used in MM are good approximations for molecular behavior only for small deviations from equilibrium. Chemical reactions cannot be reliably modeled. Second, without an explicit description of the electrons, electronic properties cannot be calculated. Lastly, the two, three, and four-body potentials are often extremely situation specific, so specific that one almost needs to know the answer in order to select the appropriate potentials to use in the problem. A simple example of this limitation is calculating the minimum energy structure of acetylene. It is known from *ab initio* quantum calculations that the carbon-carbon bond in acetylene is the sp hybrid. In an MM calculation, one must define the types of interactions between all atoms in advance. In order to obtain the correct structure for acetylene, the C-C interaction must be described with the sp interaction potential. One could also obtain a converged MM result for acetylene using the sp^2 or sp^3 potential C-C interaction potentials, though this converged result would be wrong. In contrast, for an *ab initio* calculation one would merely specify two carbon atoms and two hydrogen atoms in an approximate equilibrium configuration. The description of the C-C bonding would be a result of the electronic wavefunction solution, not an assumption made in advance of the calculation.

Alternate sets of interaction potentials have been formulated for specific problems. Stillinger and Weber [47] developed a set of two and three-body interaction potentials for

silicon and fluorine to investigate the problem of fluorination of silicon surfaces. Their potential reproduced the behavior of solid silicon, adsorbed molecules, and volatile species desorbed from the surface. These potentials, and variations of the Stillinger-Weber potential forms, have been used by other researchers for silicon and other surface investigations.

The greatest advantage of MM techniques is that the inherent simplicity of the classical mechanical description of atomic interactions enables calculations on systems with huge numbers of atoms. A representative calculation of crack formation and propagation in silicon nitride used a cluster of 100,000 atoms [48]. A cluster of this size is large enough to give a good representation of the mechanical behavior of the bulk material.

2.2.3 Density Functional Theory. Density Functional Theory (DFT) is an alternative "first principles" model for describing the electronic structure and properties of matter. In quantum mechanics, the quantity of interest is the wavefunction, which cannot be directly observed. The total energy is defined as a functional of this wavefunction, and a variational minimization yields a procedure to determine the minimum energy approximate wavefunction. In DFT, the quantity of interest is the electron density, $\rho(\vec{r})$ which is directly observable. The total energy can be defined as a functional of electron density, and a variational minimization again yields a procedure to determine the minimum energy electron density [49].

Models describing the energy as a functional of electron density date back to the earliest days of quantum mechanics. These developments proceeded without a rigorous mathematical justification that such a functional existed. These early models were all based on the simple assumption of a uniform density electron gas, and were unable to provide accurate electron densities for chemical systems because of this inappropriate assumption. Perhaps the best known of these models is the Thomas-Fermi (TF) model developed for atoms [50, 51]. A consequence of the assumption of uniform electron density was that the limiting behavior of the TF model is qualitatively wrong. The TF density does not decay exponentially as $r \rightarrow \infty$, and the electron density approaches ∞ as $r \rightarrow 0$. It was later shown that the TF model becomes exact in the limit that the number of electrons $N \rightarrow \infty$.

In 1964 Hohenberg and Kohn proved rigorously that DFT is an exact theory for describing the electronic structure of matter [52]. They proved

> *There exists a variational principle in terms of the electron density which determines the ground state energy and electron density. Further, the ground state electron density determines the external potential, within an additive constant.*

The optimum ground state electron density distribution is obtained from the functional variation

$$\delta\left\{E[\rho,\nu]-\mu\left(\int \rho d\tau - N\right)\right\}=0, \tag{2.56}$$

where $E[\rho,\nu]$ is the ground state energy as a functional of both the electron density ρ and an external potential ν, μ (the chemical potential) is a Lagrange multiplier introduced from the constraint of conservation of number of particles, and N is the number of electrons. The solution of the resulting Euler-Lagrange equation,

$$\left(\frac{\delta E[\rho,\nu]}{\delta\rho}\right)_{\nu}=\mu, \tag{2.57}$$

determines the ground state energy density and all the ground state properties of the system. Eq 2.57 is the DFT counterpart to the Schrödinger equation. The functional for the ground state energy can be partitioned as

$$E[\rho,\nu]=F[\rho]+\int \rho\nu d\tau, \tag{2.58}$$

where $F[\rho]$ is a universal functional that contains kinetic and potential energy contributions

$$\begin{aligned} F[\rho] &= T[\rho] + V_{ee}[\rho] \\ &= T[\rho] + J[\rho] + V_{xc}[\rho]. \end{aligned} \tag{2.59}$$

$T[\rho]$ is a universal kinetic energy functional, $J[\rho]$ is a Coulomb interaction functional, and $V_{xc}[\rho]$ is an electron exchange-correlation functional, much like the terms we saw in the HF-SCF Hamiltonian. At this point in the development of DFT, only a lack of exact forms of $T[\rho]$ and $V_{xc}[\rho]$ stood in the way of a practical implementation of DFT.

While this proof by Hohenberg and Kohn is extremely important, placing DFT on the same theoretical footing as the Schrödinger formalism, it is important to note that they proved the existence of a solution, but did not provide this solution. At this point, the absence of exact forms for the kinetic energy and exchange-correlation functionals precluded the development of a practical implementation of DFT. However, only one year after this initial proof, Kohn and Sham [53] solved half of this problem. The Kohn-Sham (KS) implementation of DFT is based on an orbital density description that removes the necessity of knowing the exact form of the kinetic energy functional $T[\rho]$. K-S focused on the kinetic energy of a noninteracting system of electrons as a functional of single-particle orbitals that give the exact density. Levy [54] subsequently developed a constrained search formulation of KS theory in which the kinetic energy of a noninteracting system of electrons is minimized with respect to a set of single-particle orbitals subject to the constraint that the orbitals are orthonormal and the sum of the squares of the orbitals give the exact ground state density. A time dependent formulation of KS theory is also possible within this constrained search framework [55].

While the K-S formalism removes the requirement for a universal kinetic energy functional, unfortunately, it does not remove the requirement for a universal exchange-correlation functional, $V_{xc}[\rho]$. Thus, the ability of the K-S formalism to yield quantitative results for calculated structures and properties of molecules is directly related to the accuracy of the approximation used for $E_{xc}[\rho]$, the exchange-correlation energy. Fortunately, reasonable approximations for $E_{xc}[\rho]$ have been developed [56, 57]. The consequence of using an approximation for $E_{xc}[\rho]$ is that the theory is no longer variational with respect to the true ground state energy. KS theory is variational with respect to the model system described by the approximate $E_{xc}[\rho]$.

Since approximations for $E_{xc}[\rho]$ are made by fitting calculations to experimental data, it is unclear if DFT should be categorized as an *ab initio* or semiempirical approach. *Ab initio* HF-SCF doesn't approximate terms in the electronic Hamiltonian, but does use basis sets that contain parameters optimized for specific elements. Semiempirical HF-SCF approximates the Hamiltonian by throwing away various two electron interaction terms to save time and seeks to correct this omission by adding optimizable functional forms

that do not have a direct physical interpretation. In comparison, all the terms in the KS implementation of DFT have a physical interpretation, though an analytic form for V_{xc} is not known so an approximation to this term based on experimental data must be used. Since all the terms in a DFT calculation have a clear, physical interpretation, DFT is best categorized as an *ab initio* theory with a semiempirical implementation.

The method of solution for KS DFT is very similar to HF-SCF. An approximate form of the electron density is expressed as a linear combination of basis functions. An iterative procedure is then applied to optimize the coefficients of the basis functions to provide the lowest energy electron density. As in HF-SCF, Gaussian basis functions are commonly used because of their favorable integration properties. Since a finite basis approach is used for both HF-SCF and DFT, a mangos to mangos comparison of their computational cost can be made. The computational cost of an HF-SCF computation, without correlation correction, scales as n^4 (n^3 for large systems), where n is the number of basis functions. The computational cost of approaches that include correlation corrections such as perturbation methods (MP2, MP4) and configuration interaction typically scale as n^ℓ where $\ell \geq 5$ The computational cost of DFT scales as n^4 while predicting some molecular properties with an accuracy comparable to a large basis set MP2 calculation, depending on which approximation to the exchange-correlational functional is used. No functional provodes this level of accuracy for all molecular properties.

Car and Parrinello [58] developed a computationally efficient unified scheme that combines molecular dynamics and DFT. They treated minimization of the energy of the KS functional as a complex minimization problem which could be solved using the concept of simulated annealing. Instead of the common simulated annealing strategy based on the Metropolis Monte Carlo algorithm, Car and Parrinello used a simulated annealing approach based on molecular dynamics. This approach speeds up the minimization procedure and also allows the study of finite-temperature properties. The Car and Parrinello approach is very commonly applied to simulations of surface reactions where its efficiency enables the use of a large number of atoms in the surface.

2.3 Discussion

DFT has seen widspread use in surface structure calculations because of its computational efficienvy; however, DFT has a number of significant limitations. DFT's description of atom interactions depends critically on the fit of the exchange-correlation functional to empirical data, so the reliability of a specific DFT functional is really limited to the data set from which it was derived. Unlike wavefunction based approaches, there is currently no systematic way to improve a DFT calculation by increasing the size of the basis set or using techniques analogous to post Hartree-Fock limit calculations. Very recently, alternate computation methods for HF-SCF have demonstrated linear scaling of computation time with number of basis functions [59, 60]. These techniques make large scale HF-SCF calculations competitive with DFT, and the stratgies used to speed up HF-SCF calculations can likely be adapted for methods that include correlation.

III. Merging Molecular Mechanics with Quantum Mechanics

3.1 Introduction

In spite of the progress made in *ab initio* quantum mechanics (QM) computational techniques, many molecular systems are still too large for full quantum mechanical treatments. Molecular mechanics (MM) methods give good results in predicting molecular structure and are fast enough to model very large systems [61]; however, MM potential functions are inadequate for describing chemical bond breaking or making. To get a good description of bond making and breaking, many researchers perform quantum mechanical calculations on smaller molecules that resemble pieces of interest of the large system, e.g., the reactive site on a surface. However, it is often difficult to draw conclusions about the behavior of large molecules from these small molecule models because they do not accurately represent the environment, mechanical and electronic, within the large molecule. A solution to this problem that is becoming increasingly popular is to combine QM with MM. One partitions a large molecule into a small region of interest modeled with quantum mechanics under the influence of a larger region modeled with MM [62, 63, 64, 11, 4, 65]. In this work, the small region is called the *embedded cluster* (EC), the large region is called the *bulk cluster* (BC), and the two regions together called a *hybrid cluster.*

These hybrid QM/MM methods differ in two main areas: the types of interactions between the bulk and embedded clusters, and the way the boundary between the embedded and bulk clusters is treated. The QM/MM interactions primarily include polarization of the electron distribution of the embedded cluster by the electrostatic potential of the bulk cluster, and mechanical forces on the embedded cluster from the bulk cluster. The boundary between the embedded and bulk clusters cuts across chemical bonds. Cutting these chemical bonds leaves dangling bonds at the boundary of the embedded cluster, which have to be terminated in some manner to create a realistic model for the QM description of the embedded cluster [66]. (Alternate embedded cluster termination approaches that give a better representation of the electronic environment of a large molecule are discussed in Chapter IV.) Various methods are used to link the embedded and bulk clusters.

The first part of this chapter discusses modifications to the Integrated Molecular Orbital (QM) Molecular Mechanics (IMOMM) method of Maseras and Morokuma [4] to enable hybrid modeling of surfaces. This modified IMOMM technique (MIMOMM) was implemented using the quantum chemistry code GAMESS [9], and the molecular mechanics code MM3 [6]. In IMOMM, MM forces (energy gradients) from the bulk cluster are used to augment QM forces on the embedded cluster, and this *hybrid* QM/MM gradient is used in the QM optimization of the embedded cluster. The method used to link the embedded and bulk clusters in IMOMM is unsuitable for hybrid clusters used to model surfaces, so a new linking method was developed. In addition, the hybrid QM/MM optimization method of Weiner et al. [11] was also implemented (in GAMESS and MM3) and compared to MIMOMM. In Weiner's method, the influence of the bulk cluster on the embedded cluster is communicated by using the MM portion of the hybrid optimization to determine the *positions* of the outermost atoms in the embedded cluster. The positions of these outermost atoms are then fixed in the QM portion of the hybrid optimization. The results of MIMOMM and Weiner's method are compared to each other and to full QM optimizations on some silicon cluster test cases.

Small molecular clusters have often been been used to represent surfaces of bulk materials because the size and computational cost of *ab initio* QM techniques restricts their application to small systems. The second half of this chapter investigates the ability of small silicon clusters to represent dimer formation on the silicon(001) surface. The effect of adding a representation of mechanical effects of an extended is investigated using MIMOMM. It was found that the particular model silicon cluster investigated actually gives a quite good representation of surface dimerization. While MIMOMM doesn't provide a qualitative improvement in the optimized geometry of the cluster, one can obtain useful insight in designing small clusters to model surfaces of bulk materials.

3.2 Construction of the Hybrid System

Since various portions of the hybrid systems are modeled differently, the first step in setting up a hybrid optimization is partitioning the system into regions. Figures 3.1 and 3.2 show the partitioning of a silicon carbide QM/MM hybrid model system needed to

apply IMOMM, the hybrid optimization technique of Maseras et al. [4] (the terminology used in this section is based on this reference).

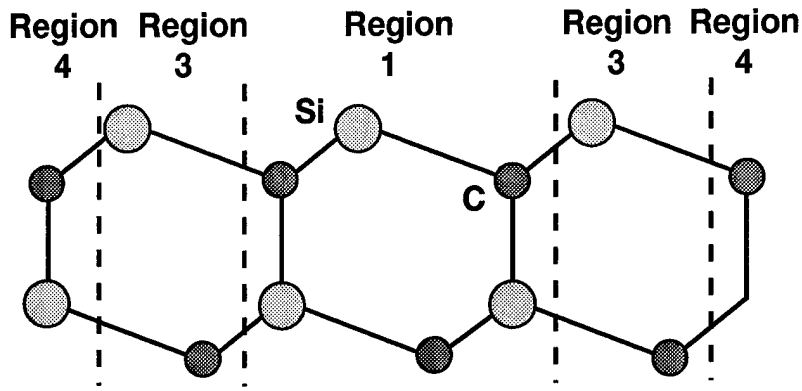

Figure 3.1 Hybrid system partitioning, IMOMM.

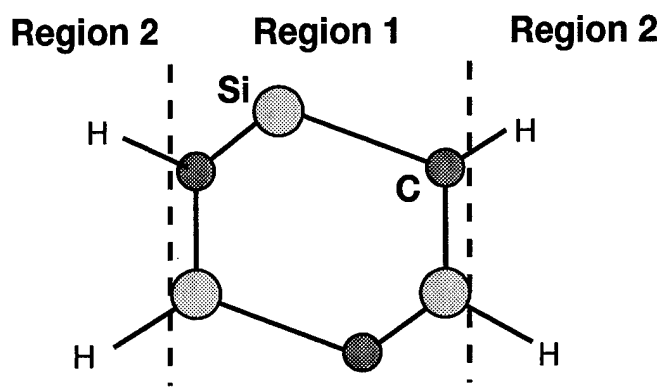

Figure 3.2 Embedded cluster partitioning, IMOMM.

The embedded cluster that is modeled in the *ab initio* code is composed of Region 1 and Region 2 atoms. Region 1 atoms make up the site of interest, for example, a reactive site on the SiC surface. Region 1 atoms are present in both the *ab initio* EC and the MM full system. Region 1 atoms are unconstrained in the *ab initio* portion of the optimization process. Region 2 and Region 3 define the linkage between embedded cluster and the bulk cluster in the hybrid cluster. Region 2 atoms are present only in the EC, and are replaced by Region 3 atoms in the MM bulk cluster. Region 2 is made up of atoms, generally hydrogen, that are used *only to terminate Region 1 atoms in the model system.* Region 3 is made up of bulk cluster atoms, Si or C in this SiC example. Region 2 atoms

stand-in for Region 3 atoms in the *ab initio* portion of the hybrid optimization process (HOP), and have been referred to as link atoms or junction dummy atoms [67, 68]. The positions of the Region 3 atoms are frozen in the MM portion of IMOMM, and so their positions are determined from the positions of the Region 2 atoms in the *ab initio* portion of IMOMM. Other hybrid QM/MM schemes have allowed the Region 3 atoms to move in the MM portion of the HOP, which means that the positions of Region 2 are determined by the MM portion of the hybrid QM/MM optimization [11]. Both approaches have been implemented in this work.

A limitation of IMOMM is that both the Region 2 and Region 3 atom positions are determined by the user, *not by energy and gradient minimization.* This limitation can be overcome by creating a new set of atoms and using a new partitioning scheme, illustrated in Figure 3.3 and Figure 3.4, which eliminates Regions 2 and 3. In this new approach, Region 1 in the embedded cluster is expanded and terminated by Region 5 H atoms, *which have no equivalents in the bulk cluster.* Region 3 is eliminated from the bulk cluster, which is now composed exclusively of Region 4 atoms. In the QM portion of IMOMM, Regions 1 and 5 are optimized without constraints. In making the transition from the QM to the MM portions of IMOMM, Region 5 atoms are removed from the model, and Region 1 is now directly connected to Region 4. In the MM portion of IMOMM, Region 4 freely optimizes around a frozen Region 1, so the MM gradient on the Region 4 atoms is zero. The MM gradient on Region 1 atoms arising from Region 4-Region 1 interactions is non-zero since the Region 1 atom positions are frozen. (MM intra Region 1 interactions are neglected as these are already calculated in the *ab initio* portion of IMOMM.) This gradient on the Region 1 atoms is added to the QM intra-Region 1 gradient, and passed back to the QM portion of IMOMM. Region 5 is reattached to Region 1 to saturate the dangling bonds, and the QM optimization of Region 1 proceeds with the hybrid gradient. We call this new method MIMOMM for "modified" IMOMM.

Region 5 termination is also easier to define in some lattice-like hybrid clusters. Figure 3.5 shows the Si_6H_{12}/Si_9H_{12} hybrid cluster. Here, atoms 3 and 5 (4 and 6) in Region 1 are both connected to atom 7 (8) in Region 3. This means that *two* atoms in Region 2 correspond to *one* atom in Region 3. In the original IMOMM procedure, the position of

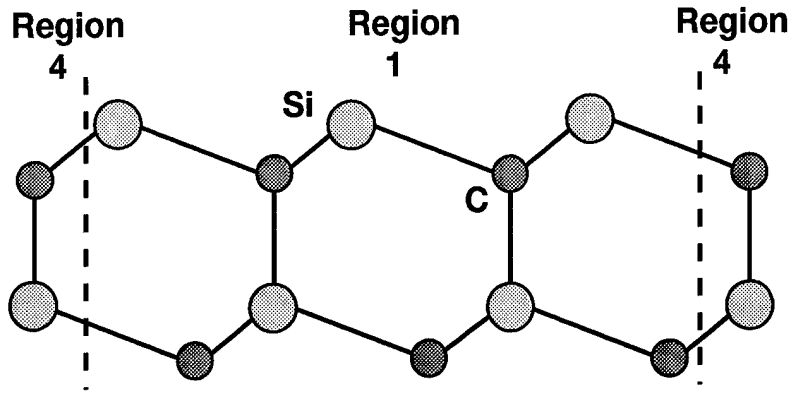

Figure 3.3 Hybrid system partitioning, modified IMOMM (MIMOMM).

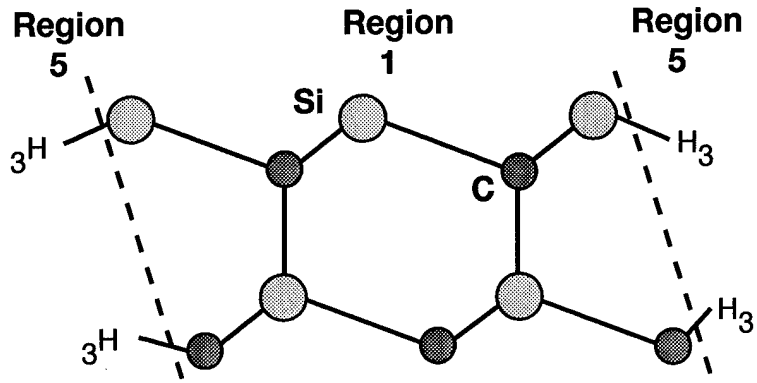

Figure 3.4 Embedded cluster partitioning, modified IMOMM (MIMOMM).

atom 7 would be determined by a simple translation of the Region 2 atom connected to atom 3. However, there is no guarantee that this position for atom 7 will be the same as the position obtained by a translation of the Region 2 atom connected to atom 5. Getting the correct position of atom 7 relative to atoms 3 and 5 is crucial, because all three atoms are fixed in the MM portion of IMOMM. The Region 4 optimization around the frozen Regions 1 and 3 would be affected, and would pass back a "corrupted" MM gradient on Region 1. This would eventually cause the IMOMM optimization to diverge. Additional constraints would have to be imposed to insure that atom 7 is properly positioned with respect to both atoms 3 and 5, increasing the user's bias imposed on the optimized result. The preferred solution is to use a larger embedded cluster in which Region 2 does have a one-to-one

correspondence to Region 3. Unfortunately, this will increase the computational cost since the cost of the HOP is really driven by the size of the *ab initio* part of the calculation.

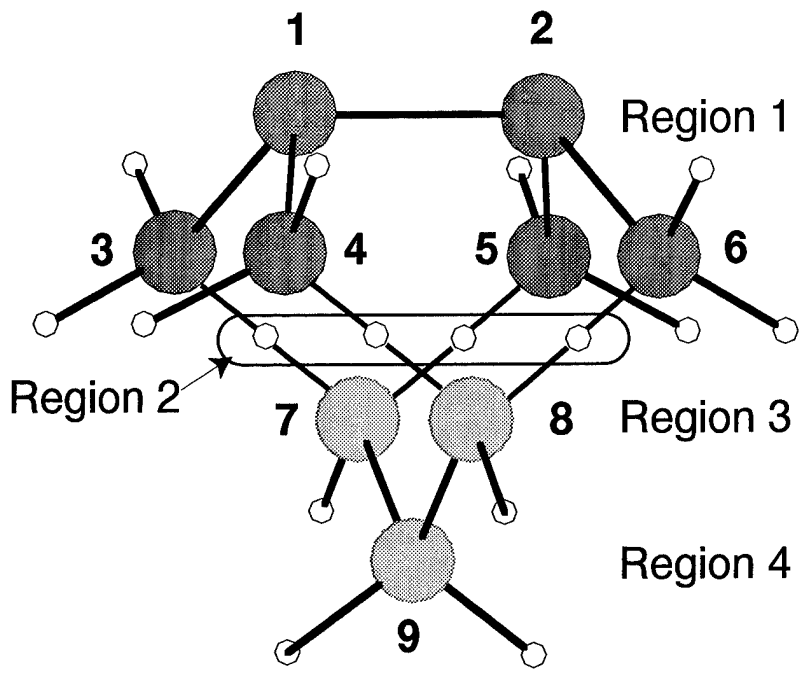

Figure 3.5 Limitation of IMOMM Region 2-3 linking. For this case, there is not a 1 to 1 correspondence between the Region 2 atoms and Region 3 atoms (7,8)

Using Region 5 termination for this same situation, atom 7 becomes part of Region 4. As Regions 2 and 3 are not defined when Region 5 is used, the problem of a non one-to-one correspondence between Regions 2 and 3 never arises.

To summarize the overall procedure of specifying a hybrid system, the following steps are described in terms of a hybrid model of a crystalline surface, though IMOMM has a much broader range of applications:

- Define a cluster large enough to give a good representation of the steric environment of the lattice. This initial cluster will be partitioned to form the hybrid cluster
- Perform a MM optimization of this cluster. This initial MM optimization aligns the cluster in principle axis coordinates, and gives a good initial geometry for the bulk portion of the hybrid cluster
- Partition the cluster into Regions 1,3, and 4 (IMOMM), or 1 and 4 (MIMMOM)
- Determine the positions of the Region 1 terminating atoms, using either Region 2-3 in IMOMM, or Region 5 in MIMOMM

3.3 The Hybrid Optimization Procedure

3.3.1 Formal Derivation of Hybrid Energy and Gradient Equations.

In IMOMM, the atomic positions of the Region 3 atoms depend on Region 1 and Region 2

$$\vec{R}_3 = \vec{R}_3(\vec{R}_1, \vec{R}_2) \tag{3.1}$$

Using Eq3.1, the total energy of the system, the sum of the *ab initio* (AI) and MM cluster energies, can be written as

$$E_{AI} = E_{AI}(\vec{R}_1, \vec{R}_2), \tag{3.2}$$

$$E_{MM} = E_{MM}(\vec{R}_1, \vec{R}_3(\vec{R}_1, \vec{R}_2), \vec{R}_4) = E_{MM}(\vec{R}_1, \vec{R}_2, \vec{R}_4), \tag{3.3}$$

$$E_T = E_{AI} + E_{MM} = E_T(\vec{R}_1, \vec{R}_2, \vec{R}_4). \tag{3.4}$$

Applying the chain rule to the calculation of the gradients

$$\frac{dE_T}{d\vec{R}_1} = \frac{\partial E_{AI}}{\partial \vec{R}_1} + \frac{\partial E_{MM}}{\partial \vec{R}_1} + \sum_{\vec{R}_3} \frac{\partial E_{MM}}{\partial \vec{R}_3} \frac{\partial \vec{R}_3}{\partial \vec{R}_1} \tag{3.5}$$

$$\frac{\partial E_T}{\partial \vec{R}_2} = \frac{\partial E_{AI}}{\partial \vec{R}_2} + \sum_{\vec{R}_3} \frac{\partial E_{MM}}{\partial \vec{R}_3} \frac{\partial \vec{R}_3}{\partial \vec{R}_2} \tag{3.6}$$

$$\frac{\partial E_T}{\partial \vec{R}_4} = \frac{\partial E_{MM}}{\partial \vec{R}_4} \tag{3.7}$$

In IMOMM, the bond separations $\vec{r}_{12}$ and $\vec{r}_{13}$ are frozen at some reasonable user selected value. (For a hybrid silicon lattice calculation, $\vec{r}_{12}$ would be an Si-H separation, while $\vec{r}_{13}$ would be an Si-Si separation.) In addition, the bond and dihedral angles between $\vec{R}_1, \vec{R}_2$ and $\vec{R}_1, \vec{R}_3$ are constrained to be the same. This choice of interfacing the two parts of the problem removes the dependence of $\vec{R}_3$ on $\vec{R}_1$, so

$$\frac{\partial \vec{R}_3}{\partial \vec{R}_1} \equiv 0. \tag{3.8}$$

With the bond distances frozen, and the angles kept the same,

$$\frac{\partial \vec{R}_3}{\partial \vec{R}_2} = \overline{\overline{I}}, \qquad \frac{\partial E_{MM}}{\partial \vec{R}_3} = \frac{\partial E_{MM}}{\partial \vec{R}_2}. \tag{3.9}$$

where $\overline{\overline{I}}$ is the identity matrix. Using 3.8 and 3.9, Equations 3.5 and 3.6 become

$$\frac{\partial E_T}{\partial \vec{R}_1} = \frac{\partial E_{AI}}{\partial \vec{R}_1} + \frac{\partial E_{MM}}{\partial \vec{R}_1}, \tag{3.10}$$

$$\frac{\partial E_T}{\partial \vec{R}_2} = \frac{\partial E_{AI}}{\partial \vec{R}_2} + \frac{\partial E_{MM}}{\partial \vec{R}_2} \tag{3.11}$$

Equations 3.1 through 3.11 define the formal optimization problem for IMOMM. As the Region 4 atom positions are allowed to freely optimize in the MM portion of IMOMM, Equation 3.7 should go to zero upon optimization. The presence of a residual gradient in Region 4 in general will cause the HOP to diverge.

Equations 3.10 and 3.11 are only valid for internal coordinates, and so the formation of the hybrid gradient must be performed using internal coordinates. *This requirement of using internal coordinates in the hybrid procedure turns out to impose significant practical problems in applying this technique to cluster models of surfaces, which are highly coupled molecular cages.* The problem of constructing "good" sets of internal coordinates for cages is discussed in Section 3.4.

3.3.2 Energy and Gradient Equations using Region 5. The formal HOP is simplified by using the MIMOMM partitioning scheme developed in this work. Since Regions 2 and 3 are never specified, terms involving $\vec{R}_2$ and $\vec{R}_3$ never appear in the optimization problem. We have

$$\frac{\partial E_T}{\partial \vec{R}_1} = \frac{\partial E_{AI}}{\partial \vec{R}_1} + \frac{\partial E_{MM}}{\partial \vec{R}_1}, \tag{3.12}$$

$$\frac{\partial E_T}{\partial \vec{R}_5} = \frac{\partial E_{AI}}{\partial \vec{R}_5} \tag{3.13}$$

$$\frac{\partial E_T}{\partial \vec{R}_4} = \frac{\partial E_{MM}}{\partial \vec{R}_4} \tag{3.14}$$

3.3.3 Double Counting. The goal of IMOMM is to include the steric influence of the outer cluster onto the embedded cluster through MM forces (gradients). However, Region 1 atoms are present both in the *ab initio* calculations of the embedded cluster and the MM calculations of the bulk cluster, so *intra-Region 1 forces would be calculated in both the ab initio and MM codes.* The intra-Region 1 MM forces need to be zeroed out in the MM calculations to avoid this double counting. Maseras et al [4] describe some simple tests to determine if a given interaction in the bulk cluster should be added to the MM gradient:

- Interactions involving atoms of Region 1 exclusively are neglected as Region 1 interactions are already accounted for in the *ab initio* code
- Region 1 - Region 3 interactions are neglected in the MM code, with the assumption that Region 1 - Region 2 interactions are properly reproduced by Region 1 - Region 2 interactions in the *ab initio* code
- "Non-bonded" (e.g., van der Waal's) interactions *between* atoms of Region 3 are kept in the MM code. These terms are sensitive to the nature of the atom, and are not adequately represented by the interactions between the Region 2 atoms (typically H atoms) in the *ab initio* calculation.
- Any interaction involving one atom of Region 4 is retained

The original IMOMM scheme used these same rules to modify calculation of the MM energy. However, modification of the MM energy calculation is not needed for two reasons. First, the atom positions of Regions 1 and 3 are kept fixed in the MM calculation. The MM energy from Regions 1 and 3 thus remains constant. Neglecting the appropriate terms in the MM energy calculation makes this constant 0, but adding a non-zero constant to an energy that is being minimized will not affect convergence. More importantly, in the *ab initio* portion of IMOMM, the geometry is considered optimized when the *hybrid gradient* falls below some tolerance value (typically 5×10^{-5} H/B), not when a criterion based on the energy is satisfied.

3.3.4 An alternate embedding approach: Weiner's method. Weiner et al [11] described an alternative approach to embedding a quantum mechanically described cluster in a MM bulk. In this approach, the influence of the bulk region on the embedded cluster is communicated by the bulk region determining the position of the boundary atoms. That is, the Region 3 atom positions are optimized in the MM calculation, and the Region 2

	IMOMM	MIMOMM	Weiner
$\vec{R}_1$ GAMESS	Optimized	Optimized	Optimized
$\vec{R}_1$ MM3	Fixed	Fixed	Fixed
$\vec{R}_2$ Stretch	Fixed	n/a	Fixed
$\vec{R}_2$ Bend	Optimized	n/a	Fixed
$\vec{R}_2$ Torsion	Optimized	n/a	Fixed
$\vec{R}_3$ Positions	Fixed	n/a	Optimized
$\vec{R}_4$ Positions	Optimized	Optimized	Optimized
$\vec{R}_5$ Stretch	n/a	Either	Either
$\vec{R}_5$ Bend	n/a	Either	Either
$\vec{R}_5$ Torsion	n/a	Either	Either
$\vec{R}_1$ Gradient	AI + MM	AI + MM	AI only

Table 3.1 Comparison of constraints on different regions of a hybrid optimization. Weiner's method may be used with or without Region 5

atom positions are frozen in the *ab initio* calculation. Once the optimized Region 3 atom positions have been determined in the MM calculation, the Region 2 atoms are placed at positions along the Region 1-Region 3 bond directions, with atom separations set at the user defined Region 1-Region 2 bond lengths. This is the opposite of the treatment of link atoms in IMOMM in which the Region 3 atoms are placed at positions along the Region 1-Region 2 bond directions, with the atom separations set at the user defined Region 1-Region 3 bond lengths. No gradient information is passed from the MM calculation to the *ab initio* calculation. The influence of the bulk cluster (BC) is limited to determining the position of the Region 2 atoms in the *ab initio* calculation. This approach provides a poorer representation of the influence of the bulk cluster on the embedded cluster; however, it is a bit faster than IMOMM, easy to implement, and provides additional insight on how to best represent the mechanical interactions of the bulk cluster onto the embedded cluster. Table 3.1 summarizes the constraints of the atoms in the different regions in the hybrid clusters in IMOMM, MIMOMM, and Weiner's method.

3.4 Internal Coordinates for Cages

Application of IMOMM requires the specification of a set of internal coordinates to add the *ab initio* and MM gradients. One need not run the *ab initio* optimization in

internal coordinates, though the MM and *ab initio* gradients need to be transformed to internal coordinates before they are added in the original IMOMM procedure. However, transition state searches and general mapping of potential energy surfaces are often aided by freezing internal coordinates. Specification of a good set of internal coordinates can become a bottleneck in using IMOMM, especially for molecular cage structures.

The optimization of the (potential) energy of a molecule is typically performed using some type of second-order Newton-Raphson minimization technique. (See Reference [46] for a detailed discussion of the optimization problem in computational procedures.) Thus, in principle one needs the energy, the gradient of the energy with respect to nuclear positions, and the second derivative, the Hessian matrix, at each molecular configuration in the optimization process. If the coordinates used to specify the molecular structure are orthogonal, a displacement along one coordinate will not change the energy contribution from another coordinate, producing the most direct search path (fewest optimization steps) to a minimum on the potential energy surface (PES). In general, the coordinates used to specify the molecular geometry are coupled to some degree. However, a good choice of coordinates leads to a diagonal dominant Hessian, which minimizes the number of optimization steps. Here are a number of commonly used coordinate systems.

Cartesian Simplest choice to specify. A molecule has 3N Cartesian degrees of freedom, while a nonlinear molecule only has 3N-6 internal degrees of freedom (6 coordinates associated with translation and rotation of the center of mass only affect the net molecular kinetic energy), so some method is typically used to remove optimization steps that involve center of mass motions. Cartesians typically require the largest number of optimization steps because the Hessian in Cartesian coordinates is highly coupled.

Internal Coordinates This type is referred to as model builder or primitive internals, and includes stretches, bends, and torsions. They are commonly used because they involve natural "chemical" parameters to describe molecular geometry. A good set of internal coordinates will produce a diagonal dominant Hessian.

Symmetry Coordinates This is a general class of coordinates that are linear combinations of primitive internal coordinates. The secular equation describing the vibrational energy of a molecule is factored to the maximum extent possible by the use of symmetry [69].

Normal Mode Coordinates A set of 3N-6 orthogonal coordinates that correspond to the spectroscopic normal vibrational modes of a molecule. Because normal modes are orthogonal, the Hessian is diagonal, so an optimization in normal mode coordinates

is quite efficient. The drawback of normal mode coordinates is that they must be calculated, which is often more time consuming than performing an optimization using a poorer set of coordinates.

Natural Internal Coordinates (NIC) These are a type of local symmetry coordinates developed by Pulay [70, 71] based on localized normal modes within a molecule.

Efficiency of geometry optimization, the number of energy and gradient calculations needed to find a minimum on the PES, depends sensitively on the choice of coordinates. In general, internal coordinates are more efficient than Cartesian coordinates, with Pulay's NIC being the most efficient. A molecule has 3N-6 (3N-5 for linear molecules) independent degrees of freedom, so one may only specify 3N-6 internal coordinates. One can specify very many more than 3N-6 internal coordinates for some highly coupled molecules, e.g., molecular cages. It is sometimes impossible to specify a set of 3N-6 primitive internal coordinates that will perform well in a geometry optimization. Pulay has developed an optimization algorithm that allows the use of more than 3N-6 internal coordinates [72], but this algorithm has not been implemented in GAMESS. As the implementation of Pulay's redundant optimization scheme would have taken more time than available, an alternate approach was used to specify internal coordinates for IMOMM in this study.

Baker et al have recently described a set of symmetry coordinates that by their construction are guaranteed to be orthogonal and non-redundant [10]. To construct their coordinates, called delocalized coordinates (DLCs), one first specifies all the possible primitive internal coordinates for a molecule. The **B** matrix, the transformation matrix between displacements in internal coordinates and Cartesian displacements is first calculated.

$$S_t = \sum_{i=1}^{3N} B_{ti}\zeta_i, \qquad t = 1, nvar$$

$$\begin{aligned} N &: \text{ number of atoms in the molecule} \\ nvar &: \text{ number of internal coordinates specified } (\geq \text{3N-6}) \\ S_t &: \text{ one of nvar internal coordinates} \\ \zeta_i &: \text{ one of 3N Cartesian displacements} \end{aligned} \tag{3.15}$$

The spectroscopic G matrix,

$$\mathbf{G} = \mathbf{B}\mathbf{B}^T \tag{3.16}$$

is then calculated and diagonalized. Of the nvar eigenvalues of the **G** matrix, *exactly* 3N-6 will be non-zero, corresponding to the 3N-6 independent degrees of freedom of the molecule [69]. The eigenvectors of the **G** matrix are orthonormal by their construction, so the eigenvectors of the non-zero eigenvalues of the **G** matrix for a set of 3N-6 orthogonal coordinates are ideal for geometry optimization. Since these coordinates may contain a contribution from every primitive internal coordinate specified for the molecule, Baker et al named these delocalized Coordinates (DLCs). Two advantages of DLCs are the ease with which an automated algorithm for their specification can be written, and their performance in optimizations of cage molecules.

In this work, a simple code to construct DLCs for use with GAMESS was pieced together using the subroutines from MM3 that define a set of stretches, angles, and torsions and the subroutines from GAMESS that construct the B matrix and diagonalize the G matrix. (See Appendix D for more details about the present implementation of DLCs.) Some modifications to the GAMESS algorithm to convert displacements in symmetry coordinates to displacements in Cartesians were also required. The full functionality of DLCs as described in Reference [10] has not yet been implemented, most notably the ability to freeze individual primitive internal coordinates, e.g., selected stretches, angles, torsions, and combinations thereof. However, IMOMM can be successfully applied to the embedded cluster cages investigated in this work using DLCs.

3.5 Summary of GAMESS/MM3 implementation

A complete listing of the program modifications required to merge GAMESS with MM3 is found in Appendix E. A brief description is presented here.

3.5.1 Program flow. The overall flow of the MIMOMM hybrid optimization procedure using GAMESS and MM3 is (RUNTYP=HYBRID):

1. Perform the normal GAMESS initialization for a RUNTYP=OPTIMIZE
2. Call interface module to initialize the HYBRID specific pieces
   (a) Read the $MM3 input file, check for syntax errors
   (b) Calculate the MM3 energy at the initial geometry to check for logical errors in the MM3 connected and attached atom definition lists

3. Pass control back to GAMESS and begin the optimization sequence
4. Calculate the GAMESS energy and gradient for Regions 1 and 2 (1 and 5)
5. Call the interface module
   (a) Convert the coordinates of Region 2 to Region 3 (if required)
   (b) Call MM3 as a subroutine, passing the Region 1 and 3 coordinates as well as lists of the atoms in each Region
   (c) Perform MM3 optimization of Region 4 around a frozen Region 1 and 3 using gradients modified to zero out inter-Region 1 terms
   (d) Convert the MM3 Cartesian gradient to internal coordinates
   (e) Add the MM3 gradient on Region 1 to the GAMESS gradient on Region 1 to form the hybrid gradient
6. Pass hybrid gradient back into the GAMESS optimization loop
7. Check for convergence and calculate the next optimization step using the hybrid gradient
8. Repeat until convergence is reached in GAMESS

The interface between GAMESS and MM3 is performed by a separate code module to minimize the changes required to GAMESS.

The modifications required to implement the HOP in GAMESS are minor. A new runtype, HYBRID, is added as an option. The input file for a HYBRID optimization contains the normal GAMESS input plus two new groups: a $MM3 group which is a standard input file for MM3, as well as a $LINK group which contains information such as the hybrid method type, lists of the atoms in each Region, and the bond lengths for atoms in Regions 2 and 3 (if used). Depending on which merging procedure is used, IMOMM, MIMOMM, or Weiner, various internal coordinates need to be frozen in the normal GAMESS input, and various atom position must be frozen (restricted to use the MM3 term) in the $MM3 group.

The modifications required in MM3 are more extensive; however, many of them are mostly bookkeeping, i.e. deconflicting COMMON blocks and subroutine names between GAMESS and MM3. As MM3 is the (significantly) smaller code, names in MM3 routines were changed to resolve the conflicts. MM3 input and output is redirected to GAMESS input and output files, and the MM3 output was significantly reduced. (Each step in the HOP involves a complete MM3 optimization, which normally produces a large output

file. Most of the information in the MM3 output isn't needed in the HOP.) The gradient subroutines in MM3 are modified so that only interaction terms that include at least one atom in Region 4 contribute to the gradient. The specific modifications are listed in Appendix E.

3.5.2 An example: the Si_6H_{12}/Si_9H_{12} hybrid system. The Si_6H_{12}/Si_9H_{12} hybrid cluster is a convenient system to show a representative result of the modified IMOMM procedure as implemented in GAMESS using MM3. Figure 3.6 shows the setup of the hybrid cluster using Region 5 termination of the embedded cluster. Si_6H_{12}/Si_9H_{12} is an odd case as there are more Region 1 than Region 4 atoms. However, *ab initio* calculations on Si_9H_{12} can be readily performed, enabling verification of the hybrid procedure by comparison with *ab initio* results at the same level of theory.

Table 3.2 shows the result of an MM3 optimization step within the overall hybrid optimization procedure in GAMESS. The magnitude of the MM3 Cartesian gradients from Region 1-Region 4 interactions (the steric interaction of the BC on the EC), is substantial, on the order of $10^{-3}\frac{Hartree}{Bohr}$. Region 4 is allowed to optimize freely, and we see that the magnitude of the MM3 Cartesian gradients in Region 4 is quite small, $\leq 3.4 \times 10^{-7}\frac{Hartree}{Bohr}$. Some of the Region 4 Cartesian gradient projects onto the internal coordinates of Region 1 in this implementation of IMOMM; however, so long as the Region 4 residual gradient is several orders of magnitude smaller than the MM3 Region 3 gradient, this projection is unimportant.

Table 3.3 shows the MM3 Cartesian gradient above converted to internal coordinates for Region 1, and added to the GAMESS gradient to form the hybrid gradient. We see that the magnitude of the GAMESS and MM3 gradients are actually quite large, as much as 0.04 $\frac{Hartree}{Bohr}$. However, the MM3 and GAMESS gradients are opposite in sign so that their sum, the hybrid gradient, satisfies the GAMESS convergence criteria of OPTOL=$e^{-5}\frac{Hartree}{Bohr}$.

The net effect of the MM3 steric forces is quite dramatic in this example. Figure 3.7 shows the results of a GVB-PP(1) optimization of Si_6H_{12} by itself. All the silicons are planar. Figure 3.8 shows the results of the hybrid optimization Si_6H_{12}/Si_9H_{12}. With the

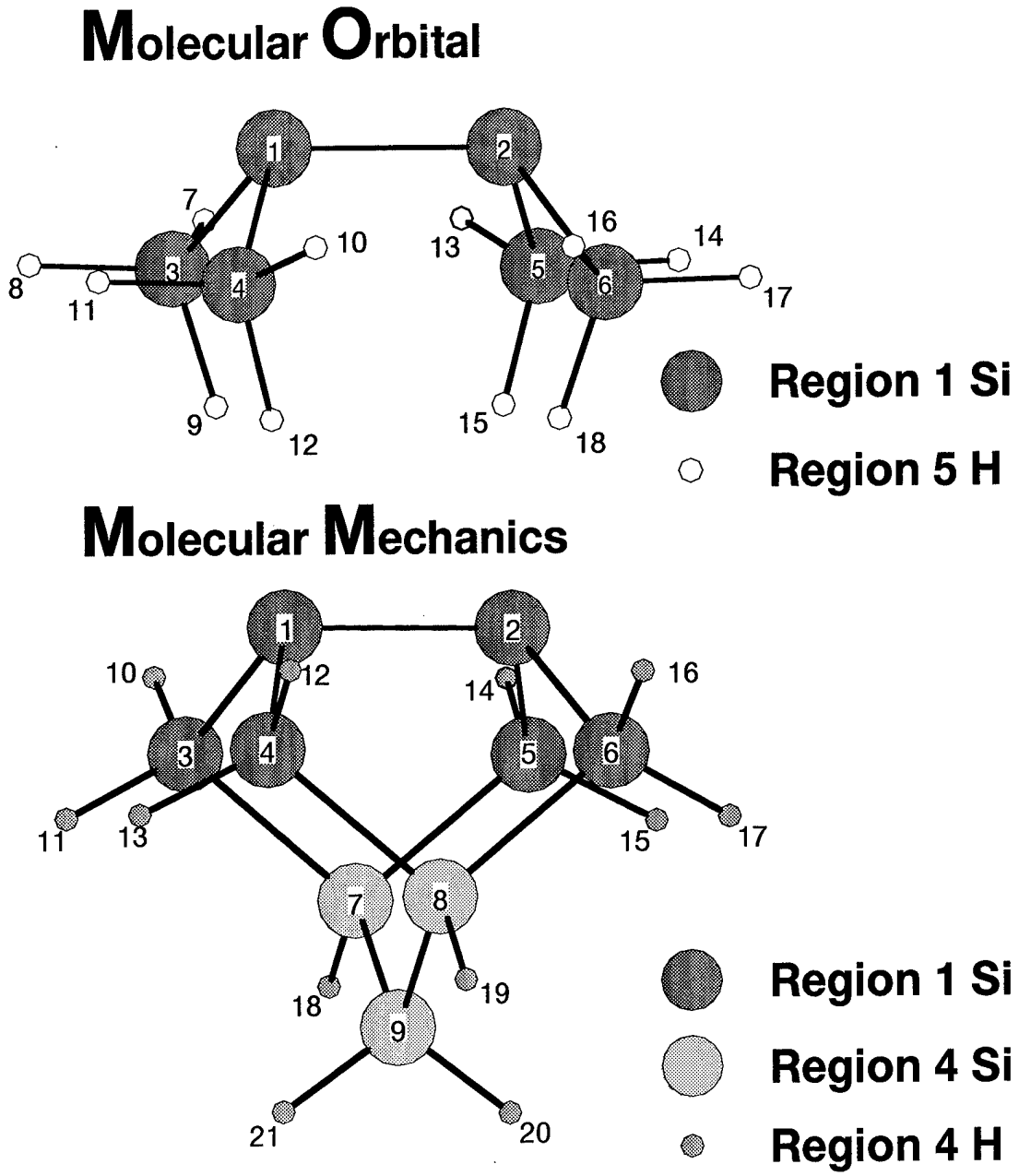

Figure 3.6 Si_6H_{12}/Si_9H_{12} embedded (MO) and hybrid (MM) clusters using Region 5 termination on the EC.

addition of the MM3 steric forces, Si_6H_{12} optimizes to a distinctly non-planar structure, which closely resembles the GVB-PP(1) optimized structure of Si_9H_{12}. Numerical comparisons are shown in Section 3.6.

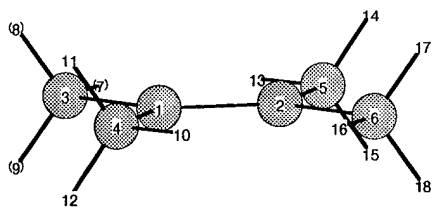

Figure 3.7 Si_6H_{12} *ab initio* optimized geometry

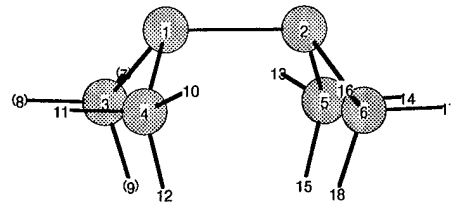

Figure 3.8 Si_6H_{12} MIMOMM optimized geometry

3.6 Comparison of methods

Table 3.4 shows a comparison of the two hybrid optimization techniques implemented in this work. The GVB-PP(1) optimized geometry of Si_9H_{12} is a result that the hybrid methods will hopefully reproduce. The MM3 optimized structure for Si_9H_{12} predicts a dimer length slightly larger than an Si-Si single bond length. The MM3 force field is parameterized only for sp^3 hybridized silicon, and so is unable to accurately model bonding in undercoordinated silicon. The results of both hybrid techniques are similar, and produce an Si_6H_{12} structure that is similar to the corresponding structure for these 6 atoms in Si_9H_{12}. As was shown qualitatively in Section 3.5.2, the hybrid structures for Si_6H_{12} are very different from the planar optimized structure for Si_6H_{12}. The differences between Weiner's method and MIMOMM are minor for this case. The largest difference is found in the last two torsion angles where MIMOMM agrees better with the full *ab initio* result. The differences in bond angles between MIMOMM and the full *ab initio* result are similar to other reported hybrid optimization results [4, 73, 65].

The primary advantage of a hybrid *ab initio*/MM method is that one can substantially increase the size of the bulk cluster while making minor impacts on the overall computational cost. Figure 3.9 shows a more representative hybrid cluster, Si_6H_{12} embedded within $Si_{38}H_{36}$. Increasing the bulk cluster size while keeping the embedded cluster

MM3 Cartesian Gradient			
Regions 1 and 3			
Atom No	X' (H/B)	Y' (H/B)	Z' (H/B)
1	.000002684	.009388175	-.009950734
2	-.000001956	-.009383519	-.009944423
3	-.002404246	-.009509900	.004962175
4	.002418841	-.009527420	.004985121
5	-.002418503	.009521604	.004985008
6	.002403241	.009510993	.004962602
Region 4 (residual)			
7	.000000159	.000000000	.000000107
8	-.000000303	-.000000007	.000000170
9	.000000042	.000000101	.000000344
10	-.000000034	.000000000	.000000021
11	.000000002	-.000000015	-.000000007
12	.000000013	.000000001	.000000010
13	-.000000005	-.000000026	-.000000013
14	-.000000027	.000000002	.000000018
15	.000000004	.000000037	-.000000016
16	-.000000001	.000000001	-.000000002
17	-.000000008	.000000057	-.000000024
18	-.000000022	.000000004	.000000016
19	.000000118	-.000000001	-.000000056
20	-.000000003	.000000009	-.000000217
21	.000000002	-.000000100	-.000000096

Table 3.2 MM3 Cartesian Gradient on frozen Region 1 atoms and optimized Region 4 atoms taken from a GAMESS .log file for an MIMOMM optimization of Si_6H_{12} embedded in Si_9H_{12}. The Region 4 gradient is $\leq 3.4x10^{-7}$ $\frac{Hartree}{Bohr}$(H/B).

Internal Coordinate	GAMESS Grad (H/B, H/R)	MM3 Grad (H/B, H/R)	HYBRID Grad (H/B, H/R)
d 2 1	-.00964296	.00964913	.00000618
d 3 1	-.00282949	.00282209	-.00000740
∠ 3 1 2	-.04046592	.04044593	-.00001998
d 4 1	-.00283912	.00283360	-.00000552
∠ 4 1 2	-.04050295	.04051407	.00001111
ω 4 1 2 3	-.02331093	.02331266	.00000173
d 5 2	-.00283716	.00282975	-.00000741
∠ 5 2 1	-.04051513	.04049657	-.00001856
ω 5 2 1 3	-.00011002	.00011170	.00000168
d 6 1	-.00282585	.00282013	-.00000572
∠ 6 2 1	-.04044872	.04045985	.00001112
ω 6 2 1 3	.02319669	-.02319692	-.00000023

Table 3.3 Converged hybrid gradient in internal coordinates taken from a GAMESS .log file from a MIMOMM optimization of Si_6H_{12} embedded in Si_9H_{12}. The *ab initio* and MM3 gradients are quite large, but opposite in sign.

Embedded (AI) Bulk (MM3)	Weiner Si_6H_{12} Si_9H_{12}	MIMOMM Si_6H_{12} Si_9H_{12}	Si_6H_{12} None	Si_9H_{12} None	None Si_9H_{12}
d 2 1	2.278	2.261	2.159	2.249	2.376
d 3 1	2.333	2.338	2.332	2.329	2.352
d 4 1	2.333	2.338	2.332	2.329	2.352
d 5 2	2.345	2.338	2.332	2.329	2.352
d 6 2	2.345	2.338	2.322	2.329	2.352
∠ 3 1 2	109.850	108.507	121.672	106.491	103.906
∠ 4 1 2	109.867	108.526	121.672	106.491	103.906
∠ 5 2 1	109.859	108.513	121.672	106.491	103.906
∠ 6 2 1	109.839	108.494	121.672	106.491	103.906
∠ 3 1 4	112.007	109.287	116.655	111.006	108.461
∠ 5 2 6	112.034	109.287	116.654	111.006	108.461
ω 3 1 2 5	0.000	-0.003	0.000	0.000	0.000
ω 4 1 2 3	123.645	118.654	0.000	118.524	113.414
ω 6 2 1 5	-123.666	-118.665	0.000	-118.524	-113.414

Table 3.4 Comparison of embedding schemes on Si_6H_{12} embedded cluster. *Ab initio* calculations are GVB-PP(1), HW ECP basis set.

constant provides useful insight on how large a bulk cluster is needed to give an accurate representation of mechanical environment of the lattice.

Table 3.5 shows a comparison of the two hybrid methods on the $Si_6H_{12}/Si_{38}H_{36}$ hybrid cluster. The *ab initio* calculations were performed using the restricted Hartree Fock (RHF) method, which incorrectly models the Si-Si dimer as a double bond. Here we see an important difference between Weiner's method and MIMOMM. With Weiner's method, MM3 fixes the positions of atoms 3,4,5, and 6, so the only way GAMESS can reduce the gradient on the dimer is to elongate that bond. In MIMOMM, MM3 provides a force on all 6 atoms that limits their displacements, but the combination of MM3 and GAMESS forces allows the structure to relax in a way more consistent with the *ab initio* model of the embedded cluster.

Use of Weiner's method requires freezing more coordinates in the embedded cluster, so that the MM calculation has a greater influence on the embedded cluster than MIMOMM. Weiner's method is also faster than MIMOMM (37 minutes on a Sun Sparc 20 compared to 107) because only one internal coordinate is relaxed in the Weiner hybrid optimization, compared to 12 relaxed internal coordinates for MIMOMM. It is undesir-

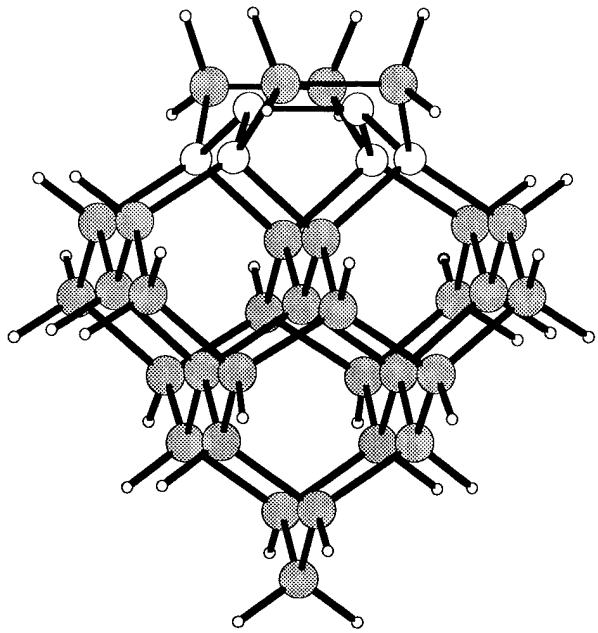

Figure 3.9 $Si_6H_{12}/Si_{38}H_{36}$ hybrid cluster. The Region 1 atoms are highlighted.

able for the MM bulk cluster to have this much influence on the embedded cluster since one considers the *ab initio* calculation on the embedded cluster to be a better theoretical model.

Weiner et al. applied their merging technique to hybrid clusters for which the embedded cluster was quite large, around 40 heavy atoms (a semiempirical method was used for the embedded cluster because of its size). The boundary of an embedded cluster this large is far enough away from the site of interest that the QM calculation still dominates. For smaller embedded clusters, the MM determined positions of the boundary atoms can dominate the *ab initio* model of the embedded cluster, so MIMOMM seems to be a better approach than Weiner.

Embedded (AI) Bulk (MM3)	WEINER Si_6H_{12} $Si_{38}H_{36}$	MIMOMM Si_6H_{12} $Si_{38}H_{36}$	Si_6H_{12} None	$Si_{38}H_{36}$ None	None $Si_{38}H_{36}$
d 2 1	2.257	2.174	2.159	2.180	2.370
d 3 1	2.373	2.337	2.322	2.338	2.350
d 4 1	2.373	2.337	2.322	2.338	2.350
d 5 2	2.373	2.337	2.322	2.338	2.350
d 6 2	2.373	2.337	2.322	2.338	2.350
∠ 3 1 2	106.244	109.333	121.672	107.005	104.252
∠ 4 1 2	106.244	109.343	121.672	107.005	104.252
∠ 5 2 1	106.244	109.340	121.672	107.005	104.252
∠ 6 2 1	106.244	109.328	121.672	107.005	104.252
∠ 3 1 4	111.444	117.683	116.655	119.100	112.858
∠ 5 2 6	111.246	117.651	116.654	119.100	112.858
ω 3 1 2 5	0.000	-0.005	0.000	0.000	0.000
ω 4 1 2 3	118.557	130.162	0.000	128.707	118.557
ω 6 2 1 5	-118.557	-130.115	0.000	-128.707	-118.557

Table 3.5 Comparison of embedding schemes on $Si_6H_{12}/Si_{38}H_{36}$ hybrid cluster. *Ab initio* calculations are RHF, HW ECP basis set.

3.7 Models of the Dimerized Si(001) Surface

3.7.1 Low Index Surfaces of a Cubic Lattice. The goal of this research is to use MIMOMM to investigate the chemistry of SiC(111) surfaces, so before we discuss calculations on hybrid cluster models of silicon surfaces, a brief description of the terminology used to describe is helpful. (See References [74, 75] for more complete discussions.) There are 14 unique 3-D Bravais lattice types. These lattice types are specified in terms of the atom spacing along 3 axes, $\vec{a_1}$, $\vec{a_2}$, and $\vec{a_3}$ and the angles between the axes, α, β, and γ. Distance along each axis is specified in terms of atom spacing, e.g., a_1 is the distance between two adjacent atoms in the $\vec{a_1}$ direction. For the three cubic Bravais lattices, cubic, body-centered cubic (bcc), and face-centered cubic (fcc):

$$a_1 = a_2 = a_3,$$
$$\alpha = \beta = \gamma = 90^\circ.$$

Silicon, diamond, and silicon carbide are all fcc lattices, the only differences among the three are the bond lengths: 2.35 $\AA$ for silicon, 1.54 $\AA$ for diamond, and 1.89 $\AA$ for silicon carbide. A surface is created by cleaving the crystal in a plane. The orientation of a crystal plane is determined by three points in the plane, provided they are not collinear. The specification of the plane is determined by where this plane intercepts the $\vec{a_1}$, $\vec{a_2}$, and $\vec{a_3}$ axes. If each point lay on a different crystal axis, the plane could be specified by giving coordinates of the point in terms of the lattice constants a_1, a_2, and a_3. However, for structure analysis it is more useful to specify the orientation of the plane determined by the following rules:

- Find the intercepts of the plane in terms of the lattice constants a_1, a_2, a_3. If the plane is parallel to one of the axes, the intercept is taken to be at ∞
- Take the reciprocal of these numbers and reduce these 3 to the smallest three integers having the same ratio. The result, enclosed in parentheses (hkl), is called the index of the plane.

This procedure is illustrated in Figure 3.10. Here, we have a plane intercepting the $\vec{a_1}$,$\vec{a_2}$,$\vec{a_3}$ axes at $3a_1$, $2a_2$, and $2a_2$. The reciprocals of these numbers are $\frac{1}{3}, \frac{1}{2}, \frac{1}{2}$ The three smallest integers having this ratio are 2,3,3, so the indices for this plane are (233). If a plane intercepts an axis on the negative side of the origin, the corresponding index is

negative, which is indicated by placing a minus sign *above* that index: $(h\bar{k}l)$. The cube faces of the cubic crystal are (100), (010), (001), $(\bar{1}00)$, $(0\bar{1}0)$, and $(00\bar{1})$. The (001), (110), and (111) planes of the cubic lattice are shown in Figure 3.11

For silicon semiconductor devices, the (001) surface is most commonly used in device fabrication. For silicon carbide, the (111) surface is of highest interest. Figure 3.12 shows a portion of the SiC lattice lattice, cleaved along the (001) and (111) directions, to highlight the initial positions of the atoms on these surfaces. (The presence of dangling bonds on the surface atoms means they are very reactive, and depending on the surface, often forming bonds each other. The movement of the surface atoms away from their lattice positions is known as reconstruction.) The (001) surface has been well characterized experimentally and theoretically, making it a good case to benchmark the modified IMOMM procedure.

3.7.2 Previous Cluster Models of the dimerized Si(001) surface. The dimerized silicon (001) surface is of high technological interest in device fabrication, and has been the subject of numerous theoretical and experimental studies [8, 31, 76, 77, 78] to name a few. Comprehensive reviews of silicon surfaces and surface chemistry are given by Haneman [79] and Neergard and Yates [80]. Figure 3.13 shows an illustration of the dimerization of the unreconstructed silicon surface. Consider a piece of crystalline silicon which has been cleaved parallel to the (001) crystal axis. Initially, the two surface silicon atoms (Layer 1 in Figure 3.13 are 3.84 $\AA$ apart, and each have two dangling bonds that had been involved in bonding with Layer 0 before cleavage. As is shown in Figure 3.13, the orientation of two of these dangling bonds is favorable for bond formation between the two surface silicon atoms. After the dimer bond is formed, the separation between the surface atoms shrinks by nearly 1.5 $\AA$ to approximately the Si lattice bond distance of 2.35 $\AA$. The effect of this large atom displacement on the surface propagates several layers down into the lattice.

An alternate configuration for a silicon surface dimer, the buckled dimer, is also shown in Figure 3.13 (A wide range of values have been reported experimentally for the 1-1 length of the buckled dimer, though most report a value greater than the Si-Si bulk separation of 2.35$\AA$. *A consensus on the minimum energy reconstruction of the dimerized Si(001) surface does not exist, though the majority of references tend to favor buckling [80].*

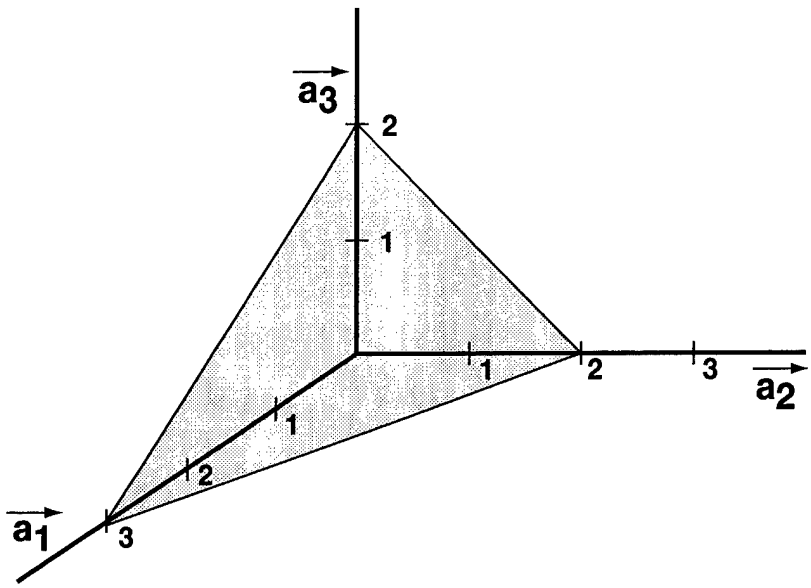

Figure 3.10 Determination of the indices of a lattice surface plane. The plane shown has intercepts of $3a_1$, $2a_2$, and $2a_3$, resulting in plane indices of (233).

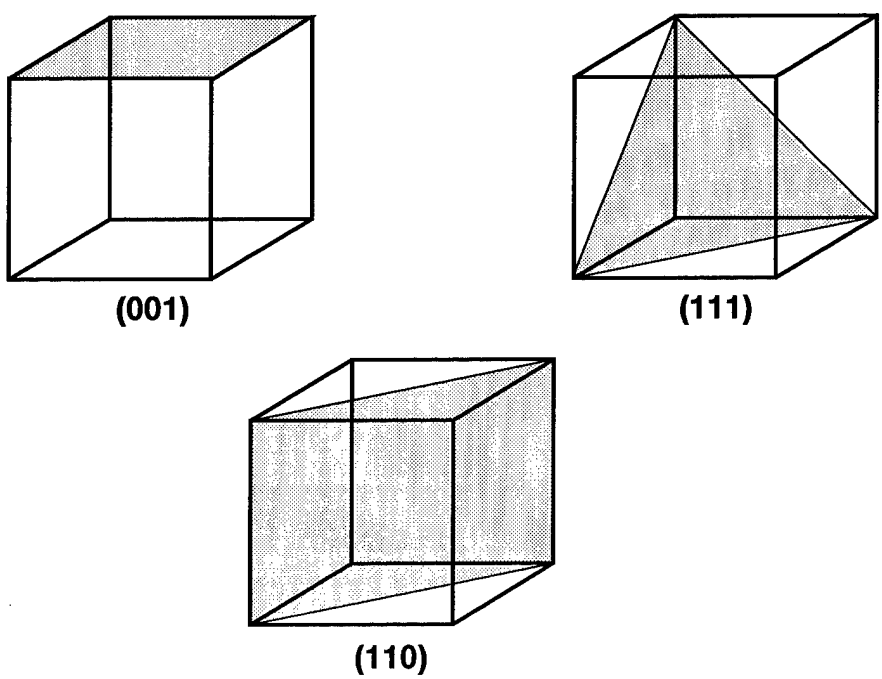

Figure 3.11 The (001), (110), and (111) planes of a cubic lattice.

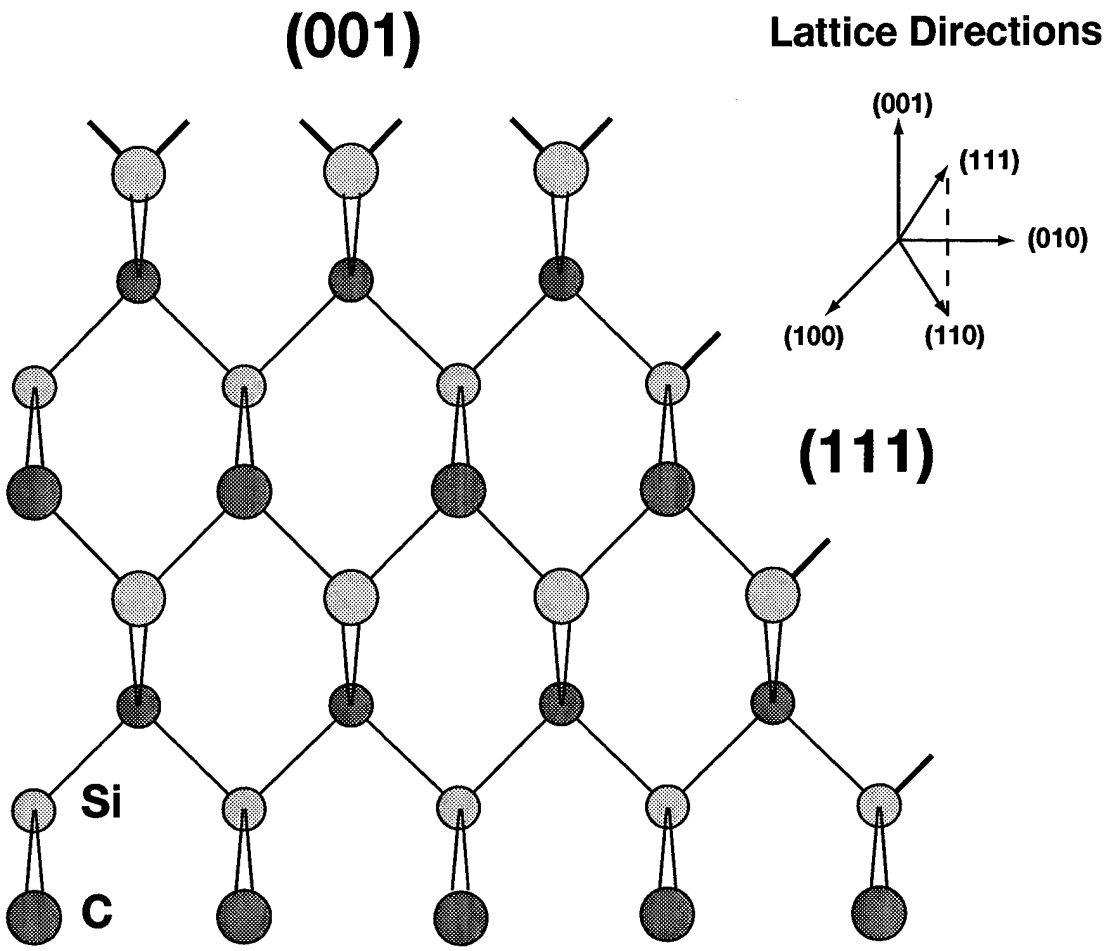

Figure 3.12 Section of an ideal tetrahedrally bonded cubic lattice showing three low index surfaces. Coplanar atoms are shown as the same size. The two planes shown parallel to the page are the (110) surface. The bonds drawn as tapering make on angle of 57.7° with the plane of the page. Dangling bonds are correctly indicated for the two ideal surfaces labeled. Each (110) surface atom also has a fourth bond, at a tetrahedral angle to the other three, to an atom above or below the (110) planes that is not shown. For bulk silicon and diamond, atoms would be either all Si or C.

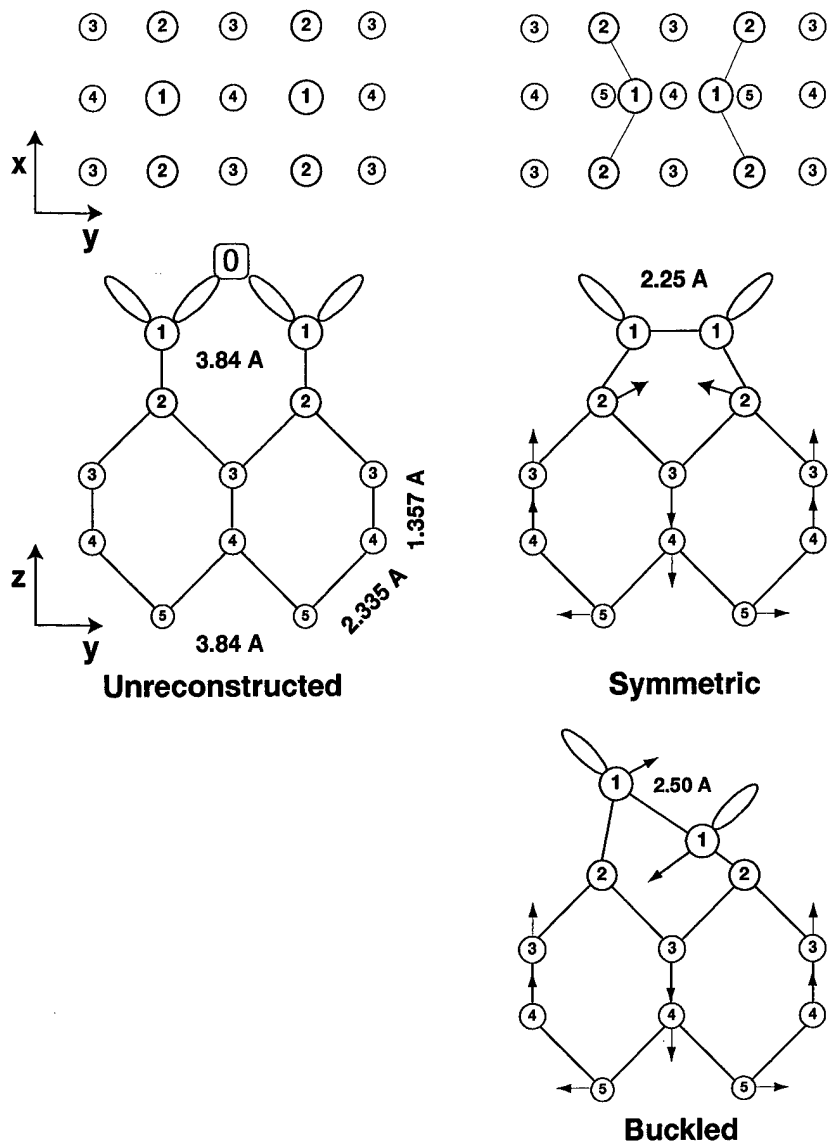

Figure 3.13 Dimerization of a silicon (001) surface. The arrows indicate the direction of atom displacements induced by the formation of the surface dimer.

Most experimental references report some degree of buckling on the surface, while most theoretical work has focused on the symmetric dimer configuration. Goddard first reported that the lowest energy configuration for a dimer in a small silicon cluster model, Si_9H_{12} shown in Figure 3.14, is the symmetric geometry [81]. The proper description of the symmetric dimer is a singlet biradical, so the lowest simplest *ab initio* theory required to accurately model the dimer is GVB-PP(1).

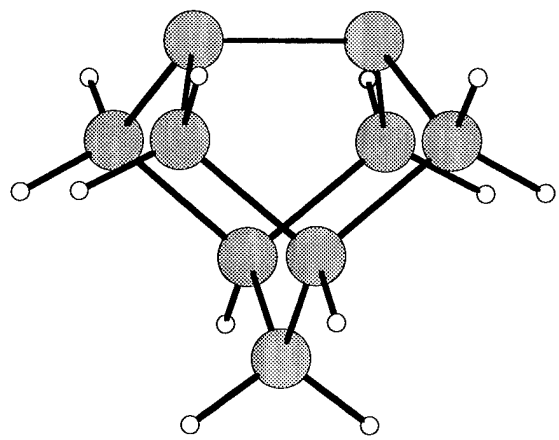

Figure 3.14 Si_9H_{12} model of a single dimer on a Si(001) surface

Si_9H_{12} has been commonly used as a model of the dimerized Si(001) surface because it is large enough to contain a silicon dimer, yet small enough to be readily modeled with *ab initio* methods (including electron correlation). However, Si_9H_{12} has two primary limitations as a model for a silicon surface. First, it seems rather small to accurately represent the steric effects of bulk silicon Second, it contains more hydrogen than silicon atoms, so one might suspect that the chemistry of this cluster is dominated by the hydrogen termination.

The dimer bond length would seem to be a simple measure of the ability of a small silicon cluster to model an actual surface dimer. Even for the symmetric geometry, reported values for the dimer length vary substantially. Table 3.6 lists a number of computational results for the length of silicon surface dimer in Si_9H_{12}.(The calculations listed in this table that were performed in this work will be discussed in Section 3.7.3.) In Table 3.6, we see

Reference	Method	Basis Set	Subsurface	Termination	Length ($\AA$)
This work	RHF	HW ECP(d)	Optimized	H	2.18
This work	TCSCF	HW ECP(d)	Optimized	H	2.24
This work	GVB-PP(1)	6-31G*	Optimized	H	2.28
[8]	GVB-PP(2)	ECP(d) *(dimer)*	Optimized	$\overline{H}$	2.25
[82]	DFT	n/a	Optimized	n/a	2.23
[83]	TCSCF	DZP *(dimer)*	Fixed (lattice)	H	2.32
[84]	CI	Dunning [85] *(dimer)*	Fixed (lattice)	H	2.40
[81]	GVB-PP(2)	ECP(d) *(dimer)*	Fixed (lattice)	$\overline{H}$	2.47
$Si_{66}H_{52}$ This work	GVB-PP(1)	HW ECP(d) Si_9	Optimized	Si	2.27
[86]	**Experiment**	n/a	n/a	n/a	2.26± 0.1

Table 3.6 Comparison of symmetric dimer length in Si_9H_{12}. The bulk lattice Si-Si separation is 2.35 $\AA$.

that an incorrect RHF model of the dimer produces a Si-Si double bond, resulting in a dimer separation of 2.18$\AA$. The TCSCF result from this work and Carter's GVB-PP(2) are from unconstrained optimizations of the entire Si_9H_{12} cluster ($Si_9\overline{H}_{12}$ in Carter's case). ($\overline{H}$ refers to an artificial hydrogen atom that is discussed in Chapter IV.) Modeled as a singlet biradical, the Si dimer length of 2.25$\AA$ is roughly halfway between the RHF result of 2.18$\AA$ and the Si-Si bond length in bulk silicon of 2.35$\AA$. The DFT result [82] was calculated using a periodic, 2-D slab calculation. This slab model should insure a good representation of the steric constraints of bulk silicon. Other similar DFT slab calculations also report a symmetric silicon dimer bond length around 2.26$\AA$.

The ability of Si_9H_{12} to accurately model the steric effects of bulk silicon is questionable. One method to make Si_9H_{12} behave more like the bulk material is to fix all the silicon atoms in lattice positions *except the 2 atoms in the dimer, which are allowed to move freely.* This approach was used by Nachtigall et al [83], Whitten et al [87], and Redondo and Goddard [81]. Nachtigall et al [83] used Si_9H_{12}, while Jing and Whitten [87] used a slightly larger silicon cluster, $Si_{12}H_{20}$. Redondo and Goddard [81] used $Si_9\overline{H}_{12}$, with the subsurface silicon atoms and the $\overline{H}$ atoms fixed at silicon lattice positions. We see in

Table 3.6 that the dimer length in the models which fixed the subsurface atoms are consistently longer than the dimer lengths calculated without constraints on the subsurface atoms, and longer than Wang's experimental result of 2.26± 0.1$\AA$. The $Si_{66}H_{52}$ cluster modeled in this work is an attempt to provide a better representation of the bulk silicon without having to resort to fixing atom positions. The singlet biradical model for this case results in a dimer length of 2.27$\AA$, which is more consistent with the unconstrained optimized results from the small silicon clusters, and with the experimental result.

Which of these results is best? Most of the results in Table 3.6 fall within the uncertainty of Wang et al's measurement, so based only on the dimer length it's difficult to judge which one is better than the other.(The relatively large uncertainty in the measured dimer length, compared with measurements of bond lengths in bulk crystals, reflects the difficulty of the surface measurement.) Substantial subsurface atom displacements caused by reconstruction on the surface have been measured, so the longer dimer bonds resulting from fixed subsurface atom positions seem to be an artifact of this approximation. At this juncture, a more detailed investigation of silicon cluster models of the symmetric dimer is needed.

The RHF result models the dimer as a double bond. The Si-Si single bond length in bulk silicon is 2.35$\AA$. The lowest energy configuration for the dimer includes singlet coupling of the dangling bonds, so one might expect a bond order of roughly 1.5. The GVB result of 2.26$\AA$ falls about halfway between the single and double bond lengths, and is consistent with the bond order argument. Fixing the subsurface atoms is one way to approximate the steric effects of the bulk lattice, and has the effect of increasing the dimer length to values about or larger than the Si-Si lattice separation of 2.35 $\AA$. However, this approach is slightly unphysical because the subsurface atoms are too restricted. One expects *some* subsurface atom displacement in response to the surface reconstruction [88], so these results confirm that fixing the subsurface atoms at lattice positions is not a good way to include bulk steric effects.

3.7.3 New Cluster Model of the Dimerized Si(001) Surface. The discussion of the Si(001) symmetric dimer in the previous section suggests some questions that need to be addressed:

1. How closely can a small silicon cluster match the *unreconstructed* bulk silicon geometry ?
2. How well does an ECP basis set match silicon geometry ?
3. How do atom displacements from small cluster models of the symmetric silicon dimer compare to calculated displacements in large clusters, and experiment ?

A series of *ab initio* optimizations were performed on $Si_{10}H_{16}$ and Si_9H_{12} to address the first two questions. In $Si_{10}H_{16}$, all the Si atoms are tetrahedrahelly coordinated, as is bulk silicon. Figure 3.15 shows the optimized geometries for these two molecules. The comparison of the 6-31G* optimized geometry for $Si_{10}H_{16}$ with bulk silicon lattice values shows differences between these two results of approximately 0.02$\AA$ for bond lengths and 0.4° for the bond angles. For Si_9H_{12}, the differences between the 6-31G* and HW ECP(d) optimized geometries are approximately 0.04$\AA$ for bond lengths and 0.5° for bond angles. We see the HW ECP(d) basis set gives a good prediction for the bulk geometry, and differs by a small amount from the 6-31G* predictions.

Another way of describing the change in the geometry of Si_9H_{12} from bulk-like silicon is to list the differences between the optimized atom positions and the corresponding lattice positions. This description is consistent with reports of measured atom displacements caused by surface reconstruction. For Si_9H_{12}, these displacements would be interpreted as atom displacements caused by symmetric dimer formation. Figure 3.16 shows the GVB-PP(1) optimized geometry of Si_9H_{12}. Si atom displacements from lattice positions are indicated by arrows. We see that the atoms in the dimer each move approximately 0.8$\AA$ closer to each along the y axis, and 0.15$\AA$ down from the lattice positions. The second "layer" atoms are dragged along by the surface atoms, and are drawn closer together. (Identification of layers in the atom is done for comparison with larger models and experiment.) The displacement of the second layer atoms drives the third layer atoms down roughly 0.1$\AA$, while the position of the fourth layer atom is nearly unchanged. The differences in atom displacements between the HW ECP(d) and 6-31G* basis set results are approximately 0.01$\AA$.

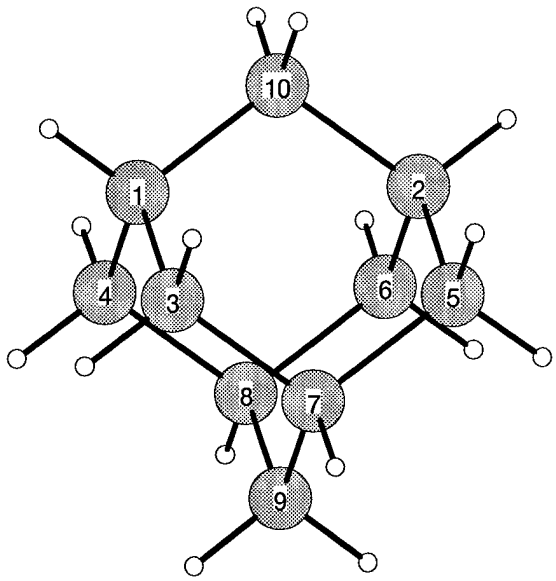

$Si_{10}H_{16}$

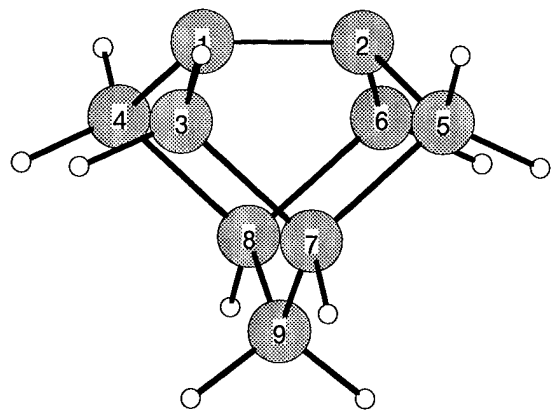

Si_9H_{12}

	LATTICE	$Si_{10}H_{16}$		Si_9H_{12}			
		RHF		RHF		GVB-PP(1)	
		HWECP(d)	6-31G*	HWECP(d)	6-31G*	HWECP(d)	6-31G*
Dist Å							
1 2	3.840	3.828	3.888	**2.151**	**2.187**	**2.241**	**2.280**
1 3	2.352	2.342	2.376	2.320	2.355	2.329	2.363
3 7	2.352	2.342	2.376	2.353	2.385	2.346	2.379
7 9	2.352	2.342	2.376	2.364	2.396	2.358	2.391
1 10	2.352	2.342	2.376	n/a	n/a	n/a	n/a
Angle°							
3 1 2	90.000	89.916	89.847	107.511	107.300	106.294	106.062
3 1 4	109.470	109.376	109.294	115.901	116.494	112.485	112.833
3 7 5	109.470	109.658	109.830	**97.877**	**97.552**	**98.249**	**97.907**
7 9 8	109.470	109.660	109.829	116.993	117.460	115.743	116.089
1 10 2	109.470	109.660	109.829	n/a	n/a	n/a	n/a

Figure 3.15 Comparison of *ab initio* optimized geometries of $Si_{10}H_{16}$ and Si_9H_{12}.

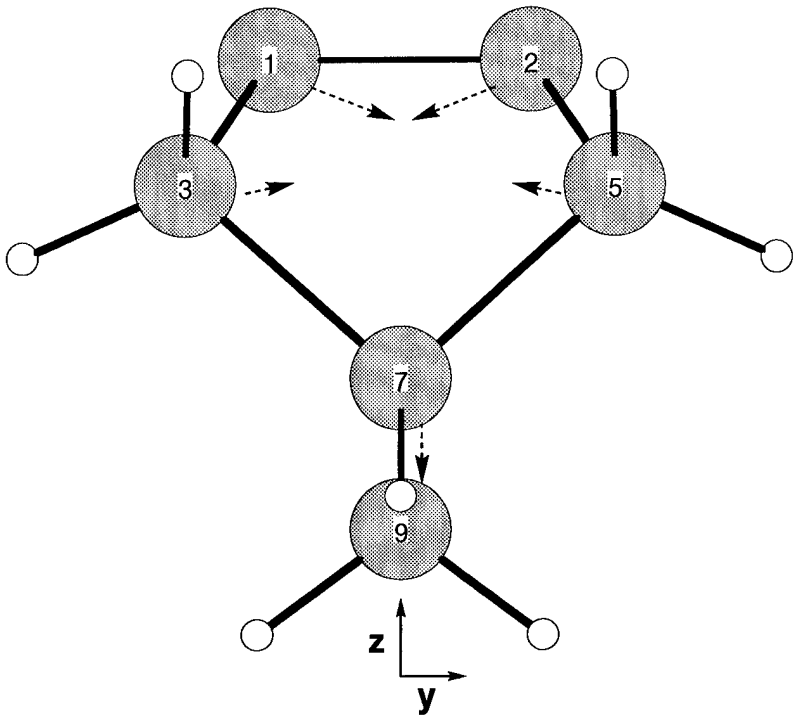

Atom Displacements ($\AA$) Caused by Symmetric Dimer Formation in Si_9H_{12} GVB-PP(1) Optimization						
Atom	HW ECP(d)			6-31G*		
	δ x	δ y	δ z	δ x	δ y	δ z
Surface						
1	0.000	0.794	-0.154	0.000	0.804	-0.152
2	0.000	-0.794	-0.154	0.000	-0.804	-0.152
Layer 2						
3	0.026	0.137	0.083	0.031	0.144	0.091
4	-0.026	0.137	0.083	-0.031	0.144	0.091
5	0.026	-0.137	0.083	0.031	-0.144	0.091
6	-0.026	-0.137	0.083	-0.031	-0.144	0.091
Layer 3						
7	0.083	0.000	-0.098	0.085	0.000	-0.095
8	-0.083	0.000	-0.098	-0.085	0.000	-0.095
Layer 4						
9	0.000	0.000	-0.003	0.000	0.000	0.004

Figure 3.16 Atom displacements induced by symmetric dimer formation in the Si_9H_{12} model of the Si(001) surface. The differences between the atom displacements calculated at the HW ECP(d) and 6-31G* basis sets are 0.01$\AA$. Layers are identified for later comparisons; in reality, identification of layers for such a small molecule is questionable.

Figure 3.17 shows the $Si_{66}H_{52}$ cluster used in this work to model symmetric dimer formation on the Si(001) surface. The atoms highlighted in this figure are the 9 silicon atoms $Si_{66}H_{52}$ has in common with Si_9H_{12}. The reason for establishing the accuracy of the HW ECP(d) basis set in predicting geometry should be readily apparent after looking at this figure. At 6-31G*, $Si_{66}H_{52}$ contains 1358 basis functions, which makes a geometry optimization impractical at this level. At HW ECP(d), $Si_{66}H_{52}$ contains 1028 basis functions, still too large for a geometry optimization. As a compromise, the HW ECP(d) basis set was used for the 9 silicon atoms which $Si_{66}H_{52}$ has in common with Si_9H_{12}. The HW ECP was used for the remaining atoms in the cluster. With this compromise, the cluster contained 686 basis functions. *A GVB-PP(1) geometry optimization of $Si_{66}H_{52}$ using C_{2v} symmetry took 100 hours on 32 processors on an IBM SP2.*

Two additional views of $Si_{66}H_{52}$ are shown in Figures 3.18 and 3.19. Figure 3.18 shows the view of the surface. The displacement of the surface atoms forming the dimers is clear in this view. $Si_{66}H_{52}$ contains both a bare surface dimer (atoms 1 and 2) and two hydrogenated surface dimers (atoms 10-12 and 11-13). Because the H atoms saturate the dangling bonds on the surface dimer, the Si-Si bond in a hydrogenated dimer is best described as a Si-Si single bond. The calculated length of the hydrogenated dimer in $Si_{66}H_{52}$ is 2.41$\AA$, with a Si-H bond length of 1.475$\AA$, and a Si-Si-H bond angle of 111.795°. Craig et al [89] report values of 2.37$\AA$, 1.51$\AA$, and 108.5° respectively, for the same parameters from a slab MINDO calculation of the hydrogenated symmetric dimer. Northrup [90] reports values of 2.40$\AA$, 1.54$\AA$, and 109° for the hydrogenated dimer from a periodic DFT model. Wang et al [91] report experimental values for the symmetric, hydrogenated dimer of 2.97$\AA$ Si-Si separation, 1.22±0.15$\AA$ for the Si-H bond length, and 133±8° for the Si-Si-H bond angle. Wang et al derived these values by fitting their data to a symmetric dimer model. These values are difficult to believe for a symmetric dimer, and one suspects that their data is more consistent with the presence of buckled dimers in their experiment.

Table 3.7 lists the displacements from lattice positions for the atoms in $Si_{66}H_{52}$. We see that this calculation predicts that the formation of dimers on the surface displaces atoms 8 "layers" down. For a given layer, atom displacements near the edges tend to be slightly larger than for atoms closer to the center. The Si_9 atoms that $Si_{66}H_{52}$ has in common with

Si_9H_{12} are buried in the center of the molecule, and so these atom displacements are most representative of bulk silicon.

Now for the real test. Table 3.8 shows a comparison of the GVB-PP(1)/HW ECP(d) calculated atom displacements using the Si_9H_{12} and $Si_{66}H_{52}$ clusters with two experimental measurements of subsurface atom displacements induced by dimer reconstruction of the Si(001) surface. Felici et al [92] used X-ray diffraction in their measurements. Tromp et al [93] report results from ion beam crystallography. Also included in this table is Roberts' and Need's [94] slab (periodic) DFT calculations on the dimerized Si(001) surface, which includes results for both symmetric and buckled dimers. One observes that:

- The predicted atom displacements from the Si_9H_{12} and $Si_{66}H_{52}$ agree qualitatively, but differ quantitatively from each other.
- Atom displacements for buckled and symmetric dimers show the greatest differences in the first two layers where the displacement are largest, but differences persist as far as 4 layers below the surface
- The atom displacements from the calculated symmetric dimer obtained by Roberts and Need and from the the $Si_{66}H_{52}$ cluster model calculated in this work agree better with the experimental results than the displacements from their buckled dimer model.

A very interesting result from Roberts' and Need's calculations is that the energy difference between the buckled and symmetric dimer is predicted to be very small, *with the buckled dimer only 0.35* $\frac{kcal}{mol}$ *lower in energy than the symmetric dimer, roughly* $\frac{1}{2}$ *thermal energy at room temperature.* In the cluster results from this work, the use of C_2v symmetry on $Si_{66}H_{52}$ forced symmetric dimer formation. Buckled dimers were not observed in optimizations Si_9H_{12} even when no symmetry constraints were applied. However, if one uses lattice positions as the starting point for Si_9H_{12}, the inherent C_2v symmetry in this structure may favor symmetric dimers. A limited search for buckled dimer formation on the Si_9H_{12} was performed using the AM1 semiempirical method by starting from asymmetric geometries. No buckled dimers resulted from this attempt; however, with such a small energy difference between the buckled and symmetric dimers one expects difficulty in converging to the buckled result with a cluster probably biased towards the symmetric result.

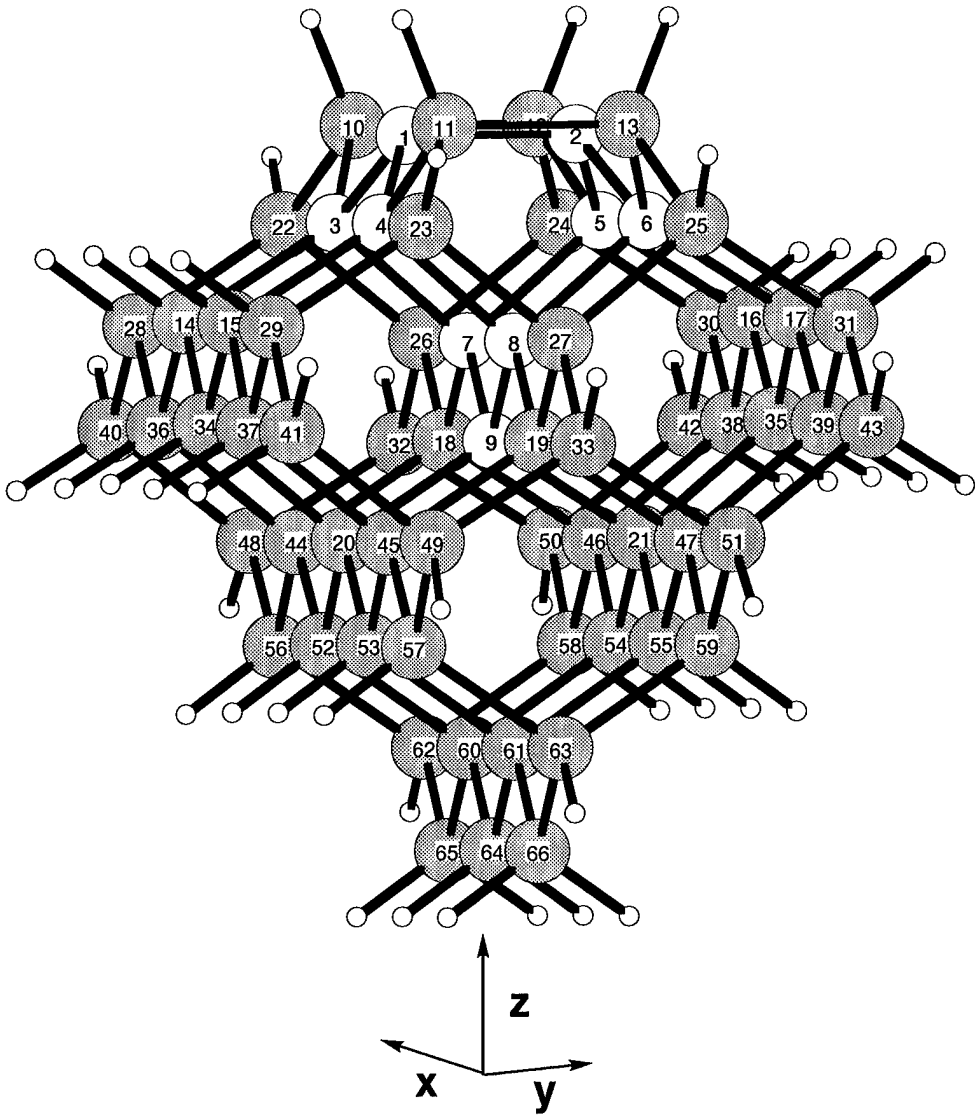

Figure 3.17 *Ab initio* GVB-PP(1) optimized geometry of $Si_{66}H_{52}$, HW ECP(d) basis set. This view is rotated slightly off the yz plane so that all the atom numbers are visible.

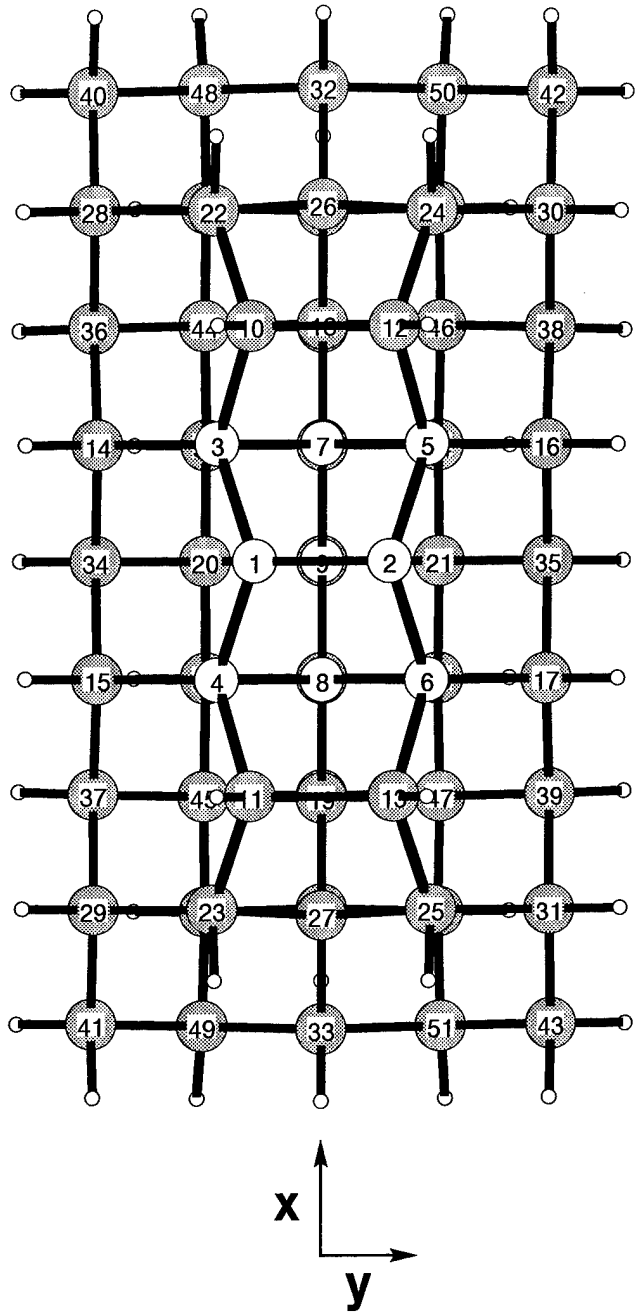

Figure 3.18 *Ab initio* GVB-PP(1) optimized geometry of $Si_{66}H_{52}$, HW ECP(d) basis set. Atoms 1,2 10,12 and 11,13 are in the surface. Atoms 1,2 form the bare dimer. Atoms 10,12 and 11,13 form hydrogenated dimers. The length of the hydrogenated dimers is 2.41$\AA$, slightly longer than the Si-Si bulk bond length of 2.35$\AA$.

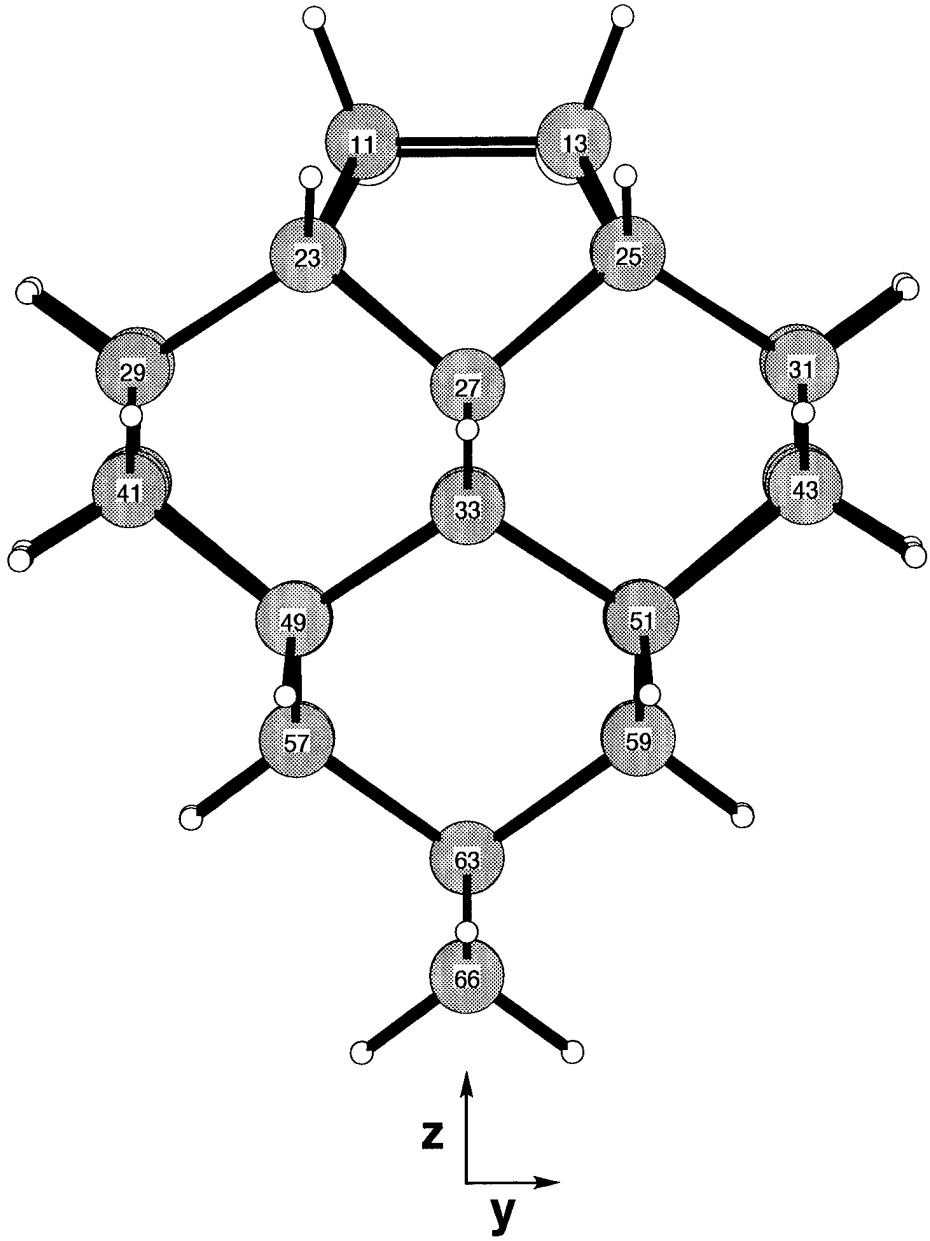

Figure 3.19 *Ab initio* GVB-PP(1) optimized geometry of $Si_{66}H_{52}$, HW ECP(d) basis set, subsurface view.

Atom Displacements (Å) Caused by Symmetric Dimer Formation in $Si_{66}H_{52}$							
Atom	δ x	δ y	δ z	Atom	δ x	δ y	δ z
Surface				Layer 5			
1	**0.000**	**0.786**	**-0.254**	20	0.000	-0.033	-0.034
2	**0.000**	**-0.786**	**-0.254**	21	0.000	0.033	-0.034
10	-0.044	0.713	-0.131	44	-0.044	-0.049	-0.060
11	0.044	0.713	-0.131	45	0.044	-0.049	-0.060
12	-0.044	-0.713	-0.131	46	-0.044	0.049	-0.060
13	0.044	-0.713	-0.131	47	0.044	0.049	-0.060
Layer 2				48	-0.055	-0.066	-0.050
3	**-0.041**	**0.168**	**0.003**	49	0.055	-0.066	-0.051
4	**0.041**	**0.168**	**0.003**	50	-0.055	0.066	-0.051
5	**-0.041**	**-0.168**	**0.003**	51	0.055	0.066	-0.051
6	**0.041**	**-0.168**	**0.003**	Layer 6			
22	-0.030	0.097	-0.027	52	-0.016	-0.012	-0.031
23	0.030	0.097	-0.027	53	0.016	-0.012	-0.031
24	-0.030	-0.097	-0.027	54	-0.016	0.012	-0.031
25	0.030	-0.097	-0.027	55	0.016	0.012	-0.031
Layer 3				56	-0.058	-0.021	-0.053
7	**-0.043**	**0.000**	**-0.172**	57	0.058	-0.021	-0.053
8	**0.043**	**0.000**	**-0.172**	58	-0.058	0.021	-0.053
14	-0.020	0.105	0.116	59	0.058	0.021	-0.053
15	0.020	0.105	0.116	Layer 7			
16	-0.020	-0.105	0.116	60	-0.012	0.000	-0.033
17	0.020	-0.105	0.116	61	0.012	0.000	-0.033
26	-0.127	0.000	-0.140	62	-0.018	0.000	-0.033
27	0.127	0.000	-0.140	63	0.018	0.000	-0.033
28	-0.024	0.048	0.055	Layer 8			
29	0.024	0.048	0.055	64	0.000	0.000	-0.015
30	-0.024	-0.048	0.055	65	-0.021	0.000	-0.024
31	0.024	-0.048	0.055	66	0.021	0.000	-0.024
Layer 4							
9	**0.000**	**0.000**	**-0.109**	36	-0.008	0.041	0.087
18	-0.070	0.000	-0.116	37	0.008	0.041	0.087
19	0.070	0.000	-0.116	38	-0.008	-0.041	0.087
32	-0.108	0.000	-0.156	39	0.008	-0.041	0.087
33	0.108	0.000	-0.156	40	-0.021	0.010	0.050
34	0.000	0.070	0.134	41	0.021	0.010	0.050
35	0.000	-0.070	0.134	42	-0.021	-0.010	0.050
				43	0.021	-0.010	0.050

Table 3.7 Atom displacements induced by symmetric dimer formation in the $Si_{66}H_{52}$ model of the Si(001) surface, GVB-PP(1)HW ECP(d) optimized geometry. Atoms 1-9 form the silicon cage in i_9H_{12}. The dimers 10-14 and 11-13 were saturated so that the cluster contained only one unsaturated surface dimer to be consistent with the Si_9H_{12} model of a single unsaturated surface dimer.

Compared to the other effects that are not considered in an *ab initio* cluster calculation, thermal vibrations, surface diffusion, cooperative interactions between adjacent dimers on the surface, the errors resulting from the use of symmetric rather than buckled dimer model are expected to be small.

Comparison of Displacements From Lattice Positions Caused by Si Surface Dimer Formation									
	Experiment				Calculated				
	Felici Ref [92]		Tromp Ref [93]		This Work			Roberts Ref [94]	
	Buckled		Buckled		Symmetric			Sym.	*Buckled*
	Label	Value ($\AA$)	Label	Value	Label	Si_9H_{12}	$Si_{66}H_{52}$	Slab	
1	d1	0.5 ±0.05	(0,0,0)ΔR_x	0.478	δy_1	0.795	0.786	0.803	0.990
1	d2	0.31 ±0.1	(0,0,0)ΔR_z	0.100	δz_1	-0.154	-0.254	-0.330	-0.530
1	d3	-0.83 ±0.02	(2,0,0)ΔR_x	-1.071	δy_2	-0.795	-0.786	-0.803	-0.650
1	d4	-0.61 ±0.1	(2,0,0)ΔR_z	-0.459	δz_2	-0.154	-0.254	-0.330	0.270
2	d5	0.07 ±0.008	(0,0,-1)ΔR_x	0.094	δy_3	0.137	0.168	0.103	0.120
3	d6	-0.027±0.02	(1,1,-2)ΔR_z	-0.025	δz_7	-0.098	-0.172	-0.146	-0.180
3	d6	0.027±0.02	(3,1,-2)ΔR_z	0.031	δz_{14}	n/a	-0.116	0.119	0.098
4	d7	-0.054±0.008	(4,0,-4)ΔR_x	-0.056	δy_{44}	n/a	-0.049	-0.011	-0.016
4	d7	0.054±0.008	(2,0,-4)ΔR_x	0.042	δy_{46}	n/a	0.049	0.011	0.011
5	d8	-0.031±0.008	(4,1,-5)ΔR_x	-0.021	δy_{52}	n/a	-0.012	n/a	n/a
5	d8	0.031±0.008	(2,1,-5)ΔR_x	0.019	δy_{54}	n/a	0.012	n/a	n/a

Table 3.8 Comparison of atom displacements caused by dimer formation on the Si(001) surface. The number is the first column is the layer; Layer 1 is the surface.The two experimental references are from measurements on buckled surface dimers. The notation for the calculated displacements in this work refers to Table 3.7. E.g., δy_{44} is the y displacement for Si atom 44 in $Si_{66}H_{52}$. The calculated atom displacements from the Si_9H_{12} model of the dimer are qualitatively consistent with the calculated displacements from the $Si_{66}H_{52}$ model, though the two results differ quantitatively. The DFT results of Roberts using a periodic slab surface model are shown for comparison. Roberts was able to model both symmetric and buckled dimers.

3.7.4 Cluster Model of Two Surface Dimers. Yang et al [95] have very recently published an "embedded" cluster model of two dimers on the Si(001) surface and purport to show that the lowest energy configuration consists of two *buckled* surface dimers. There are a number of glaring discrepancies in this reference. The authors' use of the term embedded is extremely misleading; in fact, their cluster is merely a hydrogen terminated silicon cluster *without* mechanical or electronic embedding. The motion of the subsurface atoms is partially restricted in their model, which we've seen is an inappropriate method for reproducing the steric environment of a bulk material. Their comparisons of the energy difference between unbuckled and unbuckled dimer pairs is based on RHF 6-31G and DFT calculations that model the dimers as Si-Si double bonds, which is known to be the wrong model for these singlet diradicals (Ref [81]). Their calculated energy difference between the unbuckled and buckled configurations is huge, 0.51eV, compared to previous calculations that predict energy differences between the two configurations to be approximately thermal energy at room temperature.

In order to check the results of Reference [95], the two dimer cluster model used in this reference, $Si_{15}H_{16}$, was optimized in a GVB-PP(2), 6-31G* calculation. The dangling bonds on the atoms in each dimer were used to form the GVB pairs, the same approach used in the Si_9H_{12} model of a single surface dimer. Reference [95] modeled unbuckled dimers by applying C_{2v} symmetry to $Si_{15}H_{16}$, and modeled buckled dimers by applying C_2 symmetry. *To remove the question of symmetry bias on dimer buckling, the GVB-PP(2) optimization on $Si_{15}H_{16}$ was performed without any symmetry constraints.*

The GVB-PP(2), C_1 optimized geometry of $Si_{15}H_{16}$ is shown in Figure 3.20. (The cluster $Si_{18}H_{24}$, used to provide a set of bulk silicon lattice positions for $Si_{15}H_{16}$, is also shown in this figure.) *Without the application of symmetry, a correlated description of the dimer bonds results in a pair of unbuckled dimers. A GVB-PP(2) 6-31G* Hessian calculation resulted in no imaginary frequencies, confirming this geometry as a stable point on the PES.* A comparison of the unbuckled C_{2v}, buckled C_2 6-31G RHF optimized geometries from Reference [95] and the unbuckled C_1 GVB-PP(2) optimized geometry is listed in Table 3.9. (Table 3.9 is based on Table II from Reference [95].) The dimer separations from Reference [95], d(1-1), are very large for silicon double bonds that result from a RHF

model of the dimer bond (a value of 2.17$\AA$ at 6-31G* was obtained in this work). This result is most likely caused by artificially constraining the motion of the subsurface atoms, as is shown in Table 3.6. The dimer bond separations in the GVB-PP(2) model are 2.28$\AA$, consistent with the dimer length in the 6-31G* GVB-PP(1) model of a single surface dimer obtained in this work. For comparison with our previous results, Table 3.10 lists the atom displacements from lattice positions caused by formation of the surface dimers. The results of C_{2v} and C_2 RHF 6-31G* calculations also performed in this work are listed as well.

The energies for $Si_{15}H_{16}$ obtained in this work are:

Symmetry	Model	Energy (H)	ΔE ($\frac{kcal}{mole}$)
C_{2v}	RHF	-4343.016112	0.0
C_2	RHF	-4343.016112	0.0
C_1	^{5}ROHF	-4343.024193	-5.0
C_1	^{1}GVB-PP(2)	-4343.081277	-40.9

We see that the C_1 GVB-PP(2) model is 40.9$\frac{kcal}{mole}$ lower in energy than the RHF result.

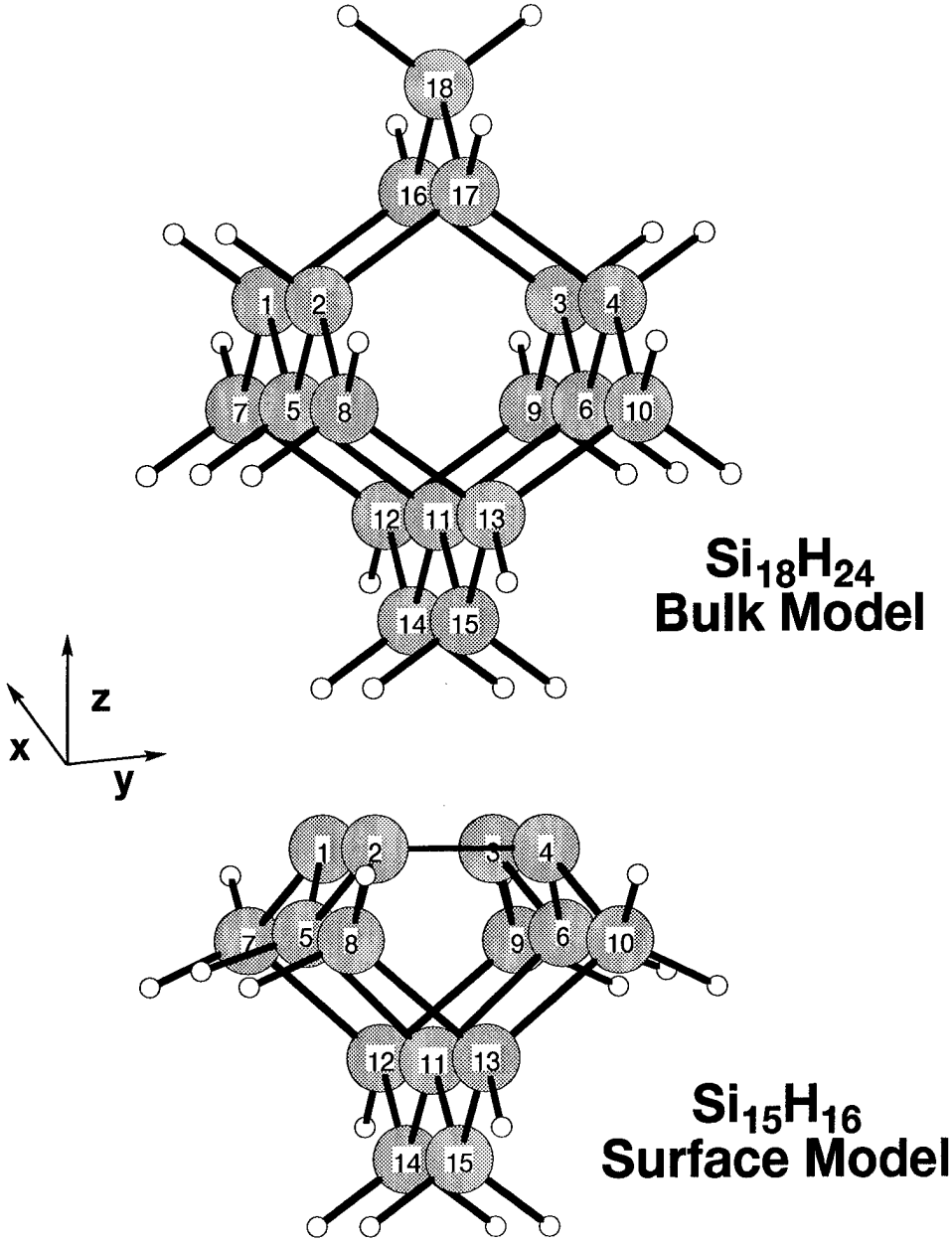

Figure 3.20 GVB-PP(2) 6-31G* optimized geometry of the $Si_{15}H_{16}$ cluster model of two adjacent dimers on the Si(001) surface. The cluster $Si_{15}H_{18}$ used to provide a set of silicon lattice poritions is also shown.

	Reference [95] 6-31G RHF		This Work 6-31G* GVB-PP(2)
	C_{2v} Unbuckled	C_2 Buckled	C_1 Unbuckled
h(1-2)(Å)	1.191	1.275	1.110
h(2-3)	1.718	1.661	1.677
h(3-4)	1.381	1.383	1.328
d(1-1)	2.239	2.384	2.282
d(1-1)	SYM	SYM	2.282
d(1-2)	2.239	2.384	2.360
d(1-2)	SYM	2.323	2.366
d(2-2)	3.464	3.545	3.604
d(2-3)	2.439	2.429	2.380
d(3-4)	2.365	2.366	2.394

Table 3.9 Comparison of $Si_{15}H_{16}$ optimized geometry, RHF and GVB-PP(2) models. The distances listed in column 1 are used in Ref [95]. h(i-j) is the separation along the z-axis between layers i and j. d(h-k) is the distance between nearest neighbor atoms in layers h and k.

Atom Displacements (Å) Caused by Dimer Formation in $Si_{15}H_{16}$									
Atom	Restricted Hartree Fock 6-31G*						GVB-PP(2) 6-31G*		
	C_{2v}			C_2			C_1		
	δ x	δ y	δ z	δ x	δ y	δ z	δ x	δ y	δ z
1	-0.089	0.852	-0.138	-0.089	0.852	-0.138	-0.064	0.803	-0.037
2	0.089	0.852	-0.138	0.089	0.852	-0.138	0.064	0.803	-0.037
3	-0.089	-0.852	-0.138	-0.089	-0.852	-0.138	-0.064	-0.803	-0.037
4	0.089	-0.852	-0.138	0.089	-0.852	-0.138	0.064	-0.803	-0.037
5	0.000	0.218	0.255	0.000	0.218	0.255	0.000	0.222	0.255
6	0.000	-0.218	0.255	-0.000	-0.218	0.255	0.000	-0.222	0.254
7	-0.098	0.136	0.152	-0.098	0.136	0.152	-0.033	0.137	0.137
8	0.098	0.136	0.152	0.098	0.136	0.152	0.033	0.137	0.137
9	-0.098	-0.136	0.152	-0.098	-0.136	0.153	-0.033	-0.137	0.137
10	0.098	-0.136	0.152	0.098	-0.136	0.153	0.033	-0.137	0.137
11	0.000	0.000	-0.007	0.000	0.000	-0.008	0.000	0.000	0.002
12	-0.147	0.000	-0.037	-0.147	-0.000	-0.037	-0.100	0.000	-0.041
13	0.147	0.000	-0.037	0.147	0.000	-0.037	0.100	0.000	-0.041
14	-0.085	0.000	0.012	-0.085	-0.001	0.012	-0.055	0.000	-0.003
15	0.085	0.000	0.012	0.085	0.001	0.012	0.055	0.000	-0.003

Table 3.10 Atom displacements induced by dimer formation in $Si_{15}H_{16}$

3.8 MIMOMM Optimization of Si_9H_{12}

3.8.1 Hybrid Cluster Model of Si(001) Surface. Now that we've quantified the differences between the Si_9H_{12} and $Si_{66}H_{52}$ models of a symmetric surface dimer, we need to examine the effect of a MIMOMM optimization of the $Si_9H_{12}/Si_{66}H_{52}$ *hybrid* cluster. In Section 3.5.2, we saw that the MIMOMM optimized geometry of Si_6H_{12}/Si_9H_{12} was *qualitatively* different than the *ab initio* optimized geometry of Si_6H_{12}. *For this case, the optimized geometries of the embedded and bulk clusters are very different, so it makes sense that the ab initio and MIMOMM results are very different.* However, for the $Si_9H_{12}/Si_{66}H_{52}$ hybrid system, the *ab initio* optimized geometry of the embedded cluster is very similar to the bulk cluster. One expects that an MIMOMM optimization may only produce small structural changes for a case like this.

Table 3.11 shows a comparison of Si_9H_{12} optimized alone, the $Si_9H_{12}/Si_{66}H_{52}$ hybrid system, a full *ab initio* GVB-PP(1) optimization of $Si_{66}H_{52}$, and the MM3 result. Table 3.11 also shows that the large bulk cluster adds a small additional computational cost to the *ab initio* calculation. As before, we see that MM3 predicts a significantly longer dimer than the *ab initio* results. MM3 is only parameterized for sp^3 "hybridized" silicons, and cannot accurately model singlet diradiacal bonding. Overall, we see small differences between the Si_9H_{12}, the $Si_9H_{12}/Si_{66}H_{52}$ hybrid result, and the full *ab initio* results. This result suggests that *localized* steric forces, i.e., steric effects arising from nearest and second nearest neighbor atoms, are most important for determining the qualitative structure of the dimer. However, as we will see in Chapter V, steric effects from third, fourth, and higher nearest neighbor atoms are very important when one attempts to model adsorption or other processes which induce large atom displacements in the cluster. Small cluster models are unacceptable for these cases.

3.9 Discussion

3.9.1 Guidance on Embedded Cluster Design. The MIMOMM optimized geometry for Si_6H_{12} is very much different from its *ab initio* optimized geometry, while the MIMOMM and *ab initio* geometries for Si_9H_{12} are almost identical. Some consideration of these cases reveals the fundamental difference between these two cases, and provides

Embedded (AI) **Bulk (MM3)**	*Ab initio* Si_9H_{12} None	MIMOMM Si_9H_{12} $Si_{66}H_{52}$	*Ab Initio* $Si_{66}H_{52}$ None	MM None $Si_{66}H_{52}$
d 2-1 (Å)	2.261	2.265	2.267	2.370
d 3-1	2.344	2.344	2.333	2.347
d 4-1	2.344	2.344	2.333	2.347
d 5-2	2.344	2.344	2.333	2.339
d 6-2	2.344	2.344	2.333	2.339
d 7-3	2.360	2.351	2.329	2.339
d 7-5	2.360	2.351	2.329	2.339
d 8-4	2.360	2.351	2.329	2.339
d 8-6	2.360	2.351	2.329	2.339
d 9-7	2.368	2.368	2.353	2.348
d 9-8	2.368	2.368	2.333	2.348
∠ 3 1 2(°)	106.320	105.987	105.378	104.129
∠ 3 1 4	111.298	112.761	114.352	112.146
∠ 3 7 5	98.600	98.245	97.579	97.479
∠ 4 8 6	98.600	98.245	97.579	97.479
∠ 7 9 8	115.944	114.400	113.085	112.017
SP2 Nodes	8	8	**32**	1
Basis Functions	150	150	**416**	n/a
Calc Time	118 min	129 min	**100 hours**	30 sec

Table 3.11 Effect of bulk cluster on Si_9H_{12} structure. All *ab initio* calculations were GVB-PP(1), with the dangling bonds on the dimer forming the GVB pair. 321G* basis set was used for the Si_9H_{12} cases. HW ECP(d) basis set used for 9 Si atoms in $Si_{66}H_{52}$, HW ECP used for rest of the atoms.

some guidance for embedded cluster design. Finite cluster models of crystal lattices will be cage-like molecules. A cluster that is an open cage, like Si_6H_{12}, distorts away from a lattice-like geometry when allowed to optimize freely. The addition of MM steric forces that*close the cage* have a pronounced effect, driving the MIMOMM optimized geometry close to the bulk geometry. However, for a cluster that is already a closed cage, like Si_9H_{12} the addition of MM steric forces will have a minor effect on the optimized geometry. Si_9H_{12} may provide a reasonable representation of the bulk steric environment for a single Si surface dimer, *except in modeling reactions which produce large distortions in its geometry.* The computational cost of a hybrid optimization is driven by the *ab initio* calculations on the embedded cluster. Thus, for surface models, it makes more sense to put as many of the embedded cluster atoms as possible in the surface layers, and use the less expensive

MM atoms to close off the structure underneath. This is only one of a number of factors that must be considered in EC design, and will not make sense for every system.

3.9.2 Molecular Mechanics Potentials. The addition of MM forces from a bulk cluster to an *ab initio* optimization of an embedded cluster has been shown to cause large changes in the embedded cluster's optimized geometry consistent with the geometry of the bulk cluster. How closely the embedded cluster matches the structure of the real system of interest depends on the specific MM force field (collection of interaction potentials) used, the level of *ab initio* theory used, and the consistency of the two sets of forces from these two different calculation. MM force fields are usually derived from experiment. *Ab initio* calculations can reproduce experimental data when a sufficiently large basis set is used in conjunction with methods that consider electron correlation. It is unclear how closely the particular MM force field being used in MIMOMM will match the interaction potentials from the level of *ab initio* theory actually being used. If the derivatives of the angle bend potentials in MM3 were twice as large as the *ab initio* energy gradients in the EC, the MM gradient would dominate the QM gradient, and the MIMOMM optimization driven by the hybrid gradient could converge at a very bad answer.

The only way to insure consistency between the *ab initio* and MM interaction potentials is to derive an MM force field from *ab initio* calculations. This procedure must be performed for every different system investigated. Krimm et al [96] have devised a general method to transform a set of forces (energy gradients) from *ab initio* calculations into a MM force field that lends itself to automation. This method does require considerable expertise in specifying the components of the MM force field; however, it provides the advantage of applying MIMOMM to systems for which force field parameters do not currently exist.

3.10 Recommendations

The 1992 version MM3 of was selected as the MM code for this work because its performance had been demonstrated in the original implementation of IMOMM by Maseras et al [4], because it is the last version for which source code is available, and because a

public domain MM code was thought unavailable. MM3 has two main limitations: the MM3 force field has been superseded by other force fields, and since MM3 is a commercial code, it cannot be distributed freely along with the source code for GAMESS. Near the end of this research, we became aware of the MM code Tinker, which is a very powerful public domain MM package [97]. Tinker is written in standard Fortran, includes a number of different MM force fields (including MM3), and can readily accept user defined force fields. Follow-on work implementing the modified version of IMOMM described in this chapter using GAMESS and Tinker is in progress. This effort should be completed and an agreement that would allow the distribution of the required portions of the Tinker package along with GAMESS should be made.

IV. Modifying the electronic environment of finite cluster models of surface reaction sites

4.1 Introduction: The Problem of Cluster Termination

A finite cluster model of a surface reaction site will contain a number of unbonded electrons, "dangling bonds" at the edges of the cluster that would normally be involved in bonding to other lattice atoms if the cluster were part of an infinite lattice. These dangling bonds are highly reactive, and can interact with each other to cause large distortions in the in the cluster's structure (surface reconstruction causing subsurface atom displacement) so that the cluster is no longer a faithful model of a surface reaction site. Even if they don't interact, a cluster with dangling bonds on all boundaries is still a poor chemical model of the surface of a crystal, which only has dangling bonds on one of its boundaries (the "surface"). In cluster calculations, dangling bonds are commonly terminated with hydrogen atoms to prevent these problems. However, H atom termination introduces a different problem. The H atoms used to terminate the cluster will not have the same electronegativity and polarizability as the lattice atoms they replace. E.g., the chemical behavior of a small silicon cluster terminated with H atoms may be qualitatively different than the chemical behavior of a real silicon surface.

A simple, brute-force approach to minimize the influence of termination is to use a cluster large enough that the reaction site is "far" removed (say 3 or more bond lengths) from the H atom termination. (The actual distance will vary with the specific material.) Of course, the problem with this approach is computational cost. Lattice-like clusters are 3-D structures. Moving the cluster termination one additional bond length away from the reactive site requires adding an additional *shell of atoms* around the edges of the entire cluster. (The number of atoms in each layer is roughly proportional to l^2, where l is the number of layers between the reactive site at the edges of the cluster.) I.e., the number of atoms in the cluster can quickly become prohibitively large for a quantum chemistry calculation without appreciably reducing the effect of H termination. Several researchers have attempted to achieve tractable computational costs in large cluster calculations by using basis sets of varying size throughout the cluster: the largest basis in the vicinity of a

reactive site, smaller basis sets farther away from a reactive site [98, 99]. This technique is known as the mixed basis set approach. Unfortunately, the use of mixed basis sets introduces basis set superposition error (BSSE) at the boundary between the higher and lower basis set, which degrades the accuracy of the calculation. In a cluster calculation, the savings in computational cost scales linearly per atom. Since the number of atoms per shell scales quadratically, use of mixed basis set does not appreciably increase the size of the cluster in terms of distance in bond lengths from the reactive site to the termination.

Since the use of very large clusters is computationally prohibitive, a number of researchers have explored methods to modify the electronic environment of a small cluster so that it behaves as if it were part of an extended material. Collectively, these methods are referred to as embedded cluster calculations [100, 101, 102, 103]. In Whitten's procedure (one of the earliest reported) one first performs an *ab initio* calculation on a large cluster, but using a small basis set. The orbitals from this Hartree-Fock wavefunction are localized and partitioned into an embedded cluster and a bulk cluster (the terminology used in Chapter III is based on Reference [100]). An effective electrostatic potential is derived from the the orbitals in the bulk cluster, and this potential is imposed on the embedded potential in subsequent calculations as a representation of a bulk electronic environment.

An alternate embedding approach, applicable where symmetry permits, is to define a unit cell and apply periodicity to crystal symmetry groups to embed the unit cell in an "infinite" material. This approach is used in both Hartree-Fock based codes such as CRYSTAL95 [104] as well as DFT codes [105, 106]. CRYSTAL95 includes point symmetry groups for molecules, 1-D symmetry for polymers, 2-D symmetry for surfaces, and 3-D symmetry for bulk materials. A companion code to CRYSTAL, EMBED [107], is used to model adsorption on crystalline surfaces. A limitation using periodic surface models is that the adsorbates must also be represented periodically. In order to insure that each adsorbate atom or molecule does not interact with its periodically created "clones", the size of the unit cell may become so large that these calculations also become prohibitively expensive.

Instead of trying to eliminate the problem of cluster termination, one could try to use the terminating atoms to trick the cluster atoms into believing they were actually

part of a bulk material. This approach was first attempted by Redondo and Goddard [7] who created artificial one-electron "atoms", dubbed siligen, for terminating small silicon clusters. (Wu and Carter [8] refer to these "atoms" as $\overline{H}$s, the term which is used in this work.) One creates the $\overline{H}$s in a small molecular model system which is taken to represent bulk silicon, and then uses the $\overline{H}$s in place of H atoms in subsequent cluster calculations. $\overline{H}$s are an attractive option for making a small cluster behave chemically more like a bulk material because they have the same low computational cost as H atoms in *ab initio* calculations, and unlike the embedded cluster methods described above, $\overline{H}$s are not limited to one specific code.

$\overline{H}$ termination has been used under very limited conditions: they were created using the same model system and the same medium-sized basis set. It is unclear how well $\overline{H}$ termination will work in applications other than silicon, and especially in two component systems such as SiC. In Chapter III the effect of adding molecular mechanics forces to the optimization of the geometry of small clusters was investigated. In this chapter, the additional effect of termination with $\overline{H}$ is evaluated. This chapter explores the use of alternative model systems and basis sets for creating $\overline{H}$s, as well as the possibility of creating $\overline{H}$s to terminate silicon carbide clusters

Since we seek to match the electronic environment of a bulk material, we must first discuss how the the electronic environment within a molecule is defined. The modification of the electronic properties of H atoms using a finite basis set expansion is next discussed. The method used to create $\overline{H}$ atoms for silicon by Goddard and Carter is then discussed, as well as questions left open from this work. Variation's of Goddard's method, as well as new methods for creating $\overline{H}$ atoms, are then presented. The ability of the different $\overline{H}$ atoms created in this work to mimic the electronic environment is compared. Tests of other molecular properties are performed using the "best" $\overline{H}$ to see what other effects the use of $\overline{H}$ atoms may have.

To provide a comparison with bulk silicon behavior, full quantum calculations were performed on large, hydrogen terminated silicon molecules, $Si_{66}H_{52}$, $Si_{66}H_{53}$, and $Si_{66}H_{54}$. ($Si_{66}H_{52}$ is shown in Figure 3.17). The terminating H atoms in these molecules are several bond lengths away from the silicon atoms which are compared, and so are judged to be

"reasonable" approximations for bulk silicon. As was mentioned in Chapter III, a GVB-PP(1) optimization of ($Si_{66}H_{52}$ took 100 hours on 32 nodes of an IBM SP2. Full *ab initio* calculations on larger silicon clusters were impractical for this study.

4.2 The Electronic Environment of a Molecule

The proper description of the electronic environment of a molecule is the electron density distribution (EDD), obtained from the square of the electronic wavefunction. The EDD has two desirable characteristics. First, the EDD can be measured. Second, as one improves an *ab initio* calculation, by increasing the size of the basis set or including correlation, the square of the approximate wavefunction approaches the experimental EDD. However, in practice there are several drawbacks to using the EDD as a metric for creating $\overline{H}$s. Since the goal is to match the electronic environment of a bulk material in a small cluster, one would first have to have a bulk-like EDD. This could be obtained from the optimization of a very large cluster model. Then, one would have to define a smaller, model system terminated with $\overline{H}$s. One would then have to monitor the EDD of the model cluster as the properties of the $\overline{H}$s are changed until the EDD of the model system matched the bulk-like EDD. The computation and analysis time involved in a process such as this was judged to be too long for the purposes of this work.

A commonly used simplification is to reduce the molecular EDD into a collection of atom centered charges [108]. The electron density distribution function $\rho(\vec{r})$ is defined such that $\rho(\vec{r})d\vec{r}$ is the probability of finding an electron in a volume element $d\vec{r}$. Integrating over all space,

$$\int \rho(\vec{r})d\vec{r} = n, \tag{4.1}$$

where n is the total number of electrons in the molecule. In Hartree-Fock theory, Equation 4.1 becomes,

$$\rho(\vec{r}) = \sum_{\mu}^{N}\sum_{\nu}^{N} P_{\mu\nu}\phi_{\mu}(\vec{r})\phi_{\nu}(\vec{r}), \tag{4.2}$$

where $P_{\mu\nu}$ are elements of the density matrix, and the summations are carried out over all the atom centered atomic basis functions, $\phi(\vec{r})$. Integrating Equation 4.2,

$$\begin{aligned} \int \rho(\vec{r}) &= \sum_{\mu}^{N}\sum_{\nu}^{N} P_{\mu\nu} \int \phi_\mu(\vec{r})\phi_\nu(\vec{r}) \\ &= \sum_{\mu}^{N}\sum_{\nu}^{N} P_{\mu\nu} S_{\mu\nu} = n, \end{aligned} \tag{4.3}$$

where $S_{\mu\nu}$ are elements of the overlap matrix.

Now that we have an expression for the electron density in terms of atomic orbitals, the problem which remains is how to partition the electron density among the individual atoms. The simplest recipe was proposed by Mulliken [109]. In Mulliken's procedure (called the Mulliken population analysis), the summation over pairs of atomic basis functions, Equation 4.3, is divided into diagonal ($\mu = \nu$; $S_{\mu\nu} = 1$) and off-diagonal ($\mu \neq \nu$) parts

$$\sum_{\mu}^{N}\sum_{\nu}^{N} P_{\mu\nu} S_{\mu\nu} = \sum_{\mu}^{N} P_{\mu\mu} + 2\sum_{\mu<\nu}\sum_{\nu}^{N} P_{\mu\nu} S_{\mu\nu} = n. \tag{4.4}$$

It is reasonable to assign any electrons associated with a particular diagonal element $P_{\mu\mu}$ to the atom on which the basis function ϕ_μ is centered. It is also reasonable to assign electrons associated with an off-diagonal element, $P_{\mu\nu}$, where both ϕ_μ and ϕ_ν reside on the same atom to that atom. However, how does one partition electrons from the density matrix elements $P_{\mu\nu}$ where ϕ_μ and ϕ_ν are centered on different atoms? Mulliken's answer was to give each of the atoms half, an arbitrary, but simple choice.

Within Mulliken's scheme, we can define a gross population, q_μ, for each basis function ϕ_μ,

$$q_\mu = P_{\mu\mu} + \sum_{\mu\neq\nu} P_{\mu\nu} S_{\mu\nu}. \tag{4.5}$$

Atomic populations, q_A, and atomic charges, Q_A, are then defined as

$$q_A = \sum_{\mu} q_{\mu A}, \qquad Q_A = Z_A - q_A, \tag{4.6}$$

where $q_{\mu A}$ is a basis function centered on atom A, and Z_A is the atomic number of atom A.

The Mulliken population analysis has a number of significant limitations. Equal partitioning of charge density is improper for heteronuclear molecules. This partitioning becomes less well defined as one increases the size of the basis set, and adds in diffuse functions with large spatial extent. For example, one could calculate the electronic wavefunction for H_2O using a set of increasingly diffuse basis functions centered on only the O atom. Because all these basis functions are centered on the O atom, a Mulliken analysis would assign the O atom a charge of -2, and each H atom a charge of +1, i.e., water would appear to be purely ionic! The primary advantage of the Mulliken population analysis is the ease with which it can be calculated. If one is careful in setting up a model system and in choosing the basis set, using Mulliken charges as the metric for defining $\overline{H}$ atoms is probably not too bad. Previous efforts relied on Mulliken charges to create $\overline{H}$ atoms [7, 8]. Mulliken charges are also used in this work for creating $\overline{H}$ atoms; however, other implications of their use are also investigated.

Other schemes for reducing the EDD into a set of atom centered point charges have been developed [110, 111, 112]. However, it is important to remember that the EDD is really a molecular property, so any scheme that seeks to represent the EDD as a collection of nuclei-centered charges will have limitations.

4.3 Altering the Electronegativity of a Hydrogen Atom

In an *ab initio* model of a molecule, each atom is represented with a nuclear charge, nuclear mass, and a set of basis functions that describe the atomic electronic wavefunction. The most commonly used basis functions are Gaussian Type Orbitals (GTOs), or Gaussian expansions of Slater Type Orbitals (STO-NG), where N is the number of Gaussians [19]. The parameters in the atomic orbitals are optimized to produce minimum energy solutions for the atomic electronic wavefunction. To alter the electronegativity of an atom modeled this way, one could modify the atom's nuclear-electron attraction by either (artificially) changing the nuclear charge, or by changing the average radial distance of the atom's electrons by changing the radial parameters of the atom's basis functions. Both methods have been used in previous work [66]. This work focused on changing the parameters of the atomic orbitals because changing nuclear charges of only some of the atoms removes

overall charge neutrality in the molecule. This non-neutrality may produce inappropriate surface charging, and unphysically bias the surface chemistry.

Since the $\overline{H}$s are only used to give a better representation of the electronic environment of a bulk material, it is desirable to use the smallest functional expansion of the atomic orbital, basis set, to keep the computational cost as low as possible. A number of functional forms are used for basis sets. One of the earliest, proposed by Slater, is called a Slater Type Orbital (STO) [17]. The normalized 1s Slater Type Orbital (STO), centered at $\vec{R}_A$ has the form [19]

$$\phi_{1s}^{SF}(\zeta, \vec{r} - \vec{R}_A) = \left(\frac{\zeta}{\pi}^{\frac{3}{2}}\right) \exp^{-\zeta|\vec{r}-\vec{R}_A|} \tag{4.7}$$

The parameter ζ controls the radial extent of the orbital. With $\zeta = 1.0$, Equation 4.7 is an exact solution for the ground state of atomic hydrogen. STO's give a good representation of the physical behavior of atomic wavefunctions; however, they are difficult and time consuming to integrate numerically. Another functional form used for basis sets are Gaussian Type orbitals (GTOs). GTOs do not give as good a representation of the wavefunction as STOs, but can be integrated very efficiently. A normalized 1s GTO has the form:

$$\phi_{1s}^{GF}(\alpha, \vec{r} - \vec{R}_A) = \left(\frac{2\alpha}{\pi}^{\frac{3}{4}}\right) \exp^{-\zeta|\vec{r}-\vec{R}_A|^2}. \tag{4.8}$$

A compromise between the better physics of the STO and the better numerics of the GTO is to expand a STO with N GTOs [24].

$$\phi_{1s}^{STO-NG}(\zeta, \vec{r} - \vec{R}_A) = \sum_{i=1}^{N} c_i \phi_{1s}^{GF}(\zeta^2 \alpha_i, \vec{r} - \vec{R}_A) \tag{4.9}$$

The unnormalized STO-3G basis set for atomic hydrogen used in molecular calculations is [24, 113]

$$\begin{aligned}\phi_{1s}^{STO-3G}(\zeta = 1.24, \vec{r} - \vec{R}_A) &= 0.154\phi_{1s}^{GF}(1.24^2 \times 2.227, \vec{r} - \vec{R}_A) + \\ &\quad 0.535\phi_{1s}^{GF}(1.24^2 \times 0.405, \vec{r} - \vec{R}_A) + 0.444\phi_{1s}^{GF}(1.24^2 \times 0.109, \vec{r} - \vec{R}_A).\end{aligned} \tag{4.10}$$

Here, $\zeta = 1.24$ reflects the fact that the hydrogen's electron density shrinks in towards the nucleus in molecules, so the minimum energy solution for hydrogen in molecules requires the use of a smaller orbital.

Figure 4.1 shows the radial profile of the hydrogen 1s STO-3G basis function for several values of ζ. As ζ is decreased, the average value of r increases. It is interesting to

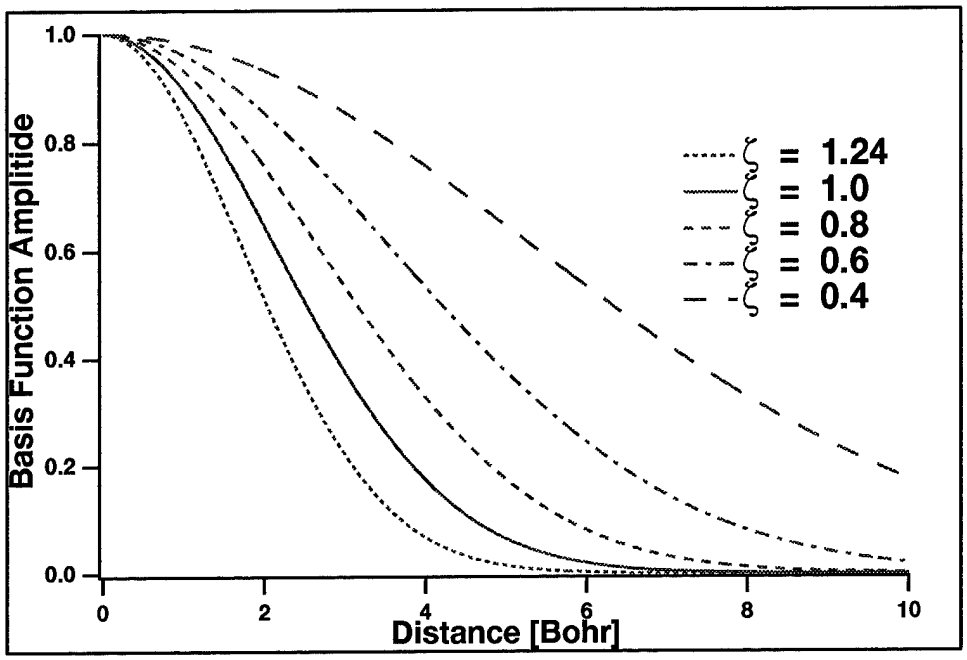

Figure 4.1 ζ dependence of the STO-3G basis set

note that electronegativity is actually a quadratic function of ζ for a hydrogenic 1s basis function [7, 66]. The definition of the ionization potential (IP) of an atom or molecule x is

$$IP = E_{x^+} - E_x. \tag{4.11}$$

The electron affinity is defined as

$$EA = E_x - E_{x^-}. \tag{4.12}$$

Combining Equations 4.11 and 4.12, one finds for a hydrogenic 1s orbital (x=H) [7]

$$\chi = \frac{1}{2}(IP + EA) = \frac{1}{2}E_{H-} = -\frac{1}{2}\zeta^2 + \left(Z - \frac{5}{16}\right)\zeta \tag{4.13}$$

Equation 4.13, the electronegativity as a function of ζ, is plotted in Figure 4.2. Also shown in Figure 4.2 are the Mulliken charges for a silicon atom connected to an $\overline{H}$ in a model molecule as a function of ζ used in the $\overline{H}$ (cf Table 4.3), which show a similar quadratic behavior.

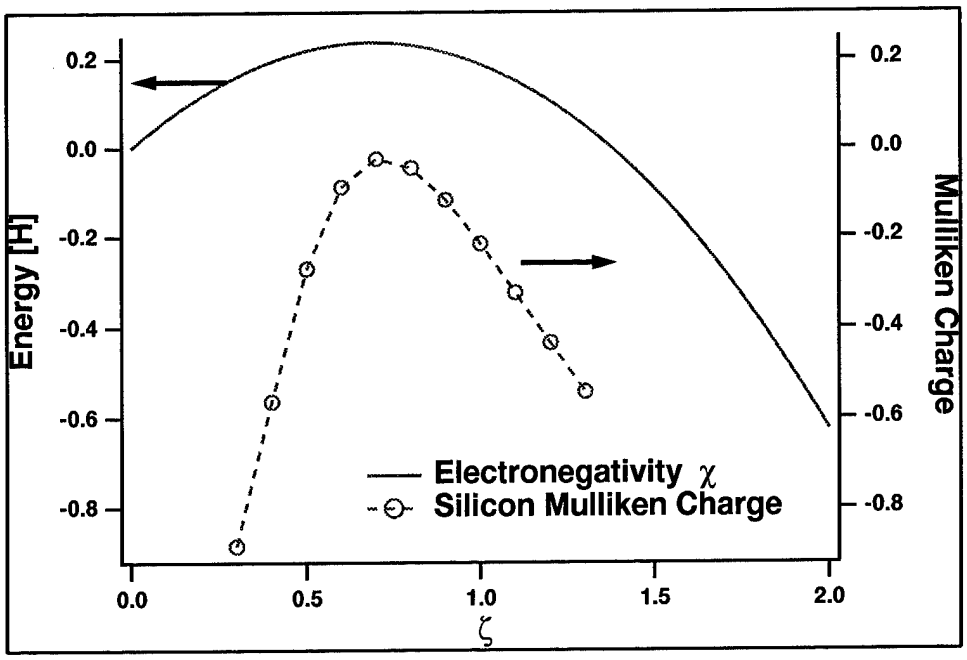

Figure 4.2 ζ dependence of hydrogen electronegativity. Also plotted is the Mulliken charge on silicon atom 1 from Table 4.3 as a function of ζ on the $\overline{H}$

This behavior of the electronegativity is an artifact of the STO description of the hydrogen atom, and demonstrates that one cannot ascribe physical significance to a value of ζ that produces a desired Mulliken charge. When ζ for a hydrogenic 1s basis function is arbitrarily adjusted to mimic the electronegativity of another material, ζ should only be considered to be a system, basis set, and geometry-dependent parameter that ensures proper electronic boundary conditions for the cluster [66]. The silicon valence shell contains

both s and p atomic orbitals, so one should not expect an $\overline{H}$ atom created using only an s orbital with a scaled value of ζ to perfectly reproduce all of silicon's properties.

4.4 Creation of $\overline{H}$s: Three Approaches

4.4.1 Previous Work. Figure 4.3 shows the model system used by several [7, 8, 114] groups to generate $\overline{H}$s that match the electronegativity of bulk silicon. This molecule, Si_5H_{12}, has tetrahedral (T_d) symmetry, so only 3 of the 15 atoms are unique, which greatly reduces calculation times. All nuclear separations are set to the silicon lattice value of 2.35 Å. (As will be discussed in Section 4.4.4, the choice of Si-$\overline{H}$ separation is somewhat arbitrary, as one can find a value of ζ that produces the desired Mulliken charge on the silicon atoms in the model molecule over a wide range of separations.) In this model

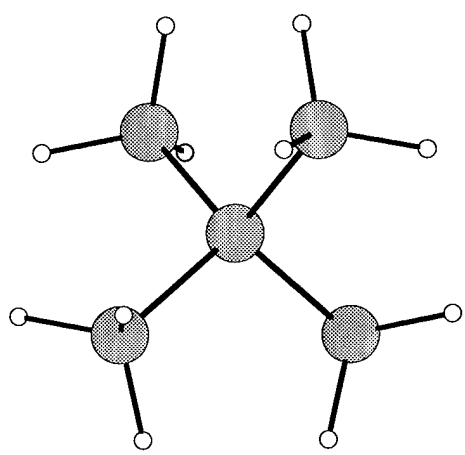

Figure 4.3 Si_5H_{12} model system used to create $\overline{H}$ atoms

system, the central silicon atom is bonded only to other silicon atoms. Since all the nearest neighbor atoms to this central silicon are also silicon, Goddard et al judged the Mulliken charge to be an adequate measure of neutrality for the central atom. This same model can also be used to create $\overline{H}$s for bulk diamond by using carbon instead of silicon (with diamond lattice separations). An alternate metric for determining whether the $\overline{H}$ model bulk-like silicon is to use the Mulliken charges on all the silicons instead of just the Mulliken charge on the central silicon.

In creating their $\overline{H}$s, Goddard et al [76] used an Effective Core Potential (ECP) basis set for the silicons, with a 3-21G split for the valence electrons. The STO-3G basis set for hydrogen was used as the starting point. The value of ζ was varied until the Mulliken charge on the central silicon became 0.0, the value one would find in bulk silicon. In subsequent calculations on the $Si_9\overline{H}_{12}$ model of a silicon surface dimer, the Si-$\overline{H}$ separation was fixed at the lattice value of 2.35Å.

Carter et al [8] used this procedure on the same model system and ECP basis set for the silicons. However, instead of just varying the the overall radial scaling factor ζ of a hydrogen STO-3G basis set, Carter et al varied all six parameters, 3 coefficients and 3 exponential terms, individually until the Mulliken charge on the central Si atom in the model system went to 0.0. Carter's functional fit, three independent Gaussians, is a triple zeta (TZ) basis set, as the ratio of the three Gaussian basis functions is not fixed. Once optimum values of these 6 parameters were determined, they were fixed and used as a single linear combination, a triple zeta basis function contracted to a "STO-3G"-like single basis function for computational efficiency. *However, unlike Goddard, in subsequent calculations on $Si_9\overline{H}_{12}$, Carter et all allowed the Si-$\overline{H}$ separations to vary as the overall $Si_9\overline{H}_{12}$ geometry was optimized.* The optimized Si-$\overline{H}$ separation was 1.72Å.

Allowing the Si-$\overline{H}$ separation to vary in these calculations seems odd because the basis set for $\overline{H}$ depends on the (fixed) Si-$\overline{H}$ separation used in the model system. Fixing the Si-$\overline{H}$ separation would seem to be crucial. However, the Mulliken charges reported by Carter for $Si_9\overline{H}_{12}$ are more representative of bulk silicon than Si_9H_{12}. The $Si_9\overline{H}_{12}$ optimizations performed in this work allowed the Si-$\overline{H}$ separation to vary because these calculations were performed using Cartesian coordinates due to difficulties encountered in specifying internal coordinates for this molecule. Internal coordinates such as bond lengths cannot be fixed using Cartesian coordinates.

4.4.2 Creation of $\overline{H}$ Atoms Using Si_5H_{12} Model System. For comparison with the work of Goddard and Carter, $\overline{H}$s were created using the Si_5H_{12} model system. In this study, the Hay Wadt ECP basis set [115] in GAMESS [9] was used, which is similar to the ECP basis set used by Goddard and Carter. Although including d functions in

the basis set is known to be required for accurate results in silicon, d functions were not used in the Si_5H_{12} model system by either Goddard or Carter to create their $\overline{H}$s. In this prior work, d functions were used in subsequent calculations on $Si_9\overline{H}_{12}$ model of a surface dimer, but *only on the 2 Si atoms in the dimer, which are not bonded to any $\overline{H}$s.* This is an important distinction because the value of ζ used in the $\overline{H}$ to produce the desired Mulliken charge in the model system depends on the basis set used in the model system. Thus, it is inappropriate to use an $\overline{H}$ created with the HW ECP basis set to terminate a silicon atom described with the HW ECP(d) basis set. In this study, $\overline{H}$s were created using the Si_5H_{12} model system using HW ECP and HW ECP(d) to quantify the effect of adding d functions on the optimum value of ζ, and to enable calculations on $Si_9\overline{H}_{12}$ to be performed in which d functions are added to all nine Si atoms.

Table 4.1 shows the Mulliken charges for the $Si_5\overline{H}_{12}$ model system as a function of ζ obtained in this work. Neither Reference [7] nor [8] provide comparable data, so the differences between using a single parameter or six parameters to define the $\overline{H}$ atoms is unclear. The first row in Table 4.1 shows the Mulliken charges for the hydrogen terminated molecule. The last column in this table, labeled Δ, is the sum of the absolute value of the Mulliken charges for the silicons. In bulk silicon, Δ would be zero. The last row in Table 4.1 shows the Mulliken charges from a $\overline{H}$ created by putting the HW ECP Si 3s basis functions on a hydrogen nucleus. At a fixed position, this last approach produces near neutral Mulliken charges on all atoms in the model system.

The best match of the Mulliken charge on the central silicon is obtained with $\zeta = 0.380$ on the hydrogen STO-3G basis set, which is close to the value of ζobtained by Goddard. The best match of the Mulliken charge on all the silicons to bulk-like values is obtained for a value of $\zeta = 0.470$. *Near neutrality on all the atoms in the model system is obtained using the Si 3s basis functions.* Based solely on this result, one would conclude that simply using a valence s orbital from the atom whose electronegativity one is trying to match is the best method to create an $\overline{H}$. However, this hypothesis proved to be false when additional tests, described in Section 4.5 were performed.

Table 4.2 shows the results of this same procedure applied to $Si_5\overline{H}_{12}$, but with the addition of d functions to the basis set for the silicon atoms. The addition of d functions

ζ	Mulliken Charge			Δ Si Mull Charge
	Si_{center}	Si_{outer}	$\overline{H}$	
1.240	-0.393	+0.580	-0.160	n/a
0.370	+0.019	-0.548	+0.181	2.194
0.380	+0.002	-0.489	+0.163	1.958
0.450	-0.107	-0.113	+0.047	0.550
0.462	-0.125	-0.056	+0.030	0.348
0.470	-0.136	-0.019	+0.018	0.213
0.480	-0.144	+0.025	+0.004	0.243
0.483	-0.153	+0.024	+0.001	0.305
0.484	-0.155	+0.045	-0.001	0.326
0.485	-0.156	+0.112	-0.002	0.335
0.490	-0.174	+0.112	-0.019	0.582
Si 3s	-0.055	-0.024	+0.013	0.015

Table 4.1 Mulliken charges on the $Si_5\overline{H}_{12}$ molecule, HW ECP basis set. Si_{center} refers to the center atom in Figure 4.3. Si_{outer} refers to any of the four equivalent Si atoms bonded to the center atom in this figure. The first row shows the results for using real H atoms.

substantially changes the value of ζ needed to produce a neutral Mulliken charge on the central silicon.

ζ	Mulliken Charge			Δ Si Mull Charge
	Si_{center}	Si_{outer}	$\overline{H}$	
1.240	-0.283	+0.372	-0.100	n/a
0.30	+0.414	-1.056	+0.318	4.638
0.485	+0.120	-0.007	-0.008	0.147
0.50	+0.100	-0.056	-0.030	0.326
0.51	+0.090	+0.096	-0.040	0.474
0.52	+0.079	+0.134	-0.051	0.615
0.60	+0.007	+0.367	-0.123	1.475

Table 4.2 Mulliken Charges on the $Si_5\overline{H}_{12}$ molecule, HW ECP(d) basis set.

There are several limitations in this approach to creating $\overline{H}$s. First one must know the Mulliken charges for the bulk crystal a priori in order to create the $\overline{H}$s. Defining the Mulliken charge for an infinite, single component crystal is trivial; however, one cannot predict Mulliken charges for heterogeneous materials. One must calculate Mulliken charges on a cluster large enough to give a good representation of a bulk heterogeneous material.

Unfortunately, a cluster that satisfies this requirement may be prohibitively large for calculations. In addition, one can envision applications in which cluster models are terminated with functional groups as opposed to being part of an infinite lattice. Creating $\overline{H}$s from bulk-like model systems is inappropriate for these applications. A generic limitation is the large Si-$\overline{H}$ separation, the Si lattice separation. If one fixed the Si-$\overline{H}$ separation in a cluster model, one may find situations in which $\overline{H}$s bonded to two cluster atoms have to occupy the same location. One then has to increase the size of the cluster so that the $\overline{H}$s will not overlap.

4.4.3 Mulliken Charge Mirror Model . In order to avoid some of the limitations of creating $\overline{H}$s using the Td model, an alternate procedure was devised. Figure 4.4 shows the model system for silicon and carbon used in this procedure. First, one performs an *ab initio* optimization on the full molecule and obtains a set of Mulliken Charges that serve as the "right answer" at the selected level of theory. Next, one replaces half of the molecule with a single $\overline{H}$ located where the silicon bonded to 4 other silicons was. Then, the value of ζ of this $\overline{H}$ is adjusted until Mulliken charges on the remaining silicons best matches the Mulliken charges from the full system. This model system includes real H atoms as well as Si atom, and so does not represent bulk silicon as well as the tetrahedral model. However, it is a good model system for terminating a cluster with $Si(SiH_3)_3$, which may be adequate to represent the bulk. More importantly, it may be possible to create similar model systems with a mirror plane of symmetry to create $\overline{H}$ atoms for heterogeneous materials. This idea is explored for silicon carbide in Section 4.7.

Table 4.3 shows typical values of Mulliken charges obtained using this method with the HW ECP basis set. Si_1 is the silicon directly bonded to the $\overline{H}$, while Si_2 is one of the silicons one bond away from the $\overline{H}$ (the Mulliken charges on all three of these silicons are equal). While the Mulliken charge on the silicon bonded to the $\overline{H}$ is very sensitive to small changes in ζ, the Mulliken charges on the other silicons in the molecule are fairly insensitive. As these silicons are each bonded to 3 hydrogens, their Mulliken charge is dominated by the hydrogens. As was discussed in Section 4.3, the variation of the Mulliken charge with ζ is nonlinear. $\zeta = 0.485$ best matches the Mulliken charge on Si_1.

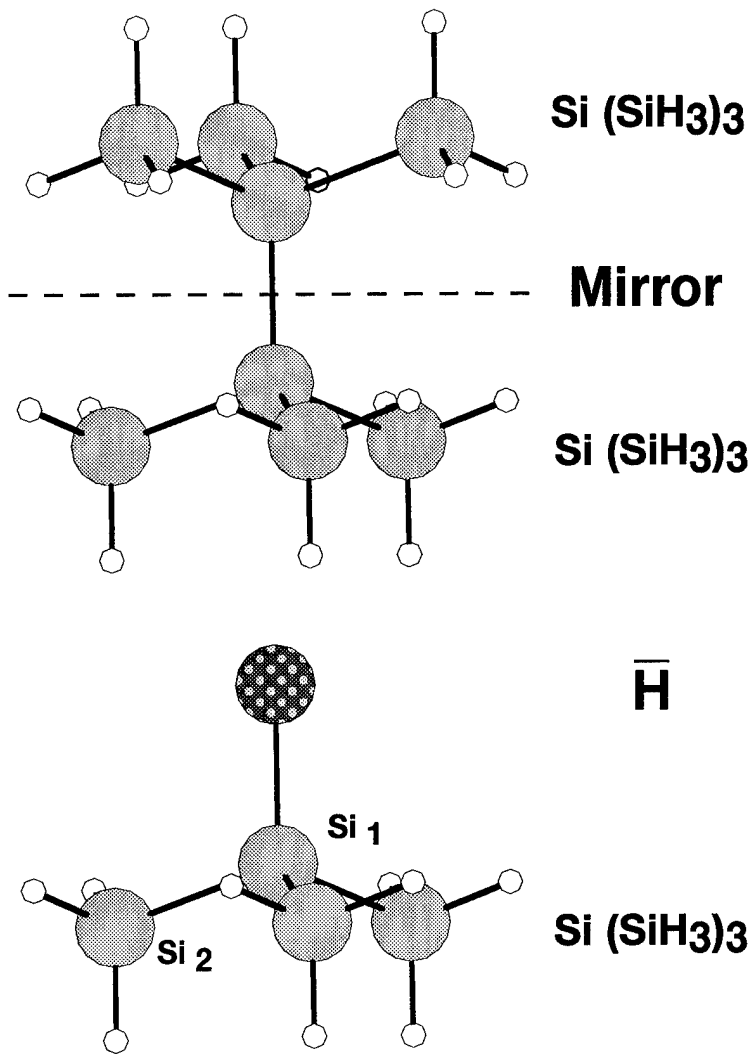

Figure 4.4 Mulliken charge mirror model system used to create $\overline{H}$ atoms. The $\overline{H}$ atom replaces one-half of the full molecule, and the radial scaling factor ζ is adjusted until the Mulliken charges on the Si atoms in $\overline{H}Si_4H_9$ are equal to the Mulliken charges in Si_8H_{18}.

ζ	Mulliken Charge		
	$\overline{H}$	Si_1	Si_2
(Full Molecule)		-0.322	+0.590
0.300	+0.544	-0.855	+0.606
0.400	+0.190	-0.564	+0.589
0.450	+0.034	-0.407	+0.579
0.462	+0.001	-0.372	+0.576
0.470	-0.021	-0.346	+0.574
0.485	-0.058	-0.309	+0.571
0.500	-0.093	-0.271	+0.579
0.600	-0.242	-0.089	+0.549
0.700	-0.272	-0.025	+0.538
0.800	-0.224	-0.046	+0.531
0.900	-0.137	-0.118	+0.530
1.000	-0.032	-0.216	+0.538
1.100	+0.075	-0.324	+0.540
1.200	+0.179	-0.434	+0.551
1.300	+0.279	-0.542	+0.559

Table 4.3 Mulliken Charges on the $\overline{H}$-$Si(SiH_3)_3$ molecule, HW ECP basis set. The row labeled Full Molecule shows the Mulliken charges on the equivalent nuclei in Si_8H_{18}. Si_1 and Si_2 are labeled in Figure 4.4. $\zeta = 0.485$ gives the best match of the Mulliken charges for the full molecule.

ζ	Mulliken Charge		
	$\overline{H}$	Si_1	Si_2
(Full Molecule)		-0.251	+0.369
0.5075	-0.211	+0.226	+0.405
0.500	-0.193	-0.249	+0.408
0.490	-0.167	-0.283	+0.411

Table 4.4 Mulliken Charges on the $\overline{H}$-$Si(SiH_3)_3$ molecule, 6-31G* basis set. The row labeled Full Molecule shows the Mulliken charges on the equivalent nuclei in Si_8H_{18}.

Table 4.4 shows the Mulliken charges for the same model system, but calculated using a 6-31G* basis set for the silicons. This procedure should produce a $\overline{H}$ atom that could be used to terminate silicon clusters calculated using the 6-31G* basis set. $\zeta = 0.50$ best matches the Mulliken charge on Si_1 at 6-31G*, quite similar to the HW ECP result.

4.4.4 Optimum Si-$\overline{H}$ separation. In previous work using $\overline{H}$s [8], the Si-$\overline{H}$ separation was (arbitrarily) fixed at the silicon lattice value while the $\overline{H}$ was created; however, when the Si-$\overline{H}$ separation was allowed to vary during the optimization of $Si_9\overline{H}_{12}$, the optimized Si-$\overline{H}$ separation was around 1.7 Å. This suggests that one might be able to use energy as a criterion to define the optimum Si-$\overline{H}$ separation in the model system used to create the $\overline{H}$. Table 4.5 shows the energies and ζs obtained at several Si-$\overline{H}$ separations in the model system shown in Figure 4.4. The same match of the Mulliken charge criteria was obtained at all 3 separations. The lowest energy is obtained at a separation of 1.70 Å; however, at this point there is not enough information to decide whether using this separation is better than the other two separations. Additional comparisons are discussed in Section 4.5.

Si-$\overline{H}$ (Å)	ζ	Energy (H)
2.36	0.485	-20.547155
1.70	0.515	-20.591807
1.20	0.520	-20.511741

Table 4.5 Energy as a function of Si-$\overline{H}$ separation. The Mulliken charge criteria was met equally well at all separation values.

4.4.5 Bulk Molecular Orbital Model of $\overline{H}$. An $\overline{H}$ is a one electron atom created to match the electronegativity of a multi-electron atom in order to create a bulk-like chemical environment within a finite cluster. The previous approaches for creating an $\overline{H}$ started with a hydrogen atom, and modified the radial scaling of its atomic orbital until a metric based on Mulliken charges was met in a model system. Instead of using the Mulliken charge and its associated limitations, it seems reasonable to base the construction of the $\overline{H}$ MO on a suitable MO from the bulk material. For example, one could use the Boys localized MO between the Si atoms on ether side of the mirror plane in Figure 4.4, take a slice along the centerline, and assume that this MO was the sum of two pieces, one from each atom. However, one still must decide how to partition this MO, the same problem that occurs in the Mulliken population analysis. If both atoms involved in the bonding MO are the same, one divides the MO into two equal pieces. If the atoms are different, as they would be in silicon carbide, dividing the MO into two equal pieces would be wrong, and it is very difficult define the "correct" partitioning. Thus, although using a Boys localized bonding MO to construct an $\overline{H}$ avoids many of the problems of the Mulliken analysis, it retains the principle problem of partitioning.

To avoid the partitioning problem, model systems representative of bulk materials that possess singly occupied MOs were investigated. Figure 4.5 shows a system that might possess a suitable one electron MO, the Si_4H_9 radical. This radical has a one-electron MO whose properties are dominated by the Si-Si bonding environment. The radial properties of this MO were used to define a basis function for $\overline{H}$. It should be noted that this MO has a distinctly directional nature, while the 1s basis function is spherically symmetric. It is unclear at this point what problems this mismatch may cause.

The following procedure was used to create a single electron MO to create the $\overline{H}$atom. To match the tetrahedral bonding environment of bulk silicon, the energy of the $Si_4H_9^{\bullet}$ was optimized with the bond and torsion angles fixed at tetrahedral lattice values, with the bond distances allowed to vary. Figure 4.6 shows a contour plot of the resulting one electron MO calculated by GAMESS with the HW ECP basis set (for consistency with other $\overline{H}$ creation schemes) as well as a radial slice of the MO along its centerline. The centerline radial profile of the single electron MO was fit to the following functional form using the

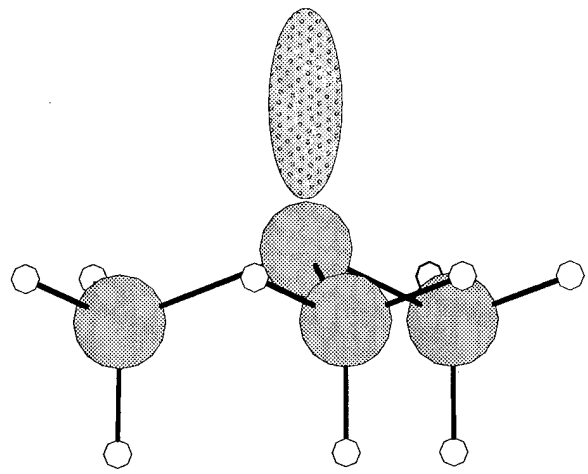

Figure 4.5 $Si_4H_9^{\bullet}$ model system. The location of the singly occupied MO is nominally indicated, i.e., this is not an accurate representation of the MO.

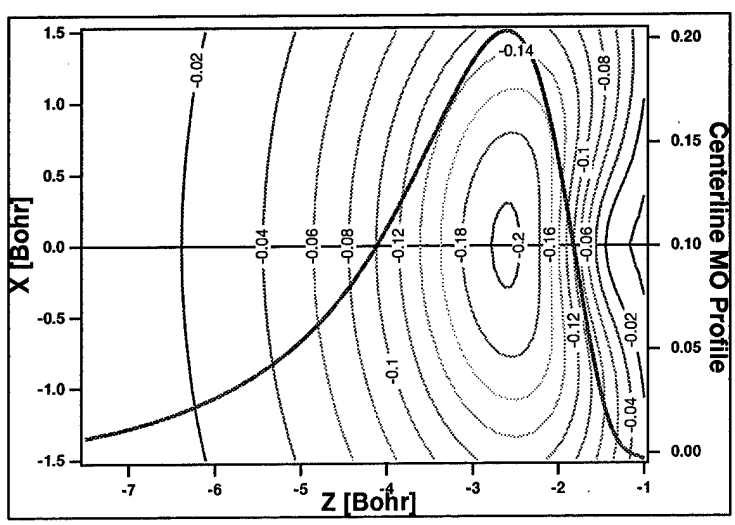

Figure 4.6 $Si_4H_9^{\bullet}$ single electron MO contours. Superimposed is the value of the MO along the Z axis. Contours appear distorted due to scaling of axes.

analysis program IGOR [116]:

$$F(r) = k_1 * \exp(-\alpha_1 r^2) + k_2 \exp(-\alpha_2 r^2) + k_3 * \exp(-\alpha_3 r^2). \tag{4.14}$$

IGOR uses the Levenberg-Marquandt nonlinear least squares curve fitting procedure, with the user supplying an initial guess to the parameters in the fit.

This fitting procedure was first applied to a known test case, a hydrogen atom MO, to quantify its performance. Figure 4.7 shows a radial slice of the GAMESS generated MO for a hydrogen atom using the STO-3G basis set [24], as well as a 3 Gaussian fit to this MO. A comparison of the fit parameters with the GAMESS STO-3G basis set is also listed. The

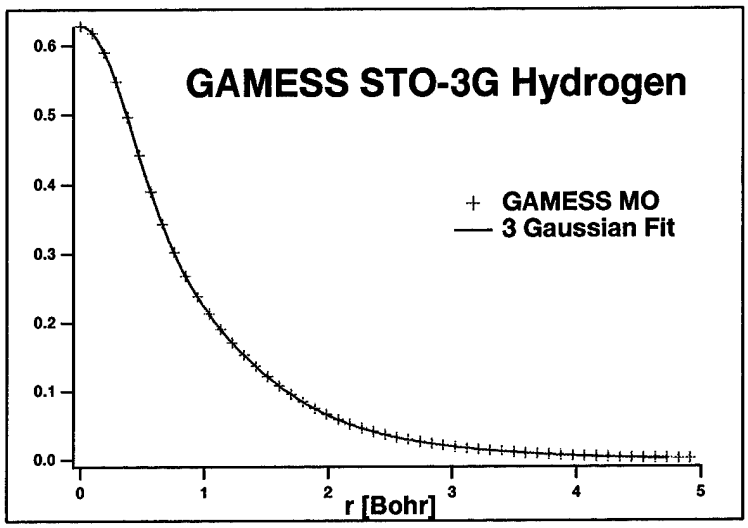

IGOR 3 Gaussian Fit		GAMESS Basis Function		
α	c	α	c (scaled)	c (input)
3.42523	0.276936	3.42525	0.2769349	0.154329
0.623908	0.267839	0.623914	0.267839	0.535328
0.168854	0.083472	0.168855	0.083474	0.444635

Figure 4.7 Fitting procedure applied to GAMESS STO-3G hydrogen atom MO.

three Gaussian fit, which had a Chi Square of 10^{-12}, (the limiting precision of IGOR), shows very good agreement to the STO-3G basis set, though one should take careful note that fitting the MO reproduces the *scaled* values of the coefficients. By convention, Gaussian

basis sets are given in the literature in the form:

$$G(\alpha, r) = \sum_{i=1}^{n} c_i \exp(-\alpha_i r^2). \tag{4.15}$$

As part of the normalization process for 1s Gaussians, new coefficients are defined as

$$c_i' = c_i \times \left(\frac{2\alpha}{\pi}\right)^{\frac{3}{4}}. \tag{4.16}$$

The fitting procedure is seen to reproduce the *scaled* coefficients. Thus in order to obtain the proper ratio of the Gaussians in the basis function, one must divide k_i by $\left(\frac{2\alpha}{\pi}\right)^{\frac{3}{4}}$ to obtain the proper scaling of the coefficients in GAMESS.

Figure 4.8 shows the calculated single electron MO in $Si_4H_9^{\bullet}$, as well as a 3 Gaussian fit to this MO. Two sets of fit parameters, obtained with slightly different initial guesses, show that the uncertainty in the fit parameters obtained in this procedure is small. Also

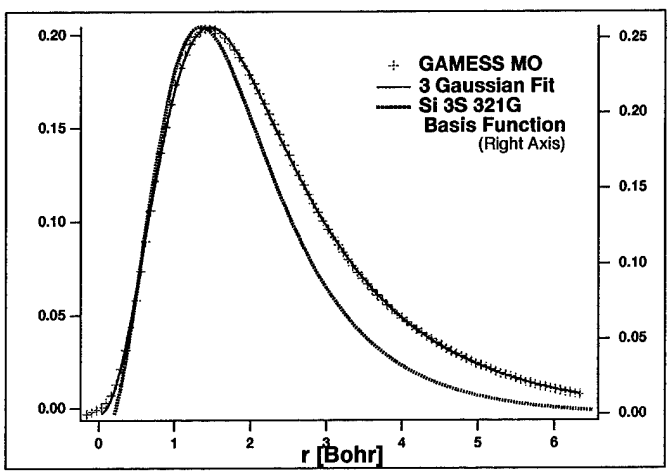

Parameter	Fit 1	Fit 2	Uncertainty
α_1	1.100390	1.100410	0.012
α_2	0.206783	0.206757	0.010
α_3	0.068053	0.068053	0.002
c_1	-0.327756	-0.327748	0.004
c_2	0.201936	0.201955	0.007
c_3	0.122519	0.122492	0.009
Error	0.000106	0.000106	

Figure 4.8 Si_4H_9 single electron MO. Si nucleus located at r=0.

shown in this figure is the input MO from the silicon 3s basis basis function from the HW ECP basis set. We see that the MO from S $i_4H_9^{\bullet}$ has a significantly larger component at larger radii than does the silicon 3s basis function. This larger radial extent of the $Si_4H_9^{\bullet}$ MO generally correlates with lower electronegativity. This may indicate that the single electron MO from $Si_4H_9^{\bullet}$ is not a good model system on which to base definition of a $\overline{H}$ for silicon.

4.5 Evaluation of Procedures used to make $\overline{H}$

4.5.1 Comparison of Model Systems. In order to determine which of the approaches described in Section 4.4 for creating $\overline{H}$s provides the best approximation to the bulk silicon environment, these $\overline{H}$s are now substituted for H atoms in the Si_9H_{12} silicon dimer model system. This same Si_9 cage can also be identified within the $Si_{66}H_{52}$ molecule shown in Figure 3.17. In $Si_{66}H_{52}$, all the atoms in the Si_9 cage are at least two bond lengths away from the terminating H atom, so the behavior of Si_9 within $Si_{66}H_{52}$ is taken to represent bulk silicon. Figure 4.9 shows the Si_9 cage, atoms 1-9, with two adsorbed H atoms, 10-11. The atom numbers used in the following discussion refer to this figure. The term "bare" dimer refers to this cage without the adsorbed H atoms.

Table 4.6 lists the Mulliken charges for Si_9 with a variety of $\overline{H}$s used in place of real H atoms. The geometries of the molecules in all these test cases was fully optimized, including the Si-$\overline{H}$ separations, as was done in Reference [8]. The first column in Table 4.6 lists the Mulliken charges for hydrogen terminated Si_9, and the last column lists the Mulliken charges for the corresponding Si atoms in $Si_{66}H_{52}$. The Mulliken charge distribution in Si_9H_{12} demonstrates the effect of H atom termination on such a small cluster. The Mulliken charge on the second layer atoms and the fourth layer atom is large, positive, and roughly equal. All these atoms all are bonded to two Si atoms, and two H atoms; hydrogen's larger electronegativity tends to move electron density away from these Si atoms, which the Mulliken analysis assigns to the H atoms (the complete structure of Si_9H_{12} is shown in Figure 3.14). The third layer Si atoms in Si_9H_{12} are each bonded to one H atom and three Si atoms, and so are not as strongly influenced by the H atom termination. The "surface" Si atoms are bonded only to Si atoms; however, the influence of the H atom termination

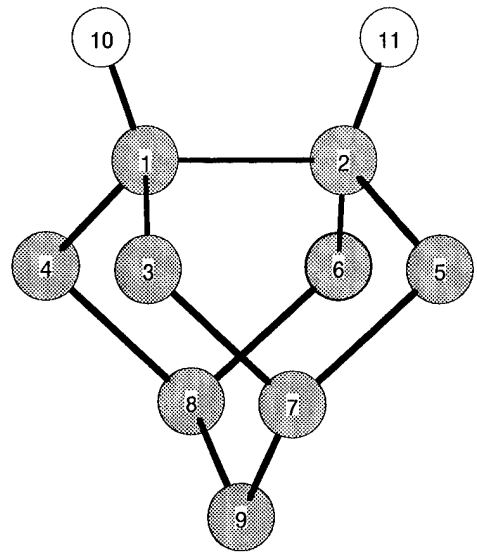

Figure 4.9 Si_9 cage with atom numbers labeled. Atoms 1-9 are silicons, 10 and 11 are hydrogen

on the second layer also affects the "surface" Si atoms. The net result is that the surface Si atoms in Si_9H_{12} have a positive Mulliken charge, in qualitative disagreement with $Si_{66}H_{52}$.

Based on the Mulliken charges in $Si_{66}H_{52}$, $\overline{H}_a$, $\overline{H}_b$, and $\overline{H}_d$ provide "plausible" representations of the bulk silicon electronic environment. The $\overline{H}_a$ results were taken from Reference [8]. $\overline{H}_c$, $\overline{H}_e$, and $\overline{H}_f$ do not provide acceptable representation of bulk silicon. The result for $\overline{H}_f$, created by grafting an Si 3s basis function onto a hydrogen nueleus, is surprising because $\overline{H}_f$ produced essentially neutral atoms for *every* atom in the $Si_5\overline{H}_{12}$ model system, the best result for any $\overline{H}$ atom investigated in this work. However, this result on the model system was obtained at a Si-$\overline{H}$ separation fixed at 2.35$\AA$, while the Si-$\overline{H}_e$ separations optimized to about 1.6$\AA$. The worst overall result is seen for $\overline{H}_e$, which was based on the fit to the single electron MO in $Si(SiH_3)_3^{\bullet}$. A possible reason for this result is that unlike the other model systems, the single electron MO in the radical is not involved in bonding , while the other model systems involve $\overline{H}$ bonded to a silicon. Since the $\overline{H}$ is intended for use in bonding, it appears that the model on which the construction of the $\overline{H}$ is based should be bonded.

		Mulliken Charge							
		H	$\overline{H}_a$	$\overline{H}_b$	$\overline{H}_c$	$\overline{H}_d$	$\overline{H}_e$	$\overline{H}_f$	$Si_{66}H_{52}$
Surface (1,2)	Si	-0.14	+0.04	+0.09	+0.17	+0.09	+0.36	+0.25	+0.10
Layer 2 (3-6)	Si	+0.39	-0.12	-0.07	-0.78	-0.18	-2.22	-0.66	-0.21
	H	-0.13	+0.05	+0.13	+0.50	+0.20	+0.98	+0.24	x
	H	-0.14	+0.04	-0.12	+0.17	-0.07	+0.97	+0.25	x
Layer 3 (7,8)	Si	+0.02	-0.01	-0.08	-0.35	-0.12	-0.48	-0.06	-0.12
	H	-0.12	+0.06	+0.12	+0.48	+0.18	+0.78	+0.19	x
Layer 4 (9)	Si	+0.33	-0.15	-0.13	-0.92	-0.23	-1.85	-0.49	-0.07
	H	-0.14	+0.06	+0.04	+0.38	+0.08	+0.80	+0.19	x
ζ		1.24	n/a	0.485	0.380	0.470	n/a	n/a	1.24

$\overline{H}_a$ Reference [8]
$\overline{H}_b$ $\overline{H}$-Si-$(SiH_3)_3$ MC Charge Match
$\overline{H}_c$ $Si_5\overline{H}_{12}$ MC Center Si Match
$\overline{H}_d$ $Si_5\overline{H}_{12}$ MC All Si Match
$\overline{H}_e$ $(SiH_3)_3$ Radical MO Fit
$\overline{H}_f$ Si 3s 321 Basis Function

Table 4.6 Mulliken charges in Si_9H_{12} obtained using a number of different $\overline{H}$ atoms for termination in place of hydrogen. The first column labeled H shows the Mulliken charges when using H atom termination. The last column shows the Mulliken charges for the same 9 Si atoms in $Si_{66}H_{52}$, which can be considered "silicon termination".

4.5.2 Effect of Si-$\overline{H}$ Separation. Now that we've seen that the Mulliken charge mirror model system can be used to create an "acceptable" $\overline{H}$ for silicon, we now examine the Mulliken charges obtained in $Si_9\overline{H}_{12}$ when these various $\overline{H}$s are used for termination. These results should indicate whether or not one can determine an "optimum" Si-$\overline{H}$ separation to use in this model system. Table 4.7 shows the Mulliken charges obtained in $Si_9\overline{H}_{12}$ using the $\overline{H}$s described in Section 4.4.4. The subscript indicates the Si-$\overline{H}$ separation used in the model system when the $\overline{H}$ was created. The Mulliken charges on the silicons in Si_9H_{12} and $Si_{66}H_{52}$ are listed in the last two columns of Table 4.7 for comparison. The columns labeled "Fixed" are single point energy calculations in which the $Si_9\overline{H}_{12}$ structure is fixed at the $Si_9\overline{H}_{12}$ RHF optimized geometry, but with the Si-$\overline{H}$ separations fixed at the values used to create the $\overline{H}$s (i.e., rSi-$\overline{H}_{1.70}$ is fixed at 1.70Å). The columns labeled "Opt" indicate geometry optimizations of the entire molecule.

	$\overline{H}_{2.36}$ Fixed	$\overline{H}_{2.36}$ Opt	$\overline{H}_{1.70}$ Fixed	$\overline{H}_{1.70}$ Opt	$\overline{H}_{1.20}$ Fixed	$\overline{H}_{1.20}$ Opt	Si_9H_{12}	$Si_{66}H_{52}$
Surface Si	-0.04	+0.09	+0.12	+0.07	+0.08	+0.07	-0.14	+0.10
Layer 2 Si	-0.03	-0.07	-0.01	+0.16	+0.42	+0.20	+0.39	-0.21
Layer 3 Si	-0.04	-0.08	+0.02	+0.02	+0.31	+0.03	+0.02	-0.12
Layer 4 Si	-0.03	-0.13	0.00	+0.09	+0.35	+0.13	+0.33	-0.07
r Si-$\overline{H}$(Å)	2.36	1.68	1.70	1.62	1.20	1.62	1.48	n/a
ζ	0.485	0.485	0.515	0.515	0.52	0.52	1.24	1.24

Table 4.7 Mulliken charges in $Si_9\overline{H}_{12}$ for $\overline{H}$s created at different Si-$\overline{H}$ separations in the model system, HW ECP basis set. $\overline{H}_{2.36}$ refers to the $\overline{H}$ created at an Si-$\overline{H}$ separation of 2.36Å, etc. The columns labeled Fixed are single point energy calculations with the Si atoms fixed at the Si_9H_{12} optimized positions and the Si-$\overline{H}$ separations fixed at the Si-$\overline{H}$ separation used in the model system. The columns labels Opt are the results from optimized $Si_9\overline{H}_{12}$ geometries.

The case for $\overline{H}_{2.36}$ in which rSi-$\overline{H}$ is fixed at 2.36Å matches the procedure used by Goddard et al, though a different model system was used to create the $\overline{H}$ atom. For this case, we see the Mulliken charges on all the silicons differ by only 0.01, and they are all very close to 0.0 (neutral). This is the kind of result one would expect for bulk silicon. The case for $\overline{H}_{2.36}$ in which rSi-$\overline{H}$ and the rest of the structure is allowed to optimize matches Carter's procedure. The optimized value of rSi-$\overline{H}$ is 1.68Å, a difference of 0.68Å. Carter used an rSi-$\overline{H}$ of 2.35Å in the $Si_5\overline{H}_{12}$ model system; the rSi-$\overline{H}$ optimized to 1.72Å

in $Si_9\overline{H}_{12}$. The silicon Mulliken charges obtained for $\overline{H}_{2.36}$ when the geometry is allowed to optimize show noticeable changes. The silicons no longer appear equivalent, and the top two "layers" now have opposite Mulliken charges. Qualitatively, this result agrees with Carter's result (see Table 4.6) and the Mulliken charges for the equivalent Si atoms in $Si_{66}H_{52}$. $\overline{H}_{1.70}$ is an $\overline{H}$ atom created in the Mulliken charge mirror model at rSi-$\overline{H}$ = 1.70$\AA$. The third column lists the Mulliken charges for the silicons in $Si_9\overline{H}_{12}$ with rSi$\overline{H}_{1.70}$ fixed to 1.70$\AA$. In this case, the silicons do not appear equivalent based on Mulliken charge. When the geometry is allowed to optimize(column 4), the Si Mulliken charges all become positive. The optimum Si-$\overline{H}$ separation in this case is 1.62$\AA$. The Mulliken charges for the case using $\overline{H}_{1.20}$ at a fixed rSi-$\overline{H}$ of 1.20$\AA$ are clearly not equivalent. The Mulliken charges obtained using $\overline{H}_{1.20}$ but allowing the geometry to optimize are smaller, but are neither equivalent nor match the charges in $Si_{66}H_{52}$.

The Mulliken charges obtained by using $\overline{H}_{2.36}$ to terminate Si_9H_{12} while keeping the Si-$\overline{H}$ separation value make the most sense. The $\overline{H}$ was created to represent the electronic environment of bulk silicon. When it is used to terminate a silicon cluster, the Mulliken charges on all the silicons are all very close to zero, which is what one expects for bulk silicon. However, these Mulliken charges are not the best match for the Mulliken charges in $Si_{66}H_{52}$. There are two possible explanations for this result. $Si_{66}H_{52}$ may be too small to give a good representation of bulk silicon, or a bulk-like model system is inappropriate for creating $\overline{H}$s to terminate surface model clusters.Before attempting a calculation on a larger silicon cluster, we shall examine how the use of $\overline{H}$ based on Mulliken charges affects other molecular properties such as geometry and hydrogenation energetics.

Table 4.7 shows how large an effect the Si-$\overline{H}$ separation has on the Mulliken charges. Recall from Table 4.1 that $\overline{H}_{321}$ made all the atoms in $Si_5\overline{H}_{12}$ essentially neutral. Table 4.6 showed that the Mulliken charges in $Si_9\overline{H}_{12}$ using $\overline{H}_{321}$ while allowing the Si-$\overline{H}$ separation to vary produced Mulliken charges that did not match $Si_{66}H_{52}$. Table 4.8 shows a comparison of the Mulliken charges in $Si_9\overline{H}_{12}$ using $\overline{H}_{321}$ with the Si-$\overline{H}$ fixed at 2.36$\AA$, the results for the optimized geometry, and the results for $Si_{66}H_{52}$. With the Si-$\overline{H}$ separation fixed, the Mulliken charges are similar to those in $Si_{66}H_{52}$, but show differences in the third and fourth layers.

	$\overline{H}_{Si3s}$ Fixed	$\overline{H}_{Si3s}$ Opt	Si_9H_{12}	$Si_{66}H_{52}$
Surface Si	0.005	+0.25	-0.14	+0.10
Layer 2 Si	-0.06	-0.66	+0.39	-0.21
Layer 3 Si	-0.03	-0.06	+0.02	-0.12
Layer 4 Si	-0.05	-0.49	+0.33	-0.07
r Si-$\overline{H}$($\AA$)	2.36	1.68	1.48	n/a

Table 4.8 Mulliken charges in $Si_9\overline{H}_{12}$ using $\overline{H}_{Si3s}$ at fixed and optimized Si-$\overline{H}$ separations.

4.5.3 Discussion on $\overline{H}$s. What can we conclude from these results ? It appears that different approaches can be used to create $\overline{H}$ atoms that behave roughly the same when used to terminated Si_9, at least in terms of Mulliken charges. Si-$\overline{H}$ separation has a significant effect on the Mulliken charges. The best matches of the Mulliken charges in $Si_{66}H_{52}$ were produced in $Si_9\overline{H}_{12}$ using $\overline{H}_{2.36}$ when the geometry of $Si_9\overline{H}_{12}$ was optimized. However, the large change in the Si-$\overline{H}$ separations observed in these optimizations, 2.36$\AA$ to 1.68$\AA$, makes one wonder what other effects the optimization has had on the molecule. *I.e., other than matching Mulliken charges, how good a model of bulk silicon is Si_9H_{12} ? Based on the results at this point, Goddard's procedure, keeping the Si-$\overline{H}$ separation fixed at the same value everytime a $\overline{H}$ is used, is the most consistent in that all the silicons in $Si_9\overline{H}_{12}$ have Mulliken charges that are close to bulk silicon values.*

4.6 Detailed Evaluation of MC Mirror $\overline{H}$

The results in Table 4.6 show that one can obtain a reasonable match to the Mulliken charges of a bulk-like silicon molecule by using $\overline{H}$s to terminate a small silicon cluster. However, it is unclear what effect the use of $\overline{H}$s has on other properties of the cluster, so additional comparisons must be made. The $\overline{H}$ atom created using the Mulliken charge mirror model, $\zeta = 0.47$, was selected for additional evaluation because this $\overline{H}$ performed well in matching Mulliken charges of the bulk silicon model, and because the Mulliken charge mirror model has potential to be used for other materials. To provide a more complete picture of the effects of $\overline{H}$ termination, optimized molecular geometry, energy of hydrogenation, and ionization energy with and without $\overline{H}$ termination will be compared. The use of $\overline{H}$s in MIMOMM optimizations will also be investigated.

Table 4.9 lists a summary of the calculations performed compare the behavior of Si_9H_{12} and $Si_9\overline{H}_{12}$ to see if $\overline{H}$ termination does make this small silicon cluster better reproduce the behavior of $Si_{66}H_{52}$, which is taken to represent bulk silicon. In Table 4.9, the term "bare" dimer refers to a dimer with two dangling bonds, as shown in Figure 3.14. The label "half-hydrogenated" dimer refers to a dimer in which one of the dangling bonds has been saturated by an *adsorbed* H atom, as shown in Figure 4.12. The label "fully hydrogenated" dimer refers to a dimer in which both of the dangling bonds have been saturated by adsorbed H atoms, as is shown in Figure 4.9.

Test Cases for $\overline{H}$ Evaluation		
Cluster	Calculation Method	Model
Hydrogen Termination		
Si_9H_{12}	*ab initio*	Si dimer, bare
$Si_9H_{12}H$	*ab initio*	Si dimer, half-hydrogenated
$Si_9H_{12}H_2$	*ab initio*	Si dimer, fully hydrogenated
$Si_9H_{12}/Si_{66}H_{52}$	MIMOMM	Si dimer, bare
$\overline{H}$ Termination		
$Si_9\overline{H}_{12}$	*ab initio*	Si dimer, bare
$Si_9\overline{H}_{12}H$	*ab initio*	Si dimer, half-hydrogenated
$Si_9\overline{H}_{12}H$	*ab initio*	Si dimer, fully hydrogenated
$Si_9\overline{H}_{12}/Si_{66}H_{52}$	MIMOMM	Si dimer, bare
"Silicon Termination"		
$Si_{66}H_{52}$	*ab initio*	Si dimer, bare
$Si_{66}H_{52}H$	*ab initio*	Si dimer, half-hydrogenated
$Si_{66}H_{52}H_2$	*ab initio*	Si dimer, fully hydrogenated

Table 4.9 Test cases used to evaluate the effect of effect of $\overline{H}$ termination on small silicon clusters. The results from calculations on $Si_{66}H_{52}$, $Si_{66}H_{52}H$, and $Si_{66}H_{52}H_2$ are taken to represent bulk silicon, i.e., the right answer.

4.6.1 Mulliken Charges. Tables 4.10 and 4.11 show the Mulliken charges for the bare and hydrogen saturated dimer in the Si_9 embedded cluster. The results can be summarized as:

- As discussed in Section 4.5, use of $\overline{H}$ terminated Si_9 with rSi-$\overline{H}$ allowed to optimize provides a better match of the Mulliken charges in $Si_{66}H_{52}$ than hydrogen termination.
- MIMOMM optimization has no effect on the Mulliken charges in the H terminated cluster, and a small effect on Mulliken charges in the $\overline{H}$ terminated cluster.

- Hydrogen saturation of the dimer substantially changes the Mulliken charges at the surface. $\overline{H}$ termination provides a better match of Mulliken charges in the bulk-like molecule than H termination
- MIMOMM optimization causes a small change (0.01) in the magnitude of the Mulliken charges in the H and $\overline{H}$ terminated clusters, but does not change the overall trends

		Mulliken Charges				
		Ab Initio	*Ab Initio*	MIMOMM	MIMOMM	*Ab Initio*
Embedded		Si_9H_{12}	$Si_9\overline{H}_{12}$	Si_9H_{12}	$Si_9\overline{H}_{12}$	$Si_{66}H_{52}$
Bulk		None	None	$Si_{66}H_{52}$	$Si_{66}H_{52}$	None
Surface	Si	-0.14	+0.09	-0.14	+0.099	+0.10
Layer 2	Si	+0.39	-0.12	+0.39	-0.099	-0.21
Layer 3	Si	+0.02	-0.08	+0.01	-0.084	-0.12
Layer 4	Si	+0.33	-0.13	+0.35	-0.119	-0.07

Table 4.10 Comparison of Mulliken Charges, Bare Dimer (HW ECP basis set), in *ab initio* and MIMOMM optimized systems.

		Mulliken Charges				
		Ab Initio	*Ab Initio*	MIMOMM	MIMOMM	*Ab Initio*
Embedded		Si_9H_{14}	$Si_9\overline{H}_{12}H_2$	$Si_9H_{12}H_2$	$Si_9\overline{H}_{12}H_2$	$Si_{66}H_{54}$
Bulk		None	None	$Si_{66}H_{54}$	$Si_{66}H_{54}$	None
Surface	Si	+0.02	+0.25	+0.02	+0.276	+0.21
Adsorbed	H	-0.10	-0.08	-0.14	-0.086	-0.04
Layer 2	Si	+0.36	-0.12	+0.37	-0.148	-0.23
Layer 3	Si	+0.00	-0.09	0.00	-0.099	-0.14
Layer 4	Si	+0.34	-0.10	+0.34	-0.112	-0.08

Table 4.11 Comparison of Mulliken Charges, hydrogenated Dimer (HW ECP basis set), in *ab initio* and MIMOMM optimized systems.

The results in Tables 4.10 and 4.11 were obtained using the HW ECP basis set for two reasons: to facilitate comparisons with previous ECP basis set results, and to enable full *ab initio* calculations on $Si_{66}H_{52}$. However, better basis sets are required for more reliable results. Since the value of ζ for an $\overline{H}$ atom depends on the basis set, *a different $\overline{H}$ must be created for each basis set.* An $\overline{H}$ atom was created using the Mulliken charge mirror model system with the 6-31G* basis set for use in 6-31G* calculations (Table 4.4). Table 4.12 shows the Mulliken charges obtained in $Si_9\overline{H}_{12}$ calculated with the 6-31G* basis set, as well as HW ECP basis set results for $Si_{66}H_{52}$. Comparing the H atom terminated

Si_9 results at the HW ECP and 6-31G* basis sets, we see that while the magnitude of the Mulliken charges changes, the qualitative behavior remains the same. However, the Mulliken charges obtained using $\overline{H}$ termination and the 6-31G* basis set are quantitatively and *qualitatively* are different than both the HW ECP results using $\overline{H}$ termination, and the Mulliken charges in $Si_{66}H_{52}$ using the HW ECP basis set.

	Mulliken Charges				
	Si_9H_{12} HW ECP	$Si_9\overline{H}_{12}$ HW ECP	Si_9H_{12} 6-31G*	$Si_9\overline{H}_{12}$ 6-31G*	$Si_{66}H_{52}$ HW ECP
Surface Si	-0.14	+0.09	-0.17	+0.001	+0.10
Layer 2 Si	+0.39	-0.12	+0.26	+0.75	-0.21
Layer 3 Si	+0.02	-0.08	+0.02	+0.40	-0.12
Layer 4 Si	+0.33	-0.13	+0.25	+0.75	-0.07

Table 4.12 Comparison of Mulliken Charges, bare dimer, for $\overline{H}$ atoms created to be used with the 6-31G* basis set.

The differences between the HW ECP and 6-31G* results highlight the basis set dependence of the Mulliken population analysis. The extra flexibility provided by the larger 6-31G* basis set makes the Mulliken partitioning of charges less appropriate, and suggests that use of $\overline{H}$s created using Mulliken charge as a metric is unreliable for larger basis sets.

4.6.2 Structure. A comparison of the HW ECP optimized structures of Si_9H_{12} and $Si_9\overline{H}_{12}$ is listed in Table 4.13. (The atom numbers are defined in Figure 4.9.) A comparison of Si atom displacements from lattice positions caused by formation of the surface dimer is listed in Table 4.14. We saw in Chapter III that the geometry and atom displacements of Si_9H_{12} gave a reasonable representation of the geometry and displacements caused by dimer formation from both larger scale calculations and experiment. Here, we see that $\overline{H}$ termination produces a significantly different structure. The motion of the second layer atoms in $Si_9\overline{H}_{12}$ along the y axis is approximately a factor of 6 smaller than in Si_9H_{12}. The motion of the third layer atoms along the z axis is down in Si_9H_{12}, but up in $Si_9\overline{H}_{12}$. The fourth layer atom in Si_9H_{12} moves $0.008\mathring{A}$ up along the z axis, while in $Si_9\overline{H}_{12}$, this atom moves up $0.314\mathring{A}$. Similar results for the hydrogenated dimer are listed

in Table 4.15. Similar distortions in cluster geometry are seen when $\overline{H}$ atoms are used for termination.

These results can be summarized as:

- The structure of real hydrogen terminated Si_9 matches the structure of $Si_{66}H_{52}$ better than $\overline{H}$ terminated Si_9
- The differences seen in $\overline{H}$ terminated Si_9 are significant because a silicon cage should be a fairly stiff system
- The MIMOMM optimized structure of Si_9H_{12} differs slightly from the *ab initio* optimized results (as was discussed in Chapter III)
- The steric forces in the MIMOMM optimization have a larger effect on $\overline{H}$ terminated Si_9, and drive the coordinates closer towards the values seen for $Si_{66}H_{52}$. However, significant differences between the hybrid optimizations and the *ab initio* optimized geometry of $Si_{66}H_{52}$ remain

Table 4.16 shows a comparison of the optimized geometries obtained for $Si_9\overline{H}_{12}$ using the $\overline{H}$s created at several different separations in the Mulliken charge mirror model, $\overline{H}_{2.36}$, $\overline{H}_{1.70}$, and $\overline{H}_{1.20}$. The optimized geometries for all three $\overline{H}$s are very similar, and all show significant differences from the structures of Si_9H_{12} and $Si_{66}H_{52}$.

Lastly, Tables 4.17 and 4.18 show a comparison of the optimized geometries and atom diplacements obtained using the $\overline{H}$ atom created to match the 6-31G* basis set. We see that the overall results are the same as obtained using the HW ECP basis set: the geometry of Si_9H_{12} matches other theoretical results and experiment better than $Si_9\overline{H}_{12}$. Figures 4.10 and 4.11 show the optimized geometries of Si_9H_{12} and $Si_9\overline{H}_{12}$ (respectively). In addition to the differences in the Si positions, these figures also highlight the differences in H-Si-H and $\overline{H}$-Si-$\overline{H}$ angles in these cases.

Embedded Bulk	*Ab Initio* Si_9H_{12} None	*Ab Initio* $Si_9\overline{H}_{12}$ None	MIMOMM Si_9H_{12} $Si_{66}H_{52}$	MIMOMM $Si_9\overline{H}_{12}$ $Si_{66}H_{52}$	*Ab Initio* $Si_{66}H_{52}$ None
Dimer (Å)	2.170	2.182	2.172	2.178	2.160
∠ 3 1 4°	114.658	100.682	115.021	104.020	118.010
∠ 3 1 2°	107.724	109.997	107.502	108.630	106.948
∠ 3 7 5°	98.381	109.805	98.404	105.295	97.616
∠ 7 9 8°	116.979	119.223	115.049	115.020	114.141

Table 4.13 Comparison of Si_9 structure, bare dimer, HW ECP basis set. RHF results are listed.

Atom	Atom Displacements (Å)					
	H termination			$\overline{H}$ termination		
	δ x	δ y	δ z	δ x	δ y	δ z
Surface						
1	0.000	0.829	-0.214	0.000	0.823	0.020
2	0.000	-0.829	-0.214	0.000	-0.823	0.020
Layer 2						
3	0.055	0.115	0.098	-0.104	0.017	0.109
4	-0.055	0.115	0.098	0.104	0.017	0.109
5	0.055	-0.115	0.098	-0.104	-0.017	0.109
6	-0.055	-0.115	0.098	0.104	-0.017	0.109
Layer 3						
7	0.113	0.000	-0.098	0.105	0.000	0.149
8	-0.113	0.000	-0.098	-0.105	0.000	0.149
Layer 4						
9	0.000	0.000	0.008	0.000	0.000	0.314

Table 4.14 Atom displacements induced by symmetric dimer formation in the Si_9H_{12} model of the Si(001) surface, HW ECP basis set.

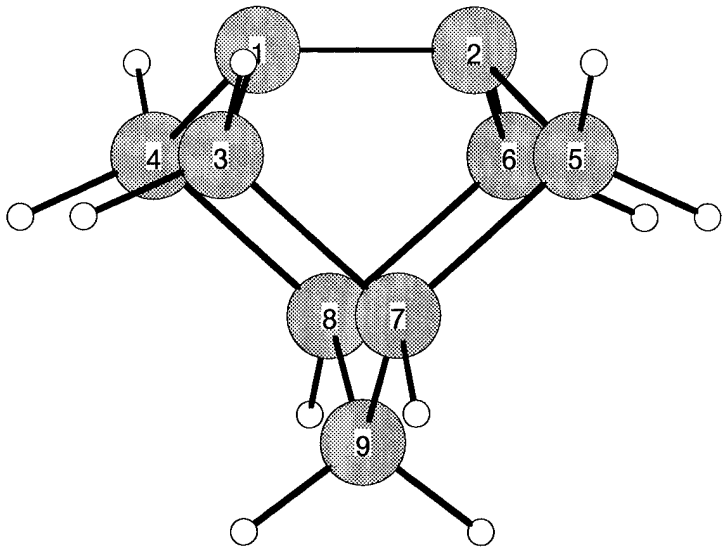

Figure 4.10 Si_9H_{12} 6-31G* optimized geometry (side view)

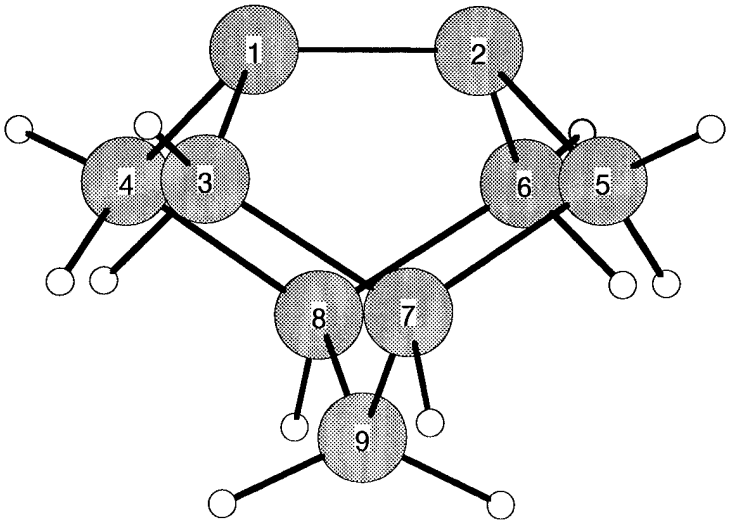

Figure 4.11 $Si_9\overline{H}_{12}$ 6-31G* optimized geometry (side view)

Embedded Bulk	*Ab Initio* Si_9H_{14} None	*Ab Initio* $Si_9\overline{H}_{12}H_2$ None	MIMOMM $Si_9H_{12}H_2$ $Si_{66}H_{54}$	MIMOMM $Si_9\overline{H}_{12}H_2$ $Si_{66}H_{54}$	*Ab Initio* $Si_{66}H_{54}$ None
Dimer($\AA$)	2.381	2.418	2.394	2.412	2.392
Si-H_{ads}($\AA$)	1.473	1.469	1.473	1.469	1.472
$\angle$ 1 2 H°_{ads}	112.851	113.857	112.442	114.955	112.195
$\angle$ 3 1 4°	105.492	94.904	108.407	98.190	110.122
$\angle$ 3 1 2°	104.938	106.483	104.326	104.992	103.800
$\angle$ 3 7 5°	99.903	110.207	99.016	104.956	98.047
$\angle$ 7 9 8°	111.653	114.272	111.839	112.380	111.113

Table 4.15 Comparison of Si_9 structure with two H atoms adsorbed on the dimer, HW ECP basis set. RHF results are listed

	$\overline{H}_{2.36}$	$\overline{H}_{1.70}$	$\overline{H}_{1.20}$	Si_9H_{12}	$Si_{66}H_{52}$
Dimer ($\AA$)	2.182	2.178	2.177	2.170	2.160
$\angle$ 3 1 4°	100.682	100.870	100.929	114.658	118.010
$\angle$ 3 1 2°	109.997	110.178	110.207	107.724	106.948
$\angle$ 3 7 5°	109.805	109.700	109.705	98.381	97.616
$\angle$ 7 9 8°	119.223	118.440	118.292	116.979	114.171
ζ	0.485	0.515	0.520	1.24	n/a

Table 4.16 Comparison of Si_9 *ab initio* optimized structure, unsaturated dimer using $\overline{H}$s created at different Si-$\overline{H}$ separations in the model system (HW ECP basis set, RHF results).

	Si_9H_{12} 6-31G*	$Si_9\overline{H}_{12}$ 6-31G*	$Si_{66}H_{52}$ HW ECP
Dimer(Å)	2.187	2.188	2.160
∠ 3 1 4°	116.495	100.982	118.010
∠ 3 1 2°	107.299	111.031	106.948
∠ 3 7 5°	97.552	112.700	97.616
∠ 7 9 8°	117.460	120.629	114.171

Table 4.17 Effect of $\overline{H}$ termination on Si_9H_{12} *ab initio* optimized geometry, 6-31G* basis set.

Atom	Atom Displacements (Å)					
	H termination			$\overline{H}$ termination		
	δ x	δ y	δ z	δ x	δ y	δ z
Surface						
1	0.000	0.850	-0.254	0.000	0.850	-0.116
2	0.000	-0.850	-0.254	0.000	-0.850	-0.116
Layer 2						
3	0.065	0.144	0.098	-0.118	-0.003	0.020
4	-0.065	0.144	0.098	-0.118	-0.003	0.020
5	0.065	-0.144	0.098	-0.118	0.003	0.020
6	-0.065	-0.144	0.098	0.118	0.003	0.020
Layer 3						
7	0.104	0.000	-0.099	0.121	0.000	0.126
8	-0.104	0.000	-0.099	-0.121	0.000	0.126
Layer 4						
9	0.000	0.000	0.023	0.000	0.000	0.315

Table 4.18 Atom displacements induced by symmetric dimer formation in the Si_9H_{12} model of the Si(001) surface, RHF 6-31G* basis set. The atom displacements for the $Si_9\overline{H}_{12}$ *qualitatively and quantitavely disagree with calculated displacements in* Si_9H_{12}.

4.6.3 Energetics. Another check on the effect of $\overline{H}$ termination is to look at the energy of hydrogenation of the silicon dimer. Nachtigall et al [83] performed a series of calculations including correlation corrections on the energy of hydrogenation of Si_9H_{12}. For comparison, the energies for the same reactions of Si_9H_{12} using the HW ECP basis set with d functions on all silicons for both the hydrogen and $\overline{H}$ terminated clusters were calculated in this work. For comparison with bulk silicon, the same reactions have been modeled on $Si_{66}H_{52}$ (Figure 3.17). $Si_{66}H_{52}$ has only a single unsaturated surface dimer, so it provides a good comparison for hydrogenation of Si_9H_{12}, which is a model of a single surface dimer.

Table 4.19 lists the energies of the final states used to calculate the reaction energetics. The HW ECP basis set with d functions was used for all the Si_9X_{12} (X=H or $\overline{H}$) molecules. Use of the HW ECP plus d basis set for $Si_{66}H_{52}$ gives a total of 1028 atomic orbitals, which is prohibitively large for an optimization. To reduce the size of the calculation, d functions were only placed on the 9 silicon atoms common to Si_9H_{12}, giving a total of 686 AOs for $Si_{66}H_{52}$. With a numerical Hessian (calculated with the AM1 [41] semi-empirical method), the RHF optimization of $Si_{66}H_{52}$ (and $Si_{66}H_{54}$) took approximately 14 hours on 32 nodes of an IBM SP2 using C_{2V} symmetry. $Si_{66}H_{53}$, because it has only C_S symmetry, took 31 hours on 32 nodes of an SP2. Since the implementation of semi-empirical calculations in GAMESS does not include gradients for the Generalized Valence Bond (GVB) technique, the GVB-PP(1) optimization of $Si_{66}H_{52}$ used a numerical Hessian, which resulted in the lengthy optimization time of 100 hours on 32 SP2 nodes even with C_{2v} symmetry.

The results from this work, as well as those from Reference [83] are listed in Table 4.20. Nachtigall et al's calculations were performed at a higher level of theory than the calculation in this work, so their hydrogenation energies are larger. However, both Reference [83] and the present calculations on Si_9H_{12} predict a larger energy for the addition of the second hydrogen than the first. The calculations on $Si_9\overline{H}_{12}$ predict that the energy of hydrogenation for each H atom is roughly the same. The calculations on $Si_{66}H_{52}$ also predict a larger energy for the addition of the second hydrogen than the first. So, the

Molecule	Model	Symmetry	Energy (H)
Si_9H_{12}	^{1}RHF	C_{2v}	-40.928623
Si_9H_{12}	^{3}UHF	C_{2v}	-40.932507
Si_9H_{12}	^{1}TCSCF	C_1	-40.960589
Si_9H_{13}	^{2}ROHF	C_s	-41.559510
Si_9H_{14}	^{1}RHF	C_{2v}	-42.169727
$Si_9\overline{H}_{12}$	^{1}RHF	C_{2v}	-39.190375
$Si_9\overline{H}_{12}$	^{3}UHF	C_{2v}	-39.206553
$Si_9\overline{H}_{12}$	^{1}TCSCF	C_1	-39.227388
$Si_9\overline{H}_{12}H$	^{2}ROHF	C_s	-39.836747
$Si_9\overline{H}_{12}H_2$	^{1}RHF	C_{2v}	-40.444197
$Si_{66}H_{52}$	^{1}RHF	C_{2v}	-278.552983
$Si_{66}H_{52}$	GVB-PP(1)	C_{2v}	-278.586510
$Si_{66}H_{53}$	^{2}ROHF	C_s	-279.189470
$Si_{66}H_{54}$	^{1}RHF	C_{2v}	-279.799806
H	^{2}ROHF	n/a	-0.496979
H_2	^{1}RHF	C_1	-1.121680

Table 4.19 State energies used to calculate energy of hydrogenation, H and $\overline{H}$ terminated molecules.

predicted hydrogention energetics from a small H terminated silicon cluster agrees better with the bulk silicon model system than the $\overline{H}$ terminated silicon cluster.

					Δ E (kcal/mole)			
					X=Si_9H_{12} Ref [83]	Si_9H_{12}	$Si_9\overline{H}_{12}$	$Si_{66}H_{52}$
XH_2	$\rightarrow$	XH	+	H	81	71	69	71
XH	$\rightarrow$	X	+	H	76	63	71	66
XH_2	$\rightarrow$	X	+	H_2	56	54	59	57

Table 4.20 Comparison of energy of hydrogenation, H and $\overline{H}$ terminated molecules.

In addition to the differences in energy, the $\overline{H}$ terminated optimization of $Si_9\overline{H}_{12}H$ also produced a structure with a noticeable amount of distortion in the silicon cage, shown in Figure 4.13. A similar distortion was not seen in the hydrogen terminated cluster $Si_9H_{12}H$.

4.6.4 Ionization Potential. Redondo and Goddard [7] used the ionization potential (IP) of the $Si(SiH_3)_3$ radical as an additional test of the ability of $\overline{H}$s to mimic the

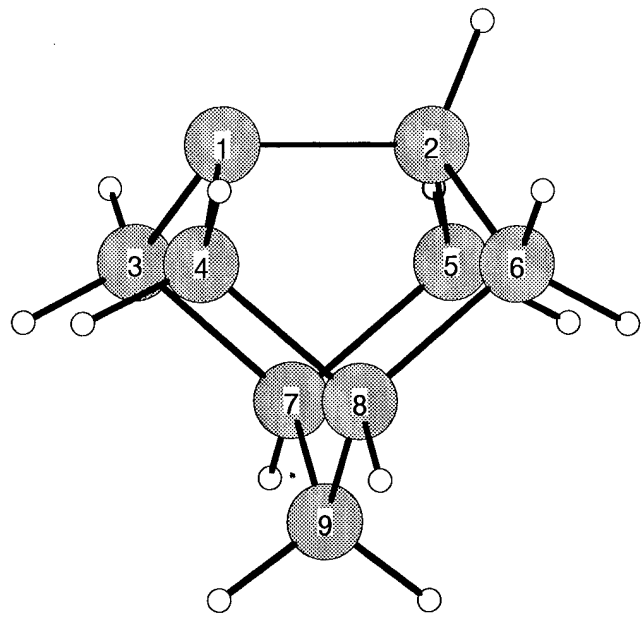

Figure 4.12 $Si_9H_{12}H$ optimized geometry, C_s symmetry.

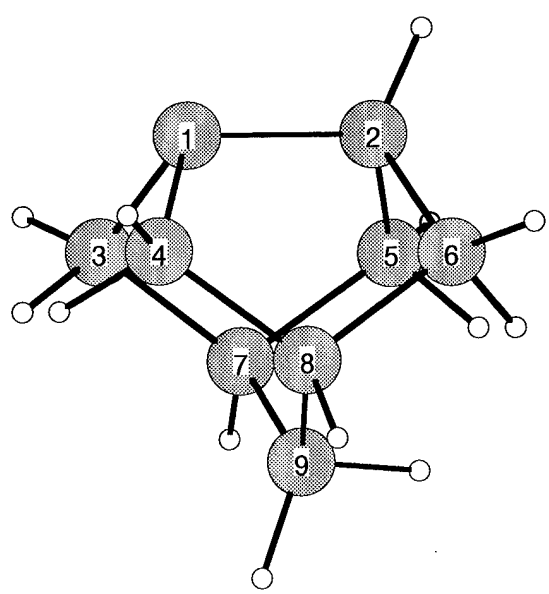

Figure 4.13 $Si_9\overline{H}_{12}H$ optimized geometry, C_s symmetry.

Reference [7]	
ζ	IP (eV)
H atom	
1.24	7.90
$\overline{H}$	
0.2944	5.95

This Work	
ζ	IP (eV)
H atom	
1.24	7.83
$\overline{H}$	
0.60	8.81
0.485	8.02
0.380	6.97
0.30	6.05

Table 4.21 Ionization potential of a silicon dangling bond in $Si(SiH_3)_3$ and $Si(Si\overline{H}_3)_3$ as a function of radial scaling parameter, HW ECP(d) basis set. $\zeta = 0.485$ produced the smallest deviation from neutrality for all the Si atoms in the Si_5H_{12} bulk silicon model. (Table 4.2) $\zeta = 0.60$ satisfied Goddard's criteria for neutrality on the central Si atom in this work for the HW ECP(d) basis set. $\zeta = 0.38$ satisfied this criterion for HW ECP basis set. $\zeta = 0.30$ was used to compare with Goddard's value of ζ. Bulk silicon IP is 5.5-5.9 eV [7].

electronic environment of bulk silicon. To compare the present work with Reference [7], we shall look at some IP results using $\overline{H}$s created using Redondo and Goddard's tetrahral model system. The ionization potential for this molecule is defined as

$$IP = E(Si(SiX_3)_3{}^+) - E(Si(SiX_3)_3{}^\bullet), \tag{4.17}$$

where X is either a hydrogen atom or a $\overline{H}$. To simulate bulk silicon, the bond angles are fixed at lattice (tetrahedral) values, though the Si-Si separation are allowed to vary. For the $\overline{H}$ terminated radicals and ions, the Si-$\overline{H}$ separation was kept fixed at Si-Si lattice separations. For the hydrogen terminated molecule, the Si-H separation is allowed to vary. For the $\overline{H}$ terminated molecule, the Si-$\overline{H}$ separation is fixed at the Si-Si lattice value.

A comparison of the results from Reference [7] and this work is listed in Table 4.21. We see that the $\overline{H}$ that provided the best match for neutrality for all the Si atoms in the tetrahedral bulk silicon model system, Si_5H_{12} (all values are taken from Table 4.2), with a value of $\zeta = 0.485$, produces a larger IP than the hydrogen terminated system. $\zeta = 0.60$ is the value obtained in this work that achieves (near) neutrality on the central silicon in the $Si_5\overline{H}_{12}$ model system, i.e., satisfies Redondo and Goddard's criterion. $\zeta = 0.60$ gives a larger IP than the hydrogen terminated system. $\zeta = 0.30$ was selected because it was

close to the value used in Reference [7]. While $\zeta = 0.30$ produces an IP quite close to that found in Reference [7] and experiment, $\zeta = 0.30$ produced a Mulliken charge of +0.414 on the central silicon in $Si_5\overline{H}_{12}$, and Mulliken charges of -1.056 on the other 4 silicons.

The observation that the IP is not a linear function of ζ is a consequence of the fact that the electronegativity of a hydrogenic 1s basis function is a quadratic function of ζ (see Figure 4.2). The reason for the differences between the IP results in this work and Reference [7] are unclear. However, it is very disconcerting that an IP calculated using an $\overline{H}$ that was shown to produce bulk-like Mulliken charges in Si_9 is larger than the IP calculated using hydrogen atoms.

As an additional test, the IP of a dangling bond in Si_9H_{12} and $Si_9\overline{H}_{12}$ ($\zeta = 0.485$) were also calculated. Because removal of a dangling bond creates a significant change in the overall electronic configuration of this molecule, full geometry optimizations were performed for both cases. For Si_9H_{12}, the calculated IP is 6.94 eV, about 1 eV larger than the experimental value. For $Si_9\overline{H}_{12}$, the calculated IP is 7.45 eV, larger than both the experimental and hydrogen terminated calculated value.

4.6.5 Discussion of Silicon $\overline{H}$s. Summarizing the results on $\overline{H}$s:

- Mulliken charges with $\overline{H}$ termination and variable Si-$\overline{H}$ separations agree better with bulk-like results than with hydrogen termination using the HW ECP basis set
- Mulliken charges with $\overline{H}$ termination and variable Si-$\overline{H}$ using the 6-31G* basis set do not agree better with bulk-like results than H atom termination
- Optimized geometries with H termination agree better with calculated bulk results (on $Si_{66}H_{52}$) and experiment than with $\overline{H}$ termination
- Energies of hydrogenation of a silicon dimer with H atom termination agree better with bulk-like results than $\overline{H}$ termination
- Ionization potentials with $\overline{H}$ termination are slightly higher than results using hydrogen termination. Both results are significantly larger (around 50 kcal/mole) than experimental results for bulk silicon.

The $\overline{H}$ atoms used in this study were constructed using Mulliken charges as a criterion, and they do indeed produce Mulliken charges in small clusters that agree better with bulk-like results, though this advantage disappears at larger basis sets. For the other properties listed above, which do not have the ambiguity of the Mulliken analysis, $\overline{H}$

termination does not reproduce bulk-like results for small clusters better than H atom termination *when the Si-$\overline{H}$ separation is allowed to vary.* These results greatly diminish the confidence one would have in calculations that use $\overline{H}$ termination. H atom termination, with the caveat that the H termination will hamper correlation of small cluster results with bulk results, is the preferred solution.

4.7 Terminating Silicon Carbide

The results from the attempts to create $\overline{H}$ atoms show that not fixing the Si-$\overline{H}$ separation in a Si cluster optimization produces questionable results. Freezing Si-$\overline{H}$ separations in the cage-like clusters used in this research is not possible because the partial implementation of delocalized coordinates in GAMESS does not include this feature. However, creation of $\overline{H}$ atoms to terminate SiC can still be investigated.

4.7.1 Mulliken Population of SiC. Determining a metric based on Mulliken charges for bulk silicon or diamond is trivial. In both materials, all atoms are equivalent, and since they are all the same type, the Mulliken charge on each should be 0.0. The Mulliken charges in bulk SiC aren't clear. Orlando et. al. performed periodic Hartree Fock optimizations on a number of bulk semiconductors, including SiC using the program CRYSTAL [104]. With the 6-21G* basis set, they report Mulliken charges of ± 1.81 (!)for silicon and carbon (respectively) in SiC, with an uncertainty of ± 0.2 [117]. These Mulliken charges are huge, especially for a covalent material like SiC. Sabisch et al [118] report Mulliken charges from a DFT calculation on SiC of ± 0.14, but it is unclear how Mulliken charges from a DFT calculation compare with HF.

Since cluster models are used in this work, Mulliken charges on a moderately large sized SiC cluster, $Si_{18}C_{18}H_{42}$, were calculated using a number of basis sets. The geometry of $Si_{18}C_{18}H_{42}$ was first optimized using the 6-31G* basis set, and single point energy calculations using different basis sets were performed at the 6-31G* geometry to obtain Mulliken charges. The 6-31G* optimzed geometry of $Si_{18}C_{18}H_{42}$ is shown in Figure 4.14. Included in this figure is a listing of the Mulliken charges from the HW ECP, HW ECP(d), 6-31G*, DZP, and TZP basis sets. (This molecule has C_3 symmetry, so only unique

Mulliken charges are listed.) Here, we see how strongly the Mulliken charge depends on basis set. The largest Mulliken charges are obtained from the HW ECP basis set, the only one used without d functions. The Mulliken charges from the basis sets that included d functions are smaller than the HW ECP charges, and smaller than Orlando et al's result, but are still very large. In addition, we see that the Mulliken charges for a C or Si atom depend on the atom's location within the molecule. For a bulk material, one expects all atoms of the same type to have the same properties.

4.7.2 Creating $\overline{H}$ Atoms for SiC: Equivalence. Reconciling the Mulliken charge with any physical properties is difficult if not impossible for a highly polar material like SiC. *However, all atoms of the same type should be equivalent in a bulk material.* Instead of trying to match some value of the Mulliken charges to some physically realistic value, one can use equivalence, and seek to create $\overline{H}_{Si}$ and $\overline{H}_C$ atoms that make all the Si and C atoms in an SiC cluster equivalent. However, one needs to design a model system for this.

A modified version of the Mulliken charge mirror model was first investigated for creating $\overline{H}_{Si}$ based on equivalence. For SiC, the model system has the same configuaration as that shown in Figure 4.4. However, C atoms are now substitutued in alternating "layers", resulting in the chemical formula

$$(SiH_3)_3\text{–}C\text{–}Si\text{–}(CH_3)_3.$$

Table 4.22 shows the results from this procedure for the $\overline{H}Si(CH_3)_3$ molecule. A good match of the Mulliken charge for the full molecule was not found in varying ζ over a wide range of values. We conclude that this model is unsuitable for creating $\overline{H}$s for SiC using the Mulliken charge mirror procedure.

Designing a model system to create $\overline{H}$ atoms for SiC is more difficult than designing a model system for silicon. The bulk-like model cluster Si_5H_{12} was attractive because its T_d symmetry greatly reduced computation times. One could adapt Si_5H_{12} for SiC, making SiC_4H_{12} and CSi_4H_{12}. However, the 4 to 1 ratio of Si to C (or C to Si) atoms in these clusters is a poor match of the 1 to 1 ratio of bulk SiC, and is a poor representation of the bulk. Extending this tetrahedral model out one additional layer would produce $SiC_4Si_{12}H_{36}$

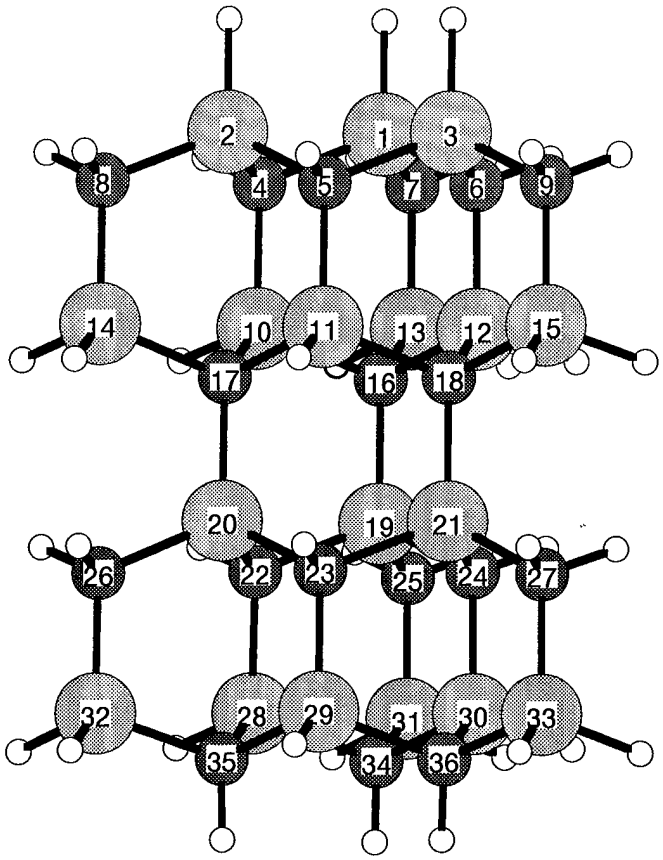

		Mulliken Charges				
Atoms	Type	HW ECP	HW ECP(d)	6-31G*	DZP	TZP
1-3	Si	1.566	1.102	0.812	1.034	0.774
4-6	C	-1.604	-1.174	-0.932	-1.262	-0.957
7-9	C	-1.312	-1.017	-0.820	-1.004	-0.873
10-12	Si	1.587	1.028	0.845	1.107	0.713
13-15	Si	1.258	0.854	0.717	0.892	0.698
16-18	C	-1.894	-1.313	-1.029	-1.568	-0.870
19-21	Si	2.014	1.428	1.085	1.354	0.958
22-24	C	-1.655	-1.215	-0.988	-1.299	-1.025
25-26	C	-1.352	-1.058	-0.854	-1.055	-0.871
28-30	Si	1.565	1.046	0.810	1.039	0.721
31-33	Si	1.236	0.855	0.683	0.873	0.675
34-36	C	-1.583	-1.159	-0.910	-1.236	-0.933
Energy(H)		-770.081	-770.905	-5907.055	-5907.214	-5907.577
Basis Functions		390	498	696	786	972

Figure 4.14 $Si_{18}C_{18}H_{42}$ molecule evaluated as a model system for creation of $\overline{H}$s. (6-31G* optimized geometry shown) Molecule has C_3 symmetry, so only unique Mulliken charges are listed.

ζ	Mulliken Charge		
	$\overline{H}$	Si_1	C_2
(Full Molecule)		+1.826	-1.027
0.40	+0.230	+0.796	-0.974
0.50	-0.166	+1.179	-0.963
0.60	-0.405	+1.441	-0.976
0.70	-0.461	+1.532	-0.984
0.80	-0.402	+1.503	-0.988
0.90	-0.293	+1.417	+0.987

Table 4.22 Mulliken Charges in the $\overline{H}Si(CH_3)_3$ molecule, HW ECP basis set. The row labeled Full Molecule shows the Mulliken charges on the equivalent nuclei in $(SiH_3)_3CSi(CH_3)_3$

and $CSi_4C_{12}H_{36}$. $SiC_4Si_{12}H_{36}$ is shown in Figure 4.15. The ratio of Si to C atoms in these clusters is approximately 3 to 1, better but still too large. A bigger problem with this model can readily be seen in Figure 4.15. In lengthening the Si-$\overline{H}$ and C-$\overline{H}$ separations to 1.89Å, the SiC lattice separation, the $\overline{H}$ atom positions are so close that their mutual interactions will be significant. $Si_{18}C_{18}H_{42}$ (Figure 4.14) contains an equal number of Si and C atoms. However, this cluster has only C_3 symmetry, so the computation time for each attempt in the process of creating a $\overline{H}$ would be lengthy. In addition, one would have to *simultaneously* create $\overline{H}_{Si}$s and $\overline{H_C}$s if $Si_{18}C_{18}H_{42}$ were used as a model system. The consequences of this added complication are unclear.

As an alternative to creating two types of $\overline{H}$ atoms in an SiC model system, one could use $\overline{H}_{Si}$ and $\overline{H}_C$ atoms created in *homogeneous* model systems. Table 4.1 presented the Mulliken charges as a function of ζ for $Si_5\overline{H}_{12}$ for the HW ECP basis set. Table 4.1 presented similar results for the HW ECP(d) basis set. Here, Table 4.23 lists these results for $C_5\overline{H}_{12}$ for the HW ECP basis set. (The specification for carbon is the same in both the HW ECP and HW ECP(d) basis sets.) Now we define the optimum value of ζ as the value which produces *equal* Mulliken charges in all the Si or C atoms in the model system (makes all the atoms look equivalent, as they would in a bulk material). For Si using the HW ECP basis set, $\zeta = 0.45$ satifies this criterion, and for C $\zeta = 0.7$ satifies this criteria. As we also see in Table 4.1, the $\overline{H}$ created by grafting the Si 3s basis function onto a hydrogen nucleus also satifies the equivalence criterion. For C using the HW ECP (and

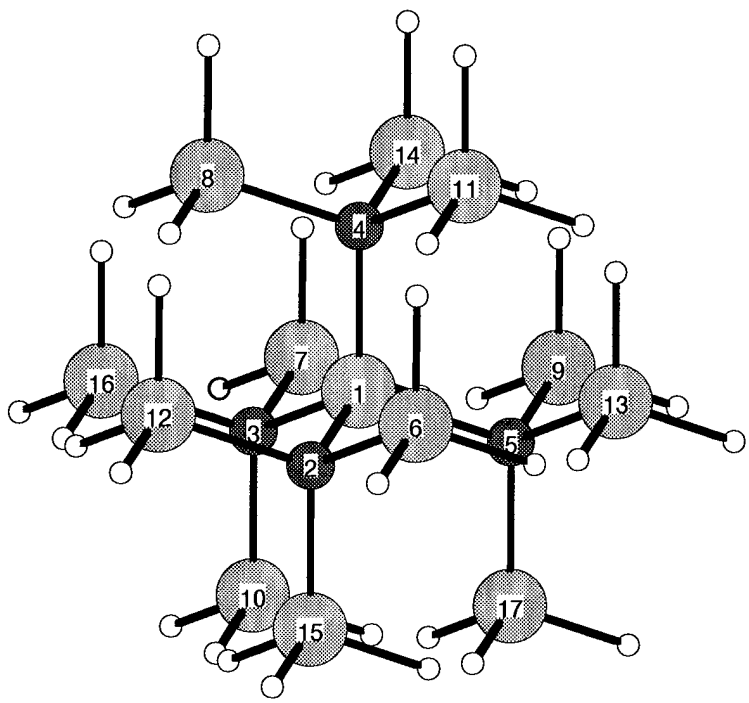

Figure 4.15 $SiC_4Si_{12}H_{36}$ tetrahedral model for bulk SiC. Notice that the $\overline{H}$ are very close to each other in this cluster.

HW ECP(d)) basis set, $\zeta = 0.7$ makes the C atoms equivalent. Also seen in this table is that grafting the C 2s basis function onto a hydrogen nucleus doesn't meet the equivalence criterion as well as was seen for silicon, but works fairly well.

	Mulliken Charge		
ζ	C_{center}	C_{outer}	$\overline{H}$
1.24	-0.353	-0.450	0.132
0.40	0.030	-1.082	0.358
0.43	-0.002	-0.976	0.326
0.45	-0.022	-0.908	0.304
0.50	-0.066	-0.743	0.253
0.60	-0.150	-0.450	0.163
0.70	-0.233	-0.230	0.096
0.80	-0.307	-0.098	0.058
0.90	-0.360	-0.061	0.051
1.00	-0.383	-0.116	0.071
C 2s	-0.221	-0.302	+0.119

Table 4.23 Mulliken charges on the $C_5\overline{H}_{12}$ molecule, HW ECP basis set. The geometry of $C_5\overline{H}_{12}$ is the same as $Si_5\overline{H}_{12}$ shown in Figure 4.3, with the bond distances shortened from $2.35\mathring{A}$ to $1.54\mathring{A}$.C_{center} refers to the center atom; C_{outer} refers to any of the four equivalent C atoms bonded to C_{center}.

From Table 4.1, we see that ζ=0.45 produces equal Mulliken charge of -0.11 in Si_5H_{12} for the HW ECP basis set. For HW ECP(d), ζ=0.51 produces equal Mulliken charges in Si_5H_{12}. A value of ζ=0.70 was found to produce equal Mulliken charges in C_5H_{12} for the HW ECP basis set.

To evaluate the utility of this approach for creating $\overline{H}$ atoms for terminating SiC, the $\overline{H}$ atoms described above were used to terminate the $Si_{18}C_{18}H_{42}$ shown in Figure 4.14. When one uses an $\overline{H}_X$ atom for termination, the X-$\overline{H}_X$ separation should be fixed at the X-$\overline{H}_X$ separation used to create the $\overline{H}_X$ atom. Thus, when $\overline{H}_{Si}$ and $\overline{H}_C$ created in single component model systems are used to terminate SiC, the Si-$\overline{H}_{Si}$ separation is fixed at $2.35\mathring{A}$, and the C-$\overline{H}_C$ separation is fixed at $1.54\mathring{A}$. (If a two component model system were used, the Si-$\overline{H}_{Si}$ and C-$\overline{H}_C$ separations would be fixed at $1.89\mathring{A}$, the SiC lattice separation.)

		Mulliken Charges					
		HW ECP			HW ECP(d)		
Atoms	Type	$\overline{H}_\zeta$	$\overline{H}_{321s}$	H	$\overline{H}_\zeta$	$\overline{H}_{321s}$	H
1-3	Si	1.502	1.370	1.566	1.242	0.996	1.102
4-6	C	-1.518	-1.510	-1.604	-1.112	-1.074	-1.174
7-9	C	-1.196	-1.188	-1.312	-0.942	-0.901	-1.017
10-12	Si	1.340	1.341	1.587	0.997	0.907	1.028
13-15	Si	0.805	0.806	1.258	0.802	0.533	0.854
16-18	C	-1.841	-1.840	-1.894	-1.271	-1.252	-1.313
19-21	Si	2.229	2.082	2.014	1.688	1.535	1.428
22-24	C	-1.531	-1.555	-1.655	-1.122	-1.119	-1.215
25-26	C	-1.101	-1.173	-1.352	-0.851	-0.879	-1.058
28-30	Si	1.438	1.360	1.565	1.131	0.956	1.046
31-33	Si	0.850	0.858	1.236	0.797	0.596	0.855
34-36	C	-1.486	-1.479	-1.583	-1.072	-1.037	-1.159

Table 4.24 Mulliken Charges in the $Si_{18}C_{18}\overline{H}_{42}$ molecule, HW ECP and HW ECP(d) basis sets. The columns labeled $overline H_\zeta$ indicate use of $overline H_{Si}$ and $overline H_C$ using the hydrogen STO-3G basis set with different values of ζ. The columns labeled $overline H_{321}$ indicate use of $overline H$s that use the valence shell s function, 3-21G split, from the HW ECP basis set.

The results of these attempts are listed in Table 4.24 for the HW ECP and HW ECP(d) basis sets. If $Si_{18}C_{18}$ were terminated "properly", all the C atoms would have the same Mulliken charge, and all the Si atoms would have the same Mulliken charge (though the Si and C Mulliken charges would be different). As in seen in Table 4.24, this result was not obtained using the $\overline{H}_{Si}$ and $\overline{H}_C$ atoms created using pure Si and C model systems. This result suggests that the composition of the model system used to create $\overline{H}$s should be the same as the system one desires to terminate.

4.8 Recommendations

$\overline{H}$s are highly dependent on basis set, geometry, and the model system in which they are created. *For specific systems of interest in single component materials, for some basis sets, one may be able to use Mulliken charge to create $\overline{H}$s to mimic some aspects of bulk-like behavior.* $\overline{H}$ atoms derived from Mulliken charges do not have much generic utility. The use of $\overline{H}$ atoms was introduced to because of the limits on the size of molecules

that can be modeled with *ab initio* techniques. With the spread of large scale parallel computers, and advances in algorithm development [59, 60], it is likely that calculations on molecules large enough to give an acceptable representation of bulk materials will soon be possible. Development of better Effective Core Potential (ECP) basis sets would also enable calculations on larger molecules.

V. *Silicon Carbide and Silicon Surface Chemistry Studies*

5.1 Introduction

In stark contrast to the wealth of theoretical (and experimental) studies of silicon and diamond surfaces, surprisingly few theoretical models of the SiC surface have been published. The bulk of the published models have focused on the SiC(001) surface because of its similarity to the (001) surface of silicon and diamond. However, the SiC(111) surface is actually of higher interest for device fabrication. This chapter presents the first application of MIMOMM for modeling the reconstruction, hydrogenation, and oxidation of Si and C-terminated SiC(111) surfaces. Literature models of the reconstruction of SiC(001) surface will first be described to show of the status of the understanding of this surface. The crystal structure of SiC(111) and the origin of the variety of different types of SiC is then discussed, as well as the rationale for the specific SiC model system used in this study. The design of the Si and C terminated hybrid SiC clusters is then discussed in some detail to highlight the factors one must consider in designing a hybrid cluster to use with MIMOMM. Results of MIMOMM models of reconstruction, hydrogenation, oxidation, and surface vacancies are described and compared with conventional *ab initio* models. Lastly, the underlying reasons for the observed differences between oxidation of Si and C terminated SiC(111) surfaces are discussed.

5.2 SiC(111) Structure: Polytypes

SiC is the most prominent of a family of close-packed materials that display a one-dimensional polymorphism called polytypism. SiC polytypes are distinguished by the stacking sequence of the tetrahedrally bonded SiC bilayers. The bond lengths and the local atomic environments of the different polytypes are nearly identical. However, the bulk electronic characteristics, e.g. electron mobility, vary by factors of 3 among the various polytypes [119].

A shorthand has been developed to catalog the different polytypes based on the fact that each SiC bilayer can occupy one of three positions with respect to the lattice, called A,B, and C. Depending on the stacking order, the bonding between Si and C atoms in

adjacent bilayers can either be zinc-blende (cubic) or wurtzite (hexagonal). The different bonding arrangements are shown in Figures 5.1 and 5.2. The purely cubic zinc-blende structure results from a stacking sequence of ABCABC (Figure 5.3), and is called 3C SiC. The purely hexagonal wurtzite form results from a stacking sequence of ABABAB (Figure 5.4) and is called 2H SiC. (In this notation, bulk silicon and diamond both have 3C stacking sequences.) All other SiC polytypes have mixtures of hexagonal and cubic bonded sites [119].

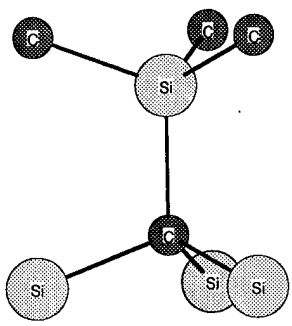

Figure 5.1 Wurtzite (hexagonal) bonding between Si and C atoms in adjacent bilayers.

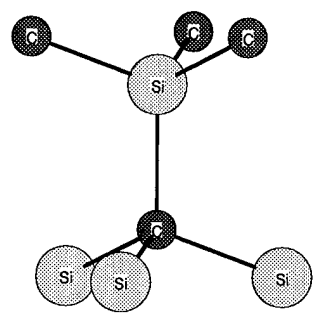

Figure 5.2 Zinc-blende (cubic) bonding between Si and C atoms in adjacent bilayers.

Among the SiC polytypes, 6H (stacking periodicity of 6 bilayers) is most easily prepared and best studied. The 3C and 4H polytypes have attracted more attention because of their superior electronic properties. The 4H polytype shown in Figure 5.5 is currently of highest interest to the Air Force for device applications [1].

5.3 Previous research on SiC Surfaces

Sabisch et al. [118] have reported the most extensive results on the reconstruction of the SiC (001) surface. They used a slab periodic model of the surface with Density Functional Theory (DFT) calculations to investigate the reconstruction of both the Si and C-terminated SiC(001) surfaces. Figure 5.6 shows the structure of the Si-terminated SiC(001) surface. (The structure of the SiC(001) surface is essentially the same as the Si(001) surface, except the atom separations are 20% smaller because of the Si-C bondlength is 1.89$\mathring{A}$

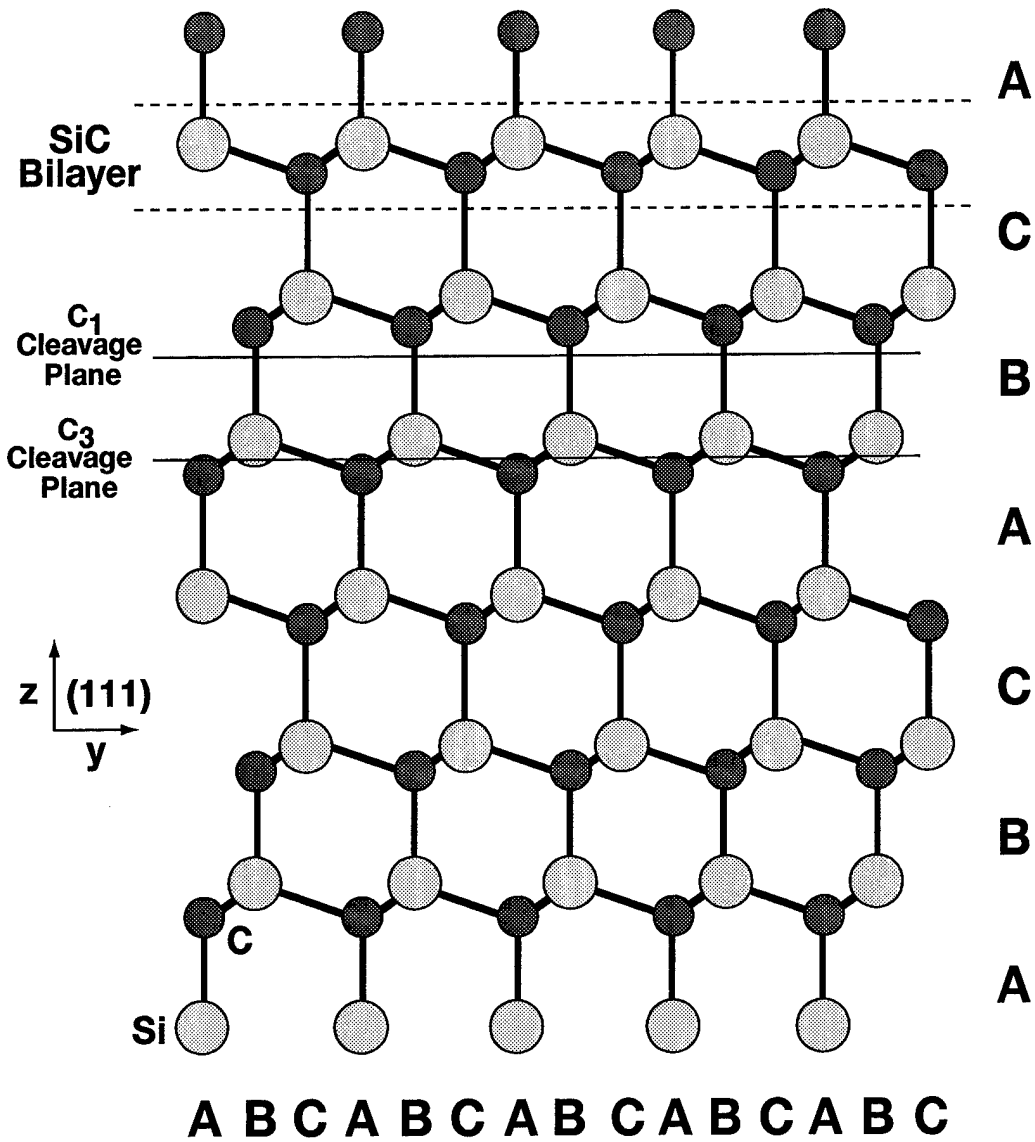

Figure 5.3 Crystal structure of the purely cubic SiC 3C polytype. The (111) crystal axis is aligned with the z axis. On a surface created by cleaving the crystal in the C_1 plane, each surface atom has 1 dangling bond. For the C_3 cleavage plane, each surface atom has 3 dangling bonds.

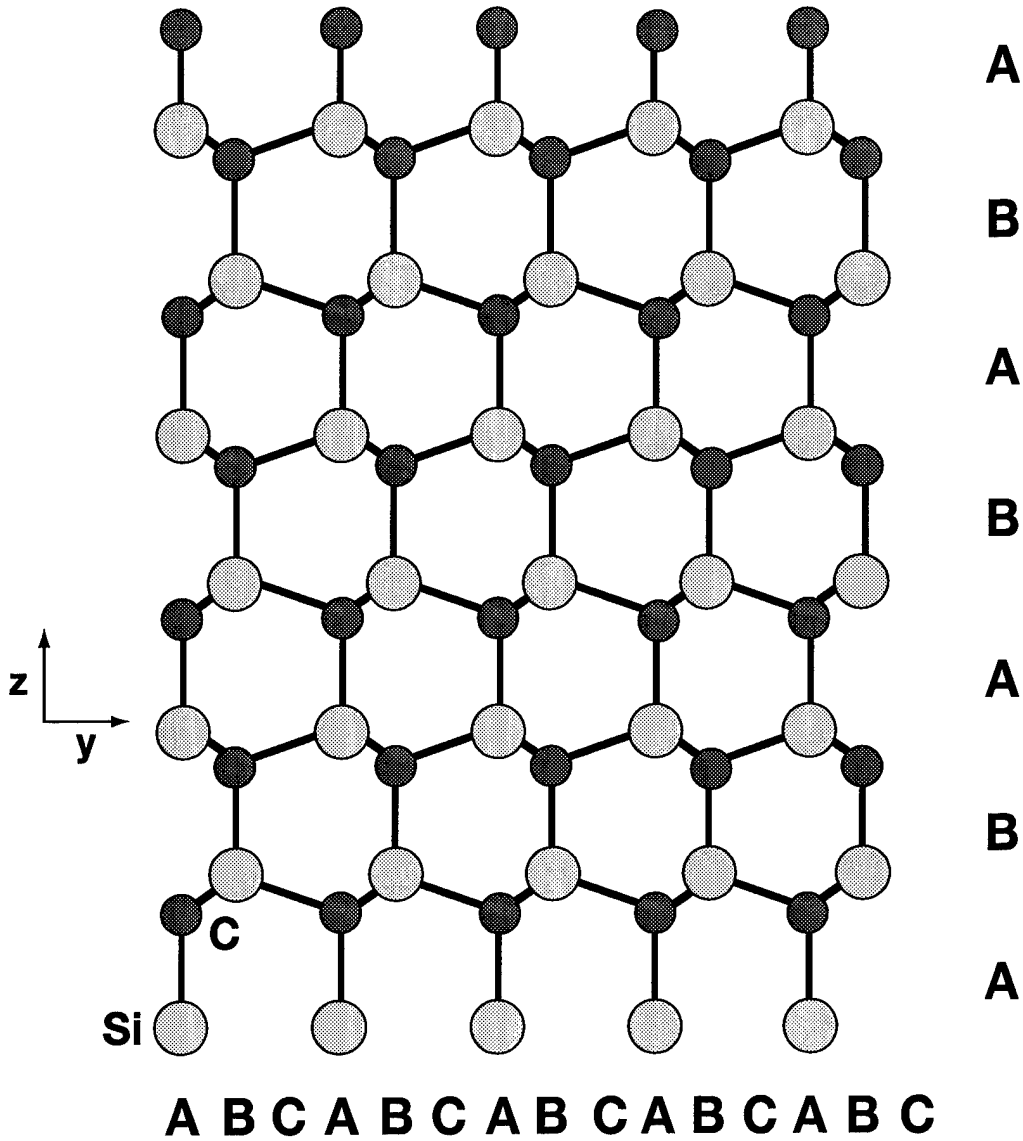

Figure 5.4 Crystal structure of the purely hexagonal SiC 2H polytype.

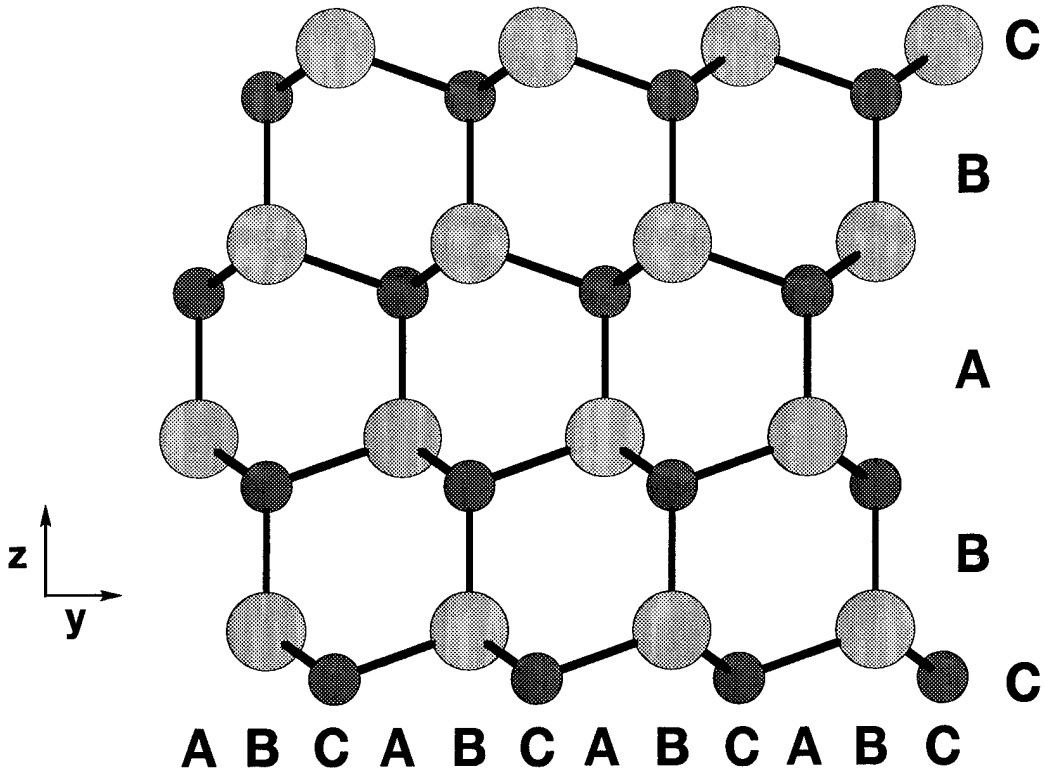

Figure 5.5 Crystal structure of SiC 4H polytype.

compared to 2.35$\AA$ for bulk silicon, and the atom layers along the vertical axis alternate between silicon and carbon.) Sabisch et al. describe the reconstruction of the SiC(001) in terms of the distances d_1, d_2, d_3, and d_4 that are labeled in Figure 5.6c. Table 5.1 (based on a similar table from Reference [118]) gives a comparison of various reported results for the reconstruction of the Si-terminated SiC(111) surface. In contrast to the Si(001) surface, Sabisch et al. found that the Si-terminated SiC (001) surface does not dimerize, *even though the lattice separation of the Si surface atoms in SiC is 3.08 Å, nearly 0.8 Å closer than in bulk silicon* [80]. Sabisch et al. attribute this result to the fact that SiC is stiffer than Si, so the forces driving the Si dimer bond formation are insufficient to displace the subsurface atoms enough to allow the bond to form. This result predicting no dimerization

agrees with a similar DFT result listed in Table 5.1, but disagrees with other theoretical and experimental results.

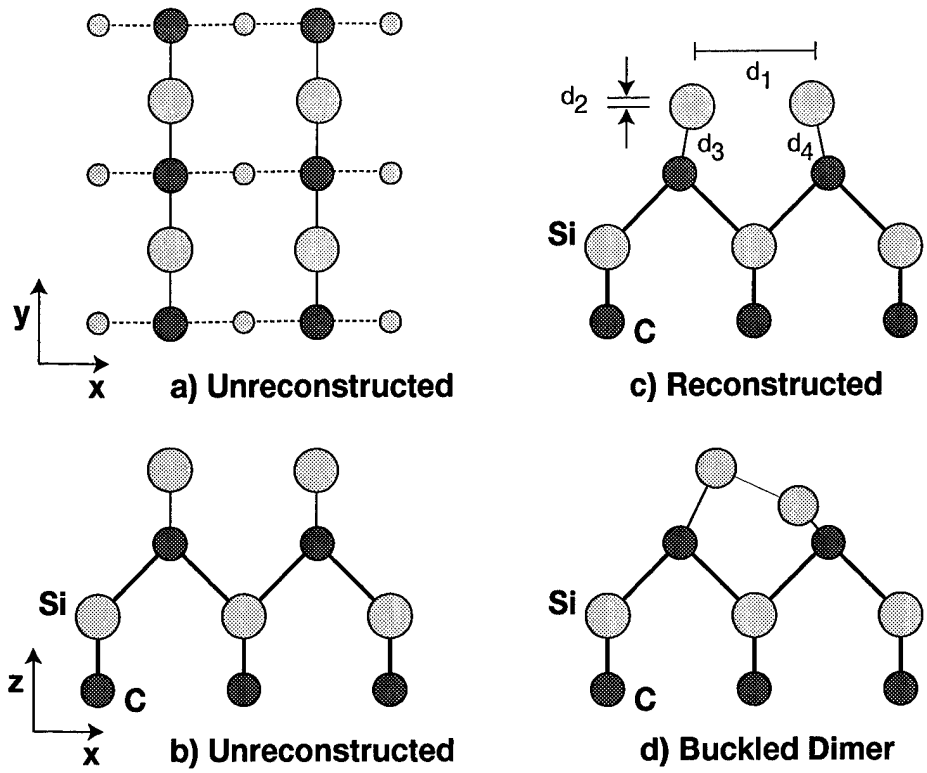

Figure 5.6 SiC(001) Si-terminated surface reconstruction. A top view of the unreconstructed surface is shown in a). Surface Si atoms and the first two subsurface layers are shown. At lattice positions, the top layer Si atoms are 3.08$\AA$ apart. A side of the unreconstructed surface is shown in b). The atoms shown are not all in the same plane. Sabisch's DFT result for the reconstructed surface is shown in c). Sabisch's result for d_1, 2.74$\AA$, is too large to say that dimerization has occurred. An alternate reconstruction observed in experiment, a buckled dimer, is shown in d).

Parameter	Ref. [118]	Ref. [120]	Ref. [121]	Ref. [89]	Ref. [122]	Ref. [123]
$d_1(\AA)$	2.73	2.75	2.26	2.33	2.16	2.31
$d_2(\AA)$	0.00	0.00	0.05	0.20		0.20
$d_3(\AA)$	1.89			1.78		
$d_4(\AA)$	1.89			1.78		
Method	DFT	DFT	DFT	MM	SE	Exp. LEED

Table 5.1 Structural parameters for Si-terminated SiC(001)-(2X1) surface. Parameters are defined in Figure 5.6. The values from [121] are from a (2X2) unit cell. LEED is a Low Energy Electron Diffraction measurement

Mehandru et al's semiempirical result of 2.16 Å for the Si dimer length looks like a Si-Si double bond length, which by analogy with the Si(001) surface is almost certainly not the minimum energy bond configuration for a dimer. The other results observing dimerization predict dimer lengths similar to those seen for silicon. Sabisch et al were able to match the results of reference [121] if they imposed additional symmetry constraints on their model. The experimental result of reference [123] is consistent with the presence of buckled dimers on the surface (see Figure 5.6).

The overall conclusion one can draw from Table 5.1 is that the reconstruction of the Si-terminated SiC(001) surface is not yet well understood, and needs additional investigation. Considering the dimerization of the Si(001) surface, and the spatial extent of a silicon dangling bond, DFT predictions of an undimerized Si-terminated SiC(001) surface are very curious. On the experimental Si(001) surface, the buckled dimer is the most likely reconstruction, though thermal vibrations of a buckled average out to a symmetric configuration.

There is better agreement in the literature on the reconstruction of the C-terminated SiC(001) surface. Sabisch et al report that the C-terminated (001) surface readily undergoes dimerization in a number of configurations, as the forces driving the formation of the C-C dimer on the surface are large enough to distort the subsurface atoms. The (2X1) dimer row configuration was found to be the minimum energy structure.

Kackell et al [124] investigated the vacancy induced reconstruction of the Si-terminated SiC(111) surface. They performed a DFT calculation using a slab periodic SiC model. They report small displacements from lattice positions for the normal Si-terminated SiC(111) surface, with dangling bonds on the surface Si atoms pointing roughly perpendicular to the (111) plane. The reconstruction caused by removing a Si atom is characterized by small lateral displacements, around 0.1 Å, and larger vertical displacements, around 0.5 Å of the Si atoms adjacent to the vacancy.

5.4 Designing an SiC(111) Surface Model

In order to run an MIMOMM optimization, one first needs to design embedded and bulk clusters for the *ab initio* and MM regions of the calculation. It is unlikely that one can define a procedure for designing the embedded and bulk clusters that will work for every possible situation. However, the considerations used for designing embedded and bulk clusters for the SiC(111) surface model used in this study can be generalized for other applications of MIMOMM, and so a description of the design process is presented here.

5.4.1 SiC(111) Embedded Cluster Design Considerations. The major fraction of the computational cost in MIMOMM is the *ab initio* calculations on the embedded cluster (EC), thus the overall goal in designing the EC is to make the smallest possible molecule that satisfies the model requirements. The factors used in the EC design are:

- *Need* (111) orientation for the surface
- *Need* more than one active site on the surface so that ontop and bridge bonding of adsorbates can be modeled
- *Need* to keep active sites from being directly bonded to a terminating H atom, as this would provide an unacceptable representation of the chemical environment
- *Need* to use at least the 6-31G* basis set in the *ab initio* calculations, which limits the embedded cluster to 15 to 30 heavy atoms to keep the number of basis functions manageable
- *Desire* similar Si and C-terminated clusters for clear comparisons
- *Desire* 4H structure

The embedded cluster for a silicon terminated SiC(111) surface that resulted from these design considerations, $Si_9C_{13}H_{25}$, is shown in Figure 5.7. While reproducing the 4H structure was desired, an initial attempt made it clear that a 4 bilayer EC included too many heavy atoms and was computationally intractable. Instead, a two bilayer EC with zinc-blende bonding was used. The most natural way to produce a surface with more than one active site was to take advantage of SiC(111)'s C_{3V} symmetry and include 3 active sites, undercoordinated Si atoms, on the surface. The Si atoms at the surface are connected to C atoms in the lower layer of the top bilayer, forming a non-planar ring. One C atom outside this ring was added so that the surface Si atoms are not directly bonded to a terminating H atom. All the C (Si) atoms in the lower layer of the top bilayer are

bonded to Si atoms in the top layer of the bottom bilayer, and C (Si) atoms in the lower layer of the bottom bilayer were added to complete the zinc-blende structure. Using the 6-31G* basis set, this Si-terminated EC contains 416 basis functions, which can be readily handled on available parallel computers.

Notice that the considerations of the system of interest here resulted in a closed cage structure. One would predict that mechanical embedding may not have a major influence on a closed cage except in reactions involving large atom displacements.

The EC for the C-terminated SiC(111) surface, $C_9Si_{13}H_{25}$, is shown in Figure 5.8. This EC was created by swapping the Si and C atoms in the Si terminated SiC(111) EC. In addition to providing direct comparisons with the Si terminated EC, swapping atom types also means that both the Si and C-terminated ECs have consistent atom numbers. Thus, the same MM3 input file can be used in the hybrid GAMESS-MM3 optimization for both the Si and C-terminated calculations, resulting in a substantial setup time savings. The C-terminated EC contains 432 basis functions using the 6-31G* basis set, a few more than the Si-terminated EC because the C-terminated EC contains more Si than C atoms.

5.4.2 Bulk Cluster Design Considerations. Since the computational cost of the MM calculations in MIMOMM are so small, the primary design consideration for the Bulk Cluster (BC) is to provide a "good" representation of the steric environment of the SiC lattice. However, the definition of "good" is difficult to quantify. One approach would be to design a number of BCs of increasing size, and use convergence of some property of the EC as a function of BC size to determine the optimum BC. This approach has two main drawbacks. First, this process could be very time consuming. Second, if the optimized EC structure is not very sensitive to the BC, e.g., a closed cage SiC cluster, it may be difficult to find a suitable property of the EC to use as a convergence criterion. In addition, because SiC has not been extensively investigated, little guidance on BC design could be obtained from the literature.

Since an optimum BC for SiC could not be predetermined, two contrasting BCs were designed. One BC emphasized steric forces parallel to the (111) crystal axis (vertical), the other emphasized steric forces perpendicular to the (111) (horizontal) axis. Figure 5.9

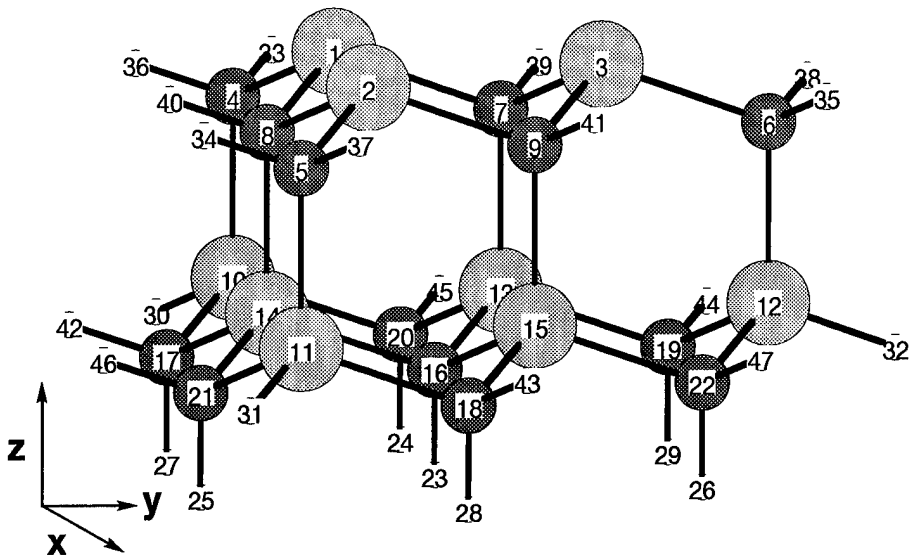

Figure 5.7 $Si_9C_{13}H_{25}$ (unreconstructed) EC used to model the Si-terminated SiC(111) surface. Using the 6-31G* basis set, this EC contains 416 basis functions.

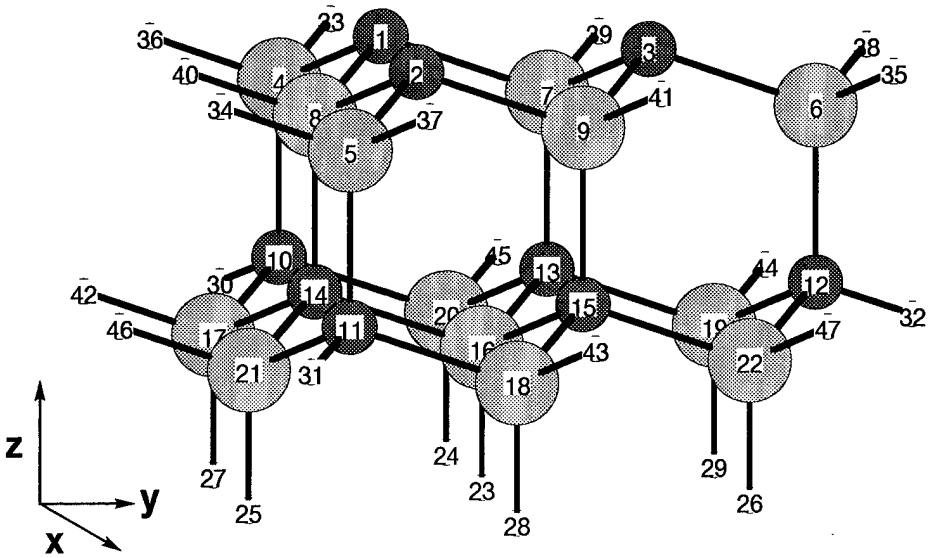

Figure 5.8 $C_9Si_{13}H_{25}$ (unreconstructed) EC used to model the C-terminated SiC(111) surface. Atoms 1,2, and 3 are the undercoordinated Si active sites. Atoms 1-22 belong to Region 1. H atoms 22-29 belong to Region 1 when this EC is used in a 2 layer hybrid cluster, but belong to Region 5 when this EC is used in a 4 layer hybrid cluster. H atoms 30-47 always belong to Region 5. Using the 6-31G* basis set, this EC contains 432 basis functions.

shows a side view of a 4 bilayer BC designed to emphasize vertical steric forces. This BC contains 2 bilayers of MM atoms below the EC, in addition to a adding a thin "ring" of MM atoms around the EC. Four bilayers were included to reproduce the 4H stacking sequence. Figure 5.10 shows a view of the Si-terminated surface of this BC. This 4 bilayer BC contains 70 Si atoms, 70 C atoms, and 87 H atoms. MM3 defines 322 bonds, 831 angles, and 2088 torsion angles for this molecule. Starting with the atoms at lattice positions, an MM3 optimization of this cluster took 13.6 minutes on one node of an IBM SP2.

Figure 5.11 shows a side view of a 2 bilayer BC, designed to emphasize horizontal steric forces. A surface view of this BC with the EC highlighted is shown in Figure 5.12. The number of atoms in this BC was kept approximately equal to the number of atoms in the 4 bilayer BC to keep the MM cost of the MIMOMM calculations constant for both BCs. This BC has 73 Si, 69 C, and 109 H atoms. MM3 defines 337 bonds, 843 angles, and 2025 torsion angles for this BC. Starting with the atoms at lattice positions, an MM3 optimization of this BC took 19.5 minutes on one node of an IBM SP2.

C-terminated BCs were created by swapping Si and C atoms in these Si-terminated BCs. The structures of these BCs are identical to those shown in Figures 5.9 to 5.12, and so are not shown.

Before the SiC calculations discussed in this chapter were performed, it was unclear whether the differences between MIMOMM optimizations using the 2 and 4 bilayer BCs would be large enough to pick a clear winner. However, in analyzing the SiC oxidation results, it became obvious that the 4 bilayer BC was better *when a reaction caused large atom displacements in the EC.* After this conclusion was reached, the 2 bilayer BC was no longer used. The SiC calculations discussed in this chapter are not presented in chronological order, so the use of the 2 and 4 bilayer BCs may seem inconsistent.

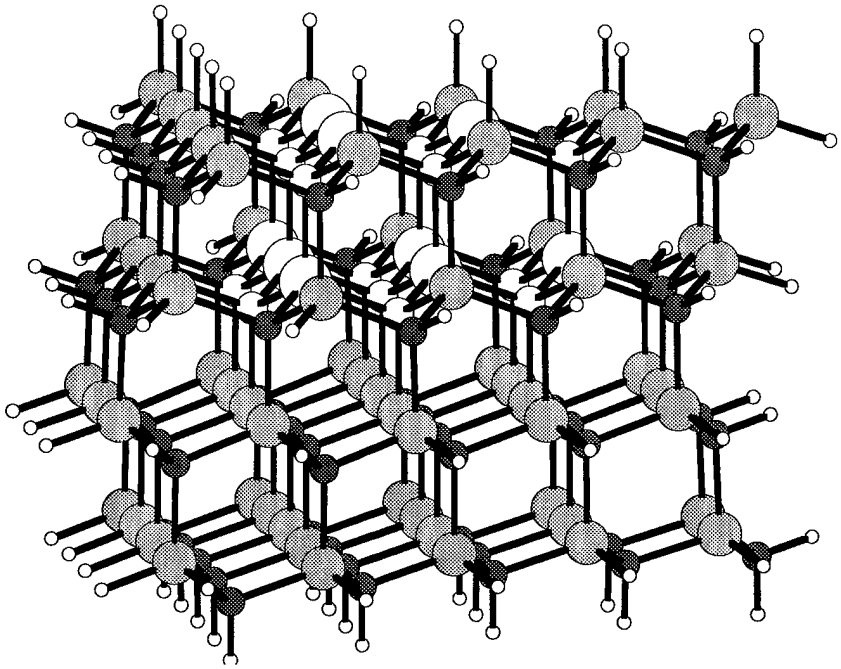

Figure 5.9 SiC 4 layer bulk cluster, Si-terminated (111) surface. The EC atoms in the middle of the cluster are shown as large white circles. The small white circles around the periphery of the cluster are H atoms.

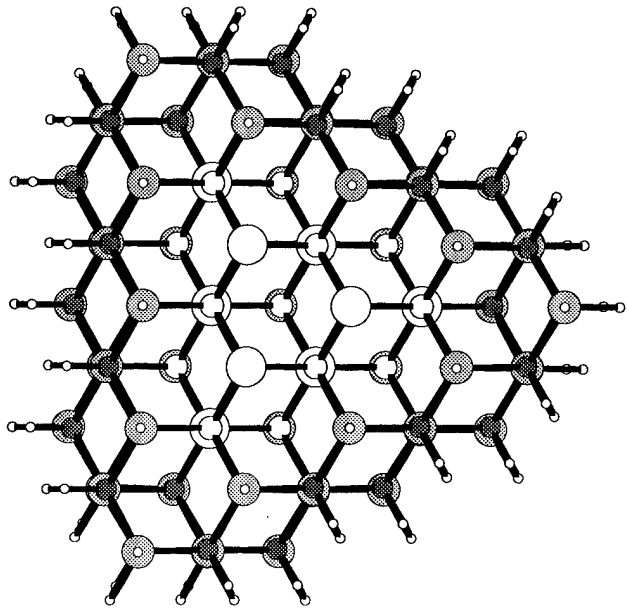

Figure 5.10 Si-terminated (111) surface of SiC 4 layer bulk cluster. The outermost EC atoms in the top bilayer are 2 bonds away from the edge of this cluster.

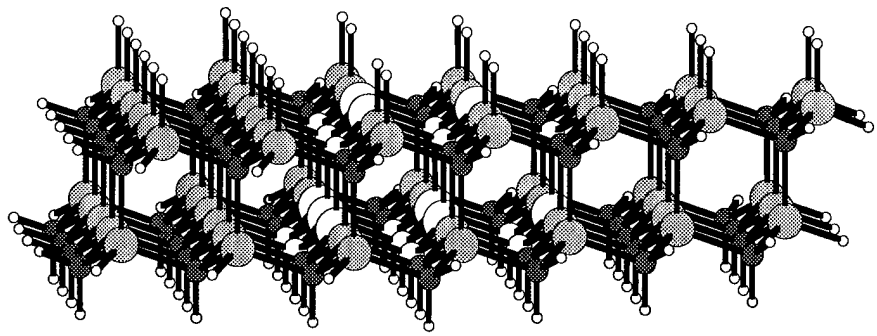

Figure 5.11 SiC 2 layer bulk cluster, Si-terminated (111) surface. The EC atoms are shown as white circles.

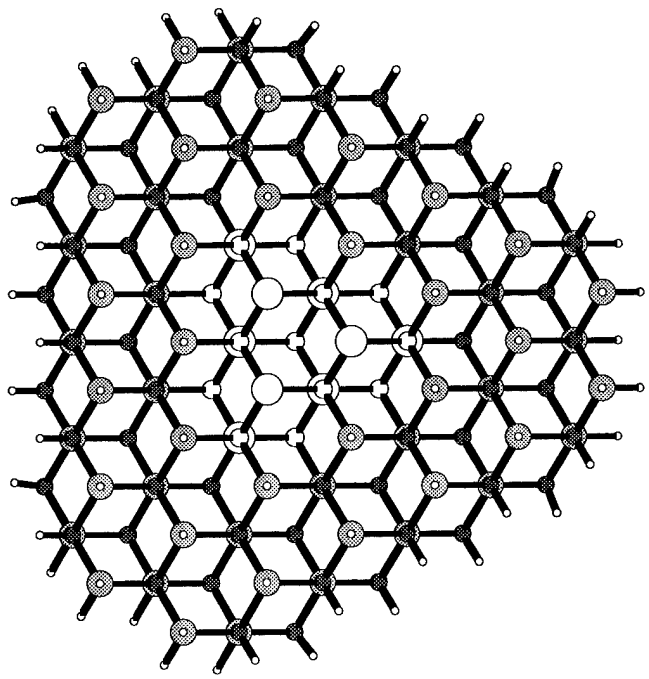

Figure 5.12 Si-terminated (111) surface of SiC 2 layer bulk cluster. The outermost EC atoms in the top bilayer are 4 bonds away from the edge of this cluster.

5.5 *SiC(111) Surface Reconstruction*

5.5.1 Energetics. Reconstruction of the clean surface of a cluster must always be investigated before adsorption studies are performed because surface chemistry depends on the surface reconstruction. One expects the reconstruction of the SiC(111) surface to be very different from the SiC(001) surface. On the unreconstructed SiC(001) surface, the undercoordinated surface atoms, Si or C, each have two nearest neighbor connections to the subsurface, and two dangling bonds oriented approximately 54.7° with respect to the surface. Dangling bonds on Si or C atoms in adjacent rows are pointed towards each other, a favorable orientation for dimer bond formation (though as we saw in Section 5.3 there are conflicting results in the literature on the dimerization of the Si-terminated SiC(001) surface). The atoms on the SiC(111) surface (C_1 cleavage plane) make three nearest neighbor connections to the subsurface, and have one dangling bond oriented normal to the surface, a less orientation for dimer bond formation. Both these factors make dimerization (or other reconstructions involving large atom displacements) unlikely on the SiC(111) surface.

Since the Si and C-terminated ECs used in this study have 3 dangling bonds on their surfaces, one can define the overall spin of the wavefunction as either 4 (quartet) or 2 (doublet). The quartet spin configuration should keep spins in the dangling bonds aligned, which will reduce the likelihood of dimerization. The doublet spin configuration will pair two of the dangling bond spins, which may favor dimer bond formation, though this bond formation would have to overcome the steric forces of the cluster.

Table 5.2 lists the quartet and doublet state energies for the Si and C-terminated ECs. These calculations were performed using the Restricted Open shell Hartree Fock (ROHF) and Generalized Valance Bond (GVB) modules in GAMESS. We see that the energy difference between the *ab initio* and MIMOMM optimized results are quite small, 0.6 $\frac{kcal}{mol}$. These small energy differences are consistent with the small differences in *ab initio* and MIMOMM optimized geometries, which are described in the following sections.

The energy differences between the quartet and doublet results are more striking. For the Si-terminated EC, we see that the ^{2}ROHF optimized geometry is 35.3 $\frac{kcal}{mol}$ higher

in energy than the ^{4}ROHF result, and is accompanied by a large distortion in the cluster geometry. The ^{2}ROHF MIMOMM (4 bilayer BC) optimized geometry shows much less distortion, but with a larger energy difference, 44.3 $\frac{kcal}{mol}$, higher than the ^{4}ROHF MIMOMM (4 bilayer BC) result. Another doublet state that is relatively easy to define for this EC is a ^{2}GVB-PP(1) with one open shell. The two Boys localized singly occupied ^{4}ROHF orbitals centered on Si atoms 1 and 2 were used to form the GVB pair. The ^{2}GVB-PP(1) energy for the cluster is only 1.1 $\frac{kcal}{mol}$ higher than the ^{4}ROHF energy. From this result, one can conclude that the ^{4}ROHF surface reconstruction is the lowest energy configuration for this cluster.

Reconstruction				
		6-31G* Energy (H)		
Molecule	Model	*ab initio*	MIMOMM 2 Bilayer	MIMOMM 4 Bilayer
($Si_9C_{13}H_{25}$)	^{4}ROHF	-3107.287434	-3107.285539	-3107.286685
($Si_9C_{13}H_{25}$)	^{2}ROHF	-3107.231180	-	-3107.216090
($Si_9C_{13}H_{25}$)	^{2}GVB-PP(1)	-3107.285713	-	-
($C_9Si_{13}H_{25}$)	^{4}ROHF	-4111.394766	-4111.393840	-4111.393770
($C_9Si_{13}H_{25}$)	^{2}ROHF	-4111.297933	-	-
($C_9Si_{13}H_{25}$)	^{2}GVB-PP(1)	DNC	-	-

Table 5.2 6-31G* energies of SiC clusters, doublet surface reconstruction. - indicates that a calculation was not performed. DNC indicates a calculation was attempted, but did not converge.

The results for the ^{2}ROHF C-terminated surface are similar. The ^{2}ROHF energy for the C-terminated EC is 60.8 $\frac{kcal}{mol}$ higher than the ^{4}ROHF result, almost twice the quartet-doublet energy difference for the Si-terminated EC. Several ^{2}GVB-PP(1) calculations for the C-terminated EC were attempted, but none converged. The Boys localized orbitals on the surface carbon atoms do not form a good GVB pair, unlike the silicon case (a comparison of the Si and C orbitals is discussed in Section 5.12). Based on the results from the GVB-PP(1) optimization of the Si-terminated EC, the quartet-doublet energy difference for the C-terminated EC was judged sufficient to conclude that the ^{4}ROHF reconstruction is energetically favored.

5.5.2 Quartet Surface Reconstruction: Structures. Figure 5.13 shows a comparison of the bulk SiC(111) lattice with the reconstructed (6-31G* optimized) Si and C-terminated ECs. The internal coordinates of the reconstructed Si and C-terminated ECs are listed in Table 5.3. Dimerization has not occurred, and overall the optimized structures are similar to the lattice geometry. There is one noticeable difference between the Si and C terminated ECs. In the Si-terminated EC, the surface Si atoms are 0.66 $\AA$ above the C atoms in the top bilayer, close to the lattice value of 0.63 $\AA$. In the C-terminated EC, the surface C atoms have sunk down 0.18 $\AA$ closer to the Si atoms in the top bilayer, a separation of only 0.45$\AA$. The overall multiplicity for both the Si and C-terminated calculations was set equal to 4, i.e., 3 unpaired electrons. In the Si-terminated case, the spin density population at each surface Si atoms is large, 0.43, indicating the existence of localized dangling bonds on the Si atoms. In the C-terminated EC, the spin density on all nuclei is small, at most 0.05, and is distributed throughout the molecule. This spin density distribution for the C-terminated EC indicates that describing the singly occupied MOs as localized dangling bonds isn't appropriate. Instead of forming dangling bonds like Si, the surface C subsurface Si bonding is strengthened, causing the C atoms to draw down closer to the subsurface.

How much do the MIMOMM optimized ^4ROHF structures differ from the conventional *ab initio* results? Table 5.4 lists a comparison of the optimized structure of the Si-terminated SiC(111) EC, as well as the the MIMOMM optimized structure of the EC embedded within the 4 layer and 2 layer BCs described in Section 5.4.2. The effect of both BCs on the optimized geometry of Si-terminated the EC are small. The IMOMM optimized geometries for the C-terminated EC also show small differences from the non-IMOMM geometry. (The C-terminated EC showed similarly small differences.) The structural differences between the 2-bilayer and 4-bilayer BC MIMOMM results are too small to conclude that one BC is better than the other.

5.5.3 Doublet Surface Reconstruction: Structures. A comparison of the ^{2}ROHF and ^{2}GVB-PP(1) *ab initio* optimized geometries for the Si-terminated EC is shown in Figures 5.14 and 5.15. Si atoms 1 and 2 have formed a bond in the ^{2}ROHF case, each

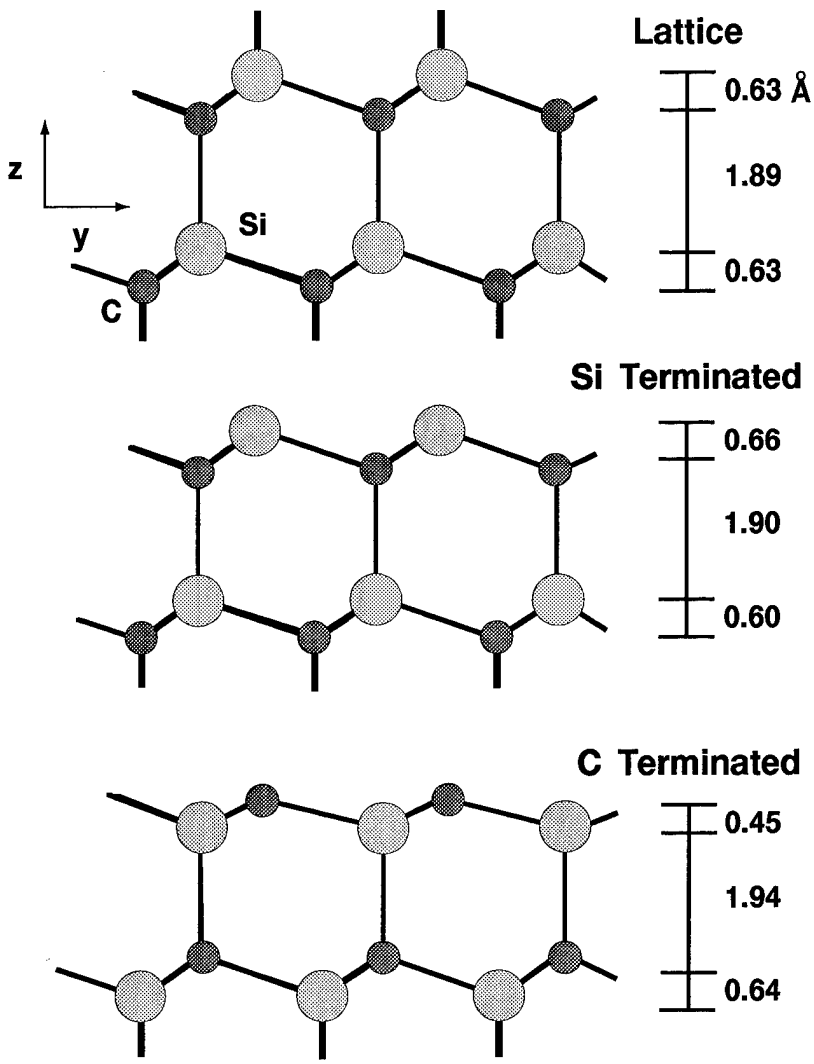

Figure 5.13 Reconstruction of Si and C-terminated embedded cluster models of SiC(111) surfaces. The Si-terminated cluster shows small deviations from the lattice geometry. The C-terminated cluster shows larger adjustments, with the surface C atoms moving approximately 0.2 $\AA$ closer to the subsurface Si atoms.

	Silicon Terminated	Carbon Terminated		Silicon Terminated	Carbon Terminated
Dist (Å)			Angle(°)		
1 2	3.147	3.151	4 10 17	108.150	110.592
2 3	3.147	3.151	5 11 18	108.150	110.592
3 1	3.147	3.151	6 12 19	108.150	110.592
1 9	3.641	3.661	7 1 8	107.174	114.316
2 7	3.641	3.661	8 2 9	107.174	114.316
3 8	3.641	3.661	9 3 7	107.174	114.316
1 8	1.903	1.871	4 10 16	97.944	101.348
1 7	1.903	1.871	Torsion(°)		
2 8	1.903	1.871	5 11 6 12	-179.999	179.999
2 9	1.903	1.871	5 11 4 10	-179.999	179.999
3 7	1.903	1.871	4 10 6 12	-179.999	179.999
3 9	1.903	1.871	18 22 17 20	179.999	179.999
7 13	1.909	1.923	10 11 12 14	0.248	-0.311
8 14	1.909	1.923			
9 15	1.909	1.923			

Table 5.3 Comparison of reconstruction of Si and C-terminated embedded clusters, conventional *ab initio* optimization, 6-31G* basis set. Atom numbers in this table refer to Figure 5.7. In an unreconstructed SiC lattice, bond lengths would be 1.89 Å, bond angles (except for 4 10 16) would be 109.5°, and all the atoms in the torsion angles listed would be planar.

Silicon Terminated SiC(111) EC							
	Ab Initio	IMOMM 2 Bilayer	MIMOMM 4 Bilayer		*Ab Initio*	IMOMM 2 Bilayer	MIMOMM 4 Bilayer
Dist (Å)				Angle(°)			
1 2	3.147	3.143	3.135	4 10 17	108.150	107.982	108.816
2 3	3.147	3.143	3.135	5 11 18	108.150	107.982	108.814
3 1	3.147	3.143	3.135	6 12 19	108.150	107.979	108.820
1 9	3.641	3.641	3.633	7 1 8	107.174	107.144	107.226
2 7	3.641	3.641	3.633	8 2 9	107.174	107.144	107.235
3 8	3.641	3.641	3.633	9 3 7	107.174	107.143	107.235
1 8	1.903	1.904	1.900	4 10 16	97.944	98.803	98.372
1 7	1.903	1.904	1.900	Torsion(°)			
2 8	1.903	1.904	1.900	5 11 6 12	-179.999	0.001	-0.002
2 9	1.903	1.904	1.900	5 11 4 10	-179.999	180.000	179.997
3 7	1.903	1.904	1.900	4 10 6 12	-179.999	179.999	180.000
3 9	1.903	1.904	1.900	18 22 17 20	179.999	-179.942	180.000
7 13	1.909	1.910	1.915	10 11 12 14	0.248	0.139	0.092
8 14	1.909	1.910	1.915				
9 15	1.909	1.910	1.915				

Table 5.4 Comparison of *ab initio* (6-31G*) and MIMOMM optimized geometries of the silicon terminated SiC(111) EC. Atom numbers in this table refer to Figure 5.7. No significant differences are observed among these three cases.

moving 0.35Å along the X axis toward each other. These atoms drag their neighbors along with them, which also drag *their* neighbors with them, resulting in considerable distortion of the cluster. In contrast, the ^{2}GVB-PP(1) optimized geometry differs little from the ^{4}ROHF optimized geometry. (MIMOMM optimizations were not performed with ^{2}GVB-PP(1) calculations because it was known from the ^{4}ROHF results that MIMOMM would make little difference in these cases.) This result indicates having the electrons in the dangling bonds unpaired is lower in energy than forcing them into bond pairs, which is what the ^{2}ROHF configuration does. The ^{4}ROHF spin configuration for these clusters would correspond to a (1 x 1) reconstruction, i.e., the unit cell for the surface is a single, unbonded atom. The modeled surface reconstruction is limited by the size of the cluster, thus we can only state that the (1 x 1) surface reconstruction is the minimum energy solution for the clusters considered in this work.

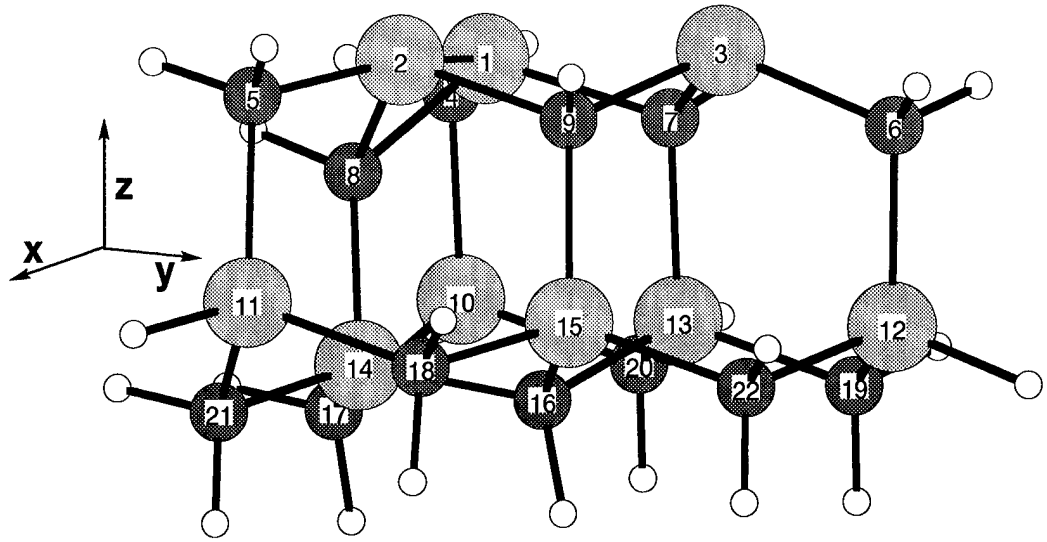

Figure 5.14 *Ab initio* ^{2}ROHF (6-31G*) optimized Si-terminated SiC(111) cluster. Si atoms 1 and 2 have moved along the x axis to bond, causing considerable distortion in the cluster. The ^{2}ROHF optimized geometry is 35.3 $\frac{kcal}{mol}$ *higher* in energy than the ^{4}ROHF optimized geometry.

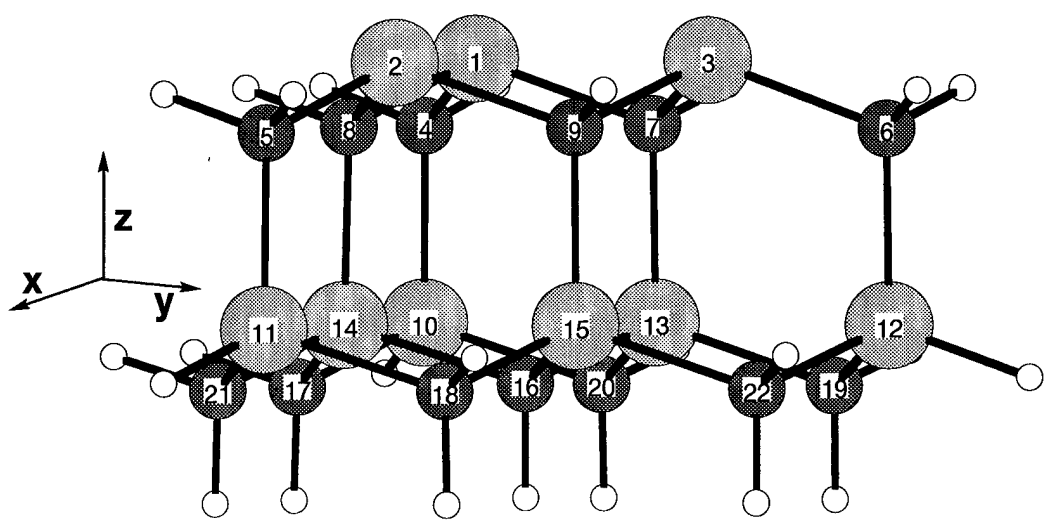

Figure 5.15 *Ab initio* ^{2}GVB-PP(1) (6-31G*) optimized Si-terminated SiC(111) cluster. The ^{2}GVB-PP(1) geometry shows small differences from the ^{4}ROHF result. The ^{2}GVB-PP(1) optimized geometry is only 1.1 $\frac{kcal}{mol}$ higher is energy than the ^{4}ROHF result.

5.6 Hydrogenation of SiC(111) Surface

Hydrogenation is the simplest possible atom adsorption reaction, thus is a logical starting point for adsorption studies of the SiC(111) surface. Since H atoms can only form one bond, they can only chemisorb to ontop sites on the SiC(111) EC. One anticipates that ontop adsorption will only cause minor changes to the EC structure, so the MIMOMM results should show minor differences from conventional *ab initio* results.

5.6.1 Si-terminated SiC(111) Surface. Hydrogen adsorption was modeled by placing an H atom 1.5 $\AA$ directly above a surface Si atom and allowing the geometry to optimize. The *ab initio* optimized geometries of the Si-terminated cluster with 0 (clean surface), 1, 2, and 3 H atoms adsorbed is shown in Figure 5.16. We see in this figure that H atom adsorption does not cause noticeable changes in the cluster geometry, which leads one to predict that the addition of bulk steric forces in a MIMOMM optimization will have little effect on the optimized geometry. This prediction is confirmed by a more detailed analysis. Figure 5.17 shows a comparison of the of the *ab initio* and MIMOMM (2 bilayer BC) optimized geometries of the Si-terminated cluster with 1 H atom adsorbed. We see that the differences in bond lengths between these cases are on the order of $10^{-3}\AA$. Differences in bond and torsion angles are are at most 0.7°. Figures 5.18 and 5.19 show similar results for adsorption of 2 and 3 H atoms. We also see that the geometries of the clusters in all 3 cases are essentially identical, indicating that there is little interaction between the adsorbed H atoms.

Since the *ab initio* and MIMOMM optimized geometries are so similar, the optimized energies should be nearly equal. Table 5.5 lists the Hartree-Fock 6-31G* energies of the Si terminated SiC(111) EC with 0 (clean surface), 1, 2, and 3 (fully saturated) H atoms adsorbed. The addition of the steric forces from the 2 bilayer BC raises the calculated energy of the EC by approximately 0.002 H in all cases, a very small amount. Since the MIMOMM optimization amounts to adding constraints to the *ab initio* optimization, the MIMOMM optimized result should always be *higher* in energy than the *ab initio* optimize result. The MP2 energy calculated at the 6-31G* optimized geometry is also listed in Table 5.5.

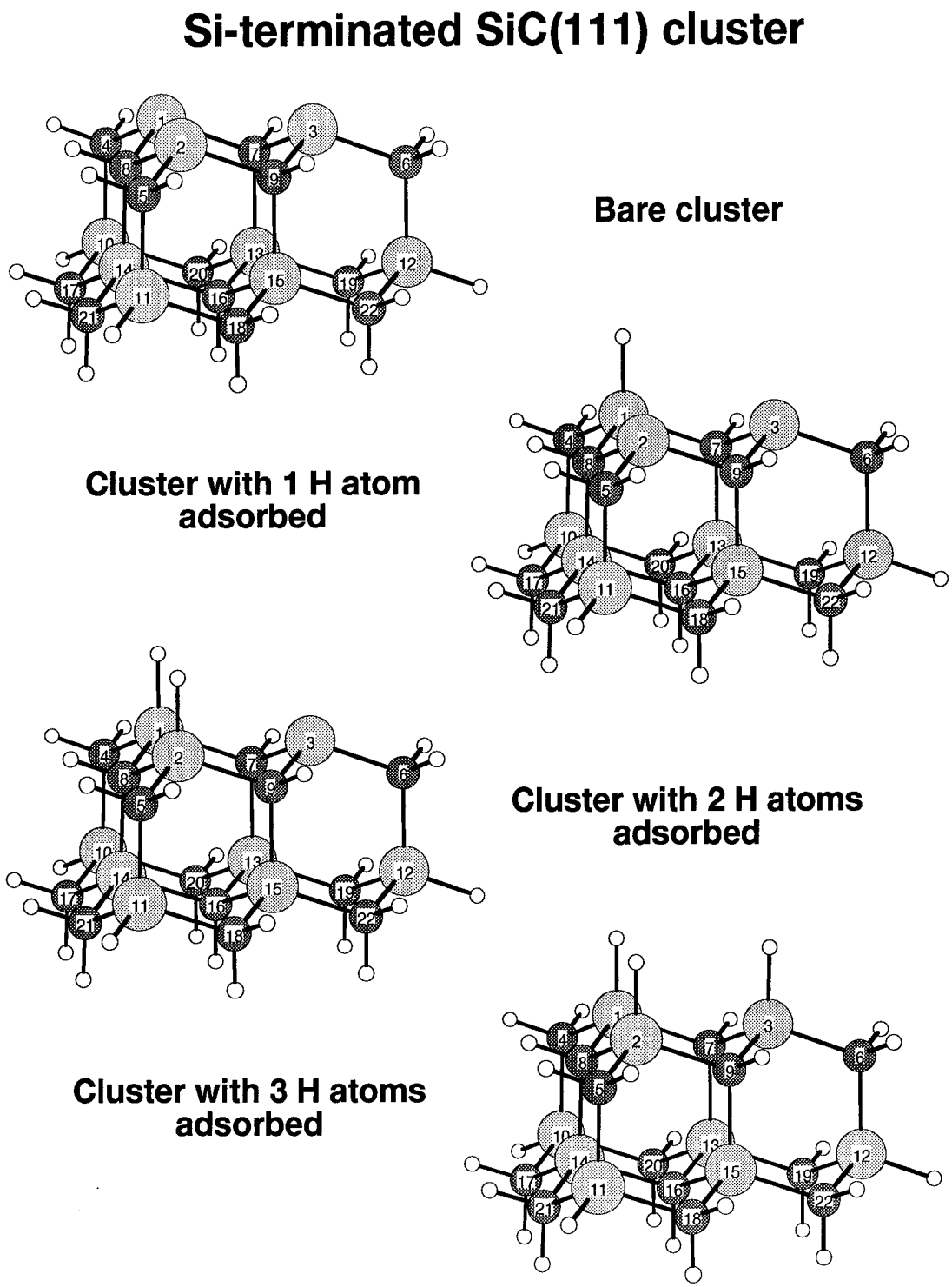

Figure 5.16 H atom adsorption onto the Si-terminated SiC(111) cluster.

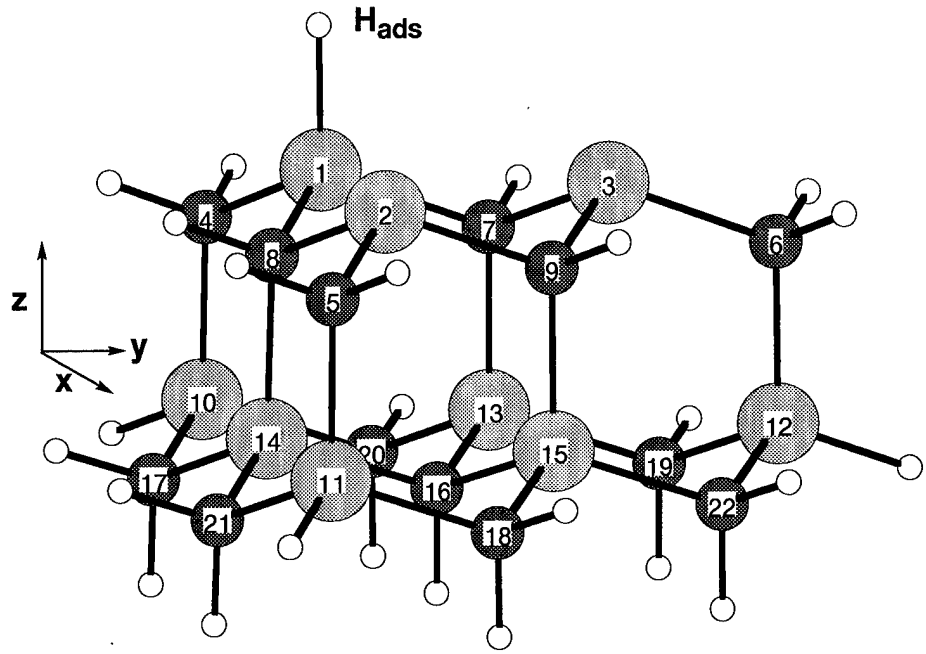

	Ab Initio	MIMOMM 2 Bilayer		*Ab Initio*	MIMOMM 2 Bilayer
Dist ($\AA$)			Angle (°)		
1 H_{ads}	1.486	1.487	H_{ads} 1 2	91.224	90.559
1 2	3.146	3.142	H_{ads} 1 3	91.221	90.570
2 3	3.146	3.142	H_{ads} 1 8	110.315	110.139
3 1	3.144	3.142	7 1 8	107.028	107.046
1 9	3.642	3.642	8 2 9	107.150	107.127
1 8	1.897	1.903	9 3 7	107.150	107.126
1 7	1.897	1.903	Torsion(°)		
7 13	1.908	1.909	5 11 4 10	-179.858	-179.892
8 14	1.908	1.909	4 10 6 12	179.858	179.897
9 15	1.908	1.909	10 11 12 14	0.311	0.174

Figure 5.17 Comparison of *ab initio* and MIMOMM optimized Si-terminated SiC(111) cluster geometry with 1 H atom adsorbed. 6-31G* basis set used in all calculations.

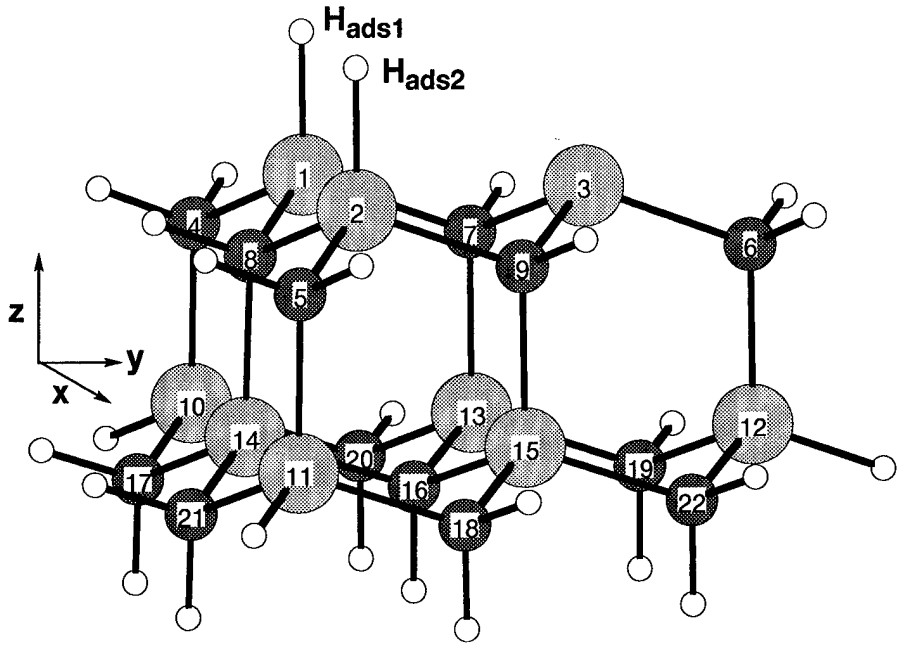

	Ab Initio	MIMOMM 2 Bilayer		*Ab Initio*	MIMOMM 2 Bilayer
Dist (Å)			Angle (°)		
1 H_{ads1}	1.486	1.487	H_{ads1} 1 2	91.054	90.548
2 H_{ads2}	1.486	1.487	H_{ads1} 1 3	91.131	90.427
1 2	3.143	3.138	H_{ads1} 1 8	110.204	110.136
2 3	3.144	3.140	H_{ads2} 2 3	91.131	90.548
3 1	3.144	3.140	H_{ads2} 2 1	91.054	90.426
1 9	3.636	3.637	H_{ads2} 2 9	110.283	110.136
1 8	1.898	1.901	7 1 8	107.032	107.063
1 7	1.897	1.900	8 2 9	107.032	107.054
7 13	1.908	1.900	9 3 7	107.097	107.092
8 14	1.907	1.909	Torsion(°)		
9 15	1.908	1.909	5 11 4 10	179.999	-179.990
			4 10 6 12	179.831	179.858
			10 11 12 14	0.315	0.171

Figure 5.18 Comparison of *ab initio* and MIMOMM optimized Si-terminated SiC(111) cluster geometry with 2 H atoms adsorbed. 6-31G* basis set used in all calculations.

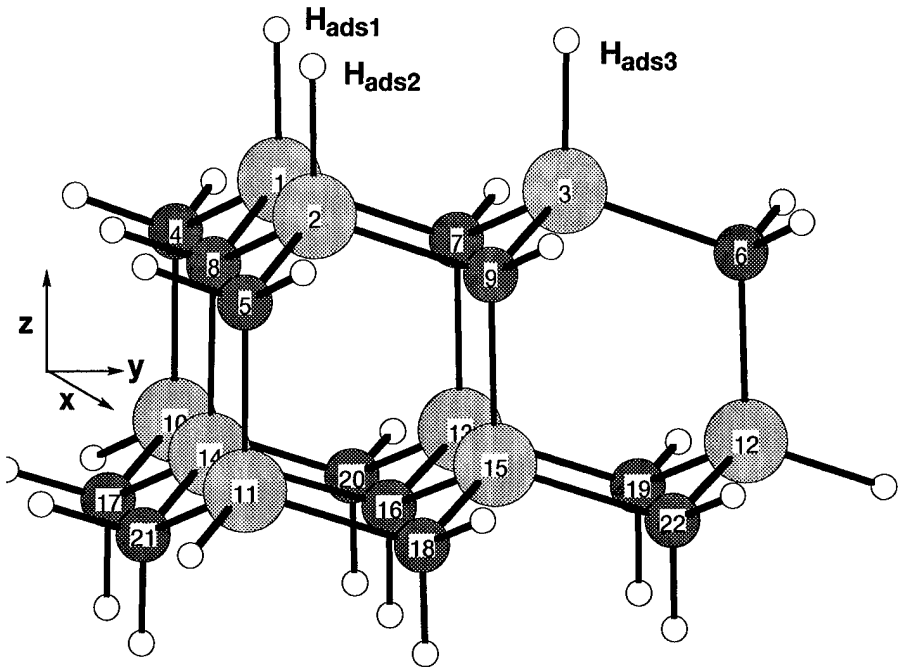

	Ab Initio	MIMOMM 2 Bilayer		*Ab Initio*	MIMOMM 2 Bilayer
Dist (Å)			Angle (°)		
1 H_{ads1}	1.487	1.486	H_{ads1} 1 2	90.978	90.344
2 H_{ads2}	1.487	1.486	H_{ads1} 1 3	90.978	90.343
3 H_{ads3}	1.487	1.486	H_{ads1} 1 8	110.174	110.188
1 2	3.140	3.138	H_{ads2} 2 3	90.978	90.343
2 3	3.140	3.138	H_{ads2} 2 1	90.978	90.343
3 1	3.140	3.138	H_{ads2} 2 9	110.172	110.188
1 9	3.630	3.632	H_{ads3} 3 1	90.978	90.342
1 8	1.897	1.902	H_{ads3} 3 2	90.978	90.343
1 7	1.897	1.902	H_{ads3} 3 7	110.174	110.188
7 13	1.907	1.902	7 1 8	107.010	106.696
8 14	1.907	1.902	8 2 9	107.010	106.696
9 15	1.907	1.902	9 3 7	107.010	106.696
			Torsion(°)		
			5 11 4 10	179.999	179.998
			4 10 6 12	-179.997	-179.996
			10 11 12 14	0.253	0.286

Figure 5.19 Comparison of *ab initio* and MIMOMM optimized Si-terminated SiC(111) cluster geometry with 3 H atoms adsorbed. 6-31G* basis set used in all calculations.

Table 5.6 lists the H atom adsorption energies energies of hydrogenation for the first, second, and third H atoms. The hydrogenation energy for each H atom is (essentially) the same, another indication that there is very little interaction between the adsorbed H atoms. MIMOMM optimization has no significant effect on the adsorption energies. The MP2 adsorption energies are approximately 6 $\frac{kcal}{mol}$ larger than the Hartree-Fock results, and about 7 $\frac{kcal}{mol}$ smaller than similar experimental results also shown in this table. These results show that neglect of electron correlation in the HF calculation does not lead to large errors for the adsorption energies.

		6-31G* Energy (H)		
		Hartree-Fock		MP2
Molecule	Model	*Ab Initio*	MIMOMM 2 Bilayer	*Ab Initio*
$(Si_9C_{13}H_{25})$	^{4}ROHF	-3107.287434	-3107.285539	-3109.704721
$(Si_9C_{13}H_{25})H$	^{3}ROHF	-3107.907559	-3107.905638	-3110.335152
$(Si_9C_{13}H_{25})H_2$	^{2}ROHF	-3108.527959	-3108.526036	-3110.965989
$(Si_9C_{13}H_{25})H_3$	^{1}RHF	-3109.146875	-3109.146875	-3111.596687

Table 5.5 6-31G* energies of Si-terminated SiC(111) clusters used in calculating energy of hydrogenation. (The 6-31G* energy for H atom is -0.498233 H.) The column labeled *ab initio* lists the results of a conventional *ab initio* calculation for adsorbing 1, 2, and 3 H atoms onto the EC. The column labeled MIMOMM lists the MIMOMM results using the 2 bilayer BC.

					Δ E (kcal/mole)		
					Hartree-Fock		MP2
					Ab Initio	MIMOMM 2 Bilayer	*Ab Initio*
$(Si_9C_{13}H_{25})H_2$	+	H	→	$(Si_9C_{13}H_{25})H_3$	-76.5	-76.5	-82.9
$(Si_9C_{13}H_{25})H$	+	H	→	$(Si_9C_{13}H_{25})H_2$	-76.7	-76.7	-83.2
$(Si_9C_{13}H_{25})$	+	H	→	$(Si_9C_{13}H_{25})H$	-76.8	-76.9	-83.1
SiH_3	+	H	→	SiH_4	-76.3		-84.2
SiH_3	+	H	→	SiH_4	**-90.3 (exp)**		
$HSi(CH_3)_3$	+	H	→	$Si(CH_3)_3H$	**-90.3 (exp)**		

Table 5.6 HF-SCF and MP2 (6-31G*) energies of hydrogenation, Si-terminated SiC(111) surface. Experimental values are taken from Ref [125].

5.6.2 C-terminated SiC(111) Surface. Hydrogen adsorption on the C-terminated SiC(111) surface was modeled by placing an H atom 1.1 Å directly above a surface C atom and allowing the geometry to optimize. The *ab initio* optimized geometries of the C-terminated cluster with 0 (clean surface), 1, 2, and 3 H atoms adsorbed is shown in Figure 5.20. We see that H atom adsorption on the C-terminated SiC(111) surface causes a subtle, change in the cluster geometry localized around the C atom to which an H atom has adsorbed. Recalling the discussion in Section 5.5, we saw that upon reconstruction, the surface C atoms in the C-terminated SiC cluster displaced down from their lattice positions by approximately 0.15Å, unlike the Si-terminated cluster in which the surface Si atoms remained nearly in lattice positions. The undercoordinated surface Si atoms form "dangling" bonds with and three Si-C single bonds. The undercoordinated surface C atoms form stronger C-Si bonds, with less electron density going into the dangling bond. Adsorption of an H atom onto the surface C atom creates 4 roughly equivalent single bonds.

Table 5.7 lists the structural changes caused by adsorption of one H atom onto the C-terminated cluster. The increase in C-Si bond length caused by the H atom adsorption is rather small, about 0.02Å, and the bond angles decrease by about 4.5°. The changes in the other internal coordinates in the cluster caused by the adsorption are very small and so are not listed. The differences between *ab initio* and MIMOMM optimized geometries are approximately the same size as was seen for the Si-terminated SiC cluster, and so are also not listed.

Table 5.8 lists the 6-31G* energies of the C-terminated SiC(111) EC with 0 (clean surface), 1, 2, and 3 (fully saturated surface) H atoms adsorbed. As was seen for the Si-terminated EC, the addition the steric forces from the 2 bilayer BC is seen to raise the energy by approximately 0.002 H in all cases, similar to the Si-terminated SiC cluster results. Table 5.9 lists the energies of hydrogenation for the first, second, and third H atoms. As was seen for the hydrogenation of Si-terminated cluster, the *ab initio* and MIMOMM results are essentially identical. H atom adsorption on the C-terminated SiC(111) cluster causes larger structural changes than for the Si-terminated cluster. However, the structural changes in the C-terminated cluster are highly localized, so the effect of bulk steric forces

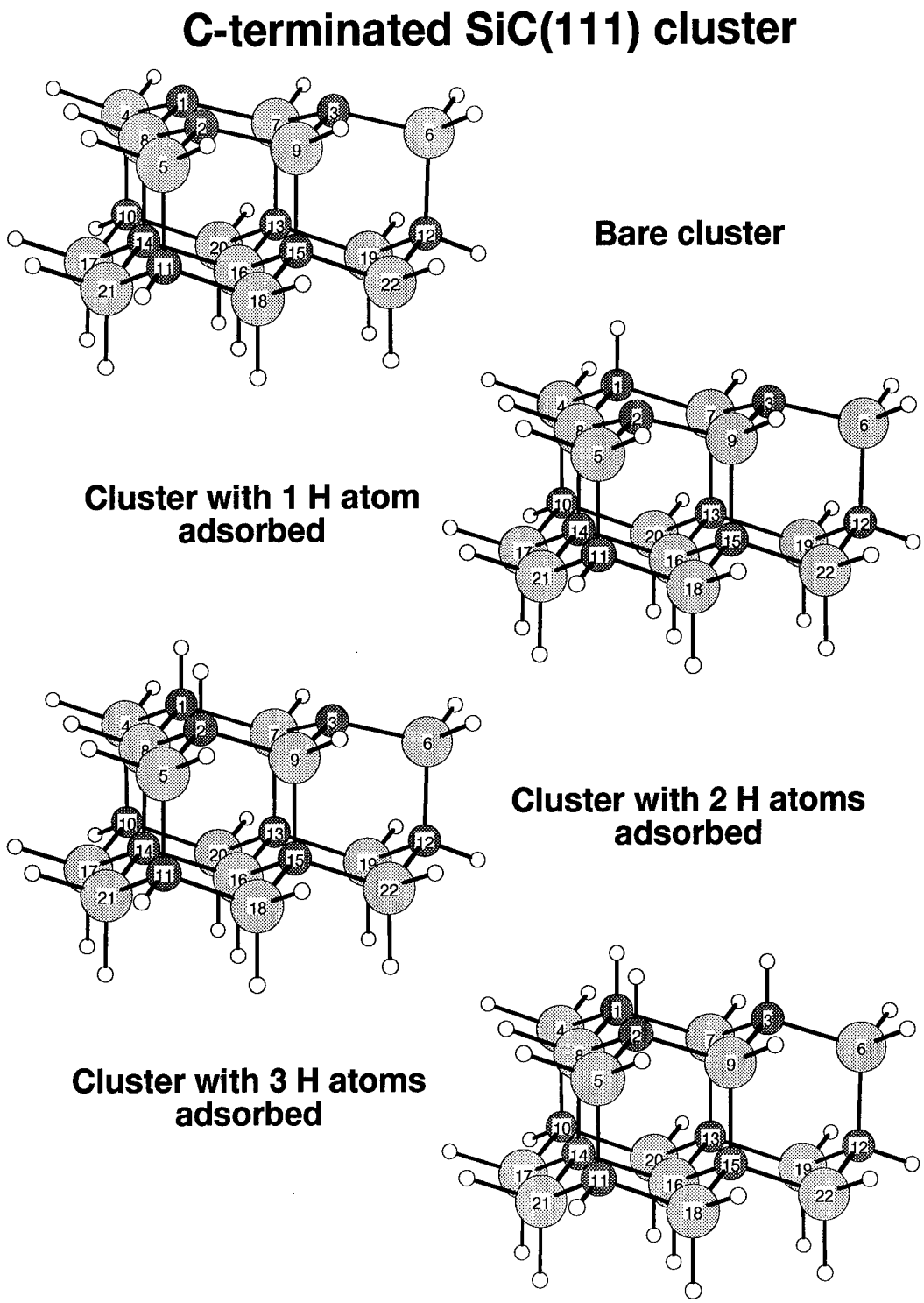

Figure 5.20 H atom adsorption on the C-terminated SiC(111) cluster. Structural changes caused by H atom adsorption are subtle, and localized, and can be best discerned by comparison with the bare cluster.

	Clean	H Adsorbed
Distance ($\AA$)		
1 4	1.876	1.896
1 7	1.870	1.893
1 8	1.870	1.893
Angle (°)		
4 1 8	114.585	110.650
8 1 7	114.315	110.573
7 1 4	114.586	110.651
ΔZ Surface Bilayer$\AA$		
C_1-Si_8	0.46	0.59
C_2-Si_8	0.46	0.45
C_3-Si_8	0.46	0.45

Table 5.7 Structural changes caused by H atom adsorption on the C-terminated SiC(111) cluster.

in the MIMOMM optimization are relatively unimportant. The energy of adsorption for each H atom is essentially identical, and the MP2 results for the cluster differ from the experimental hydrogenation energy of the CH_3 radical by 5 $\frac{kcal}{mole}$, is typical for the accuracy of MP2.

Molecule	Model	6-31G* Energy (H)		
		Hartree-Fock		MP2
		Ab Initio	MIMOMM 2 Bilayer	*Ab Initio*
$(C_9Si_{13}H_{25})$	^{4}ROHF	-4111.394766	-4111.393840	-4113.591320
$(C_9Si_{13}H_{25})H$	^{3}ROHF	-4112.027434	-4112.026682	-4114.249315
$(C_9Si_{13}H_{25})H_2$	^{2}ROHF	-4112.659983	-4112.659353	-4114.907348
$(C_9Si_{13}H_{25})H_3$	^{1}RHF	-4113.292397	-4113.291888	-4115.565393

Table 5.8 6-31G* energies of SiC molecules used in calculating energy of hydrogenation. (The 6-31G* energy for H atom is -0.498233 H.) The column labeled *ab initio* lists the results of a conventional *ab initio* calculation for adsorbing 1, 2, and 3 H atoms onto the EC. The column labeled MIMOMM lists the MIMOMM results using the 2 bilayer BC.

					Δ E (kcal/mole)		
					Hartree-Fock		MP2
					Ab Initio	MIMOMM 2 Bilayer	*Ab Initio*
$(C_9Si_{13}H_{25})H_2$	+	H	→	$(C_9Si_{13}H_{25})H_3$	-84.3	-84.5	-100.2
$(C_9Si_{13}H_{25})H$	+	H	→	$(C_9Si_{13}H_{25})H_2$	-84.3	-84.4	-100.3
$(C_9Si_{13}H_{25})$	+	H	→	$(C_9Si_{13}H_{25})H$	-84.2	-84.3	-100.3
CH_3	+	H	→	CH_4	-89.2		-104.2
CH_3	+	H	→	CH_4	**-104.8 (Exp)**		

Table 5.9 Comparison of energies of hydrogenation, C-terminated SiC(111) surface. Experimental result is taken from Ref [125].

5.7 Oxidation of SiC

5.7.1 Background. Depositing insulating layers on semiconductors is an important step in device fabrication. A commonly used method for creating insulating layers on silicon is to expose the surface to an oxygen plasma. Depending on the discharge conditions (power input, gas pressure), O atoms can be the majority neutral species in the plasma. The O atoms react with the silicon surface to form a silicon-oxide insulating layer. This approach has also been used to grow insulating layers on SiC. However, significantly degraded device performance is observed for oxide layers grown on carbon terminated SiC(111) surfaces compared to silicon terminated surfaces [126]. As was discussed in Chapter I, SiC MOSFET device performance is critically sensitive to defect formation at the insulating layer interface. Based on the observation that O atoms etch diamond surfaces, it is hypothesized that O atoms etch carbon from the C-terminated surface. After the C atoms have been etched away, the O atoms then react with the subsurface Si atoms to form a silicon oxide layer. However, the presence of C atom vacancies in this layer is believed to increase resistivity underneath the interface, causing the degraded device performance.

The mechanisms responsible for the observed differences for insulating layers grown on Si and C-terminated SiC surfaces are not understood [126]. Little characterization of oxide layers on SiC surfaces has been performed, and no theoretical treatments of the oxidation of SiC(111) surfaces have been published. Etching and other O atom reactions with SiC surfaces are likely to cause large atom displacements, so *ab initio* calculations on a small SiC cluster will likely yield unrealistic results. MIMOMM is a good way to include bulk steric effects at an acceptable computational cost.

5.7.2 Methodology for Simulating Oxidation. Mapping out the PES for O atom reactions with SiC requires the ability to freeze specific internal coordinates, which is not possible with the present implementation of delocalized coordinates in GAMESS. As an alternative, O atoms were placed in a number of starting positions relative to the SiC ECs, and the geometry of the system allowed to optimize. Figure 5.21 shows a view of the top bilayer with four starting positions labeled.

Position	Site
I	Si-O (C-O) ontop
II	Si-O-Si (C-O-C) bridge
III	Si-O-C (C-O-Si) ring insertion
IV	No adsorption calculated

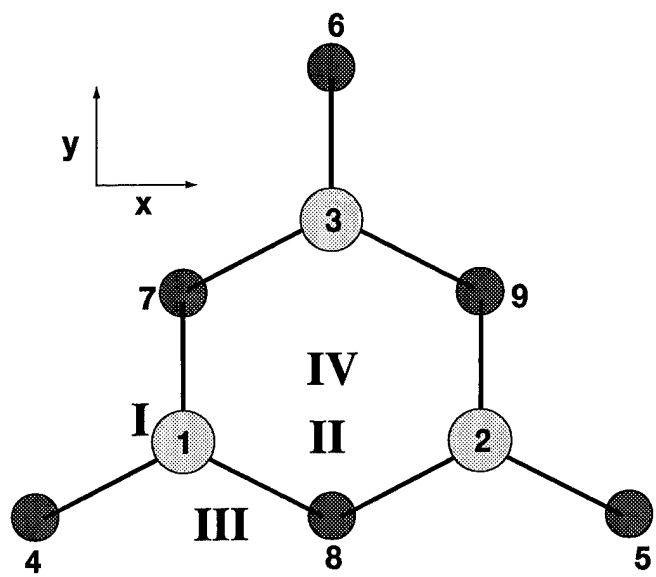

Distance from Atom 1

	Δx	Δy	Δz
I	0.0	0.0	1.5
II	1.57	0.0	1.5
III	0.79	-0.79	-0.32
IV	1.57	1.57	1.0

Figure 5.21 Starting points for O atom reactions with SiC EC. Atom numbers are the same as previous figures. Only the first bilayer is shown for clarity.

The starting positions were chosen to favor formation of specific adsorption sites. Position I, with the total spin set to 4 (quartet), favors adsorption on top of atom 1. Position II, with the total spin set to 2 (doublet), favors formation of a bridge site, Si-O-Si or C-O-C. Position III, with the total spin set to 4, favors insertion of the O atom into the Si-C surface bilayer ring. One of the mechanisms proposed for the oxidation of of Si(111) is the adsorption of a molecular oxygen precursor. After this precursor dissociates, the lowest energy configuration is for one O atom to move to an ontop site, while the other O atom inserts itself into the surface bilayer, forming an Si-O-Si ring [127]. Position III tests a similar mechanism for O atoms, creating Si-O-C (Si-terminated surface) and C-O-Si (C-terminated) rings. Position IV is above the center of the EC, and it was unclear what type of adsorption site would result from starting at this location. Position IV is 2.68$\AA$ away from all the surface atoms, a distance that is much larger than a typical Si-O bond length of 1.68$\AA$ or a C-O bond length of 1.38$\AA$. Several AM1 ^{2}ROHF optimizations, using a number of different convergence options, failed to converge in the initial SCF procedure with an O atom at Position IV. Formation of a stable *subsurface* adsorption site is likely it the O atom is placed directly below Position IV. However, because the subsurface atoms are directly bonded to H atoms, subsurface adsorption below Position IV was not investigated.

5.8 Oxidation of the Si-terminated SiC(111) Surface

5.8.1 O-Si Ontop Site Adsorption: Structure. O atom adsorption at an ontop site was modeled by initially placing an O atom 1.5 $\AA$ directly above Si atom 1 of the EC. The overall multiplicity of the molecule was set to 4, to insure the O atom could only bond to one Si atom on the surface. For the conventional *ab initio* optimization of the EC, the system was first optimized at the semi-empirical level using AM1 to enable the calculation of a numerical Hessian to initiate the 6-31G* optimization. The AM1 Hessian was also used to initiate the MIMOMM optimizations; however, *use of the AM1 Hessian in IMOMM did not provide the same reduction in number of optimization steps observed in conventional ab initio calculations.* A possible reason for this result is that the initial Hessian is updated using the gradient at each optimization step. Since MIMOMM uses the

sum of *ab initio* and MM gradients, the hybrid gradient may be unsuitable for updating the Hessian calculated for the EC alone.

The MIMOMM (2 bilayer BC) optimized Si-terminated EC with an O atom adsorbed at an ontop site (directly above an Si atom) is shown in Figure 5.22. The small distortions in the EC geometry caused by the onto O atom adsorption are similar to the H atom adsorption results. A comparison of the geometry of the clean Si terminated cluster, the *ab initio* optimized cluster with 1 O atom adsorbed, and the MIMOMM result for 1 O atom adsorbed is listed in Figure 5.22. The optimized geometries of the EC for these three cases differ very slightly.

The adsorption calculations in this research only provide final state energies for the adsorption sites, and cannot predict any barriers in the overall reaction pathway. However, the fact that O atom ontop site adsorption causes so little distortion in the cluster geometry is good evidence that there is no barrier to this reaction.

5.8.2 Si-O-Si Bridge Site Adsorption. O atom adsorption at a bridge site on the Si-terminated surface was modeled by placing an O atom 1.5 $\AA$ above the plane of the surface Si atoms, and halfway between Si atoms 1 and 2. The overall multiplicity of the EC was set to 2 to force the O atom to form two bonds with the surface Si atoms.

Adsorption of an O atom at a bridge site induces *significant* distortion of the EC. Figure 5.23 shows a view in the XZ plane of the *ab initio* optimized geometry of the Si-terminated EC. This view emphasizes the planes of Si and C atoms. Figure 5.24 shows the *ab initio* optimized structure of the Si-terminated EC with 1 O atom adsorbed at a bridge site. The displacement of Si atoms 1 and 2 to bond with the O atom is the root cause for the observed distortion of the EC. From their initial separation of 3.14 $\AA$, atoms 1 and 2 have each moved 0.34 $\AA$ closer together along the X axis, dragging atoms 4 and 5 along with them. Atoms 4 and 5 drag 10 and 11 along for the ride. Bond angle 1-8-2 squeezes down from 111° to 83°, and Atom 8 is driven 0.5 $\AA$ down from its initial position. Atom 8 drives atom 14 down 0.4$\AA$. Atoms 16 through 21 are displaced approximately $\pm 0.2\AA$ along the Z-axis in response to the displacement of the other atoms. (Atom displacements and geometry for the *ab initio* and MIMOMM optimizations for O atom bridge site adsorption

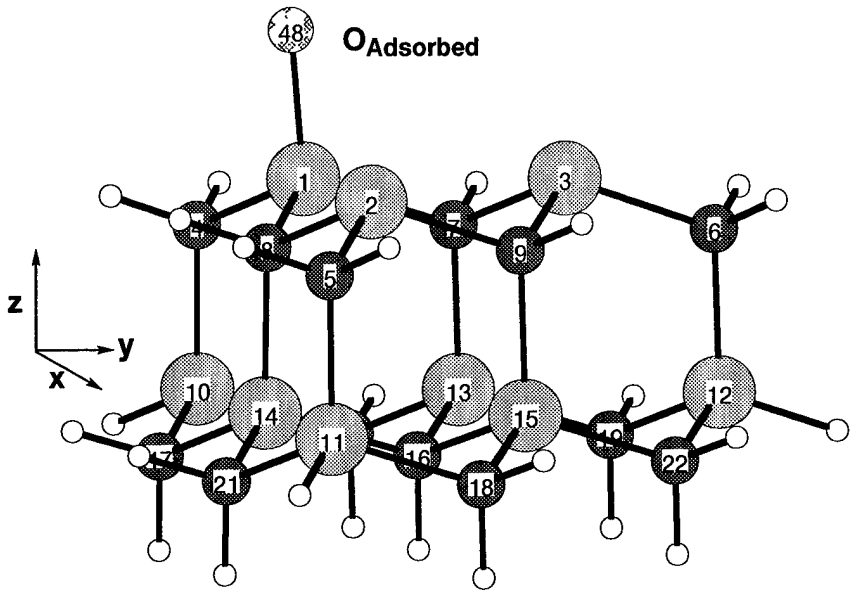

	$Si_9C_{13}H_{25}$ *Ab Initio*	$Si_9C_{13}H_{25}O$ *Ab Initio*	$Si_9C_{13}H_{25}O$ MIMOMM 2 Bilayer		$Si_9C_{13}H_{25}$ *Ab Initio*	$Si_9C_{13}H_{25}O$ *Ab Initio*	$Si_9C_{13}H_{25}O$ MIMOMM 2 Bilayer
Dist (Å)				Angle (°)			
1 O_{ads}	-	1.698	1.698	O_{ads} 1 2	-	94.560	93.785
1 2	3.147	3.155	3.149	O_{ads} 1 3	-	94.524	93.803
2 3	3.147	3.140	3.138	O_{ads} 1 8	-	111.663	111.422
3 1	3.147	3.155	3.149	7 1 8	107.174	107.450	107.566
1 9	3.641	3.647	3.643	8 2 9	107.174	106.928	106.914
1 8	1.903	1.882	1.885	9 3 7	107.174	106.928	106.917
1 7	1.903	1.882	1.885	Torsion(°)			
7 13	1.903	1.912	1.914	5 11 4 10	-179.999	-179.865	-179.922
8 14	1.903	1.912	1.914	4 10 6 12	-179.999	-179.854	179.930
9 15	1.903	1.908	1.909	10 11 12 14	0.248	0.302	0.151

Figure 5.22 Comparison of *ab initio* and MIMOMM optimized (6-31G*) Si-terminated SiC(111) cluster geometry with 1 O atom adsorbed onto an ontop site. The *ab initio* optimized bare Si-terminated EC result is listed to show the small structural change induced by O atom adsorption at an ontop site.

are listed in Tables 5.10 and 5.11). *While we saw in Chapter III that dimerization on the Si(001) surface induced large subsurface atom displacements, on the order of tenths of angstroms, bulk material doesn't "curl up '' around the edges, as this finite SiC(111) cluster appears to have done in response to a Si-O-Si bridge site being formed on the surface.*

Figure 5.25 shows the MIMOMM optimized geometry for the Si-terminated EC using the 2 bilayer BC. Significant distortion in the EC remains, and the overall pattern of the distortion is the same as in the *ab initio* optimized case. However, Table 5.10 shows that the atom displacements have been reduced. (A comparison of the optimized geometries is listed in Table 5.11.)

Figure 5.26 shows the MIMOMM optimized result using the 4 bilayer BC. The differences between this result, the *ab initio* optimized result as well as MIMOMM using the 2 bilayer BC are dramatic! Unlike the 2 bilayer BC, the 4 bilayer BC adds steric forces on the bottom layer EC atoms, atoms 16-22, along the z axis. Thus, when atom 10 is pulled up by atom 4 (which in turn is pulled by atom 1), atoms 17 and 20 now have a force from the BC restricting their motion along the z axis. Atoms 17 and 20 now pull back on atom 10, constraining its motion. (Atom displacements on the other side of the EC are likewise reduced.) Displacement of the bottom bilayer atoms still occurs, (Table 5.10), but is reduced by a factor of 3 to 4 from compared with the *ab initio* result. Experimental results for SiC are not available for direct comparisons with these, but the atom displacements observed for the MIMOMM 4 bilayer BC case are closer to MM models of subsurface displacements induced by surface reconstruction on silicon surfaces [88].

The differences between the MIMOMM optimized results using the 2-bilayer and 4-bilayer bulk clusters emphasize that thinking of a surface as a 2-D plane of atoms is a poor physical model. Cleaving a real crystal not only creates a surface, it also creates a "displacement zone" underneath the surface. This displacement layer responds to displacements of the surface atoms, as well as constraining the motions of the surface atoms. The 2-bilayer bulk cluster does not contain enough of this displacement zone to provide realistic constraints on the embedded cluster. The 4-bilayer bulk cluster contains enough of the displacement zone to provide more realistic constraints on the embedded cluster, which significantly reduces displacements along the z-axis by the atoms at the bottom of

the embedded cluster. In order to determine how much of the displacement zone is needed to provide an "acceptable" representation of the surface of a bulk material, one would need to use bulk clusters of increasing thickness in MIMOMM optimizations. Convergence of the embedded cluster atom displacements would be the criterion used to decide when the the bulk cluster is thick enough.

Atom Displacements (Å) Caused by Si-O-Si Bridge Site Adsorption									
Atom	*Ab Initio*			MIMOMM: 2 Bilayer			MIMOMM: 4 Bilayer		
	δ x	δ y	δ z	δ x	δ y	δ z	δ x	δ y	δ z
1	**0.342**	0.001	-0.098	**0.311**	-0.003	-0.058	**0.299**	0.005	-0.047
2	**-0.342**	0.001	-0.098	**-0.304**	-0.003	-0.059	**-0.290**	-0.004	-0.043
3	0.000	-0.095	-0.027	0.003	-0.056	0.013	0.009	-0.055	0.024
4	**0.278**	0.037	**0.286**	**0.183**	-0.015	**0.232**	**0.171**	-0.007	**0.187**
5	**-0.278**	0.037	**0.286**	**-0.179**	-0.012	**0.225**	**-0.165**	-0.019	**0.174**
6	0.000	-0.069	-0.101	0.003	-0.039	-0.015	0.011	-0.045	0.005
7	0.066	-0.000	-0.022	0.062	0.002	-0.009	0.063	0.005	0.003
8	0.000	0.040	**-0.505**	0.002	0.080	**-0.393**	0.006	0.102	**-0.323**
9	-0.066	-0.000	-0.022	-0.057	0.003	-0.012	-0.049	0.003	0.001
10	0.083	0.024	**0.234**	0.069	0.000	**0.164**	0.028	0.026	0.067
11	-0.083	0.024	**0.234**	-0.069	0.002	**0.157**	-0.065	-0.003	0.090
12	0.000	-0.003	-0.096	0.001	0.017	-0.012	0.005	-0.018	0.012
13	0.008	-0.006	-0.023	0.026	0.011	-0.010	0.027	0.004	0.007
14	0.000	-0.033	**-0.412**	0.000	0.017	**-0.302**	0.000	0.038	**-0.204**
15	-0.008	-0.006	-0.024	-0.027	0.012	-0.014	-0.022	-0.000	0.000
16	0.000	-0.082	**-0.188**	0.001	-0.027	**-0.145**	0.001	-0.003	**-0.064**
17	-0.083	-0.040	**-0.198**	-0.058	0.049	**-0.091**	-0.018	0.048	**-0.077**
18	0.039	0.035	**0.192**	0.019	0.016	**0.120**	-0.022	0.011	**0.040**
19	-0.026	0.000	-0.040	-0.030	-0.003	0.027	0.009	-0.003	0.022
20	-0.039	0.035	**0.192**	-0.020	0.014	**0.127**	0.018	0.006	**0.045**
21	0.083	-0.040	**-0.198**	0.056	0.050	**-0.095**	0.026	0.033	**-0.075**
22	0.026	0.000	-0.040	0.030	-0.002	0.024	-0.002	-0.004	0.014

Table 5.10 Atom displacements induced by O atom adsorption onto a bridging site of an Si-terminated SiC(111) surface. Displacements are measured from the 6-31G* optimized geometry of the $Si_9C_{13}H_{25}$ cluster. Displacements along the z axis for atoms on the bottom of EC, Atoms 16-22, using MIMOMM with the 4 bilayer BC are reduced by a factor of 3-4 from the *ab initio* result.

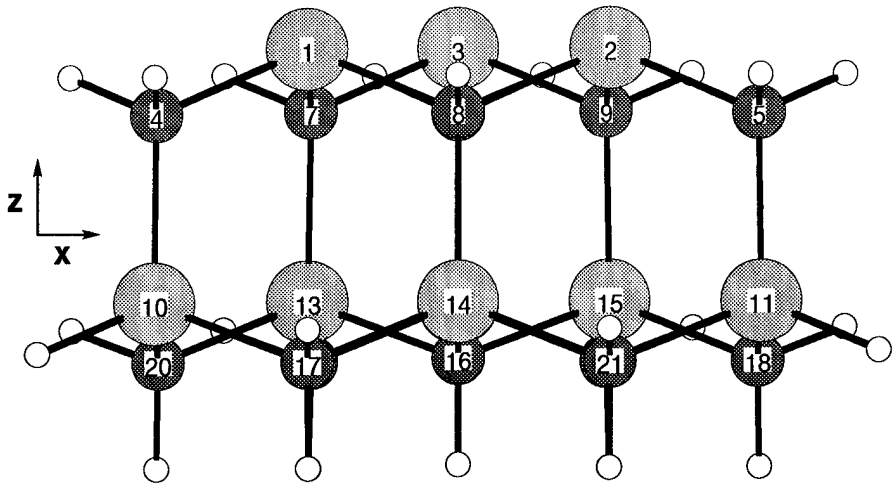

Figure 5.23 Clean Si-terminated SiC(111) embedded cluster, xz view, *ab initio* (6-31G*) optimized geometry. Notice that all the Si and C atoms lie in planes perpendicular to the z axis. This is a different view of the same EC shown in Figure 5.7. The bridge site for O atom adsorption is between Si atoms 1 and 2.

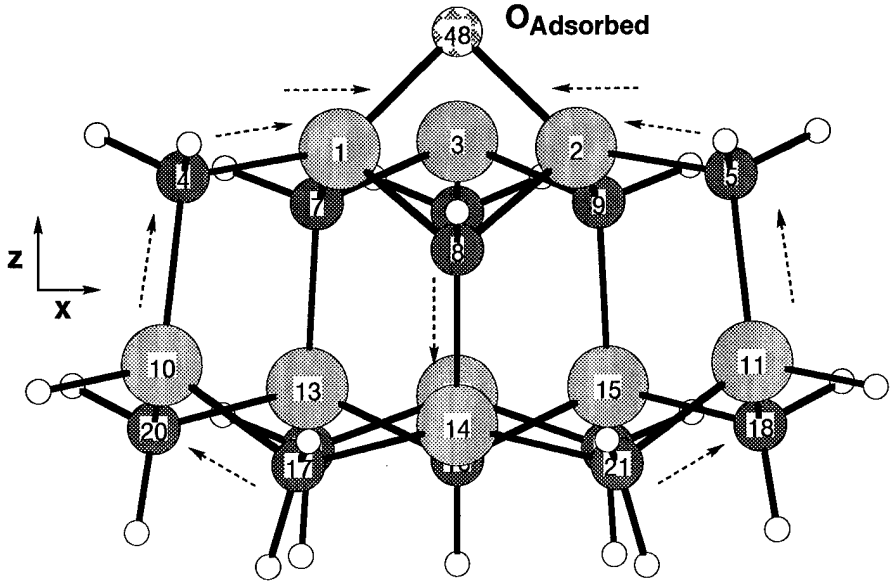

Figure 5.24 *Ab initio* optimized Si-terminated SiC(111) EC with O atom adsorbed in a bridge site. Directions of atom displacements from reconstructed EC positions are shown by arrows.

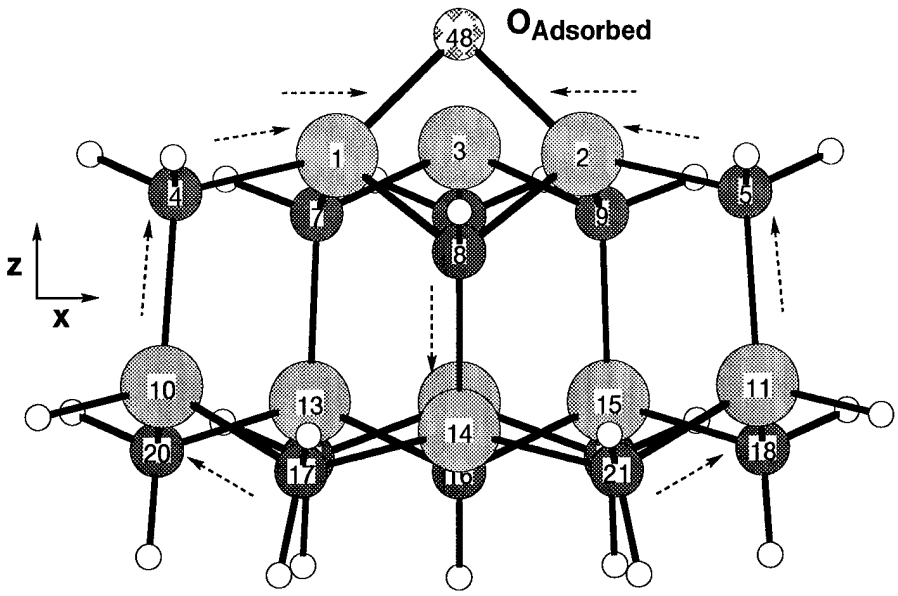

Figure 5.25 MIMOMM optimized Si-terminated SiC(111) EC with O atom adsorbed in a bridge site, 2 bilayer bulk cluster. Atom displacements are noticeably smaller than the *ab initio* result

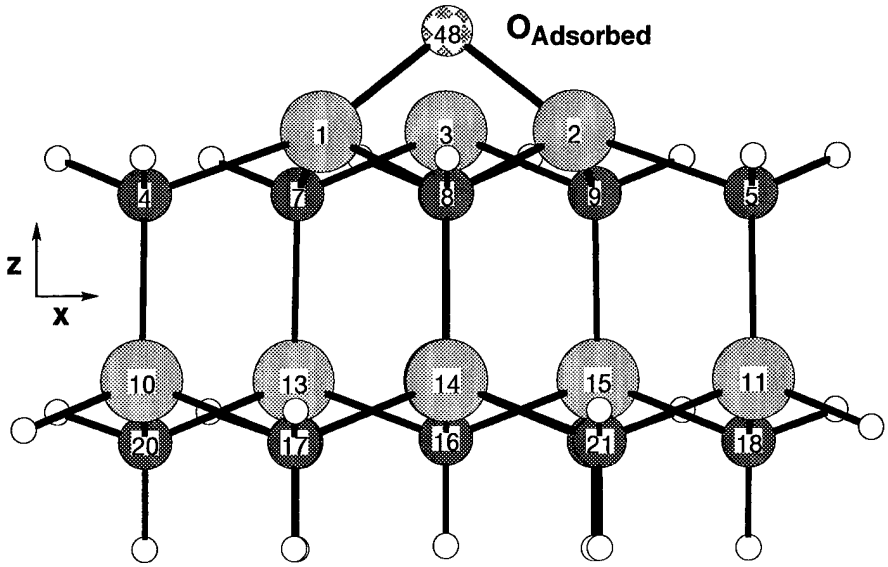

Figure 5.26 MIMOMM optimized Si-terminated SiC(111) EC with O atom adsorbed in a bridge site, 4 bilayer bulk cluster. Atoms 1 and 2 have each moved 0.3 $\AA$ away from their original positions, as in the other cases. The steric forces from the 4 bilayer on atoms 16-22, not present in the other cases, reduce their displacements and the overall distortion in the EC.

	$Si_9C_{13}H_{25}$ *Ab Initio* None	$Si_9C_{13}H_{25}O$ *Ab Initio* None	$Si_9C_{13}H_{25}O$ MIMOMM 2 Bilayer	$Si_9C_{13}H_{25}O$ MIMOMM 4 Bilayer
Dist (Å)				
1 O_{ads}	-	1.727	1.754	1.767
2 O_{ads}	-	1.727	1.754	1.765
1 2	3.147	2.463	2.531	2.546
1 4	1.904	1.878	1.928	1.942
1 8	1.903	1.848	1.852	1.842
4 10	1.896	1.960	1.968	2.037
5 11	1.896	1.960	1.968	1.998
7 13	1.903	1.913	1.911	1.911
8 14	1.903	1.816	1.817	1.795
Angle (°)				
1 O_{ads} 2	-	90.868	92.304	92.238
O_{ads} 1 4	-	136.191	141.362	142.883
1 8 2	111.593	83.592	86.166	87.404
4 1 8	110.098	104.301	105.030	104.867
8 2 9	107.174	112.077	113.011	114.139
9 3 7	107.174	101.085	102.006	102.184
Torsion(°)				
10 11 12 14	0.248	-13.480	-9.568	6.075
20 18 17 16	-1.492	-12.720	-8.356	-2.836

Table 5.11 Comparison of *ab initio* and MIMOMM optimized Si-terminated SiC(111) cluster geometry with 1 O atom adsorbed onto an *bridge* site. The bare cluster results are listed for comparison. 6-31G* basis set used in all calculations.

5.8.3 Si-O-C Ring Insertion: Structure. Initially placing an O atom halfway between a surface Si atom and a subsurface C atom, starting position III in Figure 5.21, resulted in breaking of the Si-C bond and formation of Si-O and O-C bonds. I.e., the O atom *inserted* itself into the Si-C surface bilayer, maintaining a closed ring structure. A comparison of the *ab initio* and MIMOMM (4 bilayer) optimized geometries of the Si-O-C ring insertion site on the Si-terminated SiC(111) surface is listed in Table 5.12. The major structural change caused by this O atom insertion is the 0.8Å increase in the atom 1-2 separation from the bare reconstructed cluster. This structural change has the effect of opening up the surface bilayer ring, which will help additional O atoms impinging on the surface penetrate deeper and react with subsurface atoms. Figures 5.27, 5.28, 5.29, and 5.30 show comparisons of the *ab initio* and MIMOMM (4 bilayer) optimized geometries of the Si-O-C ring insertion site on the Si-terminated SiC(111) surface. As we've seen in previous cases, the MIMOMM optimization reduces the overall distortion of the cluster.

	$Si_9C_{13}H_{25}$ *Ab Initio*	$Si_9C_{13}H_{25}O$ *Ab Initio*	$Si_9C_{13}H_{25}O$ MIMOMM 4 Bilayer
Dist (Å)			
1 2	3.147	3.917	3.822
1 4	1.904	1.895	1.877
1 7	1.903	1.895	1.887
1 8	1.903	2.832	2.766
1 9	3.641	4.063	3.997
1 48	-	1.647	1.619
8 48	-	1.427	1.430
Angle (°)			
7 1 48	-	111.114	109.021
1 48 8	-	134.114	130.052
48 8 2	-	111.142	99.700
8 2 9	107.174	108.368	106.901
2 9 3	107.174	114.700	115.113
9 3 7	107.174	112.168	112.370
3 7 1	107.174	114.847	112.724

Table 5.12 Comparison of *ab initio* and MIMOMM optimized (^{4}ROHF 6-31G*) Si-terminated SiC(111) cluster geometry with an O atom adsorbed at a Si-O-C ring insertion site. Atom 48 is the adsorbed O atom. The bare cluster results are listed for comparison.

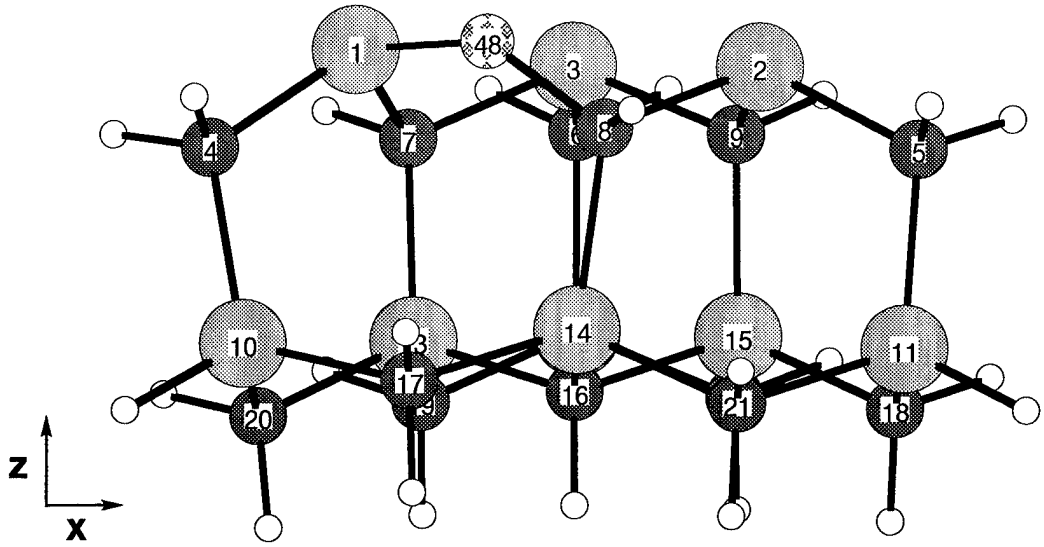

Figure 5.27 *Ab initio* optimized ^{4}ROHF (6-31G*) geometry of Si-O-C ring insertion, Si-terminated SiC(111) surface.

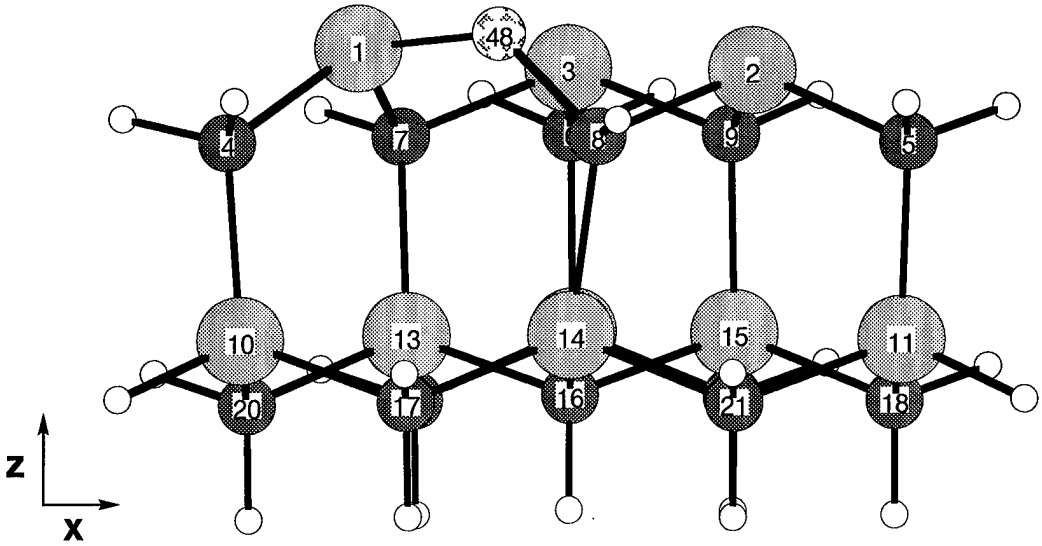

Figure 5.28 MIMOMM optimized ^{4}ROHF (6-31G*/4 bilayer BC) geometry of Si-O-C ring insertion, Si-terminated SiC(111) surface.

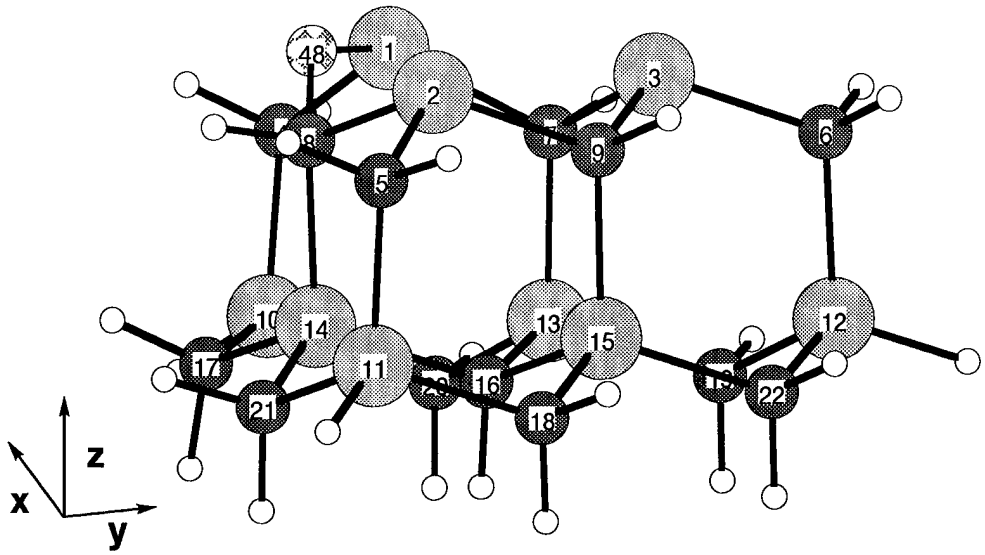

Figure 5.29 *Ab initio* optimized ^{4}ROHF (6-31G*) geometry of Si-O-C ring insertion bridge, Si-terminated SiC(111) surface.

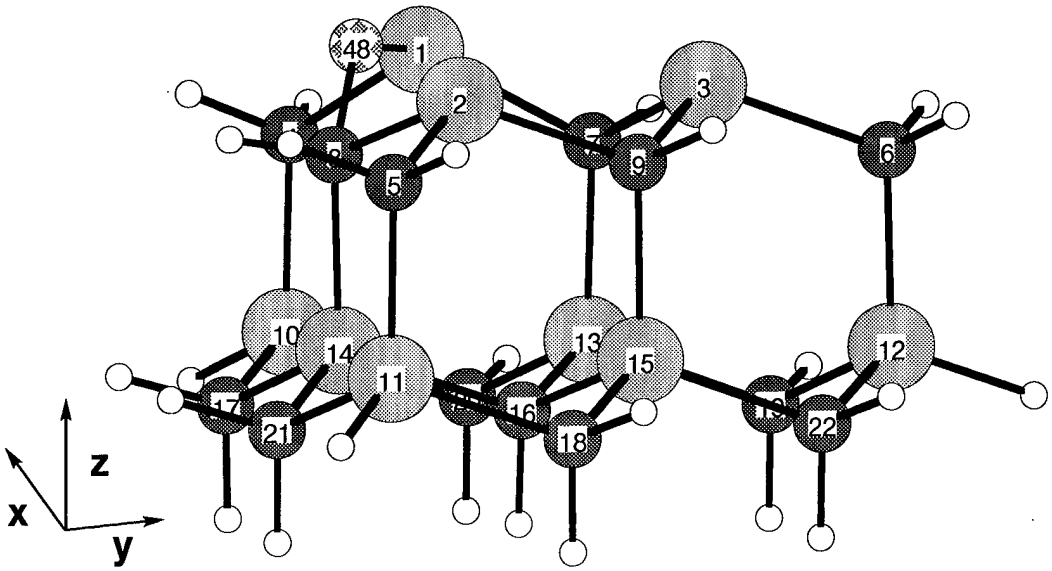

Figure 5.30 MIMOMM optimized ^{4}ROHF (6-31G*/4 bilayer BC) geometry of Si-O-C subsurface bridge, Si-terminated SiC(111) surface.

5.8.4 O-Si-O-Si Ontop and Ring Insertion: Structure. Figure 5.31 shows the *ab initio* optimized geometry of the Si-terminated SiC(111) cluster with two O atoms adsorbed. This structure was obtained by starting with the optimized geometry of the Si-terminated SiC(111) cluster with one O atom adsorbed into a ring site (between Si atom 1 and C atom 8), and placing a second O atom 1.6$\AA$ above Si atom 1. This starting point was selected to bias the optimized geometry towards Si atom 1 being bonded to both O atoms because this configuration is similar to the lowest energy product state to O_2 adsorption onto the Si(111) surface (after dissociation of the molecular precursor) [128]. This process is hypothesized to be a first step in the formation of an SiO_2 layer on Si(111) grown by exposure to oxygen. A comparison of the geometry of the bare cluster, the cluster with one O atom adsorbed in a ring site, and the cluster with two O atoms adsorbed is listed in Table 5.13.

	$Si_9C_{13}H_{25}$ *Ab Initio*	Si-O_{ring}-Si *Ab Initio*	O_{ontop}Si-O_{ring}-Si *Ab Initio*
Dist ($\AA$)			
1 O_{ontop}	-	-	1.695
1 O_{ring}	-	1.647	1.632
1 4	1.904	1.895	1.873
1 7	1.903	1.895	1.872
8 O_{ring}	-	1.427	1.428
2 8	1.903	1.913	1.914
3 7	1.903	1.911	1.915
Angle (°)			
O_{ontop}-1-O_{ring}	-	-	109.037
O_{ontop}-1-4	-	-	105.711
O_{ontop}-1-7	-	-	107.831
1-O_{ring}-8	-	134.114	133.649
O_{ring}-8-2	-	111.142	110.610
2-9-3	111.593	114.700	114.642
3-7-1	111.593	114.847	115.780
7-1-O_{ring}	-	111.095	111.151

Table 5.13 Comparison of Si-terminated SiC(111) cluster *ab initio* optimized geometry (6-31G*) with 0, 1, and 2 O atoms adsorbed.

5.8.5 Comparison of Adsorption Site Energetics. Table 5.14 lists the Hartree-Fock and MP2 6-31G* energies of the Si-terminated SiC(111) EC, the clean surface and with O atom (s) adsorbed at various sites on the cluster. (The MP2 energies were calculated

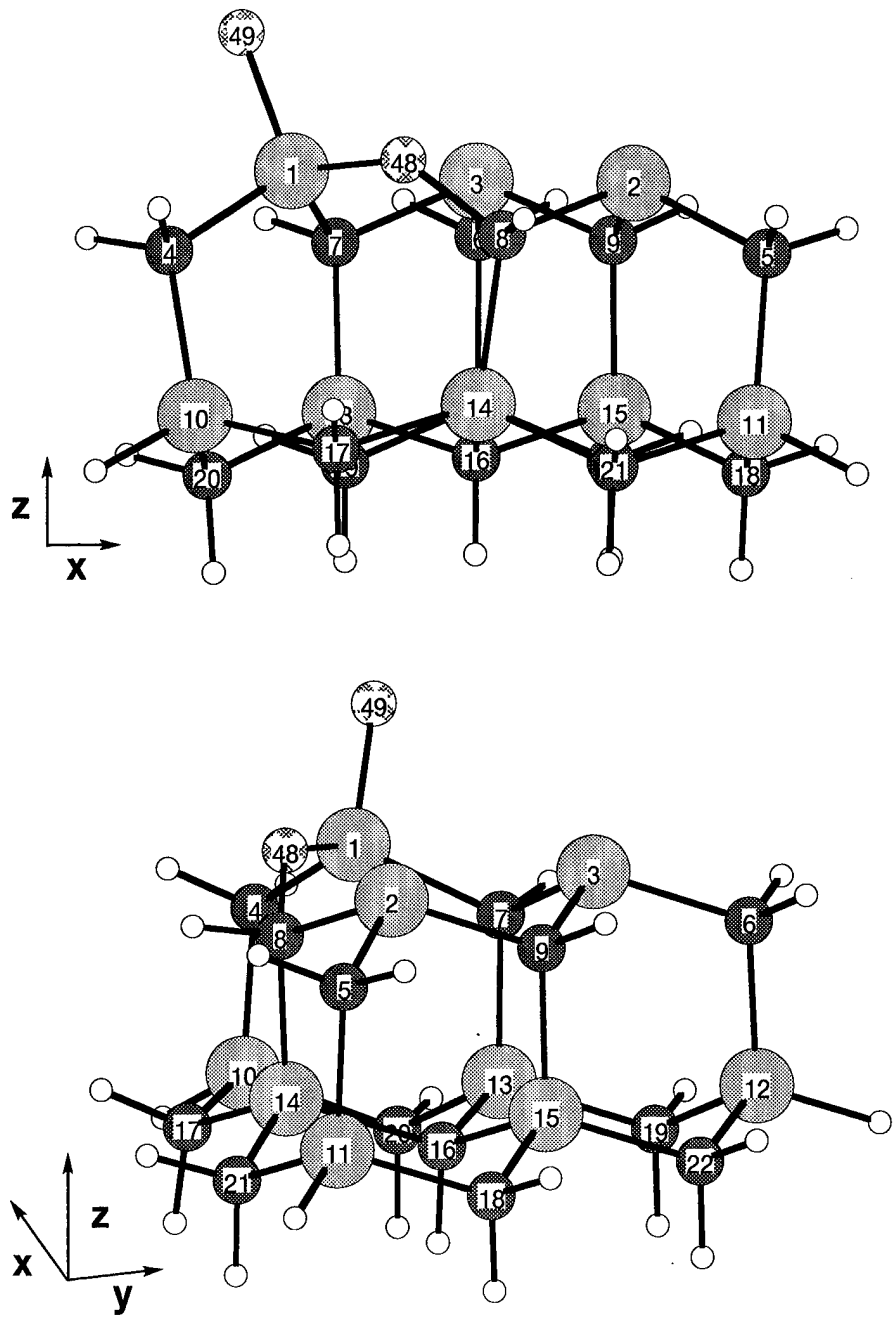

Figure 5.31 *Ab initio* optimized ^{4}ROHF (6-31G*) geometry of Si-terminated SiC(111) cluster with two O atoms adsorbed, O_{ontop}Si-O_{ring}-Si.

at the Hartree-Fock optimized geometries.) Large atom displacements in the EC were observed in bridge site oxidation, so MIMOMM calculations using both the 2 bilayer and 4 bilayer bulk clusters were performed (a discussion of the optimized structures follows). As before, we see that use of MIMOMM increases the EC energies, which one expects from a constrained optimization. Table 5.15 lists the oxidation energies for the ontop, bridge, and ring insertion sites on the Si-terminated surface. We see that the inclusion of electron correlation in the MP2 calculation has a significant effect on the predicted adsorption energies, though the relative energies of the different sites are the same at both the HF and MP2 levels of theory.As was seen in the hydrogenation results, MIMOMM has essentially no effect on the oxidation energy at the ontop site. However, use of MIMOMM decreases the oxidation energy at the bridge site by 4.5 $\frac{kcal}{mole}$ using the 2-bilayer bulk cluster, and 11.6 $\frac{kcal}{mole}$ using the 4-bilayer bulk cluster. *Overall, adsorption at a bridge site on the Si-terminated surface is energetically favored over an ontop site.*

The adsorption energy for 2 O atoms, one O atom in a ring insertion site and one O atom at an ontop site, with both O atoms bonded to the same Si surface atom, is quite large. SiO_2 is not a stable gas phase molecule, so it is unlikely that O atoms will etch the Si-terminated SiC(111) surface with this two O atom adsorption structure as an intermediate. However, this structure is predicted to be an initial state in the formation of a silicon dioxide layer on the Si(111) surface by exposing the Si(111) surface to a flux of O_2 molecules. A similar mechanism may be involved in the growth of an insulating layer, predominantly silicon dioxide, on the Si-terminated SiC(111) surface.

5.9 Oxidation of the C-terminated SiC(111) Surface

5.9.1 O-C Ontop Site Adsorption: Structure . O atom adsorption at an ontop site on the C-terminated SiC(111) surface was modeled by placing an O atom 1.1 $\AA$ directly above C atom 1 of the EC (starting position I in Figure 5.21), a distance shorter than the expected optimum. The overall multiplicity of the molecule was set to 4, to insure the O atom could only bond to one Si atom on the surface. (This is the same procedure as was used for the Si-terminated surface.) Figure 5.32 shows the *ab initio* optimized clean C terminated EC, offset about 10° from the yz plane. Figure 5.33 shows a view of the

Surface	Model	6-31G* Hartree Fock Energy (H)		
		Ab Initio	MIMOMM 2 Bilayer	MIMOMM 4 Bilayer
Si-terminated ($Si_9C_{13}H_{25}$)				
Bare	^{4}ROHF	-3107.287434	-3107.285539	-3107.286685
O-Si ontop	^{4}ROHF	-3182.185212	-3182.183299	a
Si-O-Si bridge	^{2}ROHF	-3182.236653	-3182.227517	-3182.217861
Si-O-C ring	^{4}ROHF	-3182.146984	b	-3182.137410
O_{ontop}-Si-O_{ring}-C	^{4}ROHF	-3257.051971	c	c
Si-O-C ring	^{2}ROHF	-3182.083401	b	-3182.070495
Si-O-C ring	^{2}GVB	-3182.083407	^{2}ROHF orbitals	
Si-O-C ring	^{2}GVB	-3182.083407	Huckel orbitals	
O atom	^{3}ROHF	-74.778966		

Surface	Model	6-31G* MP2 Energy (H)		
		Ab Initio	MIMOMM 2 Bilayer	MIMOMM 4 Bilayer
Si-terminated ($Si_9C_{13}H_{25}$)				
Bare	^{4}ROHF	-3109.704721	-3109.704177	-3109.704136
O-Si ontop	^{4}ROHF	-3184.750274	-3184.749495	a
Si-O-Si bridge	^{2}ROHF	-3184.862621	-3184.855145	-3184.844983
Si-O-C ring	^{4}ROHF	-3184.736188	b	-3184.726729
O_{ontop}-Si-O_{ring}-C	^{4}ROHF	-3259.788683	c	c
O atom	^{3}ROHF	-74.879847		

a Not calculated because minimal strutural change means bulk cluster has minor effect on energy

b Not calculated because 4 bilayer BC determined better

c Not calculated because MIMOMM effect on energy could be reliably estimated

Table 5.14 6-31G* energies of SiC clusters used in calculating energy of oxidation.

					Ab Initio	MIMOMM 2 Bilayer	MIMOMM 4 Bilayer
					Hartree-Fock ΔE ($\frac{kcal}{mole}$)		
($Si_9C_{13}H_{25}$)	+	O	→	($Si_9C_{13}H_{25}$)O ontop	-74.5	-74.5	-
($Si_9C_{13}H_{25}$)	+	O	→	($Si_9C_{13}H_{25}$)O bridge	-106.8	-102.3	-92.5
($Si_9C_{13}H_{25}$)	+	O	→	($Si_9C_{13}H_{25}$)O ring	-50.6	-	-45.0
($Si_9C_{13}H_{25}$)	+	2O	→	($Si_9C_{13}H_{25}$)O_2 ontop & ring	-129.6	-	-
					MP2 ΔE ($\frac{kcal}{mole}$)		
($Si_9C_{13}H_{25}$)	+	O	→	($Si_9C_{13}H_{25}$)O ontop	-104.0	-103.8	-
($Si_9C_{13}H_{25}$)	+	O	→	($Si_9C_{13}H_{25}$)O bridge	-174.5	-170.1	-163.8
($Si_9C_{13}H_{25}$)	+	O	→	($Si_9C_{13}H_{25}$)O ring	-95.1	-	-89.3
($Si_9C_{13}H_{25}$)	+	2O	→	($Si_9C_{13}H_{25}$)O_2 ontop & ring	-203.5	-	-

Table 5.15 Comparison of energy of oxidation, Si-terminated SiC(111) surface.

ab initio optimized EC with an O atom adsorbed on C atom 1. Adsorption of the O atom raises C atom 1 up out the surface plane closer to a lattice position, very similar to structural change caused by H atom adsorption. Because the overall distortion of the cluster is small, the IMOMM optimized structure results in small differences from the *ab initio* result and is not shown.

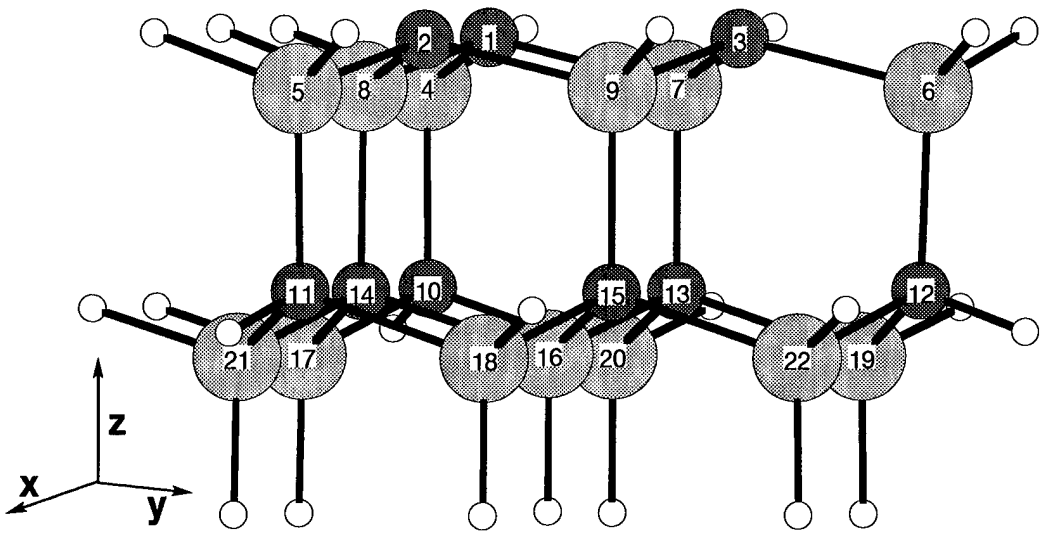

Figure 5.32 Clean C-terminated SiC(111) EC, *ab initio* optimized geometry.

5.9.2 C-O-C Bridge Site Adsorption . O atom adsorption at a bridge site on the Si-terminated surface was modeled by placing an O atom 1.5 Å above the plane of the surface Si atoms, and halfway between C atoms 1 and 2, starting position II in Figure 5.21. The overall multiplicity of the EC was set to 2 to force the O atom to form two bonds with the surface Si atoms.

As was seen in the Si-terminated EC, adsorption of an O atom at a bridge site induces *significant* distortion of the EC structure. Figure 5.34 shows the *ab initio* optimized structure of the C-terminated EC with 1 O atom adsorbed at a bridge site. The pattern of atom displacements is the same as in the Si-terminated EC, though the displacements are larger in the C-terminated cluster. Figure 5.35 shows the MIMOMM optimized structure

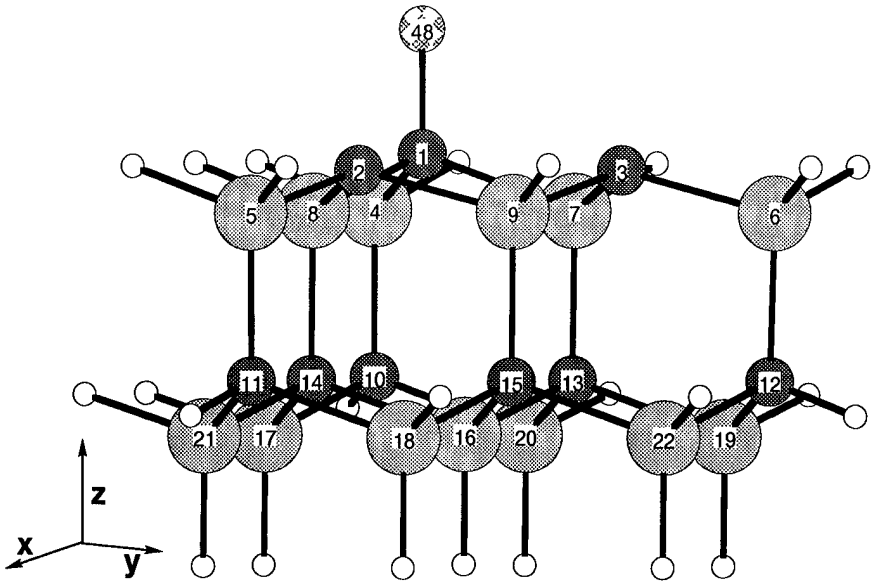

Figure 5.33 *Ab initio* optimized C-terminated SiC(111) EC with one O atom adsorbed in an ontop site, 6-31G* optimized geometry. Adsorption of the O atom raises C atom 1 out of the plane of the other surface C atoms, but otherwise causes minor structural distortions.

using the 2 bilayer BC. The magnitude of atom displacements is reduced from the *ab initio* optimized EC, though the pattern of displacements is the same. (Atom displacements for the various cases are listed in Table 5.16. A comparison of the optimized geometries is listed in Table 5.17.) Figure 5.36 shows the MIMOMM optimized EC geometry using the 4 bilayer BC. As was seen for the Si-terminated EC, *addition of steric forces underneath the EC greatly reduces the atom displacements in the EC.*

With the EC constrained by the 4 bilayer BC, O atom adsorption at a bridge site is predicted to be higher in energy than the separated EC and O atom. This result is quite strange, and indicates that a Hartree-Fock (single configuration) model of these bonds is inadequate.

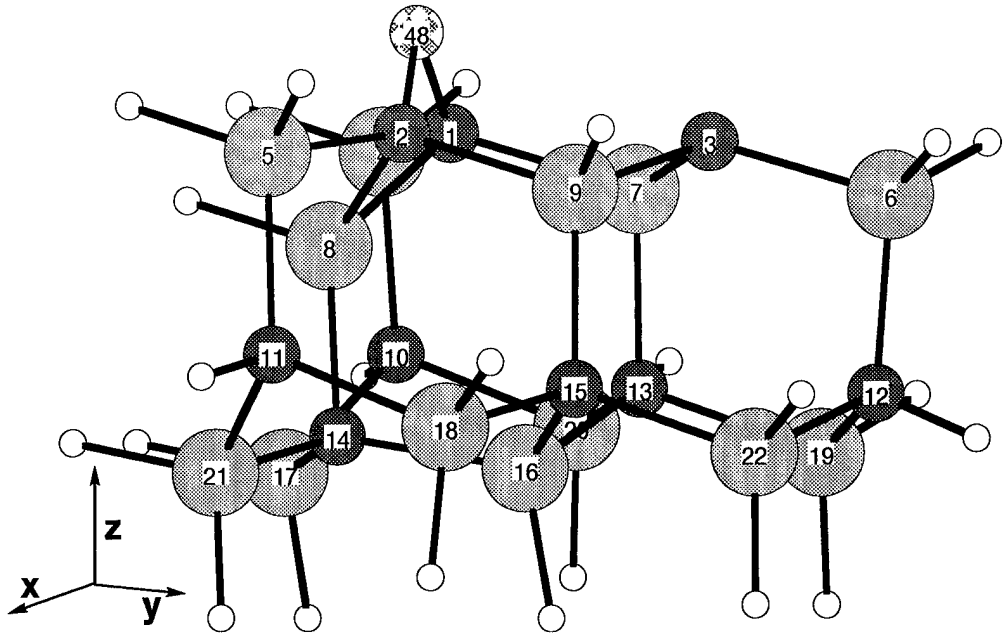

Figure 5.34 C-terminated SiC(111) *ab initio* optimized EC with 1 O atom adsorbed in a bridge site.

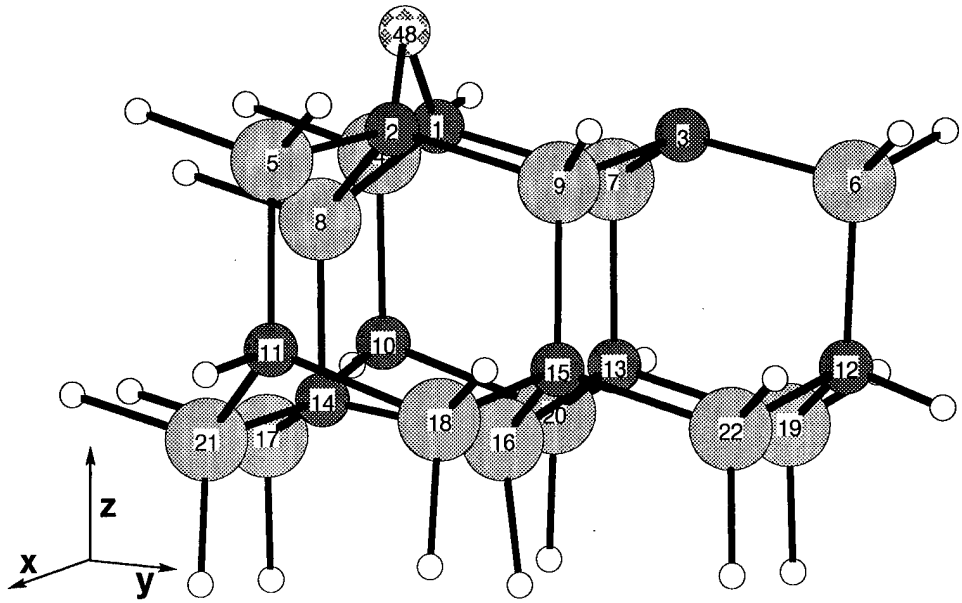

Figure 5.35 C-terminated SiC(111) surface with O atom adsorbed in a bridge site, IMOMM optimized geometry, 2 bilayer BC.

Atom Displacements (Å) Caused by C-O-C Bridge Site Adsorption									
Atom	*Ab Initio*			IMOMM: 2 Bilayer			IMOMM: 4 Bilayer		
	δ x	δ y	δ z	δ x	δ y	δ z	δ x	δ y	δ z
1	**0.418**	0.033	0.030	**0.356**	-0.041	0.038	**0.335**	-0.028	0.073
2	**-0.418**	0.033	0.030	**-0.355**	-0.041	0.041	**-0.331**	-0.034	0.075
3	0.000	**-0.143**	-0.091	0.000	**-0.106**	-0.053	-0.002	-0.097	0.010
4	**0.396**	0.063	**0.320**	**0.240**	-0.026	**0.204**	**0.213**	-0.003	**0.178**
5	**-0.396**	0.063	**0.320**	**-0.239**	-0.025	**0.204**	**-0.211**	-0.006	**0.176**
6	0.000	**-0.113**	-0.163	0.000	-0.065	-0.084	-0.001	-0.077	-0.010
7	**0.101**	-0.012	-0.076	**0.104**	-0.013	-0.073	**0.087**	-0.011	-0.019
8	0.000	0.038	**-0.574**	0.001	0.040	**-0.444**	0.001	0.073	**-0.330**
9	**-0.101**	-0.012	-0.076	**-0.104**	-0.013	-0.072	**-0.084**	-0.013	-0.018
10	**0.132**	0.018	**0.287**	**0.076**	0.007	**0.160**	**0.094**	-0.007	**0.121**
11	**-0.132**	0.018	**0.287**	**-0.076**	0.006	**0.159**	**-0.094**	-0.009	**0.119**
12	-0.000	-0.009	**-0.160**	0.000	-0.025	**-0.085**	0.001	-0.030	-0.008
13	0.008	-0.006	-0.069	0.029	-0.001	-0.063	0.029	-0.004	-0.010
14	-0.000	-0.038	**-0.487**	0.000	0.012	**-0.367**	0.000	0.036	**-0.229**
15	-0.008	-0.006	-0.069	-0.029	-0.001	-0.062	-0.028	-0.004	-0.009
16	-0.000	-0.090	**-0.224**	0.000	-0.039	**-0.181**	0.000	-0.007	**-0.074**
17	-0.094	-0.045	**-0.197**	-0.062	-0.028	**-0.118**	-0.015	0.035	**0.049**
18	-0.037	-0.004	-0.076	-0.017	0.011	-0.044	0.008	-0.010	0.004
20	-0.043	0.044	**0.206**	0.002	-0.014	**0.081**	0.035	0.010	**0.050**
21	0.094	-0.045	**-0.197**	0.062	-0.028	**-0.119**	0.015	0.036	**-0.065**
22	0.037	-0.004	-0.076	0.016	0.011	0.043	-0.010	-0.007	0.000

Table 5.16 Atom displacements induced by O atom adsorption onto a bridging site of a C-terminated SiC(111) surface. Displacements are measured from the 6-31G* optimized geometry of the $C_9Si_{13}H_{25}$ cluster.

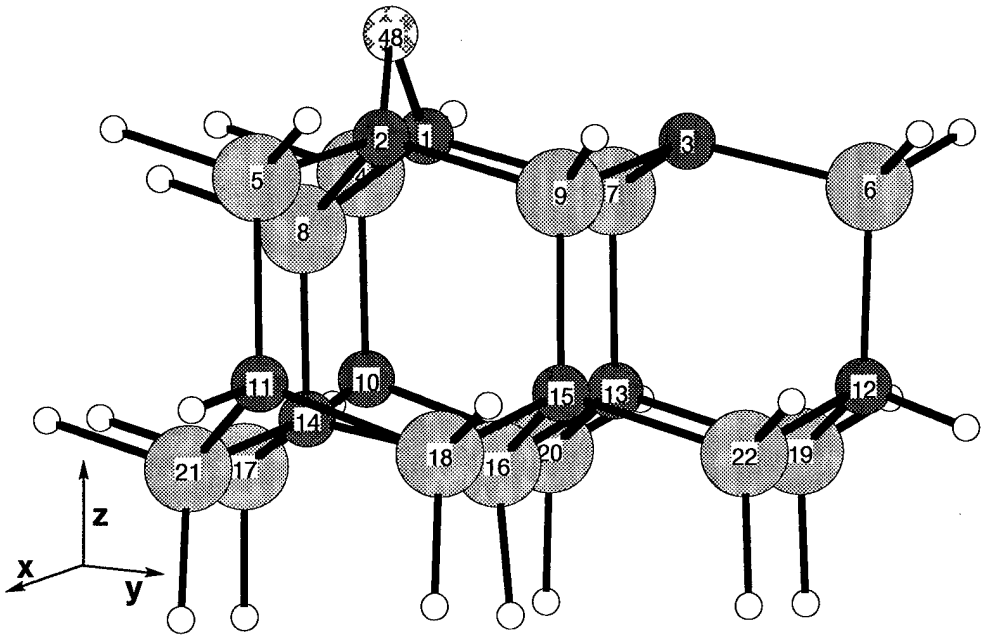

Figure 5.36 C-terminated SiC(111) surface with O atom adsorbed in a bridge site, IMOMM optimized geometry, 4 bilayer BC.

	$C_9Si_{13}H_{25}$ *Ab Initio*	$C_9Si_{13}H_{25}O$ *Ab Initio*	$C_9Si_{13}H_{25}O$ MIMOMM 2 Bilayer	$C_9Si_{13}H_{25}O$ MIMOMM 4 Bilayer
Dist ($\AA$)				
1 O_{ads}	-	1.505	1.568	1.590
2 O_{ads}	-	1.505	1.569	1.591
1 2	3.152	2.361	2.440	2.476
1 4	1.876	1.896	1.951	1.958
1 8	1.871	1.842	1.822	1.809
4 10	1.900	1.946	1.948	1.965
5 11	1.900	1.946	1.948	1.965
7 13	1.923	1.919	1.915	1.910
8 14	1.923	1.837	1.846	1.817
Angle (°)				
1 O_{ads} 2	-	100.641	102.163	102.223
O_{ads} 1 4	-	132.469	137.390	138.550
1 8 2	114.796	77.939	84.064	86.335
4 1 8	114.584	101.544	104.476	103.922
8 2 9	114.316	116.027	116.710	117.744
9 3 7	114.316	105.040	105.952	106.158
Torsion(°)				
10 11 12 14	-0.310	-16.989	-11.570	-7.765
20 18 17 16	-1.105	14.722	8.466	4.190

Table 5.17 Comparison of *ab initio* and MIMOMM optimized C-terminated SiC(111) cluster geometry with 1 O atom adsorbed onto C-O-C bridge site. The bare cluster results are listed for comparison. 6-31G* basis set used in all calculations.

5.9.3 C-O-Si Ring Insertion: Structure. A comparison of the *ab initio* and MIMOMM (4 bilayer) optimized geometries of the C1-O48-Si8 (atom numbers refer to Figure 5.37) ring insertion site on the C-terminated SiC(111) surface is listed in Table 5.18. The overall structural distortion is similar to that seen in the Si-terminated case. The major structural change caused by the O atom insertion is the 0.8Å increase in the atom 1-2 separation. This has the effect of opening up the surface bilayer ring, which will help additional O atoms impinging on the surface penetrate deeper and react with subsurface atoms. Figures 5.37, 5.38, 5.39, and 5.40 show comparisons of the *ab initio* and MIMOMM (4 bilayer) optimized geometries of the C-O-Si ring insertion site on the C-terminated SiC(111) surface. (Figures 5.39 and 5.40 are different views of the structures shown in Figures 5.37 and 5.38.) As we've seen in previous cases, the MIMOMM optimization reduces the overall distortion of the cluster. C-O-Si ring insertion is predicted to be the lowest energy O atom adsorption site on the C-terminated SiC(111) surface, unlike the Si-terminated surface, and should play a more important role in the oxidation of the C-terminated surface.

	$C_9Si_{13}H_{25}$ *Ab Initio*	$C_9C_{13}H_{25}O$ *Ab Initio*	$C_9Si_{13}H_{25}O$ MIMOMM 4 Bilayer
Dist (Å)			
1 2	3.151	3.848	3.706
1 4	1.876	1.886	1.852
1 7	1.871	1.878	1.862
1 9	3.661	4.048	3.945
1 48	-	1.378	1.361
8 48	-	1.655	1.647
Angle (°)			
7 1 48	-	119.677	119.985
1 48 8	-	128.014	119.977
48 8 2	-	113.372	106.389
8 2 9	114.316	116.235	114.479
2 9 3	114.795	117.994	118.194
9 3 7	114.316	120.988	118.563
3 7 1	114.795	117.856	116.783

Table 5.18 Comparison of *ab initio* and MIMOMM optimized (^{4}ROHF 6-31G*) C-terminated SiC(111) cluster geometry with an O atom adsorbed at a C-O-Si ring insertion site. Atom 48 is the adsorbed O atom. The bare cluster results are listed for comparison.

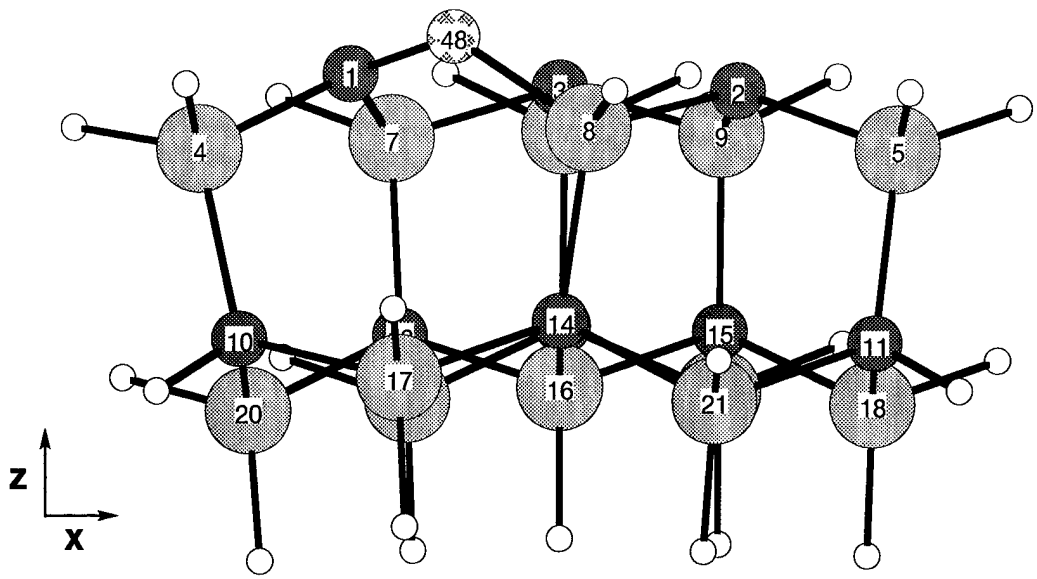

Figure 5.37 *Ab initio* optimized ^{4}ROHF (6-31G*) geometry of C-O-Si ring insertion site, C-terminated SiC(111) surface.

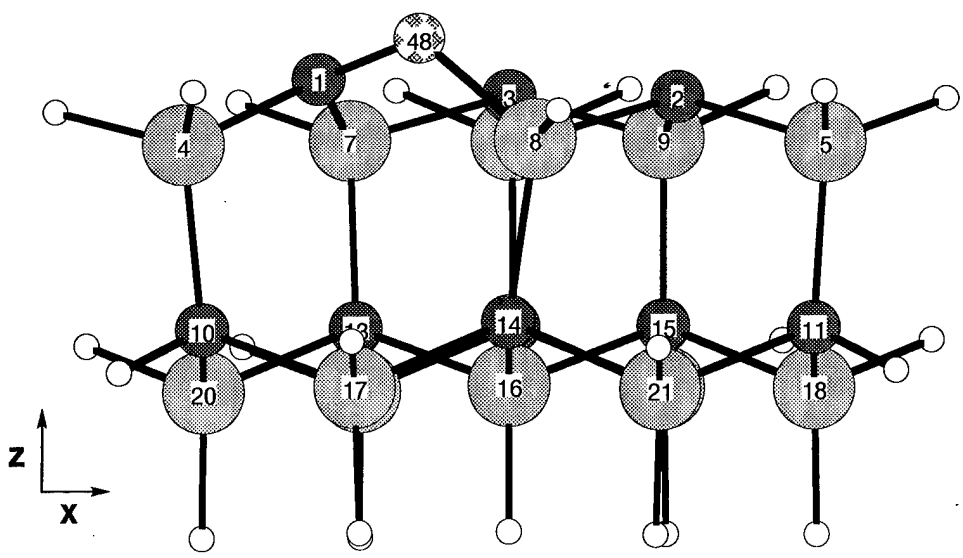

Figure 5.38 IMOMM optimized ^{4}ROHF (6-31G*/4 bilayer BC) geometry of C-O-Si ring insertion site, C-terminated SiC(111) surface, XZ view

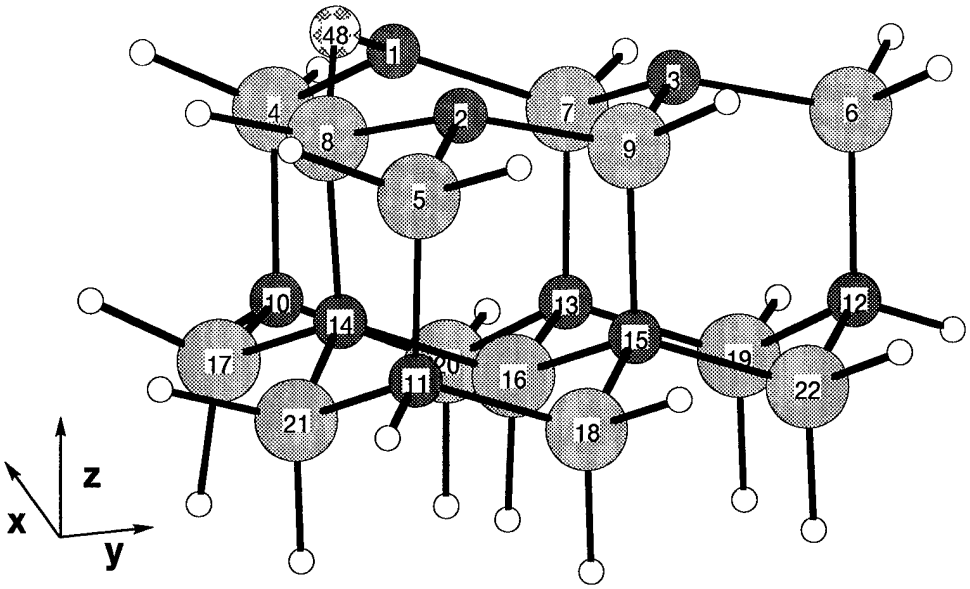

Figure 5.39 *Ab initio* optimized ^{4}ROHF (6-31G*) geometry of C-O-Si ring insertion site, C-terminated SiC(111) surface, YZ view

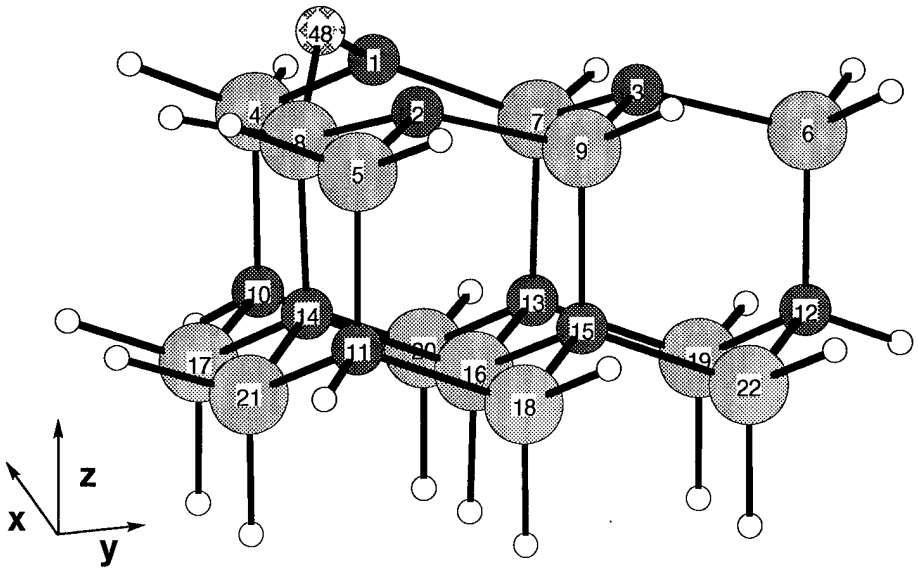

Figure 5.40 IMOMM optimized ^{4}ROHF (6-31G*/4 bilayer BC) geometry of C-O-Si ring insertion site, C-terminated SiC(111) surface, YZ view

5.9.4 O-C-O-Si Ontop and Ring Insertion: Structure. Figure 5.41 shows the *ab initio* optimized geometry of the C-terminated SiC(111) cluster with two O atoms adsorbed. This structure was obtained by starting with the optimized geometry of the C-terminated cluster with one O atom adsorbed into a ring site (between C atom 1 and Si atom 8), and placing a second O atom 1.3Å above C atom 1. This starting point was selected to bias the optimized geometry towards C atom 1 being bonded to both O atoms because this configuration is a logical intermediate state for etching of C atoms via CO_2 elimination. We see that addition of the O atom to an ontop adsorption site causes some additional distortion in the cluster geometry. We see that the C1-Si4 and C1-Si7 bond lengths are elongated by approximately 0.06Å after addition of the second O atom, and that the angle 1-O_{ring}-8 has increased by 11°. These changes are very steps in the direction of the geometry changes that would be required for the desorption of CO_2; however, these changes are too small to support any such conclusions.

	$C_9Si_{13}H_{25}$ *Ab Initio*	C-O_{ring}-Si *Ab Initio*	O_{ontop}C-O_{ring}-Si *Ab Initio*
Dist (Å)			
1 O_{ontop}	-	-	1.334
1 O_{ring}	-	1.378	1.417
1 4	1.876	1.886	1.943
1 7	1.871	1.879	1.944
8 O_{ring}	-	1.655	1.636
2 8	1.871	1.875	1.895
3 7	1.871	1.875	1.872
Angle (°)			
O_{ontop}-1-O_{ring}	-	-	110.706
O_{ontop}-1-4	-	-	108.561
O_{ontop}-1-7	-	-	105.923
1-O_{ring}-8	-	128.015	139.135
O_{ring}-8-2	-	113.372	115.056
2-9-3	114.796	117.994	117.904
3-7-1	114.796	117.856	115.505
7-1-O_{ring}	-	128.014	115.089

Table 5.19 Comparison of C-terminated SiC(111) cluster *ab initio* optimized geometry (6-31G*) with 0, 1, and 2 O atoms adsorbed.

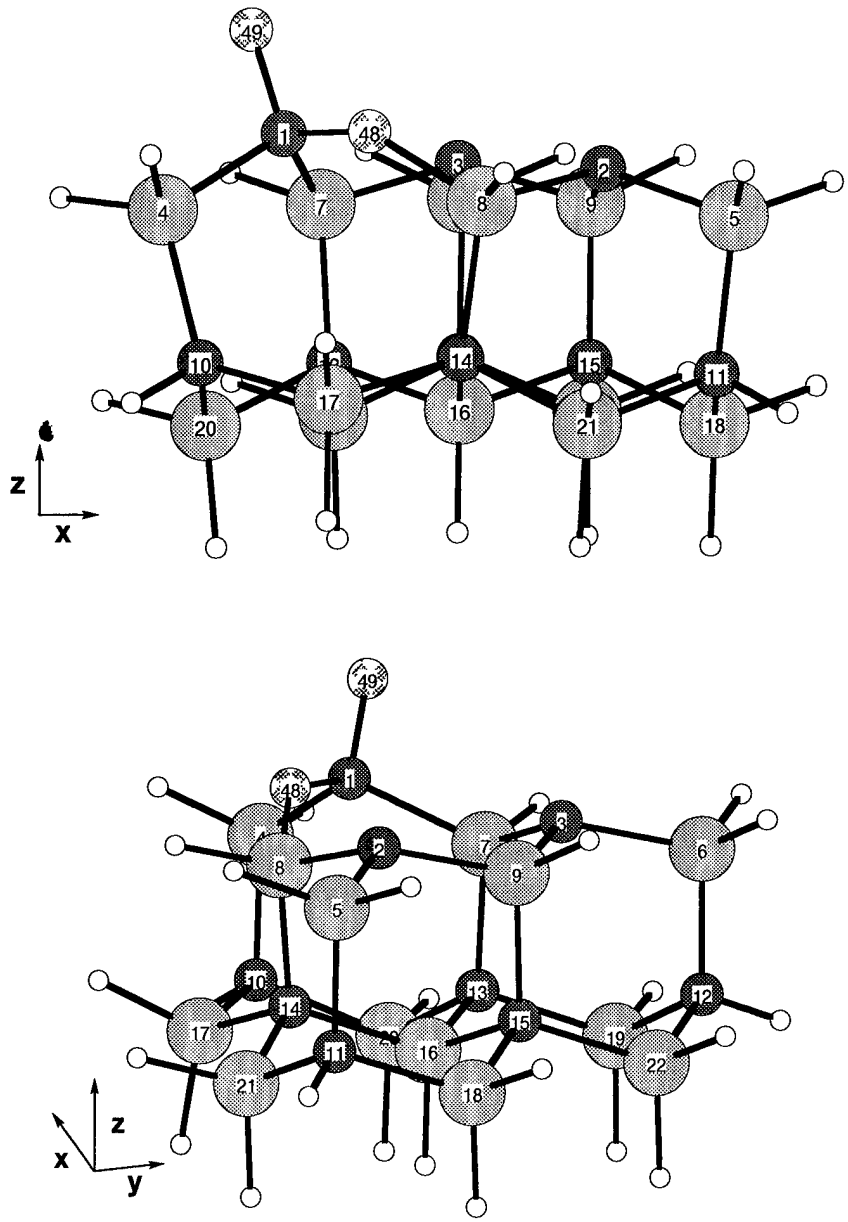

Figure 5.41 *Ab initio* optimized (^{4}ROHF 6-31G*) geometry of C-terminated SiC(111) cluster with two O atoms adsorbed, ontop and ring insertion. Addition of O at an ontop site causes no additional distortion to the cluster with an O atom adsorbed at a ring site.

5.9.5 Comparison of Adsorption Site Energetics. The behavior of Si and C-terminated SiC(111) clusters in the reconstruction and H atom adsorption calculations was very similar, both in the optimized geometries and relative energies. For O atom adsorption, we've seen that the the optimized geometries of the Si and C-terminated clusters are also quite similar. However, we shall now see that the adsorption energies of the different adsorption sites are rather different.

Before comparing O atom adsorption on the Si and C-terminated clusters, we need to emphasize the importance of electron correlation in predicting adsorption energies. Table 5.20 lists the Hartree-Fock *ab initio* and MIMOMM optimized energies of the C-terminated SiC(111) with an O atom adsorbed at ontop, bridge, and ring sites, as well as the MP2 energies calculated at the Hartree-Fock optimized geometries. Table 5.21 lists the Hartree-Fock and MP2 oxidation energies for these three sites. Immediately obvious in Table 5.21 is the significance of including electron correlation. The Hartree-Fock MIMOMM 4 bilayer binding energy involved in creating a bridge adsorption site is *positive*, which implies that this site would not form. However, the MP2 binding energy of this adsorption site is rather large and negative. The C-O bondlengths in this adsorption geometry are much larger than typical gas phase (unconstrained) C-O bondlengths, so it is not too surprising that a Hartree-Fock description of the C-O-C bridge site is so poor.

On the Si-terminated SiC(111) surface, Si-O-Si bridge site formation produced the largest binding energy, followed by ontop site formation, then ring insertion. On the C-terminated SiC(111) surface, O atom ring insertion produces that largest binding energy, followed by the C-O-C bridge, then O-C ontop adsorption. This is interesting because O atom ring insertion is a more likely first step in the formation of a CO_2 gas phase precursor, i.e., is more likely to lead towards C atom etching than bridge site formation. The binding energy of a 2 O atom adsorption structure that is a likely CO_2 gas phase precursor is also listed in Table 5.21. The energetics of C atom etching via this precursor will be discussed in Section 5.12.

Surface	Model	6-31G* Hartree-Fock Energy (H)		
		Ab Initio	MIMOMM 2 Bilayer	MIMOMM 4 Bilayer
C-terminated ($C_9Si_{13}H_{25}$)				
Bare	^{4}ROHF	-4111.394766	-4111.393840	-4111.393770
O-C ontop	^{4}ROHF	-4186.238773	-4186.237856	a
C-O-C bridge	^{2}ROHF	-4186.189023	-4186.175370	-4186.163413
C-O-Si ring	^{4}ROHF	-4186.266287	b	-4186.255885
O_{ontop}-C-O_{ring}-Si	^{4}ROHF	-4261.127424	c	c
C-O-Si ring	^{2}ROHF	-4186.216075	b	-4186.201713
C-O-Si ring	^{2}GVB	-4186.216087	^{2}ROHF orbitals	
O Atom	^{3}ROHF	-74.778966		

Surface	Model	6-31G* MP2 Energy (H)		
		Ab Initio	MIMOMM 2 Bilayer	MIMOMM 4 Bilayer
C-terminated ($C_9Si_{13}H_{25}$)				
Bare	^{4}ROHF	-4113.591320	-4113.590790	-4113.590379
O-C ontop	^{4}ROHF	-4188.605864	-4188.605138	a
C-O-C bridge	^{2}ROHF	-4188.632281	-4188.621922	-4188.611703
C-O-Si ring	^{4}ROHF	-4188.641555	b	-4188.631201
O_{ontop}-C-O_{ring}-Si	^{4}ROHF	-4263.674058	c	c
O Atom	^{3}ROHF	-74.879847		

a Not calculated because minimal strutural change means bulk cluster has minor effect on energy

b Not calculated because 4 bilayer BC determined better

c Not calculated because MIMOMM effect on energy could be reliably estimated

Table 5.20 6-31G* energies of C-terminated SiC clusters used in calculating energy of oxidation. (The 6-31G* energy for O atom is -74.778966 H.)

					Ab Initio	IMOMM 2 Bilayer	MIMOMM 4 Bilayer
					Hartree-Fock Δ E (kcal/mol)		
($C_9Si_{13}H_{25}$)	+	O	→	($C_9Si_{13}H_{25}$)O ontop	-40.8	-40.8	-
($C_9Si_{13}H_{25}$)	+	O	→	($C_9Si_{13}H_{25}$)O bridge	-9.6	-1.7	**+5.8**
($C_9Si_{13}H_{25}$)	+	O	→	($C_9Si_{13}H_{25}$)O ring	-58.1	-	-52.2
($C_9Si_{13}H_{25}$)	+	2O	→	($C_9Si_{13}H_{25}$)O_2 ontop & ring	-109.0	-	-
					MP2 Δ E (kcal/mol)		
($C_9Si_{13}H_{25}$)	+	O	→	($C_9Si_{13}H_{25}$)O ontop	-84.5	-84.5	-
($C_9Si_{13}H_{25}$)	+	O	→	($C_9Si_{13}H_{25}$)O bridge	-101.1	-94.9	-88.8
($C_9Si_{13}H_{25}$)	+	O	→	($C_9Si_{13}H_{25}$)O ring	-106.9	-	-101.0
($C_9Si_{13}H_{25}$)	+	2O	→	($C_9Si_{13}H_{25}$)O_2 ontop & ring	-202.7	-	-

Table 5.21 Comparison of energy of oxidation,C-terminated SiC(111) surface

5.10 Surface Vacancies

5.10.1 Si Vacancy at the Si-terminated SiC(111) Surface: Structure. The Si atom vacancy in the Si-terminated SiC(111) surface was modeled by removing Si atom 1 and optimizing the remaining cluster in a ^{4}ROHF configuration. Removing Si atom 1 breaks 3 SiC bonds and leaves C atoms 7, 8, and 4 with dangling bonds. The ^{4}ROHF configuration should favor bond formation between atoms 7 and 8. This is a reasonable choice for the C vacancy case (in which atoms 7 and 8 are silicons) discussed in the next section, and was used here for consistency. The initial separation between C atoms 7 and 8 is 3.14 $\AA$. This separation is too large to permit the formation of a C-C bond when the energy required to deform the cluster to enable these atoms move close enough to each other to bond is considered. This result is a consequence of the small size of the single occupied carbon orbitals compared to the lattice dimensions. Instead, Si atom 3 is observed to move 0.27 $\AA$ down along the Z axis, and the Si3-C7 bond length decreases from 1.9$\AA$ to 1.73$\AA$, i.e., the Si-C bonding has strengthened. C atom 4 has been displaced 0.66$\AA$ away from its initial position. (Atom displacements and selected internal coordinates from both cases are listed in Tables 5.22 and 5.23.) Because of the relatively minor differences between the *ab initio* and MIMOMM optimized structures, MIMOMM raises the energy for creation of a Si vacancy by only 4 $\frac{kcal}{mol}$.

The *ab initio* optimized energy for the ^{2}ROHF reconstruction around a Si vacancy was found to be 22 $\frac{kcal}{mol}$ higher in energy than the ^{4}ROHF. A ^{2}ROHF MIMOMM optimization was not performed because this was not the minimum energy reconstruction. The *ab initio* ^{2}ROHF optimized geometry is shown in Figure 5.44. In this solution, we see that *both* Si atoms 2 and 3 have sunk down along the Z axis, and the Si-C bond lengths around these Si atoms have decreased. Even the doublet spin configuration does not force bond formation between C atoms 2 and 3.

One feature of these results that should be highlighted is that the H atoms bonded to C atom 4 no longer point in lattice directions. Those H atoms belong to Region 5, so there are no constraints on their optimized geometry. This discrepancy arises because this EC is really too small to model vacancies. Ideally, all the atoms around the vacancy should be at least one bond away from a terminating H atom. Linking the EC and BC

using Morokuma's Region 2-Region 3 scheme could force the bond directions of these H atoms to be correct, but would not correct the termination problem.

5.10.2 C Vacancy in the C-terminated SiC(111) Surface. The C atom vacancy in the C-terminated SiC(111) surface was modeled by removing C atom 1 and optimizing the remaining cluster in a ^{4}ROHF configuration. Removing C atom 1 breaks 3 SiC bonds and leaves Si atoms 7, 8, and 4 with dangling bonds. The ^{4}ROHF configuration favors bonding between atoms 7 and 8, leaving three undercoordinated atoms, 4, 2, and 3, in the cluster. Figures 5.45 and 5.46 show the *ab initio* and MIMOMM (4 bilayer) optimized geometries for the C-terminated EC with a C vacancy. In both cases Si atoms 7 and 8 on either side of the vacancy have bonded, forming a 5 membered ring in the surface bilayer. This is very different from the ^{4}ROHF reconstruction observed around the Si vacancy. The dangling bond orbitals are large enough for a bond to form even though Si atoms 7 and 8 are initially separated by 3.1$\AA$. In the *ab initio* optimized result, Si atom 4 has moved 0.95$\AA$ away from its initial position. The bottom layer silicon atoms, 17-22, are seen to have been displaced by as much as 0.19$\AA$ along the Z axis in response the the reconstruction around the C vacancy. (Atom displacements and selected internal coordinates from both cases are listed in Tables 5.24 and 5.25.)

As we've seen before, the addition of the steric forces from the 4 bilayer BC in the MIMOMM optimized result greatly reduces the observed atom displacements. The displacement of Si atoms 7 and 8 have not changed much in the MIMOMM optimized result, as the steric forces of the BC have no direct effect on these atoms. However, the displacement of Si atom 4 has been reduced to 0.26$\AA$, and Si atoms 17-22 scarcely budge from their original positions. The displacements of C atoms 2 and 3 are also significantly reduced, because the atoms in the BC impose steric constraints on Si atoms 5 and 6. This force on Si atoms 5 and 6 means that C atoms 2 and 3 cannot drag them around unhindered, reducing the displacements of C atoms 2 and 3.

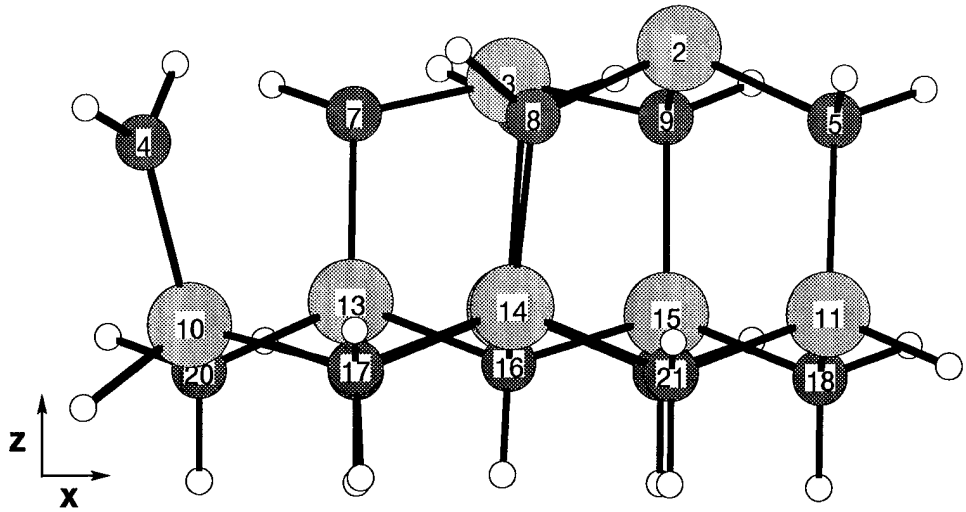

Figure 5.42 Si-terminated SiC(111) EC with a Si vacancy, *ab initio* ^{4}ROHF optimized geometry. Si atom 3 has moved down 0.27 $\AA$ along the Z axis, and the separation between Si 3 and C 7 has shortened by 0.17 $\AA$. Atom C4 has moved away from the surface bilayer, but the overall distortion of the EC is small.

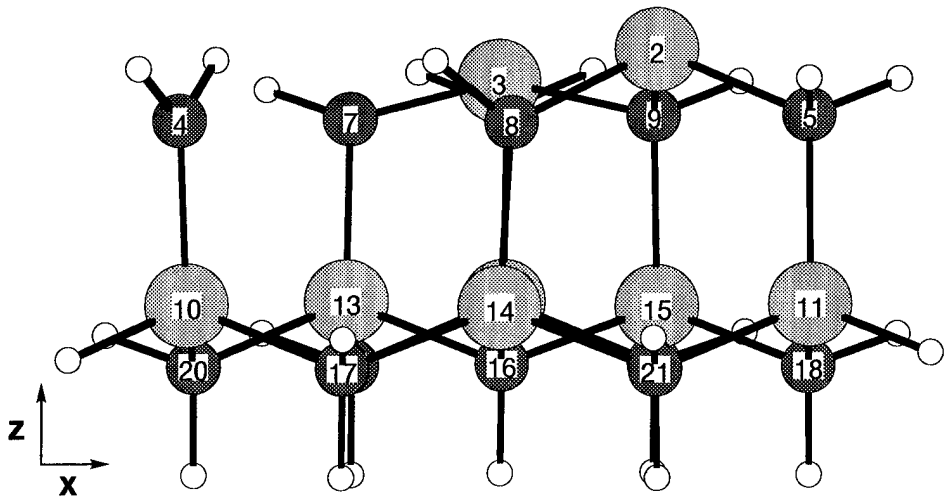

Figure 5.43 Si-terminated SiC(111) EC with a Si vacancy, MIMOMM ^{4}ROHF optimized geometry, 4 bilayer bulk cluster. MIMOMM significantly reduces the displacement of C atom 4. The effect on C8 is smaller but also noticeable.

Atom Displacements (Å) Caused by Si Vacancy						
Atom	*Ab Initio*			IMOMM: 4 Bilayer		
	δ x	δ y	δ z	δ x	δ y	δ z
1	-	-	-	-	-	-
2	**0.114**	0.006	0.034	0.013	-0.014	0.041
3	-0.023	-0.0369	**-0.274**	-0.042	-0.030	**-0.270**
4	**-0.537**	**-0.335**	**-0.203**	**-0.117**	-0.078	-0.017
5	**0.134**	0.089	-0.023	0.017	0.002	0.020
6	**0.125**	0.010	**0.102**	0.023	0.013	**0.111**
7	-0.029	**0.186**	0.042	-0.002	**0.130**	0.006
8	**0.229**	-0.096	0.008	**0.119**	-0.047	0.043
9	0.029	0.002	-0.007	0.008	-0.002	0.022
10	-0.049	-0.088	-0.099	-0.016	-0.006	0.022
11	0.041	0.020	-0.026	0.003	0.001	0.013
12	-0.014	-0.015	0.044	-0.008	0.008	0.051
13	-0.021	-0.052	**0.111**	-0.006	-0.021	0.060
14	0.024	-0.052	0.049	-0.006	-0.013	-0.004
15	-0.006	-0.029	-0.034	0.005	-0.012	-0.001
16	-0.016	-0.043	0.063	0.004	-0.001	0.018
17	0.031	-0.063	0.074	-0.006	0.005	0.002
18	0.003	0.012	-0.049	0.011	0.007	0.018
19	-0.001	-0.041	0.030	-0.002	0.010	0.034
20	0.005	-0.046	0.051	-0.001	-0.003	0.030
21	0.040	0.003	-0.004	0.009	0.005	-0.007
22	-0.026	-0.011	0.006	-0.002	0.010	0.048

Table 5.22 Atom displacements induced by a Si atom vacancy at the Si-terminated SiC(111) surface.

	$Si_9C_{13}H_{25}$ No Vacancy	$Si_8C_{13}H_{25}$ *Ab Initio*	$Si_8C_{13}H_{25}$ MIMOMM 4 Bilayer
Dist (Å)			
3 7	1.903	1.723	1.719
4 7	3.120	3.841	3.357
7 8	3.062	3.437	3.273
Angle (°)			
3 7 8	91.277	83.648	87.097
7 8 2	91.277	87.888	88.752
8 2 9	107.174	107.666	107.367
Torsion(°)			
5 11 4 10	179.999	170.213	-177.648
10 11 12 14	0.248	2.568	0.514
20 18 22 17	0.000	0.820	0.002

Table 5.23 Comparison of *ab initio* and MIMOMM optimized geometries of Si-terminated cluster with a Si surface vacancy. The results for the Si-terminated cluster without the vacancy are listed for comparison.

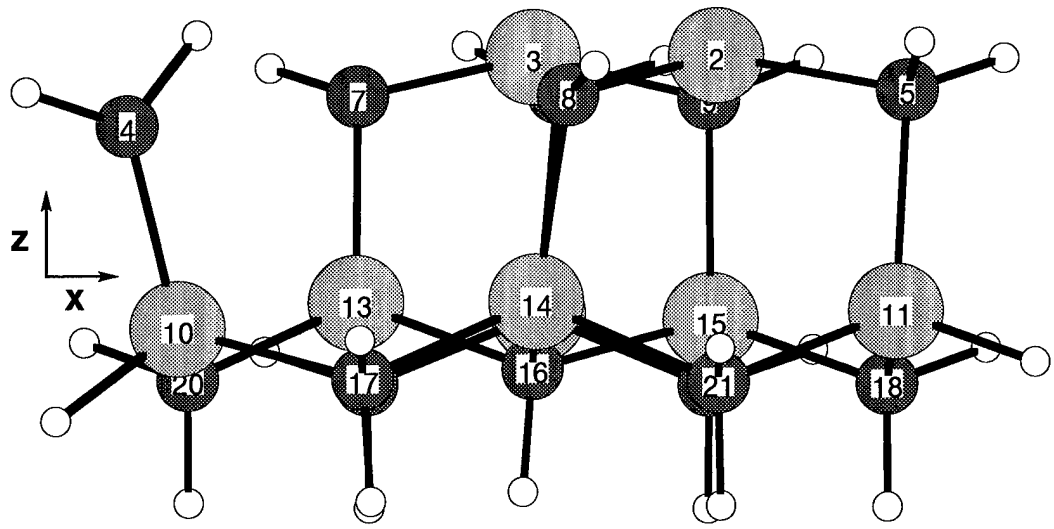

Figure 5.44 Si-terminated SiC(111) EC with a Si vacancy, ^{2}ROHF *ab initio* optimized geometry.

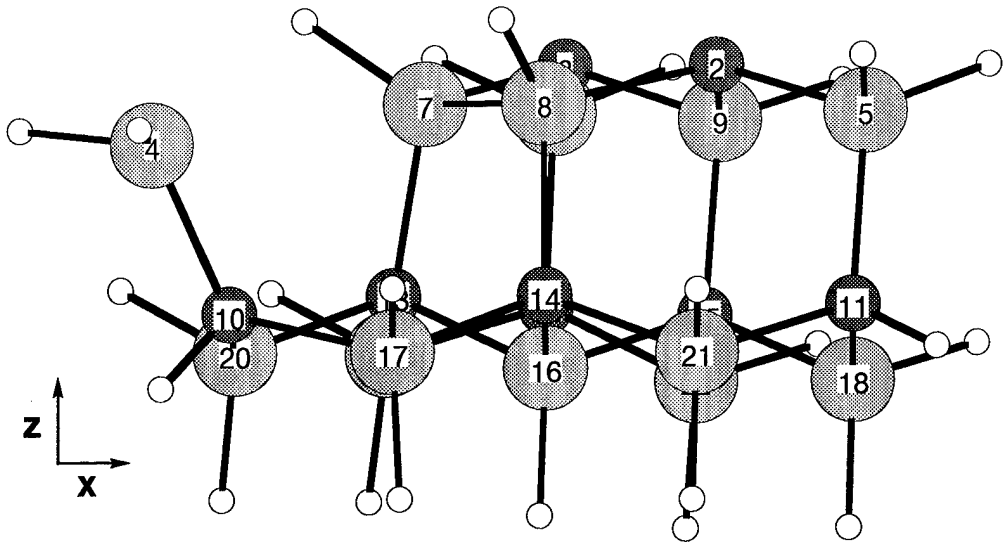

Figure 5.45 C-terminated SiC(111) EC with a C vacancy, *ab initio* optimized geometry (6-31G* basis set). Si atoms 7 and 8, which had been bonded to C atom 1 that was removed, have now moved significantly from their original positions and bonded to each other, causing distortions in the bottom bilayer. Si atom 4 has moved away from the surface bilayer.

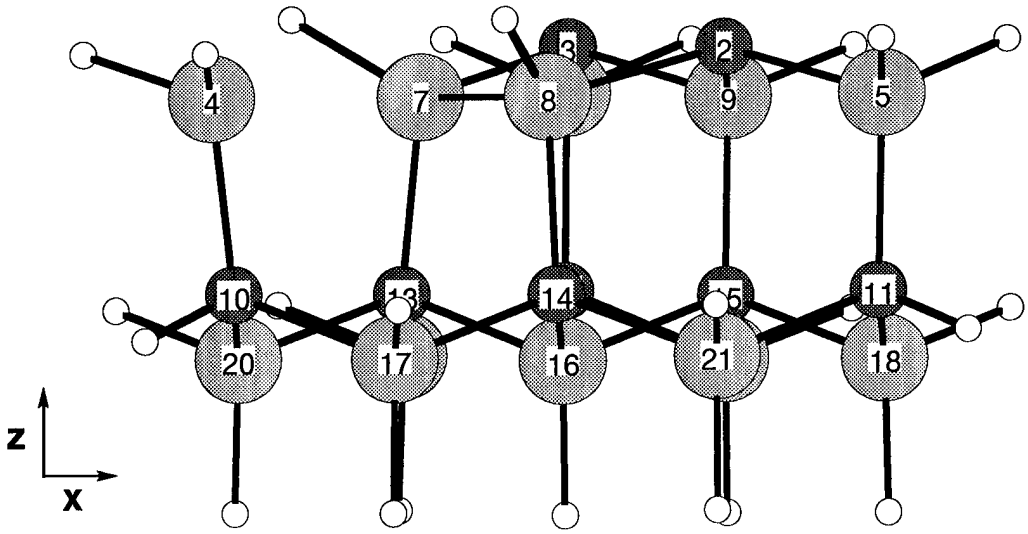

Figure 5.46 C-terminated SiC(111) EC with a C vacancy, MIMOMM optimized geometry, 4 bilayer bulk cluster (6-31G* basis set). As in the *ab initio* case, Si atoms 7 and 8 have bonded. However, the steric constraints of the BC have greatly reduced the displacement of Si atom 4. The overall distortion in the cluster is visibly reduced as well.

Atom Displacements (Å) Caused by C Vacancy						
Atom	*Ab Initio*			IMOMM: 4 Bilayer		
	δ x	δ y	δ z	δ x	δ y	δ z
1	-	-	-	-	-	-
2	**0.186**	**0.167**	0.014	0.011	0.048	0.006
3	**0.229**	0.095	0.004	0.046	-0.017	0.006
4	**-0.780**	**-0.438**	**-0.312**	**-0.231**	**-0.133**	-0.033
5	**0.118**	0.077	0.010	-0.010	0.031	-0.012
6	**0.121**	0.078	-0.009	0.020	-0.026	-0.012
7	**0.392**	**-0.193**	0.080	**0.185**	**-0.249**	0.022
8	0.019	**0.452**	0.087	**-0.116**	**0.285**	0.022
9	**0.226**	**0.139**	-0.085	0.055	0.031	0.019
10	-0.040	-0.018	-0.080	-0.042	-0.026	-0.018
11	0.038	0.021	0.014	-0.010	0.018	0.012
12	0.038	0.027	-0.005	0.008	-0.019	0.012
13	0.082	-0.008	0.114	0.020	-0.046	-0.008
14	0.029	0.080	0.124	-0.026	0.039	-0.009
15	0.067	0.040	-0.082	0.020	0.011	-0.017
16	0.041	0.024	-0.004	0.021	0.011	-0.036
17	0.057	0.004	**0.187**	-0.017	0.014	-0.005
18	0.026	-0.018	-0.098	0.016	0.008	-0.003
19	-0.005	0.006	**0.163**	0.010	-0.035	0.025
20	0.031	0.052	**0.178**	0.004	-0.025	-0.005
21	-0.001	-0.007	**0.182**	-0.022	0.026	0.025
22	-0.000	0.031	**-0.109**	0.014	0.009	-0.003

Table 5.24 Atom displacements induced by a C atom vacancy at the C-terminated SiC(111) surface.

	$C_9Si_{13}H_{25}$ No Vacancy	$C_8Si_{13}H_{25}$ *Ab Initio*	$C_8Si_{13}H_{25}$ MIMOMM 4 Bilayer
Dist (Å)			
3 7	1.871	1.887	1.884
4 7	3.152	4.072	3.277
7 8	3.143	2.398	2.500
Angle (°)			
3 7 8	90.130	100.214	98.647
7 8 2	90.130	100.214	98.653
8 2 9	114.315	105.976	105.573
Torsion(°)			
5 11 4 10	179.999	164.263	-176.232
10 11 12 14	-0.311	3.009	0.390
20 18 22 17	0.000	0.243	0.000

Table 5.25 Comparison of *ab initio* and MIMOMM optimized geometries of C-terminated cluster with a C surface vacancy (6-31G* basis set).

5.10.3 Comparison of Surface Vacancy Energetics. To determine the likelihood of etching of the SiC(111) during the oxidation process, the energies of the clusters with one Si or C atom removed must also be calculated. Creation of a surface vacancy is likely to cause substantial reconstruction within the cluster, so the use of MIMOMM will likely be required to obtain physically realistic results. Table 5.26 lists the Hartree-Fock and MP2 energies for single atom vacancies (atom 1 has been removed, see Figure 5.42) on the Si and C-terminated clusters. Table 5.27 lists the Hartree-Fock and MP2 energies required to remove an Si or C atom from these clusters. As was seen in previous results, the MIMOMM optimized results are higher in energy than the *ab initio* optimized results. The MP2 vacancy creation energies are larger than the Hartree-Fock energies, showing the importance of including electron correlation. ^{2}ROHF Hartree-Fock MIMOMM optimizations and MP2 energies were not calculated because the ^{2}ROHF *ab initio* Hartree-Fock optimized energy was signficantly higher in energy than the ^{4}ROHF Hatree-Fock results.

One note of caution about the results presented in this section is that the ECs used in this research were not designed to model surface vacancies. As a result, one of the Si (C) atoms around the C (Si) vacancy is bonded to 2 H atoms, violating the requirement that the EC atoms involved in a reaction be at least one bond length away from a terminating H atom. However, a vacancy in this EC must be used for consistent comparisons with the other results described in this chapter.

5.11 Silicon (111) Surface Calculations

The primary interest in this investigation is the oxidation of Si and C-terminated surfaces of SiC(111). However, SiC, bulk silicon, and diamond are all tetrahedrally bonded crystals. In order to adapt the embedded cluster used for SiC(111) for Si(111) or diamond(111), one merely needs to change the atom spacings in the SiC EC based on a Si-C separation of 1.89$\AA$ to 2.35$\AA$ for silicon or 1.54$\AA$ for diamond. Oxidation of the silicon surface has been investigated by numerous researchers, so comparisons of the Si(111) surface and the Si-terminated SiC(111) surface will help to extend the understanding of the oxidation of silicon to SiC. Comparisons of the C-terminated SiC surface and the diamond(111) surface would be less useful because there is considerable evidence that the "real" diamond

Surface Vacancy			
		6-31G* Hartree-Fock Energy (H)	
		Ab Initio	MIMOMM
Molecule	Model		4 Bilayer
$(Si_9C_{13}H_{25})$	^{4}ROHF	-3107.287434	-3107.286685
$(Si_8C_{13}H_{25})$	^{4}ROHF	-2818.200471	-2818.193653
$(Si_8C_{13}H_{25})$	^{2}ROHF	-2818.165306	-
Si	^{3}ROHF	-288.829374	
$(C_9Si_{13}H_{25})$	^{4}ROHF	-4111.394766	-4111.393770
$(C_8Si_{13}H_{25})$	^{4}ROHF	-4073.482303	-4073.464211
C	^{3}ROHF	-37.677126	-

		6-31G* MP2 Energy (H)	
		Ab Initio	MIMOMM
Molecule	Model		4 Bilayer
$(Si_9C_{13}H_{25})$	^{4}ROHF	-3109.704721	-3109.704136
$(Si_8C_{13}H_{25})$	^{4}ROHF	-2820.514745	-2820.512337
Si	^{3}ROHF	-288.874528	
$(C_9Si_{13}H_{25})$	^{4}ROHF	-4113.591320	-4113.590379
$(C_8Si_{13}H_{25})$	^{2}ROHF	-4074.561578	-4075.553303
C	^{3}ROHF	-37.732769	-

Table 5.26 Surface vacancy energies, Si and C-terminated SiC(111) clusters.

					ab initio	MIMOMM 4 Bilayer
					Hartree-FockΔ E $(\frac{kcal}{mole})$	
$(Si_9C_{13}H_{25})$	$\rightarrow$	$(Si_8C_{13}H_{25})$	+	Si	+161.6	+165.4
$(C_9Si_{13}H_{25})$	$\rightarrow$	$(C_8Si_{13}H_{25})$	+	C	+147.7	+158.4
					MP2 Δ E $(\frac{kcal}{mole})$	
$(Si_9C_{13}H_{25})$	$\rightarrow$	$(Si_8C_{13}H_{25})$	+	Si	+197.9	+199.1
$(C_9Si_{13}H_{25})$	$\rightarrow$	$(C_8Si_{13}H_{25})$	+	C	+186.4	+191.0

Table 5.27 Comparison of ^{4}ROHF energy of vacancy creation, Si and C-terminated SiC(111) clusters.

surface is largely graphitic [129, 130, 131]. The embedded cluster used in this study is too small to give an acceptable representation of a graphitic surface, so modeling of the diamond(111) surface was not performed.

5.11.1 Hybrid Cluster for Si(111). The embedded cluster for Si(111) has the same configuration as the SiC(111) ECs; however, the difference in bondlength between the two materials has an interesting effect on the lattice structure. Figure 5.48 shows a comparison of the Si-terminated SiC(111) embedded cluster with the Si(111) EC. This figure highlights the effect of the bondlength difference between SiC and silicon. Nearest neighbor Si atoms on the SiC(111) surface are 3.08$\AA$ apart, but 3.84$\AA$ apart on the Si(111) surface.

The bulk cluster for Si(111) is shown in Figure 5.47, with the EC atoms highlighted. A three bilayer BC for silicon was chosen for several reasons. First, the importance of including steric forces on the bottom of the EC was demonstrated by the SiC results. Second, bulk Si(111) has a 3C stacking sequence (see Figure 5.3), so one needs at least three bilayers in the BC to match the experimental structure. Since the silicon lattice is not as stiff as SiC, one might suspect that a larger BC would be needed to give an accurate representation of the steric environment of bulk silicon. However, using a 3 bilayer BC provides an additional data point for bulk cluster design guidance.

Before performing any calculations, what predictions can we make about potential differences between the Si-terminated SiC(111) and Si(111) surface? H atom adsorption on SiC was seen to cause minimal structural changes, so it seems reasonable that H atom adsorption on Si(111) will be similarly "uninteresting". The binding energy per H atom may be different because Si and SiC are different materials. For O atom reactions, adsorption at on ontop site caused minimal distortion in the SiC clusters, so one expects ontop adsorption on the Si(111) to be similar. Si-O-Si bridge formation on Si(111) will probably be less favored energetically because of the larger surface atom separation of Si(111) compared to Si-terminated SiC(111). Bridge site formation was seen to cause large distortions in the SiC(111) cluster. Because silicon is less tightly bound than SiC, one expects to see larger distortions, and perhaps larger differences between the *ab initio* and MIMOMM

calculations. O atom insertion into the puckered Si surface ring may occur more easily because of Si(111)'s larger lattice spacing. Adsorption of two O atoms on Si(111) should be similar to adsorption of two O atoms on Si-terminated SiC(111). It is unclear how the relative binding energies of the different adsorption sites on Si(111) will compare to Si-terminated SiC(111).

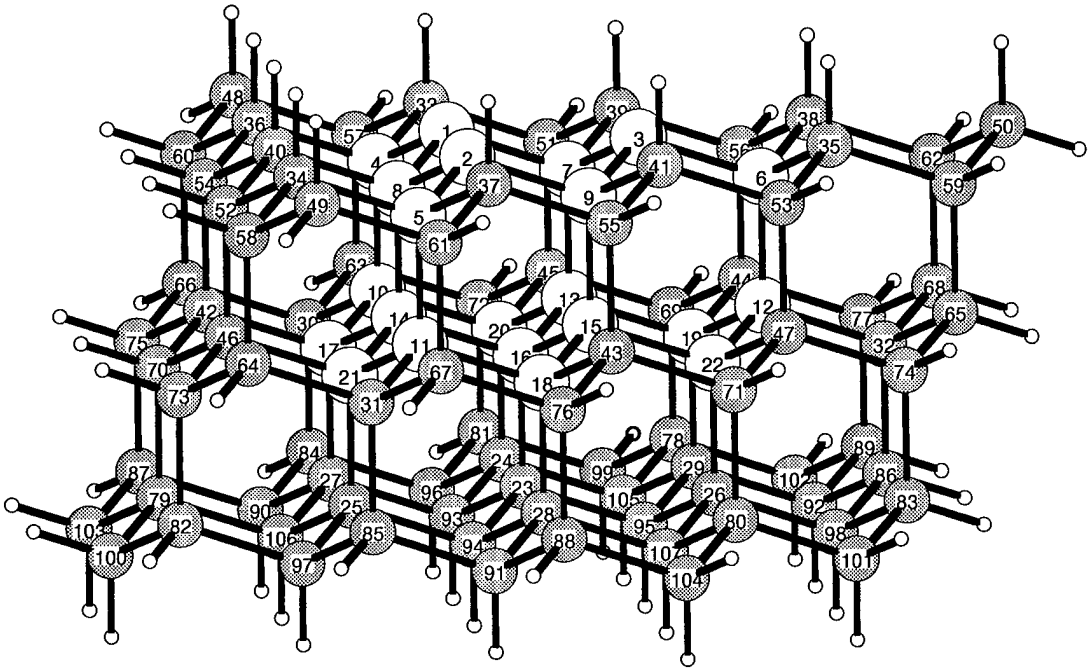

Figure 5.47 Hybrid cluster for Si(111) surface studies. EC is the same as was used for SiC(111). Three bilayer BC with 3C stacking sequence used to match bulk silicon; however, oxidation results suggest that a deeper BC may be required for silicon.

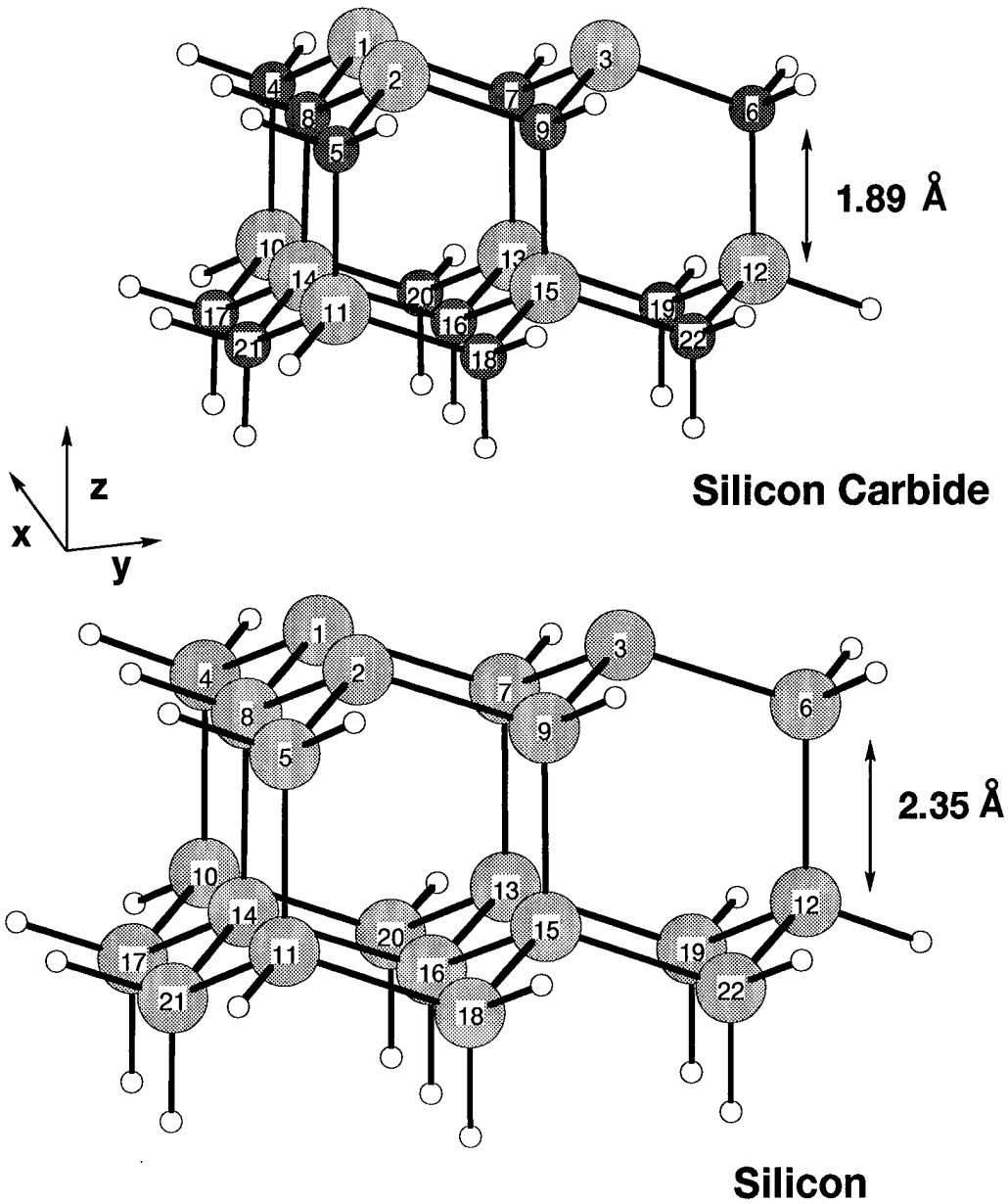

Figure 5.48 Comparison of the reconstructed (*ab initio* 6-31G* optimized) Si-terminated SiC(111) and Si(111) embedded clusters. Both figures are drawn to the same scale, highlighting the size difference of these two crystals.

5.11.2 Reconstruction of the Si(111) Surface. The reconstructed SiC(111) EC is shown in Figure 5.48. Based on experience from SiC, only a ^{4}ROHF *ab initio* optimization was performed to model surface reconstruction. The ^{4}ROHF reconstructed Si(111) surface was found to show small deviations from bulk silicon lattice structure. A comparison of bulk silicon geometry and the *ab initio* optimized (6-31G*) Si(111) cluster geometry is listed in Table 5.28.

	Bulk Silicon	$Si_{22}H_{25}$ *Ab Initio*
Dist (Å)		
1 2	3.84	3.926
1 4	2.35	2.370
1 8	2.35	2.371
4 10	2.35	2.377
5 11	2.35	2.377
7 13	2.35	2.393
8 14	2.35	2.393
Angle (°)		
1 8 2	109.47	111.835
4 1 8	109.47	110.073
8 2 9	109.47	109.621
9 3 7	109.47	109.621
Torsion(°)		
10 11 12 14	0.00	0.035
20 18 17 16	0.00	-1.288

Table 5.28 Comparison bulk silicon lattice and reconstructed (*ab initio* optimized) Si(111) cluster (6-31G* basis set).

5.11.3 Si(111) Hydrogenation Energetics. Table 5.29 lists the Hartree-Fock energetics for H atom adsorption onto the Si(111) cluster. As was seen in the SiC cases, ontop adsorption of H atoms on Si(111) causes minimal changes in cluster geometry, so these structures are not shown. The adsorption energy per H atom is also equal. The adsorption energy per H atom on the Si(111) cluster is calculated to be 10 $\frac{kcal}{mole}$ smaller than the adsorption energy on the Si-terminated SiC surface.

5.11.4 Si(111) O-Si Ontop Site Adsorption: Structure. The structure of the Si(111) cluster with an O atom adsorbed at an ontop site is shown in Figure 5.49. A

Surface	Model	6-31G* Energy (H)	
		ab initio	MIMOMM 3 Bilayer
Reconstruction			
Bare	^{4}ROHF	-6370.850792	-
Hydrogenation			
$(H\text{-}Si)_1$ ontop	^{3}ROHF	-6371.850792	-
$(H\text{-}Si)_2$ ontop	^{2}ROHF	6372.066296	-
$(H\text{-}Si)_3$ ontop	^{1}RHF	-6372.674192	-

		Adsorption Energy ($\frac{kcal}{mol}$)	
Hydrogenation			
Cluster + nH(g)	^{4}ROHF	0.0	0.0
$(H\text{-}Si)_{n=1}$	^{3}ROHF	-68.70	-
$(H\text{-}Si)_{n=2}$	^{2}ROHF	-137.45 (-68.75)	-
$(H\text{-}Si)_{n=3}$	^{1}RHF	-206.26 (-68.81)	-

Table 5.29 Hydrogenation energetics of silicon(111) cluster. As was seen for the SiC clusters, the gain in energy for the adsorption of each H atom is the same.

comparison of this structure with the bare cluster is also listed. Minimal differences in the two structures are seen.

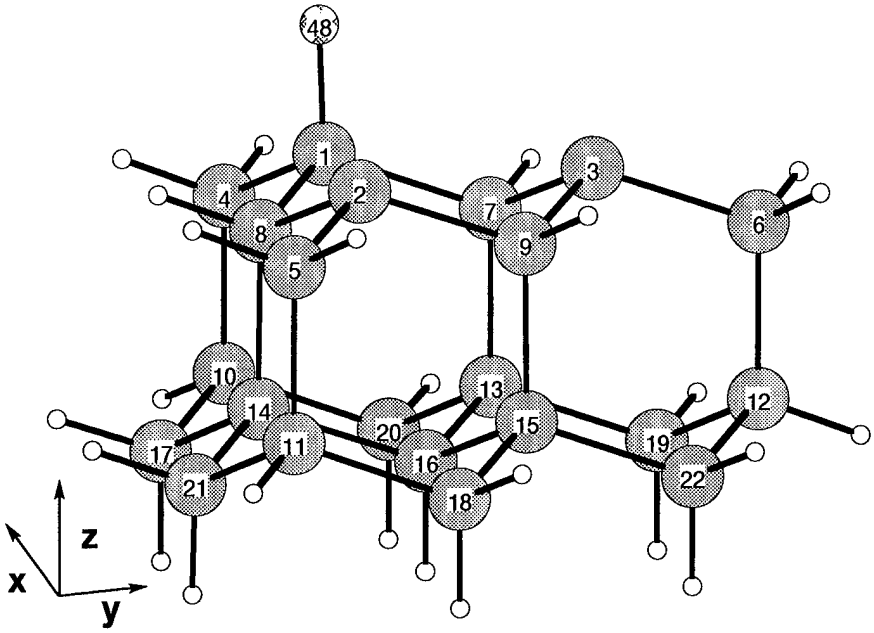

	$Si_{22}H_{25}$	$Si_{22}H_{25}O$		$Si_{22}H_{25}$	$Si_{22}H_{25}O$
	Ab Initio	*Ab Initio*		*Ab Initio*	*Ab Initio*
Dist ($\AA$)			Angle (°)		
1 O_{ads}	-	1.702	O_{ads} 1 2	-	93.700
1 2	3.927	3.929	O_{ads} 1 3	-	93.598
2 3	3.927	3.929	O_{ads} 1 8	-	110.739
3 1	3.927	3.929	7 1 8	109.621	109.107
1 9	4.564	4.568	8 2 9	109.621	109.530
1 8	2.371	2.379	9 3 7	109.621	109.533
1 7	2.371	2.379	Torsion(°)		
7 13	2.392	2.391	5 11 4 10	-179.993	-179.841
8 14	2.392	2.391	4 10 6 12	-179.993	-179.824
9 15	2.392	2.393	10 11 12 14	0.035	0.070

Figure 5.49 Comparison of *ab initio* (6-31G* basis set) optimized Si(111) cluster geometry, bare and with 1 O atom adsorbed at an ontop site. Ontop site adsorption causes small changes in cluster geometry. *This adsorption site is an AM1 saddle point.*

5.11.5 Si(111) Si-O-Si Bridge Site Adsorption: Structure. Bridge site adsorption of an O atom on the Si(111) causes the same qualitative pattern of atom displacements as was seen in the two SiC(111) surfaces. However, because of the weaker bonding in silicon, the atom displacements for the *ab initio* optimized structure are significantly larger (50%) than the corresponding displacements in the Si-terminated SiC(111) surface. The displacements in the IMOMM optimized result are again considerably reduced. The largest reductions in displacements are observed along the z-axis, again confirming the importance of including layers below the embedded cluster in the bulk cluster. A comparison of the *ab initio* and MIMOMM (3bl) optimized geometries are shown in Figures 5.50 and 5.51. The atom displacements for these two cases are listed in Table 5.31, and the internal coordinates are listed in Table 5.30.

Si-O-Si Bridge Site Si(111) Surface			
	$Si_{22}H_{25}$ *Ab Initio* None	$Si_{22}H_{25}O$ *Ab Initio* None	$Si_{22}H_{25}O$ MIMOMM 3 Bilayer
Dist (Å)			
1 O_{ads}	-	1.719	1.756
2 O_{ads}	-	1.719	1.756
1 2	3.926	2.713	2.801
1 4	2.370	2.360	2.462
1 8	2.371	2.363	2.306
4 10	2.377	2.423	2.493
5 11	2.377	2.423	2.493
7 13	2.393	2.390	2.382
8 14	2.393	2.303	2.263
Angle (°)			
1 O_{ads} 2	-	104.206	105.766
O_{ads} 1 4	-	133.809	143.855
1 8 2	111.835	71.333	74.777
4 1 8	110.073	100.234	100.226
8 2 9	109.621	113.910	118.212
9 3 7	109.621	100.071	101.875
Torsion(°)			
10 11 12 14	0.035	21.570	11.292
20 18 17 16	-1.288	-18.211	-6.749

Table 5.30 Comparison of *ab initio* and MIMOMM optimized Si(111) cluster geometry with 1 O atom adsorbed onto an *bridge* site. The bare cluster results are listed for comparison. 6-31G* basis set used in all calculations.

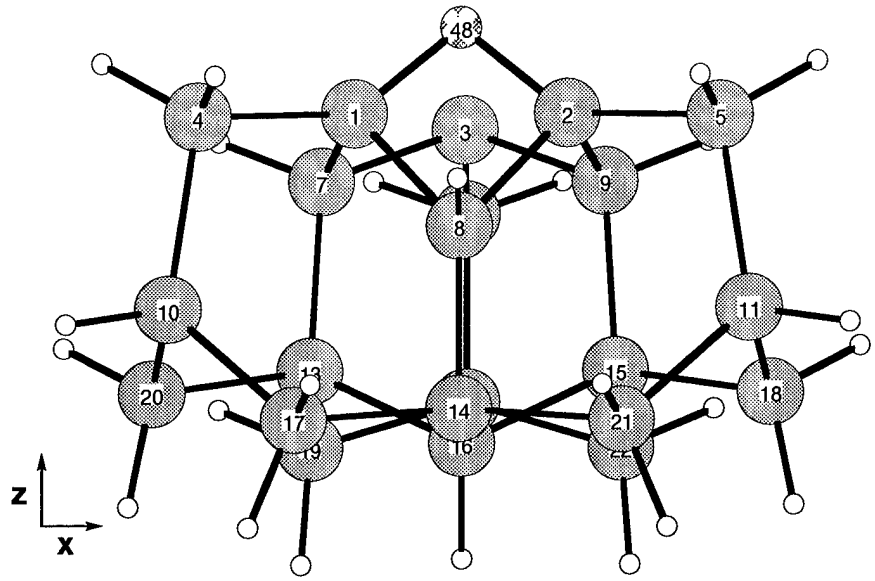

Figure 5.50 *Ab initio* optimized ^{4}ROHF (6-31G*) geometry of Si-O-Si bridge, Si(111) surface.

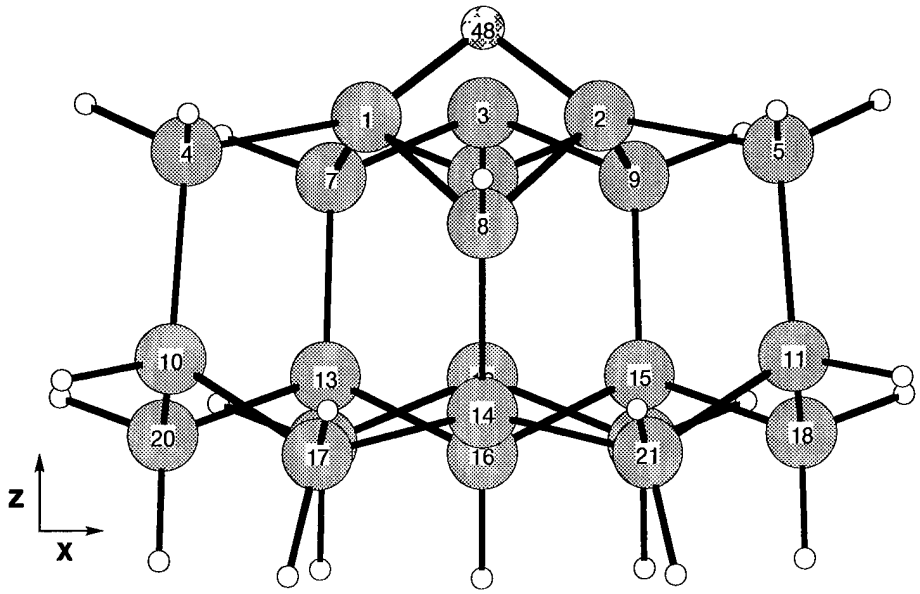

Figure 5.51 MIMOMM optimized ^{4}ROHF (6-31G*/3BL) geometry of Si-O-Si bridge, Si(111) surface.

Atom Displacements ($\AA$) Caused by Si-O-Si Bridge Adsorption Site Si(111) Surface						
Atom	*Ab Initio*			IMOMM: 3 Bilayer		
	δ x	δ y	δ z	δ x	δ y	δ z
1	**0.605**	0.042	**-0.160**	**0.562**	0.031	-0.024
2	**-0.608**	0.042	**-0.158**	**-0.563**	0.031	-0.020
3	-0.001	**0.209**	-0.084	-0.001	**0.127**	0.021
4	**0.579**	**-0.125**	**0.466**	**0.360**	0.016	**0.337**
5	**-0.582**	**-0.125**	**0.470**	**-0.362**	0.014	**0.340**
6	0.000	**0.162**	**-0.208**	0.001	**0.111**	0.007
7	**0.128**	0.034	-0.083	**0.115**	0.011	-0.005
8	0.000	-0.022	**-0.906**	0.001	**-0.181**	**-0.559**
9	**-0.130**	0.033	-0.081	**-0.116**	0.010	-0.004
10	**0.214**	-0.031	**0.443**	**0.175**	0.012	**0.229**
11	**-0.215**	-0.032	**0.448**	**-0.175**	0.011	**0.231**
12	0.000	0.018	**-0.203**	0.000	0.020	-0.010
13	0.017	0.028	-0.076	0.079	-0.012	0.005
14	0.001	0.094	**-0.816**	0.001	-0.025	**-0.427**
15	-0.016	0.027	-0.074	-0.080	-0.012	0.007
16	0.000	0.182	**-0.331**	0.000	0.022	**-0.172**
17	**-0.131**	0.070	**-0.259**	-0.024	-0.064	**-0.126**
18	0.041	-0.075	**0.337**	-0.067	-0.017	**0.103**
19	-0.051	0.021	-0.091	0.007	-0.016	-0.004
20	-0.040	-0.074	**0.332**	0.068	-0.017	0.100
21	**0.132**	0.069	**-0.256**	0.024	-0.065	**-0.125**
22	0.053	0.021	-0.089	-0.006	-0.016	-0.002

Table 5.31 Atom displacements induced by an O atom Si-O-Si bridge adsorption site on the Si(111) surface. The pattern of displacements is the same as on the SiC(111) surfaces, but the displacements are larger.

5.11.6 Si(111) Si-O-Si Ring Insertion: Structure. A comparison of the *ab initio* and MIMOMM (3 bilayer) optimized geometries of the Si-O-Si ring insertion site on the Si(111) surface is listed in Table 5.32. The major structural change caused by the O atom insertion is the 0.8$\AA$ increase in the atom 1-2 separation from the bare, reconstructed cluster. This has the effect of opening up the surface bilayer ring, which should make it easier for additional O atoms impinging on the surface to penetrate through the surface bilayer and react with subsurface atoms. Figures 5.52, 5.53, 5.54, and 5.55 show comparisons of the *ab initio* and MIMOMM (3 bilayer) optimized geometries of the Si-O-Si ring insertion site on the Si(111) surface. As we've seen in previous cases, the MIMOMM optimization reduces the overall distortion of the cluster.

Si-O-Si Ring Site Si(111) Surface			
	$Si_{22}H_{25}$ *Ab Initio*	$Si_{22}H_{25}O$ *Ab Initio*	$Si_{22}H_{25}O$ MIMOMM 4 Bilayer
Dist ($\AA$)			
1 2	3.927	4.608	4.575
1 4	2.370	2.371	2.367
1 7	2.371	2.376	2.351
1 9	4.453	4.952	4.855
1 48	-	1.657	1.636
8 48	-	1.651	1.638
Angle (°)			
7 1 48	-	110.182	102.498
1 48 8	-	152.602	157.098
48 8 2	-	111.618	100.814
8 2 9	109.621	110.931	109.170
2 9 3	111.835	114.004	115.416
9 3 7	109.621	113.982	116.147
3 7 1	111.835	113.787	109.534

Table 5.32 Comparison of *ab initio* and MIMOMM optimized (^{4}ROHF 6-31G*) Si(111) cluster geometry with an O atom adsorbed at a Si-O-Si ring insertion site. Atom 48 is the adsorbed O atom. The bare cluster results are listed for comparison.

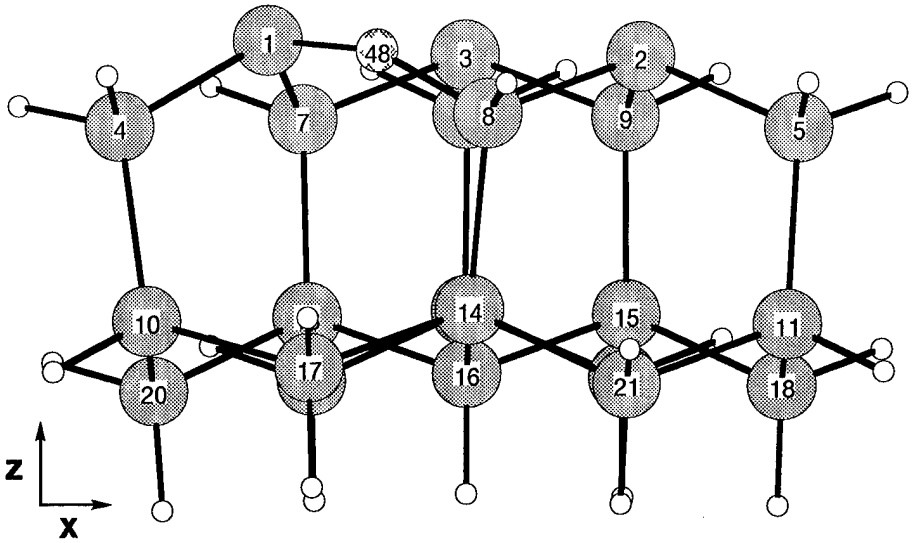

Figure 5.52 *Ab initio* optimized ^{4}ROHF (6-31G*/3BL) geometry of Si-O-Si ring insertion, Si(111) surface.

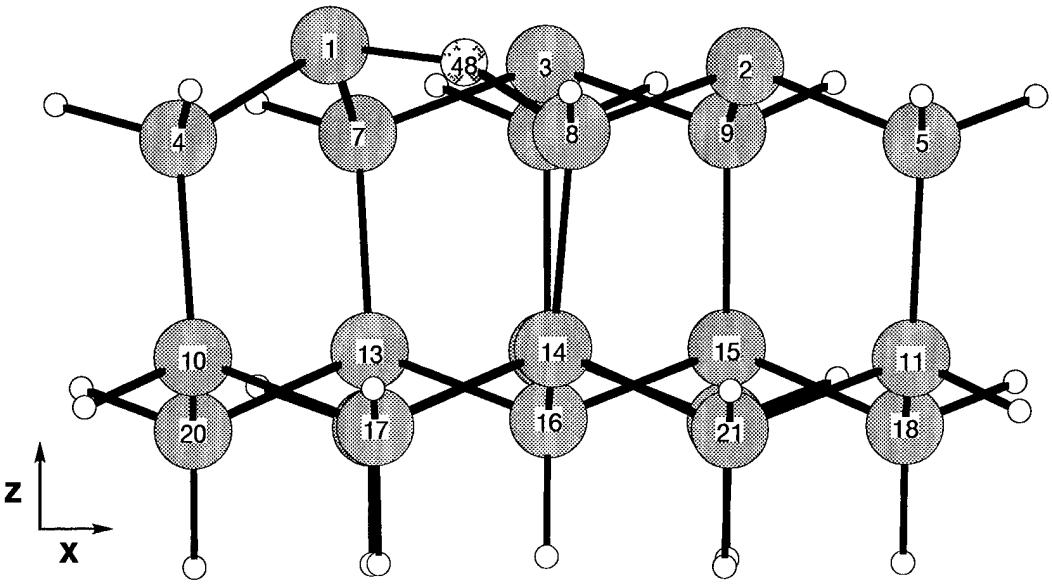

Figure 5.53 IMOMM optimized ^{4}ROHF (6-31G*/3BL) geometry of Si-O-Si ring insertion, Si(111) surface.

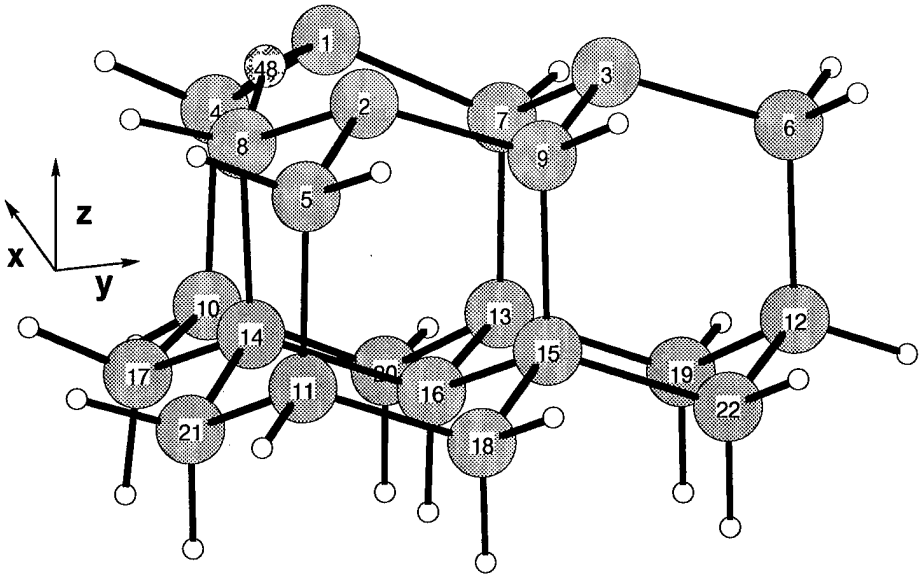

Figure 5.54 *Ab initio* optimized ^{4}ROHF (6-31G*/3BL) geometry of Si-O-Si ring insertion, Si(111) surface.

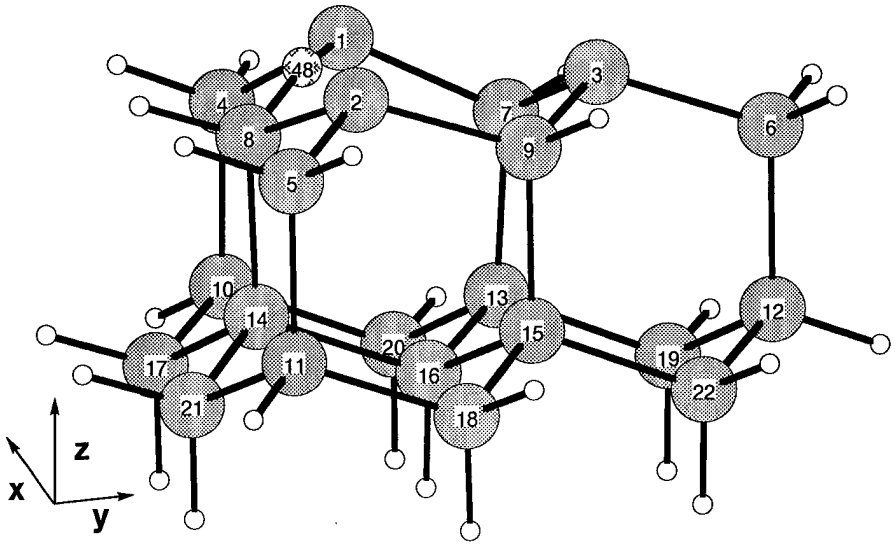

Figure 5.55 IMOMM optimized ^{4}ROHF (6-31G*/3BL) geometry of Si-O-Si ring insertion, Si(111) surface.

5.11.7 Si(111) O-Si-O-Si Ontop and Ring Insertion: Structure. Figure 5.56 shows the *ab initio* optimized geometry of the Si(111) cluster with two O atoms adsorbed. This structure was obtained by starting with the optimized geometry of the Si(111) cluster with one O atom adsorbed into a ring site (between atoms 1 and 8), and placing a second O atom 1.6Å above atom 1. This starting point was selected to bias the optimized geometry towards Si atom 1 being bonded to both O atoms because this configuration was found to be the lowest energy product state to O_2 adsorption onto the Si(111) surface (after dissociation of the molecular precursor) [128]. Unlike the single O atom adsorbed ontop Si(111), this configuration had an AM1 Hessian free of imaginary frequencies. As was mentioned earlier, this configuration is a likely early step in the formation of an SiO_2 layer on Si(111). A comparison of the geometry of the bare cluster, the cluster with one O atom adsorbed in a ring site, and the cluster with two O atoms adsorbed is listed in Table 5.33.

	$Si_{22}H_{25}$ *Ab Initio*	Si-O_{ring}-Si *Ab Initio*	O_{ontop}Si-O_{ring}-Si *Ab Initio*
Dist (Å)			
1 O_{ontop}	-	-	1.680
1 O_{ring}	-	1.598	1.640
1 4	2.367	2.366	2.366
1 7	2.371	2.333	2.372
8 O_{ring}	-	1.710	1.652
2 8	2.371	2.354	2.362
3 7	2.371	2.404	2.376
Angle (°)			
O_{ontop}-1-O_{ring}	-	-	111.068
O_{ontop}-1-4	-	-	107.932
O_{ontop}-1-7	-	-	106.264
1-O_{ring}-8	-	147.508	156.315
O_{ring}-8-2	-	112.306	111.630
2-9-3	111.835	112.551	114.174
3-7-1	111.835	116.256	114.094
7-1-O_{ring}	-	118.379	109.234

Table 5.33 Comparison of Si(111) cluster *ab initio* optimized geometry (6-31G*) with 0, 1, and 2 O atoms adsorbed.

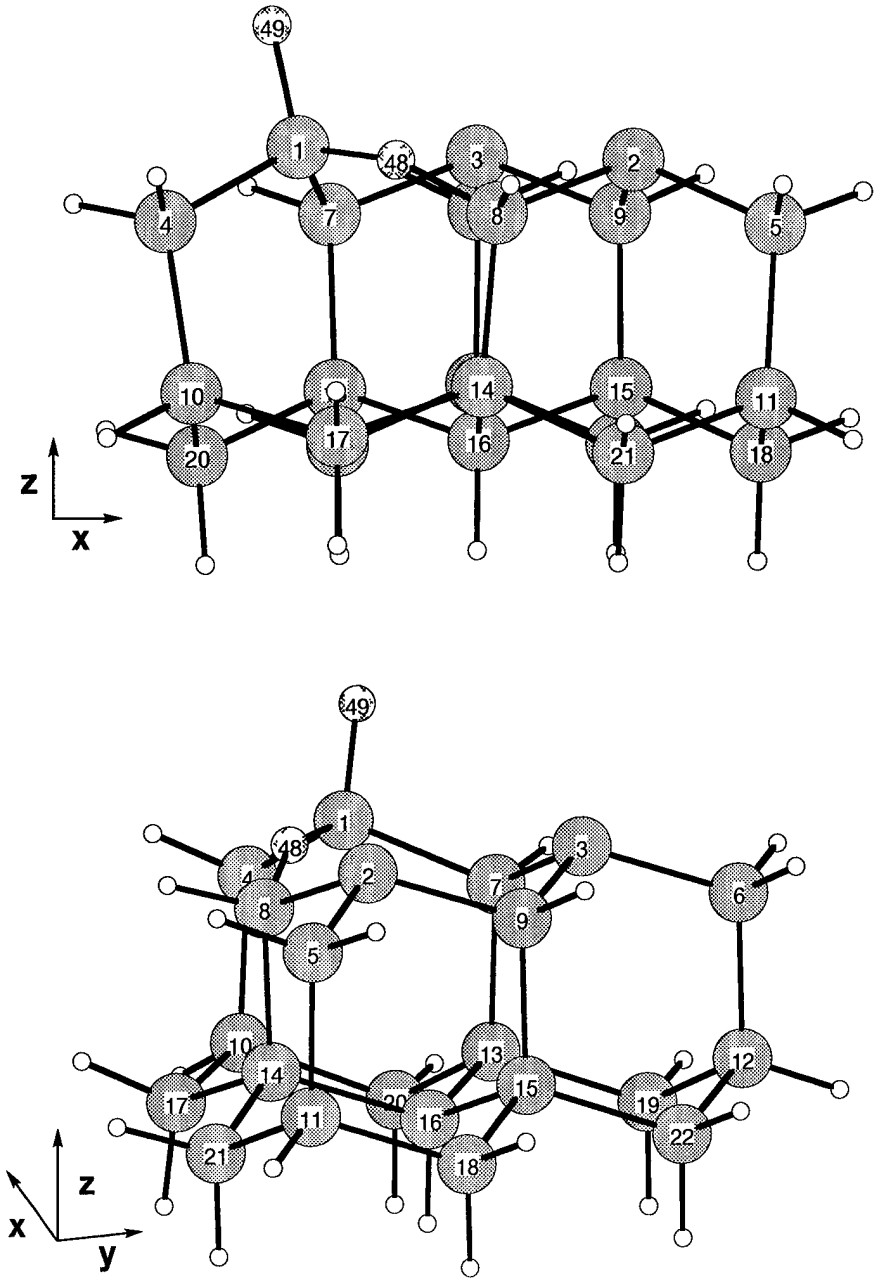

Figure 5.56 *Ab initio* optimized ^{4}ROHF (6-31G*) geometry of Si(111) cluster with two O atoms adsorbed, O_{ontop}Si-O_{ring}-Si.

5.11.8 Comparison of Si(111) Oxygen Adsorption Site Energetics. The oxidation energetics for Si(111) are summarized in Table 5.34, and we that the overall behavior of one O atom adsorbed on a Si(111) surface is actually quite different than the Si-terminated SiC(111) surface. The ontop adsorption energy on Si(111) is predicted to be $16\frac{kcal}{mole}$ smaller than on Si-terminated SiC(111). As expected, the Si-O-Si bridge adsorption site is less bound on Si(111) than on Si-terminated SiC(111), and is significantly affected by addition of sterics from the bulk cluster in the MIMOMM optimization. *Unlike the Si-terminated SiC(111) cluster, the ring adsorption site in Si(111) is the lowest energy adsorption site.* The total binding energy of 2 O atoms adsorbed, one in a ring insertion site, one ontop, is 12 $\frac{kcal}{mole}$ larger than the sum of the individual ontop and ring adsorption sites.

The O atom ontop adsorption site on Si(111) is of particular interest because of all the O atom adsorption sites reported in this work, *only the AM1 Hessian at this adsorption site contained imaginary frequencies, i.e., this is not an AM1 stationary point.* (All the *ab initio* optimizations performed in this work were preceded by AM1 optimizations and Hessian calculations.) However, the AM1 Hessian for the O ontop site *with an O atom already adsorbed at a ring insertion site* did not contain any imaginary frequencies. Adsorption of O_2 onto the Si(111) surface is believed to occur via a molecular precursor. Schubert et al [127, 128] report extended Huckel tight binding calculations of O_2 adsorption on Si(111). The lowest energy final state they report involves adsorption of an O_2 molecule at an ontop site, followed by dissociation with 1 O atom moving into a ring adsorption site and the other O atom remaining ontop. They speculate that repetition of this mechanism results in the formation of an SiO_2 layer ontop the silicon. For reactions involving atomic oxygen, our calculations predict that the atomic oxygen first burrows into the subsurface before adsorbing at ontop sites. The larger spacing of the Si(111) lattice is a likely reason why the ring insertion site is preferred over an ontop site for a single O atom.

5.11.9 Si Vacancy in the Si(111) Surface. The reconstruction induced by a surface vacancy in the Si(111) surface was modeled by removing Si atom 1 and optimizing the cluster geometry, the same procedure that was used for the SiC clusters. Table 5.35 lists the energetics of Si vacancy creation in the Si(111) cluster.

Surface	Model	6-31G* Energy (H) *ab initio*	MIMOMM 3 Bilayer
Bare	^{4}ROHF	-6370.850792	-
Oxidation			
O-Si ontop	^{4}ROHF	-6445.722146	*AM1 saddle pt*
Si-O-Si bridge	^{2}ROHF	-6445.761154	-6445.737058
Si-O-Si ring	^{4}ROHF	-6445.777182	-6445.770469
O_{ontop}-Si-O_{ring}-Si	^{4}ROHF	-6520.667840	-

		Adsorption Energy ($\frac{kcal}{mol}$)	
Oxidation			
Cluster + O(g)		0.0	0.0
O-Si ontop	^{4}ROHF	-58.0	-
Si-O-Si bridge	^{2}ROHF	-82.4	-67.3
Si-O-Si ring	^{4}ROHF	-92.5	-88.3
Cluster + 2O(g)		0.0	0.0
O_{ontop}-Si-O_{ring}-Si	^{4}ROHF	-162.6	-

Table 5.34 Oxidation energetics of Si(111) cluster. All the *ab initio* calculations were preceded with AM1 optimization and Hessian calculations to start the 6-31G* optimizations. *The O-Si ontop adsorption site is the only site reported in this work that did not optimize to an AM1 minimum.*

Because the silicon lattice isn't as stiff as SiC, we expect to see very large atom displacements upon reconstruction around the vacancy, and we expect the steric influence of the bulk cluster to be more important than in the SiC clusters. Figures 5.57 and 5.58 show a comparison of *ab initio* optimized geometries (^{4}ROHF 6-31G*) of the bare cluster and this same cluster with Si atom 1 removed. In this case, atoms 4 and 8 have bonded, with atom 4 dragging atom 10 along with it. Figures 5.59 and 5.60 show a comparison of the bare cluster and the MIMOMM optimized cluster with a vacancy. In MIMOMM optimized case, the steric forces on atom 10 make bonding between atom 4 and 8 less favorable, and we see that atoms 4 and 7 have now bonded around the vacancy. *Unlike the SiC(11) Si and C vacancy calculation, in Si(111) the ab initio and MIMOMM optimized geometries display qualitatively different reconstructions.* A comparison of the *ab initio* and MIMOMM optimized geometries for the vacancy induced reconstruction is shown in Figures 5.61 and 5.62. The atom displacements for these cases are listed in Table 5.37.

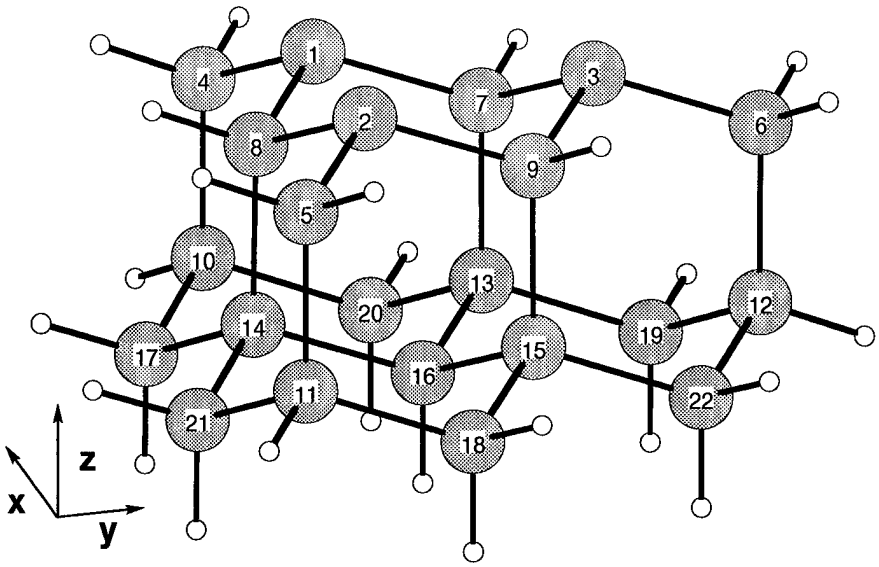

Figure 5.57 *Ab initio* optimized ^{4}ROHF (6-31G*) geometry of Si(111) cluster.

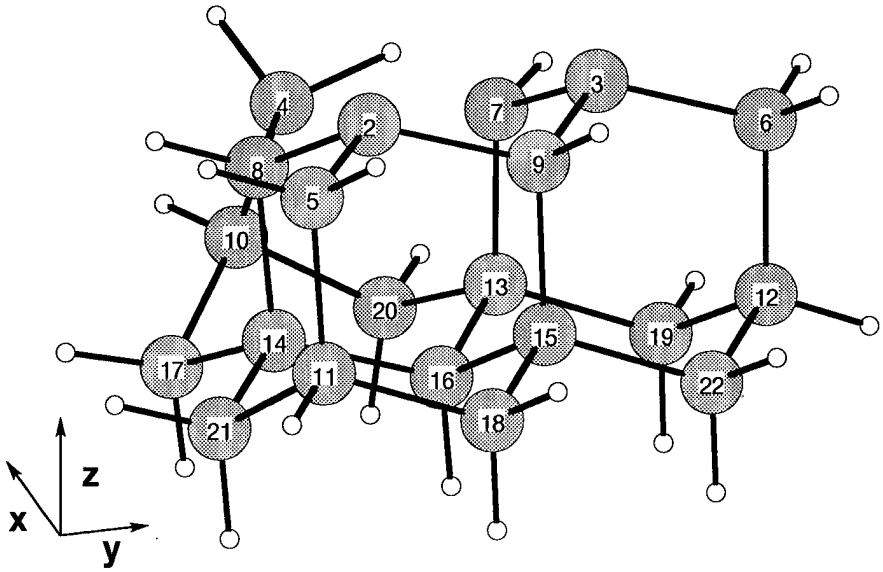

Figure 5.58 *Ab initio* optimized ^{4}ROHF (6-31G*) geometry of Si(111) cluster with a surface vacancy. Distortion of cluster much larger than in SiC

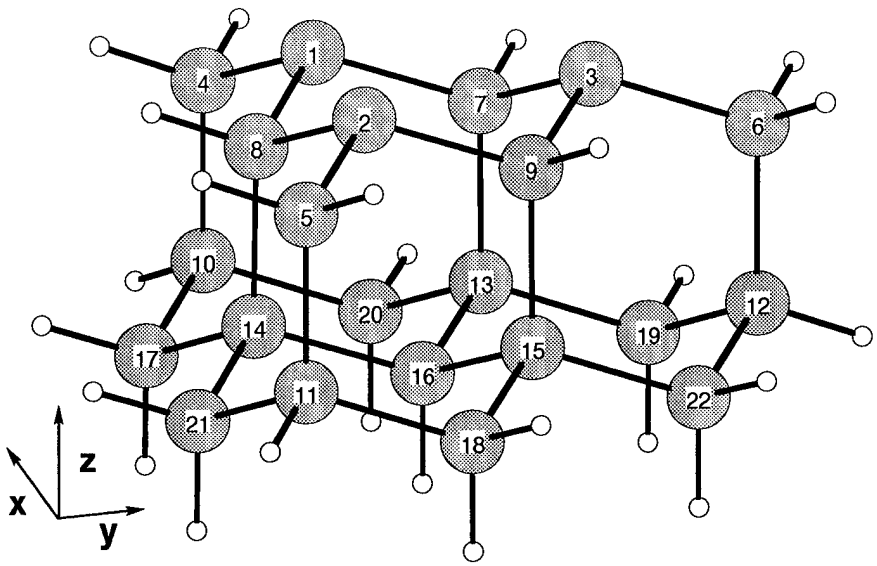

Figure 5.59 *Ab initio* optimized ^{4}ROHF (6-31G*) geometry of Si(111) cluster.

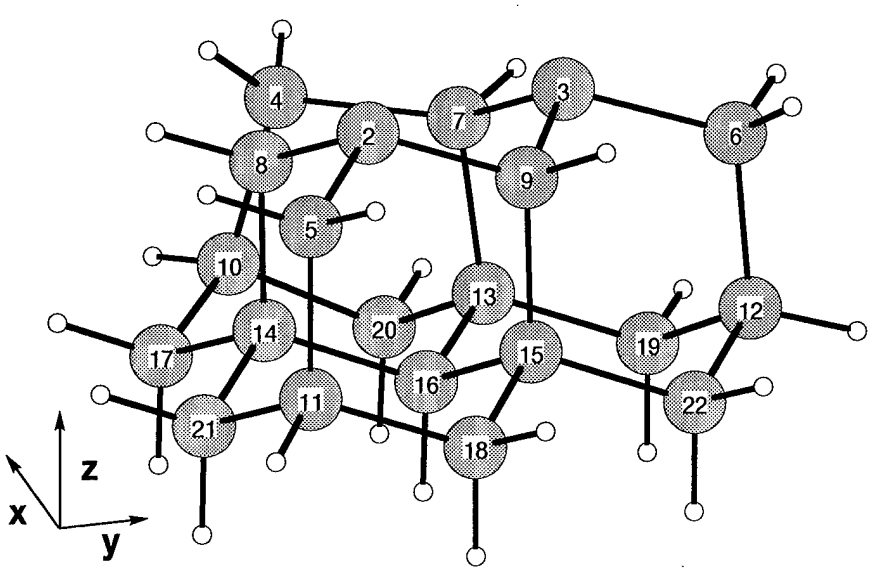

Figure 5.60 MIMOMM optimized ^{4}ROHF (6-31G*) geometry of Si(111) cluster with a surface vacancy. Distortion of cluster much larger than in SiC

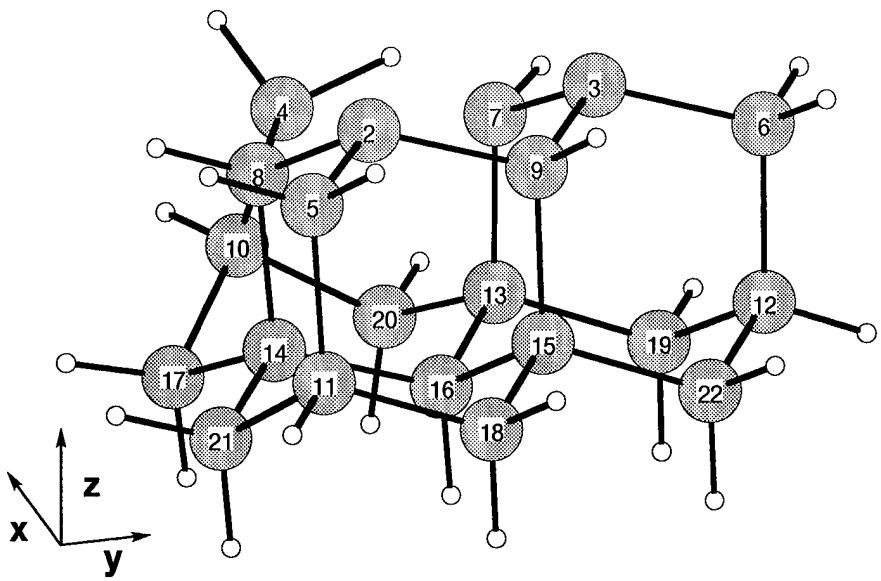

Figure 5.61 *Ab initio* optimized ^{4}ROHF (6-31G*) geometry of Si(111) cluster with a surface vacancy. Atoms 4 and 8 have bonded in the reconstruction following creation of the vacancy.

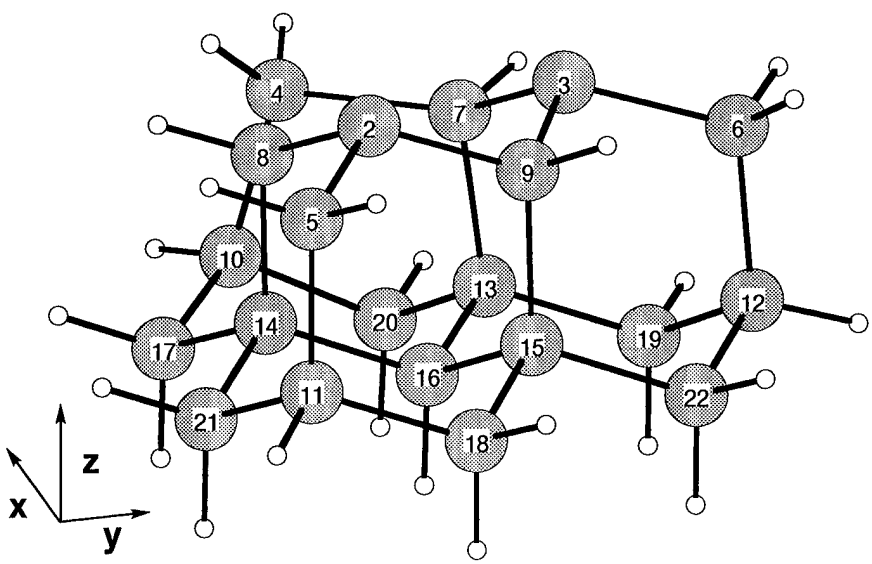

Figure 5.62 MIMOMM optimized ^{4}ROHF (6-31G*) geometry of Si(111) cluster with a surface vacancy. Atoms 4 and 7 have bonded in the reconstruction following creation of the vacancy.

Surface	Model	6-31G* Energy (H)	
		ab initio	MIMOMM 3 Bilayer
Reconstruction			
Bare	^{4}ROHF	-6370.850792	-
Si Vacancy			
$Si_{21}H_{25}$	^{4}ROHF	-6081.888239	-6081.870402

		Δ Energy ($\frac{kcal}{mol}$)	
Si Vacancy	^{4}ROHF	+83.6	+94.8

Table 5.35 Si(111) surface vacancy energetics

Atom Displacements ($\AA$) Caused by Si Surface Vacancy Si(111) Surface						
Atom	*Ab Initio*			IMOMM: 3 Bilayer		
	δ x	δ y	δ z	δ x	δ y	δ z
1	-	-	-	-	-	-
2	-0.648	-0.159	-0.040	0.151	-0.042	0.038
3	-0.151	0.187	0.009	-0.253	-0.368	-0.042
4	1.260	-0.400	-0.030	0.383	0.825	0.021
5	-0.537	-0.117	0.212	0.133	-0.040	-0.010
6	0.020	0.119	-0.154	-0.148	-0.278	0.031
7	-0.250	0.436	-0.011	-0.381	-0.279	-0.116
8	-0.291	-0.423	-0.406	0.218	-0.058	0.006
9	-0.346	-0.123	0.082	-0.074	-0.084	0.002
10	0.241	-0.177	0.205	0.097	0.239	0.065
11	-0.141	-0.052	0.240	0.026	-0.015	-0.028
12	-0.082	-0.052	-0.148	-0.042	-0.095	0.014
13	-0.104	-0.030	0.038	-0.041	-0.011	-0.077
14	-0.049	-0.078	-0.365	0.050	0.053	0.032
15	-0.121	-0.054	0.098	-0.049	-0.054	0.004
16	-0.096	0.001	-0.027	-0.030	-0.001	-0.058
17	-0.060	0.037	-0.470	0.032	0.097	0.064
18	-0.042	-0.037	0.299	-0.028	-0.004	-0.028
19	-0.075	-0.095	-0.132	-0.043	-0.021	-0.077
20	-0.121	-0.157	0.335	-0.056	0.132	-0.148
21	0.056	0.039	-0.216	-0.000	-0.005	-0.008
22	-0.047	-0.086	0.016	-0.016	-0.062	-0.003

Table 5.36 Atom displacements induced by a Si vacancy on the Si(111) surface. As was seen in the SiC clusters, the MIMOMM optimized z axis displacements are significantly smaller than the *ab initio* result. Unlike the SiC cases, the *ab initio* and MIMOMM reconstruction are also qualitatively different.

	$Si_{22}H_{25}$ No Vacancy	$Si_{21}H_{25}$ *Ab Initio*	$Si_{21}H_{25}$ MIMOMM 3 Bilayer
Dist (Å)			
2 4	6.026	4.259	5.700
2 8	2.371	2.382	2.334
4 7	3.908	4.237	2.575
4 8	3.908	2.385	3.842
4 10	2.378	2.384	2.423
Angle (°)			
4 7 3	146.295	118.500	139.338
4 8 2	146.293	126.601	133.187
7 3 9	109.621	108.081	119.421
8 2 9	109.621	120.532	104.757
7 13 12	90.028	84.870	98.407
17 10 20	108.953	106.776	112.265
Torsion(°)			
10 13 15 14	-0.035	-10.231	-2.051
17 20 22 21	0.001	8.295	-2.415

Table 5.37 Comparison of *ab initio* and MIMOMM optimized (6-31G* basis set) geometries of Si(111) cluster with a Si surface vacancy.

5.12 Discussion

5.12.1 Steric Effects on O Atom Bridge Site Formation. Of the three adsorption sites investigated, formation of the Si-O-Si bridge site is predicted to be the lowest energy adsorption site on the Si-terminated SiC(111) surface. However, the C-O-C terminated bridge site on the C-terminated surface is predicted to be weakly bound by the *ab initio* calculation, and even *higher* in energy than the EC plus a free O atom by the MIMOMM (4 bilayer) calculation. This result may seem odd at first, but can be readily understood by considering the steric constraints of the SiC lattice.

One way to understand the steric effects on reactivity is to compare the cluster calculations with a similar small molecule that does not have the same steric constraints. $H_3Si\text{-}O\text{-}SiH_3$, shown in Figure 5.63, can be used to make comparisons to the O ontop and bridge sites on the Si-terminated clusters. Two $SiH_3^{\bullet}$s and an O atom would be comparable to the Si-terminated cluster with an unbonded O atom. $SiH_3O^{\bullet}$ and $SiH_3^{\bullet}$ correspond to an O atom adsorbed at an ontop site, and SiH_3OSiH_3 corresponds to an O atom adsorbed at a bridge site. Table 5.38 lists the calculated (6-31G*) Si-O binding energies for these systems, as well as the optimized Si-O bond lengths and Si-O-Si bond angle.. The experimental bond strength for an Si-O bond in $HO\text{-}Si(CH_3)_3$ is also listed to bound these Hartree-Fock results. The corresponding results from the Si-terminated cluster calculations are listed in Table 5.39.

In Table 5.39, we see that the most striking structural difference between the cluster results and $H_3SiOSiH_3$ is in the value of the Si-O-Si bond angle. Table 5.40 lists the angles around the O-Si bond for $H_3SiOSiH_3$, and the ontop and Si-O-Si bridge adsorption sites on the Si-terminated cluster. In $H_3SiOSiH_3$, the H atoms bonded to the Si are free to move, and so can achieve a nearly tetrahedral geometry around Si for any value of Si-O-Si angle, i.e., the Si-O-Si bond angle and Si-O bond distance are free to optimize fully. In the O-Si ontop site adsorption, the structure around Si is nearly tetrahedral, so little distortion of the cluster is required to achieve an optimum geometry. However, in the Si-O-Si bridge formation, the Si atoms are bonded to C atoms in the EC, and are coupled into the entire cluster. In order to achieve a tetrahedral geometry around the Si atom, the subsurface C atoms would have to be pulled out of the lattice. There isn't enough energy in the O

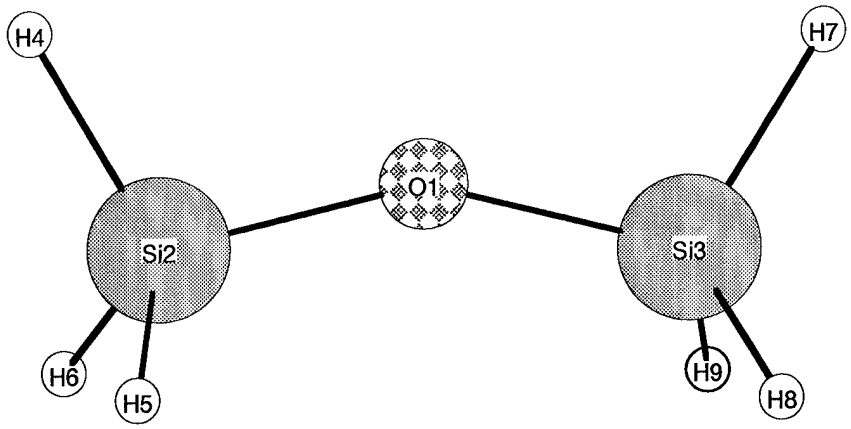

Figure 5.63 Optimized geometry of $H_3Si\text{-}O\text{-}SiH_3$, a small molecule model of an Si-O-Si O atom bridge adsorption site.

adsorption reaction to do this, though there is enough energy to cause significant distortion in the EC. Two Si-O bonds form, but at a far from optimum geometry, so the bonding energy of the Si-O-Si bridge site is much less than twice the O-Si ontop site bonding energy. The better representation of the bulk steric forces provided by MIMOMM further restrict the displacement of the C atoms, reducing the bonding energy of the Si-O-Si bridge site.

These same steric constraints on O atom bridge site formation can also be observed on the C-terminated SiC(111) cluster. For this case, the analogous small molecule model system is $H_3C\text{-}O\text{-}CH_3$. The comparisons listed in Tables 5.41, 5.42, and 5.43 shows that the steric constraints of the C-terminated cluster result in the formation of C-O bonds at less than optimal geometries, which reduces the binding energy. However, an additional effect on the C-terminated SiC(111) surface also plays a role in bridge bond formation: atomic size. The C-C bond length in diamond is 1.54Å. In bulk silicon, the Si-Si bond length is 2.35Å. In SiC, the Si-C bond length is 1.89Å. On the Si-terminated SiC surface, Si atoms 1 and 3 that form the bridge bond with the O atom are 3.1Å apart in the SiC lattice, *18% closer together* than the separation of 3.84Å on a Si(111) surface. On the C-terminated SiC surface, C atoms 1 and 3 are also 3.1Å apart, *23% farther apart* than the separation

System	$\Delta E(\frac{kcal}{mol})$ HF	MP2	Si-O ($\AA$)	∠Si-O-Si°
$SiH_3^\bullet + SiH_3^\bullet + O^\bullet$	0.0	0.0	-	-
$H_3SiO^\bullet + SiH_3^\bullet$	-67.94	-96.9	1.688	-
$H_3SiOSiH_3$	-167.70	-224.5	1.631	153.4
$HO\text{-}Si(CH_3)_3$ bond energy			128.0 **exp** Ref [125]	

Table 5.38 Small molecule models for Si-O bond energies (6-31G* basis set).

Adsorption Site	$\Delta E(\frac{kcal}{mol})$ HF	MP2	Si-O $\AA$	∠Si-O-Si°
Ontop	-74.5	-104.0	1.698	-
Bridge				
ab initio	-106.8	-174.5	1.727	90.8
MIMOMM 2 Bl	-102.3	-170.1	1.754	92.3
MIMOMM 4 Bl	-92.5	-163.8	1.767	92.3

Table 5.39 Si-O bond energies in SiC cluster models (6-31G* basis set).

of 2.62$\AA$ on the diamond (C(111)) surface, which makes bonding that involves cooperation of more than one surface C atom more difficult. This difference in oxidation adsorption between the Si and C-terminated SiC(111) surfaces caused by this size difference can be better understood by examining the Boys localized singly occupied orbitals on the bare Si and C-terminated clusters, shown in Figure 5.64. In this figure, we see that the spatial extent of the C dangling bond is much smaller that the Si dangling bond. An O atom moving towards the surface has a much higher probability of interacting with 2 adjacent

$H_3SiOSiH_3$		Si-terminated SiC(111) Cluster	O Ontop	O Bridge
$\angle Si_1\text{-}O\text{-}Si_3(°)$	153.373	$\angle Si_1\text{-}O\text{-}Si_3(°)$	-	92.304
$\angle O\text{-}Si_1\text{-}H_4$	108.923	$\angle O\text{-}Si_1\text{-}C_4$	103.762	142.883
$\angle O\text{-}Si_1\text{-}H_5$	110.234	$\angle O\text{-}Si_1\text{-}C_7$	111.800	103.356
$\angle O\text{-}Si_1\text{-}H_6$	110.234	$\angle O\text{-}Si_1\text{-}C_8$	111.663	83.083

Table 5.40 Comparison of bond angles in $H_3SiOSiH_3$ with O atom ontop and bridge adsorption sites on the Si-terminated SiC(111) surface. Atom numbers for $H_3SiOSiH_3$ are shown in Figure 5.63. Atom numbers for the Si-terminated SiC(111) cluster are shown in Figure 5.24.

Si atoms on the Si-terminated SiC surface than 2 adjacent C atoms on the C-terminated SiC surface. Formation of a bridge bond essentially passivates two surface reactive sites, while formation of an ontop adsorption site produces a new radical site above the surface. This is a possible reason why O atom exposure of the Si-terminated SiC surface leads to growth of a good insulating layer, and why the O atom exposure of the C-terminated SiC surface results in formation of a poorer insulating layer.

System	$\Delta E(\frac{kcal}{mol})$ HF	MP2	C-O ($\AA$)	∠C-O-C°
$CH_3^\bullet + CH_3^\bullet + O^\bullet$	0.0	0.0	-	-
$H_3CO^\bullet + CH_3^\bullet$	-51.7	-86.4	1.384	-
H_3COCH_3	-110.6	-179.4	1.391	113.8
H_3C-$OC(CH_3)CH_2$ bond energy			66.3 (**Exp**) Ref [125]	

Table 5.41 Small molecule models for C-O bond energies (6-31G* basis set).

Adsorption Site	$\Delta E(\frac{kcal}{mol})$ HF	MP2	C-O $\AA$	∠C-O-C°
Ontop	-40.8	-84.5	1.396	-
Bridge				
ab initio	-9.6	-101.1	1.505	100.641
IMOMM 2 Bl	-1.7	-94.9	1.568	102.163
IMOMM 4 Bl	**+5.8**	-88.8	1.590	102.233

Table 5.42 C-O bond energies in SiC cluster models (6-31G* basis set).

H_3COCH_3		C-terminated SiC(111) Cluster	O Ontop	O Bridge
$\angle C_1$-O-C_3(°)	113.811	C_1-O-C_3(°)	-	102.227
∠O-C_1-H_4	107.648	O-C_1-Si_4	106.846	138.550
∠O-C_1-H_5	111.487	O-C_1-Si_7	109.636	110.367
∠O-C_1-H_6	111.489	O-C_1-Si_8	109.634	74.172

Table 5.43 Comparison of bond angles in H_3COCH_3 with O atom ontop and bridge adsorption sites on the C-terminated SiC(111) surface. Atoms numbers for H_3COCH_3 are consistent with Figure 5.63. Atoms numbers for the C-terminated SiC(111) cluster are shown in Figure 5.34.

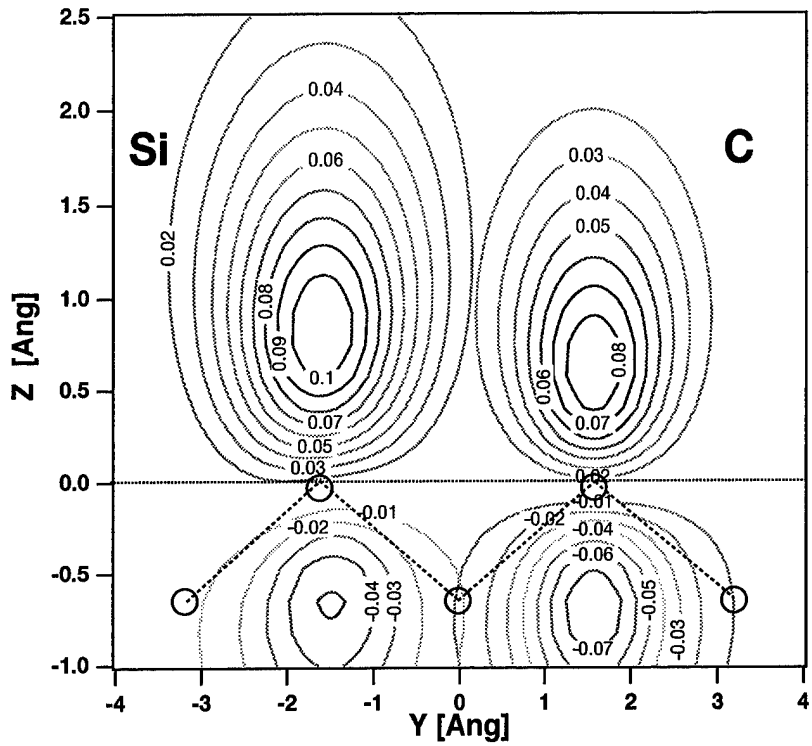

Figure 5.64 Boys localized singly occupied molecular orbitals for Si and C-terminated SiC(111) surfaces. Subsurface atom locations are accurate only for the Si-terminated surface

5.12.2 Etching of the C-terminated SiC(111) Surface. Observed differences in the performance of SiC devices have been attributed to differences between the oxidation of Si and C-terminated surfaces. O atoms are assumed to etch the C-terminated surface, producing defects at the semiconductor-insulator interface that increase the resistivity near the interface. Direct experimental evidence for carbon etching by oxygen does not yet exist. From the oxygen adsorption results in Section 5.9, one possible mechanism for carbon etching is adsorption at an ontop site, followed by formation of CO (gas) along with ^{4}ROHF reconstruction of the remaining cluster. The Hartree-Fock and MP2 energetics for this mechanism are:

					ab initio	MIMOMM 4 Bilayer
					Hartree-Fock ΔE ($\frac{kcal}{mole}$)	
$(C_9Si_{13}H_{25})O$	$\rightarrow$	$C_8Si_{13}H_{25}$	+	CO	+11.7	+22.4
CO	$\rightarrow$	C	+	O	177.0	
					MP2 ΔE ($\frac{kcal}{mole}$)	
$(C_9Si_{13}H_{25})O$	$\rightarrow$	$C_8Si_{13}H_{25}$	+	CO	+16.5	+21.2
CO	$\rightarrow$	C	+	O	254.4	
CO (^{2}ROHF)	$\rightarrow$	C (^{3}ROHF)	+	O (^{3}ROHF)	**257 (Exp)** Ref [125]	

The inclusion of electron correlation makes a large difference in the calculated binding energies; however, the Hartree-Fock and MP2 energetics of CO elimination differ by only about $6\frac{kcal}{mole}$. These calculations if reactant and product state energies do not consider the effect of thermal vibrations of the cluster on CO elimination, nor do they consider the entropic gain of reelasing a gas phase molecule. However, since the binding energy of O atom ring insertion is greater than O atom ontop site adsorption for the C-terminated SiC(111) cluster, direct elimination of CO is unlikely.

An alternate mechanism for etching of C atoms from the C-terminated surface would begin with O atom C-O-Si ring insertion, followed by subsequent ontop adsorption of a second O atom on the C atom involved in the C-O-Si ring bond. The second step is followed by desorption of a CO_2 molecule. The binding energy of CO_2 is very large, 384 $\frac{kcal}{mol}$, and the distortion caused by the initial O atom ring insertion is likely to weaken the C atom binding to SiC. The energetics for this mechanism are listed in Table 5.44. (The MP2 calculated binding energy for CO_2 listed here does not include a correction for zero point vibration energy.) We see that at the MP2 level of theory, the energy of 2 O atoms adsorbed onto the cluster is only 7 $\frac{kcal}{mole}$ lower in energy than the cluster with a C atoms vacancy and a CO_2 molecule. This result does not include the entropic gain associated with desorbing a molecule from a surface. Since the insertion of the O atom into the surface ring on the C-terminated SiC(111) surface is energetically favored, a plausible mechanism for CO_2 elimination is adsorption of an O atom at this site, adsorption of a second O atom onto a surface C atom adjacent to the first O atom. While this is a plausible mechanism, the calculations performed do not provide any information about barriers to this reaction mechanism.

					ab initio Hartree-Fock ΔE ($\frac{kcal}{mole}$)
$(C_9Si_{13}H_{25})O_2$	$\rightarrow$	$C_8Si_{13}H_{25}$	+	CO_2	+6.9
CO_2	$\rightarrow$	C	+	2O	250.0
					MP2 ΔE ($\frac{kcal}{mole}$)
$(C_9Si_{13}H_{25})_2$	$\rightarrow$	$C_8Si_{13}H_{25}$	+	CO_2	+6.8
CO_2	$\rightarrow$	C	+	2O	382.6
CO_2	$\rightarrow$	C	+	2O	**384 (Exp)** Ref [125]

Table 5.44 Energetics of CO_2 desorption from C-terminated SiC(111) cluster.

5.13 Summary of Oxidation Energetics

Table 5.45 lists the MP2 oxidation energetics for the Si and C-terminated SiC clusters and the Hartree-Fock energetics for the Si(111) cluster.

5.14 Conclusions

Our interest in oxidation of SiC(111) was spurred by the experimental observation of widely differing device SiC MOSFET device performance. The hypothesized reason for this observed difference is that SiC comes in two varieties, with silicon or carbon terminated surfaces. Oxidation of the Si-terminated surface is believed to lead to a defect-free interface between the oxide layer and the SiC underneath. Oxidation of the C-terminated surface is believed to etch carbon from the surface, producing a defect-rich interface. From the calculations presented in this chapter, we can conclude:

- Etching of C by O atom adsorption is energetically reasonable
  - Etching by elimination of CO_2 is more likely than by elimination of CO
  - Atom displacements after removal of a surface C from SiC are much larger than after removal of a surface Si atom. The effect of these displacements propagates many layers into the SiC below the interface

- The relative energetics of the single O atom adsorption sites investigated in this work on the C-terminated SiC(111) surface is the same Si(111) surface, while both differ from the Si-terminated SiC(111) surface.
- Imposing bulk steric effects on small clusters is more important when modeling processes that cause large atom displacements.
- Fabrication processes developed for silicon devices, such as growing insulating layers by exposure to atomic oxygen, may be inappropriate for SiC devices.

5.15 Recommendations

5.15.1 SiC Oxidation. The O atom adsorption calculations provide some insight into the observed differences in the oxidation of Si and C-terminated SiC surfaces. Oxidation of SiC is currently performed using "wet" chemistry, exposure to steam, or "dry" chemistry, exposure to O atoms in Plasma Enhanced Chemical Vapor Deposition (PECVD). The gas used in the PECVD process is a mixture of oxygen diluted in a rare gas buffer. The goal of this oxidation is to grow an insulating layer of SiO_2 on the SiC surface, and there's more than one way to grow SiO_2 layers. An approach commonly used to grow SiO_2 layers on silicon is PECVD using a gas mix of tetraethoxysilane (TEOS $Si(OC_2H_5)_4$) and O_2 [132]. Since the O atoms are responsible for etching the C atoms on the C-terminated surface, using TEOS/O_2 would provide a flux dissociation products containing Si-O instead of just O atoms (and other pure oxygen products). The Si-O containing TEOS dissociation products should bind to the surface C atoms, instead of etching off the C and producing surface defects.

5.15.2 MIMOMM. Optimum BC design is highly system dependent so it is difficult to specify a set of rules for designing BCs a priori. If clear guidance on the design of the BC isn't intuitively obvious, perform a conventional *ab initio* calculation on the EC. The observed deformations of the EC should provide reliable guidance for the BC design.

The use of MM3 interaction potentials raises some questions about the IMOMM results on SiC that are unanswered. First, the MM3 interaction potentials are similar to the equivalent 6-31G* potentials, but they different. It is unclear how this difference affects

the MIMOMM optimized results. The only way to guarantee consistency of the potentials is for the user to generate his own set of potentials based on *ab initio* results (using the same basis set to be used in the subsequent MIMOMM calculations). Methods for generating a set of MM potentials based on *ab initio* calculations exist, but are beyond the experience of the average user [96]. Second, the MM3 interaction potentials were parameterized using gas phase experimental data. Potentials parameterized against solid state material properties are more appropriate for reproducing the steric environment of bulk Si and SiC. Again, generating a set of parameters is beyond the experience of the average user. An easier approach is to use an MM code (other than MM3) that includes a number of different parameter sets (e.g. AMBER, CHARMM), and to select the parameterization most appropriate for the specific model system.

O Atom Adsorption Energies ($\frac{kcal}{mol}$)			
	Ab Initio	MIMOMM 2 Bilayer	MIMOMM 4 Bilayer
Si-terminated $Si_9C_{13}H_{25}$		**MP2** / HF	
Cluster + O(g)	0.0	0.0	0.0
O-Si ontop	**-104.0** / -74.5	**-103.8** / -74.5	-
Si-O-Si bridge	**-174.5** / -106.8	**-170.1** / -102.3	**-163.8** / -92.5
Si-O-C ring	**-95.1** / -50.6	-	**-89.3** / -45.0
Cluster + 2O(g)	0.0	0.0	0.0
O_{ontop}-Si-O_{ring}-C	**-203.5** / -129.6	-	-
C-terminated $C_9Si_{13}H_{25}$		**MP2** / HF	
Cluster + O(g)	0.0	0.0	0.0
O-C ontop	**-84.5** / -40.8	**-84.4** / -40.8	-
C-O-C bridge	**-101.1** / -9.6	**-94.9** / -1.7	**-88.8** / +5.8
C-O-Si ring	**-106.9** / -58.1	-	**-101.0** / -52.2
Cluster + 2O(g)	0.0	0.0	0.0
O_{ontop}-C-O_{ring}-Si	**-202.7** / -109.0	-	-

	Ab Initio		MIMOMM 3 Bilayer
Silicon $Si_{22}H_{25}$		HF	
Cluster + O(g)	0.0		0.0
Si-O ontop	-50.0		-
Si-O-Si bridge	-82.4		-67.8
Si-O-Si ring	-92.5		-88.3
Cluster + 2O(g)	0.0		0.0
O_{ontop}-Si-O_{ring}-Si	-162.6		-

Table 5.45 Summary of O atom adsorption energies on SiC(111) and Si(111). The MIMOMM 3 bilayer results for silicon are listed in the same column as the MIMOMM 4 bilayer results for SiC because both of these bulk clusters provide steric constraints on the bottom of the embedded cluster, unlike the 2 bilayer bulk cluster.

VI. *Conclusions and Recommendations*

6.1 Summary

A new hybrid quantum mechanics/molecular mechanics (QM/MM) calculation method for modeling surface chemistry was developed and applied to the study of silicon and silicon carbide surfaces in this work. This method, known as the Modified Integrated Molecular Orbital and Molecular Mechanics (MIMOMM), was based on the IMOMM method developed by Maseras and Morokuma [4]. The delocalized coordinates of Baker [10] were implemented and shown to be very useful for the highly coupled molecular clusters typically required for modeling surfaces. MIMOMM was verified on silicon clusters used to model the dimerization of the Si(001) surface by comparison with a conventional *ab initio* optimization of a large silicon cluster, $Si_{66}H_{52}$, with experiment, and with other published model calculations. As a model of a single silicon surface dimer, the small cluster Si_9H_{12} was found to reproduce experimental dimer separation, as well as subsurface atom displacements from the large cluster model.

The use of $\overline{H}$s to terminate silicon was investigated using the HW ECP and 6-31G* basis sets. While reported modification of Mulliken charges in Si_9H_{12} were reproduced, the limitations of using Mulliken charge as a metric for defining $\overline{H}$s become apparent when one moves to a larger basis set such as 6-31G*. The limitation of the Mulliken population analysis for highly polarized materials such as SiC highlights the difficulty of using Mulliken charge for the construction of $\overline{H}$s.

Studies of the surface chemistry of Si and C-terminated SiC(111) surfaces using conventional *ab initio* techniques and MIMOMM displayed the importance of including bulk subsurface mechanical effects in modeling "surface" chemistry. O atom adsorption at on-top sites (O bonded to one surface atom), bridge sites (O bonded to two adjacent surface atoms), and ring sites (O bonded to one surface atom and and adjacent subsurface atoms) was investigated. Differences in the relative adsorption energies of O atoms at these adsorption sites on the Si and C-terminated SiC(111) surfaces were calculated, and attributed to the difference in lattice spacing for cubic Si, SiC, and cubic C (diamond) crystals. Adjacent Si atoms on the Si-terminated SiC(111) are 20% *closer together* than on the Si(111)

surface, which favors formation above-surface Si-O-Si bridges. Adjacent C atoms on the C-terminated SiC(111) surface are 20% *farther apart* than on the C(111) surface, which hinders formation of above surface C-O-C adsorption sites. The relative energetics of O atoms on the Si(111) surface was found to behave more like the C-terminated SiC(111) surface than the Si-terminated SiC(111) surface.

6.2 Conclusions

Although it was previously supposed that small molecular clusters would be unable to provide an acceptable representation of the surface of a bulk material in modeling chemical reactions, in several cases investigated in this research, small cluster models were found to work quite well by using MIMOMM. In surface reconstruction, the conventional *ab initio* and MIMOMM optimized geometries of Si_9H_{12} and the Si and C-terminated SiC(111) embedded cluster proved nearly identical. These clusters, while small, are large enough to represent enough of the bulk steric effects to produce a bulk-like surface structure (the MIMOMM result). All clusters three are the smallest *closed-cage* structures one can design for the portion of the surface being modeled. In the absence of any external (MIMOMM) or arbitrarily imposed (fixing atom positions) boundary conditions, a closed cage structure is necessary for accurate modeling of surface reconstruction.

The predictions of optimized geometries of O atoms adsorbed on SiC(111) clusters highlighted the problems involved with using small clusters to simulate the behavior of bulk materials. In general, O atom adsorption caused significant distortion of SiC cluster geometry, with MIMOMM optimized results giving a better representation of bulk behavior. The exception to this trend was O atom adsorption at ontop sites on the Si and C-terminated SiC(111) surface, where the conventional *ab initio* and MIMOMM optimized geometries were virtually identical. (Similar small differences between the conventional *ab initio* and MIMOMM optimized geometries were also observed for H atom ontop adsorption on SiC.) For O atoms at ontop sites, the distortion to the cluster structure caused by the adsorption was minimal. While we are unable to simulate reaction dynamics using MIMOMM, one can conclude that the lack of distortion caused by these adsorptions implies that barriers to these reactions are probably non-existent. On the Si-terminated SiC(111)

surface, the sticking probability for an O atom at an ontop site may be larger than for a bridge site because of the small atomic displacements that are required for an ontop site to form, even though the binding energy at the bridge site is so much larger (-104$\frac{kcal}{mol}$ ontop versus -164$\frac{kcal}{mol}$ bridge), but this cannot be verified with MIMOMM. Unfortunately, because we cannot estimate the barrier heights for these two migration paths, we cannot determine whether bridge site formation or ring insertion is more probable. However, the adsorption energy at the bridge site is much larger than the ring or ontop site (-164$\frac{kcal}{mol}$ bridge, -104$\frac{kcal}{mol}$ ontop, -90$\frac{kcal}{mol}$ ring), so if bridge adsorption sites form, they should be very stable. *Experimentally, one should be able to verify the existence or non-existence of bridge adsorption sites on real Si-terminated SiC(111) surfaces.* Formation of O atoms bridge adsorption sites could passivate the Si-terminated surface, which may contribute to the hypothesized stability of insulating layers grown on Si-terminated SiC surfaces.

O atom adsorption at ontop sites on the C-terminated surface should also have a higher sticking probability than bridge adsorption sites based on considerations of cluster distortion. In addition, the adsorption energy at ontop and bridge sites on the C-terminated surface are quite close (-84$\frac{kcal}{mol}$ ontop versus -89$\frac{kcal}{mol}$ bridge site) when the bulk steric effects in the MIMOMM optimization are included. While we have no information about migration barriers, the adsorption energy of the subsurface ring site is significantly larger than either the ontop or bridge sites (-101$\frac{kcal}{mol}$ ring site, -89$\frac{kcal}{mol}$ bridge, and -84$\frac{kcal}{mol}$ ontop). Thus it seems likely that initial O atom adsorption at an ontop site would be followed by migration subsurface. This migration will lead to a likely precursor for C atom etching by CO_2 elimination, as was discussed in Chapter 5. O atom exposure is unlikely to lead to passivation of the C-terminated SiC(111) surface. Experimentally, one should be able to determine if O atoms are adsorbed preferentially subsurface at low O atom exposures. As the O atom exposure is increased, one should be able to measure CO or CO_2 being desorbed from the surface.

Overall, the use of MIMOMM was demonstrated to enable the study of surface chemistry using physically realistic model systems while requiring practical computation times. A single *ab initio* geometry optimization on a four bilayer SiC cluster is estimated to take more than a full year running on 32 nodes of an IBM SP2 supercomputer. The

equivalent hybrid cluster optimized with MIMOMM required only 24 hours on 32 IBM SP2 nodes.

6.3 Recommended Future Work

Although the basis MIMOMM approach was developed, validated, and applied, further code development, as well as Si and SiC surface chemistry studies are suggested.

6.3.1 Code development. MIMOMM should be implemented using GAMESS and Tinker so that this technique can be made available to the scientific community. Tinker has the ability to use a number of different MM potentials, including user determined potentials. MM potentials are parameterized to reproduce some set of experimental data, so no matter what MM potentials are used, there will always be some mismatch between the MM potentials and the equivalent *ab initio* potentials. It would be useful to develop a process for inputting *ab initio* based potentials into Tinker for use with MIMOMM to eliminate this mismatch. A hybrid QM/MM Hessian calculation needs to be added to the current implementation of MIMOMM to enable the location of transition states and prediction of vibrational frequencies for comparison with spectroscopy. The use of consistent MM potentials consistent with the *ab initio* calculation is likely to be more important for hybrid Hessian calculations and vibrational analyses. The sensitivity of a MIMOMM result as a function of MM potential used should be determined, and used to provide guidance for choice of optimum MM potential for various applications.

The implementation of delocalized coordinates in GAMESS needs to completed. The ability to freeze selected primitive internal coordinates is needed to enable the calculation of reaction barriers. Delocalized coordinates are required for surface cluster calculation using MIMOMM. However, use of delocalized coordinates results in significant time (and frustration) savings to the user in specifying a set of good coordinates. Delocalized coordinates would be quite useful for many types of calculations, such as determination of energy barriers, reaction coordinates, in addition to MIMOMM.

6.3.2 Silicon and SiC surface chemistry models. O atom adsorption reactions were investigated because growth of silicon dioxide insulating layers by exposure to O atoms is one of the primary processes currently being used in the fabrication of silicon and SiC semiconductor devices. Silicon dioxide layers are also grown by exposure to molecular oxygen, and some semi-empirical and DFT theoretical modeling of the adsorption of O_2 on Si(111) has been reported in the literature. It would be very interesting to investigate O_2 adsorption on Si and C-terminated SiC(111) and Si(111) surfaces using MIMOMM. O_2 adsorbed at ontop sites is a likely molecular precursor to surface dissociation. While MIMOMM cannot currently model reaction barriers, from the results already presented we know where the dissociated O atoms are likely to end up. Ultimately, one would like to map out the potential energy surfaces for the various O_2 and O atom adsorption reactions and input them into a molecular dynamics code so that a more realistic simulation of the surface could be performed while modeling chemistry on the surface with reliable reaction potentials.

Experiments characterizing the Si and C-terminated SiC(111) and Si(111) surfaces at low O atom exposures could determine the existence of the predicted stable O atom adsorption sites. Monitoring the exhaust gas in while exposing SiC surfaces to an O atom flux would be an easy way to determining which species, if any, are actually being desorbed. Alternate methods for depositing insulating layers on SiC should be explored.

Appendix A. Definition of terms

ab initio from first principles. *Ab initio* is used to describe computational methods based on solution of Schrödinger's equation for the electronic wavefunction of an atom or molecule.

$\mathring{A}$ angstrom, unit of distance equal to 10^{-10} meters.

Atomic Orbital (AO) one of a family of exact solutions for the electronic wavefunction of the hydrogen atom. Also referred to as a **Basis Function.**

Basis Set a specific collection of basis functions used to describe the electronic wavefunction for atoms in a molecule. The Hay-Wadt Effective Core Potential (HWECP) and 6-31G* are types of basis sets.

B matrix the transformation matrix between displacements in internal coordinates and Cartesian displacements.

Bohr atomic unit of distance, equal to the average ground state separation of the electron and nucleus in atomic hydrogen, $0.530\mathring{A}$.

Bulk Cluster the large, peripheral region of the cluster surrounding the embedded cluster. The bulk cluster, or bulk, does not directly interact with the adsorbate in a chemical reaction, but influences the embedded cluster

Cartesian Coordinates simplest choice of coordinated to specify for a molecule. A molecule has 3N (N is the number of nuclei) Cartesian degrees of freedom, while a nonlinear molecule only has 3N-6 internal degrees of freedom (6 coordinates associated with translation and rotation of the center of mass only affect the net molecular kinetic energy), so some method is typically used to remove optimization steps that involve center of mass motions. Cartesians typically require the largest number of optimization steps because the Hessian in Cartesian coordinates is highly coupled.

Cluster a finite collection of atoms used to simulate a solid. A cluster is generally partitioned into two regions, an Embedded Cluster which is surrounded by a Bulk Cluster

Correlation Energy the correlation energy for a certain state with respect to a specified Hamiltonian is the difference between the exact eigenvalue of the Hamiltonian and its expectation value in the Hartree-Fock approximation for the state under consideration.

Dangling Bond a singly occupied electron MO created by breaking a chemical bond. The term dangling bond is commonly used to refer to such MOs present at surfaces.

Electron Affinity (EA) the energy gained from adding an electron to an atom or molecule

Electron Correlation Schrödinger's equation for the electronic wavefunction of an atom or molecule contains a term which depends on the simultaneous position of two electrons. The motion of one electron depends on the motion of other electrons, thus electronic motion is correlate. The Hartree-Fock form of the electronic wavefunction cannot describe this electron correlation.

Electronegativity χ the power of an atom or molecule to attract electrons to itself. One definition of electronegativity is $\frac{1}{2}$(IP+EA)

Embedded Cluster a small, central subsection of a cluster that is treated at a higher level of approximation in a calculation on the cluster. An embedded cluster corresponds to the notion of an isolated reaction site on a surface.

GTO Gaussian type Orbital. a Gaussian function used to approximate an AO.

$\overline{H}$ an artificial one electron atom that has been modified to have the same electronegativity as the atom to which it is bonded by creating a customized basis set for the $\overline{H}$ atom. Used in place of real H atoms for capping a cluster.

H atom capping/saturation placing H atoms at the lattice locations to which the outermost atoms in the cluster would be bonded in an infinite solid

Hartree atomic unit of energy equal to 27.2 electron Volts (eV).

Hybrid Cluster the combination of the embedded and bulk clusters.

Internal Coordinates this type of molecular coordinates is referred to as model builder or primitive internals, and includes stretches, bends, and torsions. These are commonly used because they involve natural "chemical" parameters to describe molecular geometry. A good set of internal coordinates will produce a diagonal dominant Hessian.

Ionization Potential (IP) the energy required to remove an electron from an atom or molecule.

$\frac{kcal}{mol}$ one kilocalorie per mole, equal to 0.04 eV per molecule.

LCAO-MO approximate MO constructed from a Linear Combination of Atomic Orbitals

Molecular Mechanics (MM) a description of molecular structure based on classical inter-atomic interaction potentials such as bond stretches, bond angle ends, torsional twisting, etc.

Molecular Orbital (MO) hypothetical eigenfunction of the wave equation for a multi-electron molecule.

MP2 Möller-Plesset second order perturbation method. This technique is a perturbation expansion of the uncorrelated Hartree-Fock wavefunction to calculate the second order correction to the energy, recovering a large fraction of the correlation energy. (The first order perturbation correction to the energy is zero.)

Natural Internal Coordinates (NIC) these coordinated are a type of local symmetry coordinates developed by Pulay [70, 71] based on localized normal modes within a molecule.

Normal Mode Coordinates A set of 3N-6 (3N-5 for linear molecules) orthogonal coordinates that correspond to the spectroscopic normal vibrational modes of a molecule, where N is the number of nuclei in the molecule. Because normal modes are orthogonal, the Hessian is diagonal, so an optimization in normal mode coordinates is quite efficient. The drawback of normal mode coordinates is that they must be calculated,

which is often more time consuming than performing an optimization using a poorer set of coordinates.

Periodic Boundary Conditions the use of symmetry to connect the outermost atoms in a cluster to each other to simulate an infinite material. For example, the atoms on the right side of the cluster would be specified to be bonded to atoms on the left side of the cluster. In one dimension, this corresponds to making a linear chain of atoms into a ring.

Polytype a specific form of SiC defined by the number of layers stacked along the z axis. For example, in the 4H polytype is SiC, the position of layers repeats after 4 layers.

Slab a section of a surface several atoms layers deep and 10 to 20 atoms wide. This structure is repeated periodically in two horizontal dimensions to simulate an infinite surface

Steric relating to the arrangement of atoms in space. Large molecules can assume a number of conformations in space without breaking chemical bonds. However, effects such as atoms having to move close to each other restricts the conformations that the molecule can actually achieve.

STO Slater type Orbital. an approximate AO used in molecular wavefunction calculations.

STO-nG A STO approximated with an expansion of n Gaussians

Surface Reconstruction the change in surface structure away from the lattice positions for the surface atoms, also a particular surface structure

Symmetry Coordinates this is a general class of molecular coordinates that are linear combinations of primitive internal coordinates. The secular equation describing the vibrational energy of a molecule is factored to the maximum extent possible by the use of symmetry [69].

Termination the boundary condition imposed on the outermost atoms in a cluster to simulate the presence of an infinite solid. Without termination, the cluster as a whole would be a radical, i.e., possessing unpaired electrons, and would act like a chemically different species than the non radical solid to be simulated.

Appendix B. List of Symbols

Symbol	Definition
$\mathbf{B}$	transformation matrix between internal and Cartesian coordinates
B	Bohr
$\overline{\overline{\mathbf{C}}}$	matrix of coefficients of the atomic orbitals
eV	electron volt
EA	electron affinity
E_{AI}	*ab initio* energy of hybrid system
E_{MM}	molecular mechanics energy of hybrid system
$\overline{\overline{\mathbf{F}}}$	matrix representation of Fock Hamiltonian
$\mathbf{G}$	spectroscopic G matrix
H	Hartree, atomic unit of energy = 27.2 electron volts
$\hat{\mathcal{H}}_0$	the Hartree Fock Hamiltonian
IP	ionization potential
$J[\rho]$	DFT Coulomb interaction functional
kcal	kilo-calorie
M_A	mass of nuclei A
n^*	effective quantum number
$nvar$	number of internal coordinates specified for a molecule
N	number of nuclei in a molecule
$P_{\mu\nu}$	elements of the density matrix
q_μ	gross population for each basis function ϕ_μ
q_A	atomic Mulliken population
Q_A	atomic charge
$\vec{r}$	electron coordinate
r_{ij}	separation between electrons i and j
r_{iA}	separation between electron i and nuclei A
R	Radian
$\vec{R}$	nuclear coordinate
R_{AB}	separation between nuclei A and B

Symbol	Definition
$R_{nl}(r)$	radial part of electronic wavefunction
$\overline{\overline{\mathbf{S}}}$	overlap matrix of the atomic orbitals
$S_{\mu\nu}$	elements of the overlap matrix
S_t	one of the *nvar* internal coordinates
$T[\rho]$	density functional theory (DFT) kinetic energy functional
$V_{xc}[\rho]$	DFT exchange-correlation functional
$\hat{\mathcal{V}}$	perturbation term to the zeroth order energy
Z_A	charge of nuclei A
χ	electronegativity
χ_i	spin orbital, product of spatial and spin wavefunctions
$\vec{\varepsilon}$	eigenvalues of Roothaan equations
ϕ_j	atomic orbital j
ϕ_{1s}^{GF}	1s Gaussian function
ϕ_{1s}^{SF}	1s Slater orbital
ϕ_{1s}^{STO-NG}	Slater orbital expanded with N Gaussian functions
$\rho(\vec{r})d\vec{r}$	probability of finding an electron in volume element $d\vec{r}$
$\Psi(\vec{r})$	electronic wavefunction
$\Psi(\vec{R},\vec{r})$	total molecular wavefunction
$\Psi^{VB}(1,2)$	valence bond wavfunction for electrons 1 and 2
$\Psi^{HF}(1,2)$	Hartree-Fock wavefunction for electrons 1 and 2
$\Psi^{GVB}(1,2)$	generalized valence bond wavefunction for electrons 1 and 2
ζ	orbital scaling parameter in a 1s Slater orbital
ζ_i	one of 3N Cartesian displacements
$\mathring{A}$	Angstrom

Appendix C. SiC Model System Energies

The following tables are compilations of the relevant results from chapter 5. Table C.1 contains the energies for the small molecules used for comparisons with the cluster reactions. Table C.2 contains the Hartree-Fock results for the Si-terminated SiC(111) cluster, and Table C.3 contains the MP2 results. Table C.4 contains the Hartree-Fock results for the C-terminated SiC(111) cluster, and Table C.5 contains the MP2 results. Table C.6 contains the Hartree-Fock results for the Silicon(111) cluster.

Small Molecule Models			
		Energy (H)	
Molecule	Model	HF	MP2
H	^{2}ROHF	-0.498233	-0.498233
C	^{3}ROHF	-37.677126	-37.732769
O	^{3}ROHF	-74.778966	-74.879847
Si	^{3}ROHF	-288.829374	-288.874528
H_2	^{1}RHF	-1.126828	-1.144100
CO	^{1}RHF	-112.737870	-113.018033
CO_2	^{1}RHF	-187.634176	-188.102190
$CH_3^\bullet$	^{2}ROHF	-39.554764	-39.668170
$CH_3O^\bullet$	^{2}ROHF	-114.416236	-114.685746
H_3COCH_3	^{1}RHF	-154.007462	-154.502071
$SiH_3^\bullet$	^{2}ROHF	-290.604753	-290.675345
$SiH_3O^\bullet$	^{2}ROHF	-365.491980	-365.709630
$H_3SiOSiH_3$	^{1}RHF	656.254320	-656.588294

Table C.1 6-31G* energies of small molecules used in reaction caculations.

Si-terminated SiC(111) Cluster

$Si_9C_{13}H_{25}$

Surface	Model	Hartree-Fock Energy (H) *ab initio*	MIMOMM 2 Bilayer	MIMOMM 4 Bilayer
Reconstruction				
Bare	^{4}ROHF	-3107.287434	-3107.285539	-3107.286685
Bare	^{2}*ROHF*	-3107.231180	-	-3107.216090
Bare	^{2}GVB-PP(1)	-3107.285713	-	-
Si Vacancy				
$Si_8C_{13}H_{25}$	^{4}ROHF	-2818.200471	-	-2818.193653
$Si_8C_{13}H_{25}$	^{2}ROHF	-2818.165306	-	-
$Si_8C_{13}H_{25}$	^{2}GVB-PP(1)	-2818.165313	-	-
Hydrogenation				
H-Si ontop	^{3}ROHF	-3107.907559	-3107.905638	-
$(H\text{-}Si)_2$ ontop	^{2}ROHF	-3108.527959	-3108.526036	-
$(H\text{-}Si)_3$ ontop	^{1}RHF	-3109.146875	-3109.146875	-
Oxidation				
O-Si ontop	^{4}ROHF	-3182.185212	-3182.183299	-
Si-O-Si bridge	^{2}ROHF	-3182.236653	-3182.227517	-3182.217861
Si-O-C ring	^{4}ROHF	-3182.146984	-	-3182.137410
O_{ontop}-Si-O_{ring}-C	^{4}ROHF	-3257.051971	-	-
Si-O-C ring	^{2}ROHF	-3182.083401	-	-3182.070495
Si-O-C ring	^{2}GVB	-3182.083407	^{2}ROHF orbitals	
Si-O-C ring	^{2}GVB	-3182.083407	Huckel orbitals	

		HF Adsorption Energy ($\frac{kcal}{mol}$)		
Hydrogenation				
Cluster + nH(g)	^{4}ROHF	0.0	0.0	0.0
$(H\text{-}Si)_{n=1}$	^{3}ROHF	-76.5	-76.5	-
$(H\text{-}Si)_{n=2}$	^{2}ROHF	-153.1 (-76.7)	-153.1 (-76.7)	-
$(H\text{-}Si)_{n=3}$	^{1}RHF	-230.0 (-76.8)	-230.0 (-76.9)	-
Oxidation				
Cluster + O(g)		0.0	0.0	0.0
O-Si ontop	^{4}ROHF	-74.5	-74.5	-
Si-O-Si bridge	^{2}ROHF	-106.8	-102.3	-92.5
Si-O-C ring	^{4}ROHF	-50.6	-	-45.0
Cluster + 2O(g)		0.0	0.0	0.0
O_{ontop}-Si-O_{ring}-C	^{4}ROHF	-129.6	-	-
Si vacancy	^{4}ROHF	+161.6	-	+165.4

Table C.2 Hartree-Fock (6-31G*) energetics of Si-terminated SiC(111) clusters used in this work

Si-terminated SiC(111) Cluster

$Si_9C_{13}H_{25}$

Surface	Model	MP2 Energy (H) *ab initio*	MIMOMM 2 Bilayer	MIMOMM 4 Bilayer
Reconstruction				
Bare	^{4}ROHF	-3109.704721	-3109.704177	-3109.704136
Si Vacancy				
$Si_8C_{13}H_{25}$	^{4}ROHF	-2820.514745	-	-2820.512337
Hydrogenation				
H-Si ontop	^{3}ROHF	-3110.335152	-	-
$(H\text{-}Si)_2$ ontop	^{2}ROHF	-3110.965989	-	-
$(H\text{-}Si)_3$ ontop	^{1}RHF	-3111.596687	-	-
Oxidation				
O-Si ontop	^{4}ROHF	-3184.750274	-3184.749495	-
Si-O-Si bridge	^{2}ROHF	-3184.862621	-3184.855145	-3184.844983
Si-O-C ring	^{4}ROHF	-3184.736188	-	-3184.726279
O_{ontop}-Si-O_{ring}-C	^{4}ROHF	-3259.788683	-	-

		MP2 Adsorption Energy ($\frac{kcal}{mol}$)		
Hydrogenation				
Cluster + nH(g)	^{4}ROHF	0.0	0.0	0.0
$(H\text{-}Si)_{n=1}$	^{3}ROHF	-82.9	-	-
$(H\text{-}Si)_{n=2}$	^{2}ROHF	-166.1 (-83.2)	-	-
$(H\text{-}Si)_{n=3}$	^{1}RHF	-249.2 (-83.1)	-	-
Oxidation				
Cluster + O(g)		0.0	0.0	0.0
O-Si ontop	^{4}ROHF	-104.0	-103.8	-
Si-O-Si bridge	^{2}ROHF	-174.5	-170.1	-163.8
Si-O-C ring	^{4}ROHF	-95.1	-	-89.3
Cluster + 2O(g)		0.0	0.0	0.0
O_{ontop}-Si-O_{ring}-C	^{4}ROHF	-203.5	-	-
Si vacancy	^{4}ROHF	+197.9	-	+199.1

Table C.3 MP2 (6-31G*) energetics of Si-terminated SiC(111) clusters used in this work

C-terminated SiC(111) Cluster

$C_9Si_{13}H_{25}$

Surface	Model	Hartree-Fock Energy (H) *ab initio*	MIMOMM 2 Bilayer	MIMOMM 4 Bilayer
Reconstruction				
Bare	^{4}ROHF	-4111.394766	-4111.393840	-4111.393770
Bare	^{2}ROHF	-4111.297933	-	-
Bare	^{2}GVB	-4111.297916	^{2}ROHF orbitals	
Bare	^{2}GVB	-4111.297916	Huckel orbitals	
Bare	^{2}GVB-PP(1)	DNC	-	-
C Vacancy				
$C_8Si_{13}H_{25}$	^{4}ROHF	-4073.482303	-	-4073.464211
Hydrogenation				
H-C ontop	^{3}ROHF	-4112.027434	-4112.026682	-
$(H\text{-}C)_2$ ontop	^{2}ROHF	-4112.659983	-4112.659353	-
$(H\text{-}C)_3$ ontop	^{1}RHF	-4113.292397	-4113.291888	-
Oxidation				
O-C ontop	^{4}ROHF	-4186.238773	-4186.237856	-
C-O-C bridge	^{2}ROHF	-4186.189023	-4186.175370	-4186.163413
C-O-Si ring	^{4}ROHF	-4186.266287	-	-4186.255885
O_{ontop}-C-O_{ring}-Si	^{4}ROHF	-4261.127424	-	-
C-O-Si ring	^{2}ROHF	-4186.216075	-	-4186.201713
C-O-Si ring	^{2}GVB	-4186.216087	^{2}ROHF orbitals	

		HF Adsorption Energy ($\frac{kcal}{mol}$)		
Hydrogenation				
Cluster + nH(g)	^{4}ROHF	0.0	0.0	0.0
$(H\text{-}C)_{n=1}$	^{3}ROHF	-84.3	-84.5	-
$(H\text{-}C)_{n=2}$	^{2}ROHF	-168.6 (-84.3)	-168.8 (-84.36)	-
$(H\text{-}C)_{n=3}$	^{1}RHF	-252.8 (-84.2)	-253.1 (-84.29)	-
Oxidation				
Cluster + O(g)		0.0	0.0	0.0
O-C ontop	^{4}ROHF	-40.8	-40.8	-
C-O-C bridge	^{2}ROHF	-9.6	-1.7	+5.8
C-O-Si ring	^{4}ROHF	-58.1	-	-52.2
Cluster + 2O(g)		0.0	0.0	0.0
O_{ontop}-C-O_{ring}-Si	^{4}ROHF	-109.0	-	-
C vacancy	^{4}ROHF	+147.7	-	+158.4

Table C.4 Hartree-Fock (6-31G*) energies of C-terminated SiC(111) clusters used in this work

C-terminated SiC(111) Cluster

$C_9Si_{13}H_{25}$

Surface	Model	MP2 Energy (H) *ab initio*	MIMOMM 2 Bilayer	MIMOMM 4 Bilayer
Reconstruction				
Bare	^{4}ROHF	-4113.591320	-4113.590790	-4113.590379
C Vacancy				
$C_8Si_{13}H_{25}$	^{4}ROHF	-4075.561578	-	-4075.553303
Hydrogenation				
H-C ontop	^{3}ROHF	-4112.027434	-	-
$(H\text{-}C)_2$ ontop	^{2}ROHF	-4112.659983	-	-
$(H\text{-}C)_3$ ontop	^{1}RHF	-4115.565393	-	-
Oxidation				
O-C ontop	^{4}ROHF	-4188.605864	-4188.605138	-
C-O-C bridge	^{2}ROHF	-4188.632281	-4188.621922	-4188.611703
O_{ontop}-C-O_{ring}-Si	^{4}ROHF	-4263.674058	-	-

		MP2 Adsorption Energy ($\frac{kcal}{mol}$)		
Hydrogenation				
Cluster + nH(g)	^{4}ROHF	0.0	0.0	0.0
$(H\text{-}C)_{n=1}$	^{3}ROHF	-100.2		-
$(H\text{-}C)_{n=2}$	^{2}ROHF	-200.5 (-100.3)	-	-
$(H\text{-}C)_{n=3}$	^{1}RHF	-300.8 (-100.3)	-	-
Oxidation				
Cluster + O(g)		0.0	0.0	0.0
O-C ontop	^{4}ROHF	-84.5	-84.4	-
C-O-C bridge	^{2}ROHF	-101.1	-94.9	-88.8
C-O-Si ring	^{4}ROHF	-106.9	-	-101.0
Cluster + 2O(g)		0.0	0.0	0.0
O_{ontop}-C-O_{ring}-Si	^{4}ROHF	-202.7	-	-
C vacancy	^{4}ROHF	+186.4	-	+191.0

Table C.5 MP2 (6-31G*) energies of C-terminated SiC(111) clusters used in this work

Silicon(111) Cluster

$Si_{22}H_{25}$

Surface	Model	Hartree-Fock Energy (H) *ab initio*	MIMOMM 3 Bilayer
Reconstruction			
Bare	^{4}ROHF	-6370.850792	-
Si Vacancy			
$Si_{21}H_{25}$	^{4}ROHF	-6081.888239	-6081.870402
Hydrogenation			
H-Si ontop	^{3}ROHF	-6371.850792	-
$(H\text{-}Si)_2$ ontop	^{2}ROHF	6372.066296	-
$(H\text{-}Si)_3$ ontop	^{1}RHF	-6372.674192	-
Oxidation			
O-Si ontop	^{4}ROHF	-6445.722146	*AM1 saddle pt*
Si-O-Si bridge	^{2}ROHF	-6445.761154	-6445.737058
Si-O-Si ring	^{4}ROHF	-6445.777182	-6445.770469
O_{ontop}-Si-O_{ring}-Si	^{4}ROHF	-6520.667840	-

		HF Adsorption Energy ($\frac{kcal}{mol}$)	
Hydrogenation			
Cluster + nH(g)	^{4}ROHF	0.0	0.0
$(H\text{-}Si)_{n=1}$	^{3}ROHF	-68.70	-
$(H\text{-}Si)_{n=2}$	^{2}ROHF	-137.45 (-68.75)	-
$(H\text{-}Si)_{n=3}$	^{1}RHF	-206.26 (-68.81)	-
Oxidation			
Cluster + O(g)		0.0	0.0
O-Si ontop	^{4}ROHF	-58.0	-
Si-O-Si bridge	^{2}ROHF	-82.4	-67.3
Si-O-Si ring	^{4}ROHF	-92.5	-88.3
Cluster + 2O(g)		0.0	0.0
O_{ontop}-Si-O_{ring}-Si	^{4}ROHF	-162.6	-
Si Vacancy	^{4}ROHF	+83.6	+94.8

Table C.6 Hartree-Fock (6-31G*) energies of silicon(111) clusters used in this work

Appendix D. Generation and use of Delocalized Coordinates

This appendix discusses the use of the program Deloc.x to generate set of delocalized coordinates as described by Baker et al [10]. The main driver program, delocal.f, is fairly well commented. Source code of this program is included at the end of this appendix. The names of the subroutines copied from GAMESS that must be linked with delocal.o are listed, but only the modifications to these routines are listed. *Delocal.x does not give useful error messages from crashes due to errors in the input file, or due to the limits set on the B matrix etc being too small for the molecule being considered.*

There are three basic steps in the generation of dlcs:

1. Generate a set of primitive internal coordinates (PIC), bond stretches, bond angles, and torsional angles
2. Calculate and diagonalize the G matrix for this set of coordinates *without inverse mass weighting* (This requires a change in the GAMESS subroutine GINV).
3. Write a $ZMAT card for GAMESS

Modifications to several GAMESS routines are required to enable use of DLCs.

D.1 Generation of DLCs

This DLC generation code is another GAMESS/MM3 merger. I copied and modified the routines in MM3 that read the lists of connected an attached atoms and define all possible stretches, bends, and torsions. I then set up an GAMESS IZMAT array and use the appropriate routines from GAMESS (with minor modifications) to calculate the B matrix, and create and diagonalize the G matrix. The column vectors of the G matrix that correspond to non-zero eigenvalues become the DLCs.

D.1.1 Source Code Description. The following routines were copied from MM2, collected in the main driver program delocal.f, and modified

```
C       SUBROUTINE BONDTB                MM2
C       SUBROUTINE THETA                 MM2
C       SUBROUTINE OMEGA                 MM2
C       SUBROUTINE KSORT(NK,K,KK)        MM2
C       FUNCTION IPACK4(M,I,J,K,L)       MM2
C       SUBROUTINE UNPACK4               MM2
```

delocal.f is fairly well commented. The reader is directed to the source code for more details.

The following routines from GAMESS must be linked with delocal:

```
 9598 Sep 25  1996 abrt.f
 5619 Sep 25  1996 bend.f
16739 Sep 25  1996 blas.f
 6181 Sep 25  1996 bmat.dlc.f
 1027 Sep 25  1996 bstr.f
 1398 Sep 25  1996 cstr.f
 3516 Sep 25  1996 dgedi.f
 2787 Sep 25  1996 dgefa.f
 2172 Sep 25  1996 dgop.f
74411 Sep 25  1996 eigen.f
 2163 Sep 25  1996 fillzm.f
 6277 Jun  8 11:29 ginvr.dlc.f
  964 Sep 25  1996 nxtval.f
  927 Sep 25  1996 prsq.f
  276 Sep 25  1996 synch.f
 1801 Sep 25  1996 tfsqu.f
 3267 Sep 25  1996 tors.f
 2601 Sep 25  1996 trang.f
  458 Sep 25  1996 vclr.f
 4991 Sep 25  1996 zmat2.f
```

eigen.f and blas.f are complete GAMESS modules. The diagonalization of the G matrix used so many subroutines from these modules that is was easier to use them in their entirety. The other files are individual subroutines copied from GAMESS modules.

bmat.dlc.f and ginvr.dlc.f are modifications of the GAMESS routines of the same name. The bulk of the modifications involve commenting out operations not needed, like writing the IZMAT array to scratch file, calculating the B inverse matrix, etc. The rest of the modifications are mainly for writing diagnostic information to the screen. The modifications are easy to find by diff'ing these files against the original GAMESS source code.

D.1.2 Using Delocal.x. Figure D.1 shows an input file for the program Delocal.x. *This input file is for fluoroethylene, the example described in exquisite in Baker's paper [10]. The eigenvalues of the G matrix, the DLCs, etc generated by Delocal.x can be directly compared with the results in this paper.*

The first line of the input file is an 80 character header. The second line gives the number of atoms. Line 3 gives the number of Connected Atom Lists, which are given in Lines 4 through 9. The line after the last Connected Atom List gives the number of Attached Atom lists, which are listed in the following two lines. In the MMn series of programs, a connected atom is bonded to more than one atom, while an attached atom

is bonded to only one atom. (The format for the connected and attached atom lists is column specific, and can be found in delocal.f.) The line after the attached atom lists defines the unit used in the Cartesian coordinates for the atoms, ANGSTROM or BOHR. The Cartesian coordinates for the atoms in GAMESS Cartesian format comes last.

NOTE: Some care is needed in defining connected atom lists. If the same atom pair is given in more than one connected atom list, the PIC assignment algorithm from MM2 will likely blowup.

```
FLUOROETHYLENE Test case from Baker's paper          HEADER A80
NAT            6                                     12X I3
NCON LISTS     3                                     12X I3
    3    1     4
    5    2     6
    1    2
NATTCH         0                                     12X I3
ANGSTROM
C       6.0   -0.061684    0.67379   0.00000
C       6.0   -0.061684   -0.72621   0.00000
F       9.0    1.174443    1.33105   0.00000
H       1.0   -0.927709    1.17379   0.00000
H       1.0   -0.927709   -1.22610   0.00000
H       1.0    0.804342   -1.22610   0.00000
```

Figure D.1 Fluorethylene input file for program Delocal.x

When you execute Delocal.x, you will be asked for the input file name. The program read the input file, defines a set of internal coordinates and echoes them to the screen. The B and G matrices are then calculated, and the G matrix is diagonalized, with the eigenvalues of the G matrix echoed to the screen. There will be *EXACTLY* 3N-6 numerically non-zero eigenvalues of the G matrix. Delocal.x then creates a file named ZMAT that contains a $ZMAT deck for the GAMESS input file, and writes an additional $CONTRL card with the appropriate value for NZVAR.

Figure D.2 shows the information dumped to the screen while generating DLCs for fluoroethylene. Figure D.3 is the $ZMAT deck that is created in the file ZMAT.

D.2 Frozen Primitive Coordinates in DLCs

One can freeze individual primitive coordinates when using DLCs; however, this will require more extensive modifications GAMESS. As described in Reference [10]:

```
 INPUT FILE NAME =
Fluoro.dlc
    ATOM     TYPE     CHARGE     MASS (AMU)
      1       C        6.00       12.0000
      2       C        6.00       12.0000
      3       F        9.00       18.9984
      4       H        1.00        1.0078
      5       H        1.00        1.0078
      6       H        1.00        1.0078

 NUMBER OF BONDS                 5
 NUMBER OF ANGLES                6
 NUMBER OF TORSIONS              4
 TOTAL NUMBER OF PRIMITIVES      15

 LENGTH OF IZMAT ARRAY           60

                 IZMAT ARRAY

    IZMAT(1)=
       1,     1,     2,
       1,     1,     3,
       1,     1,     4,
       1,     2,     5,
       1,     2,     6,
       2,     2,     1,     3,
       2,     2,     1,     4,
       2,     3,     1,     4,
       2,     1,     2,     5,
       2,     1,     2,     6,
       2,     5,     2,     6,
       3,     3,     1,     2,     5,
       3,     3,     1,     2,     6,
       3,     4,     1,     2,     5,
       3,     4,     1,     2,     6,

   INTERNAL COORDINATES            G Matrix Diagonalization
  1    2.6456163828106          Eigenvalue  1   -2.7794929616583D-16
  2    2.6456168334623          Eigenvalue  2   -9.6603238681852D-17
  3    1.8897253269082          Eigenvalue  3    8.3253051443601D-18
  4    1.8896214005176          Eigenvalue  4   0.25282297912648
  5    1.8896230371584          Eigenvalue  5   0.40164265930883
  6    2.0594882747752          Eigenvalue  6   0.62952826897820
  7    2.0943953042855          Eigenvalue  7   0.89161474745617
  8    2.1293017281189          Eigenvalue  8   0.95520136151152
  9    2.0943000362294          Eigenvalue  9    1.1555879572794
  10    2.0942995362845         Eigenvalue  10    2.0228419499204
  11    2.0945857346657         Eigenvalue  11    2.3717845988896
  12    3.1415926535898         Eigenvalue  12    2.6162906671169
  13  0.                        Eigenvalue  13    3.9764819217071
  14  0.                        Eigenvalue  14    4.2059895026748
  15    3.1415926535898         Eigenvalue  15    4.7120460400846
                                NUMBER OF ZEROES IN G MATRIX   3
```

Figure D.2 Screen dump from DLC generation for fluoroethylene

```
 $ZMAT      IZMAT(1)=
      1,     1,     2,
      1,     1,     3,
      1,     1,     4,
      1,     2,     5,
      1,     2,     6,
      2,     2,     1,     3,
      2,     2,     1,     4,
      2,     3,     1,     4,
      2,     1,     2,     5,
      2,     1,     2,     6,
      2,     5,     2,     6,
      3,     3,     1,     2,     5,
      3,     3,     1,     2,     6,
      3,     4,     1,     2,     5,
      3,     4,     1,     2,     6,
 IJS(1)=
   666,666
 SIJ(1)=
-.1751, -.1135, 0.1134, 0.0157, -.0771, -.6251, 0.4187, 0.2064,
0.3649, -.4365, 0.0716, 0.0000, 0.0000, 0.0000, 0.0000,
-.6979, -.0848, -.1289, -.1851, -.0625, -.0718, -.3045, 0.3763,
-.3388, 0.0291, 0.3097, 0.0000, 0.0000, 0.0000, 0.0000,
0.1283, -.2241, 0.3893, -.3307, 0.3723, -.3243, 0.2708, 0.0535,
-.3822, 0.4493, -.0670, 0.0000, 0.0000, 0.0000, 0.0000,
-.1325, -.6505, -.4710, -.0155, 0.0802, 0.1267, 0.3126, -.4394,
-.0770, -.0480, 0.1250, 0.0000, 0.0000, 0.0000, 0.0000,
-.0640, -.0876, -.0810, -.5975, -.5938, 0.0066, 0.0143, -.0209,
0.2124, 0.2129, -.4254, 0.0000, 0.0000, 0.0000, 0.0000,
0.0000, 0.0000, 0.0000, 0.0000, 0.0000, 0.0000, 0.0000, 0.0000,
0.0000, 0.0000, 0.0000, 0.7286, 0.5664, 0.3411, 0.1789,
0.0000, 0.0000, 0.0000, 0.0000, 0.0000, 0.0000, 0.0000, 0.0000,
0.0000, 0.0000, 0.0000, -.4423, 0.1461, 0.2581, 0.8464,
-.1276, 0.1555, 0.5365, -.1595, -.3372, 0.2215, 0.2127, -.4342,
-.1963, -.2116, 0.4079, 0.0000, 0.0000, 0.0000, 0.0000,
0.0045, -.5471, 0.3880, 0.5470, -.3996, 0.0180, -.1623, 0.1444,
-.0409, 0.1639, -.1230, 0.0000, 0.0000, 0.0000, 0.0000,
0.5590, 0.0390, -.3363, -.0095, -.4270, -.2487, 0.0522, 0.1964,
-.3783, -.0015, 0.3798, 0.0000, 0.0000, 0.0000, 0.0000,
0.3397, -.4169, 0.1976, -.4173, 0.1918, 0.1957, -.3912, 0.1955,
0.1957, -.3926, 0.1970, 0.0000, 0.0000, 0.0000, 0.0000,
0.0000, 0.0000, 0.0000, 0.0000, 0.0000, 0.0000, 0.0000, 0.0000,
0.0000, 0.0000, 0.0000, 0.1535, -.6386, 0.7530, -.0392,
 $END
 $CONTRL NZVAR=  15 $END
```

Figure D.3 $ZMAT deck for fluoroethylene DLCs

What is done is to take a unit vector with unit component corresponding to the primitive internal (stretch, bend, or torsion) that one wishes to keep constant. This vector is then projected onto the full active subspace, normalized, and then all (n, say) active vectors are Schmidt orthogonalized in turn to the normalized, projected constraint vector. The last vector taken in the active space should drop out (since it will be linearly dependent on the other vectors and the constraint vector) leaving (n-1) active vectors and one constraint vector.

The calculation of the nuclear displacements in the optimization process and the iterative conversion of internal coordinates to Cartesians uses different combination of the original DLCs and the Schmidt orthogonalized set. This will require a change in the storage of the S matrix in GAMESS, and probably a separate subroutine to update coordinates using DLCs. One will also need to store the S inverse matrix to track the values of the PICs to correct for sign changes in bends and torsions in the iterative conversion of internals to Cartesians. Frozen PICs was not implemented in this work due to time constraints.

D.3 Modifications to GAMESS to enable the use of DLCs

D.3.1 Reading the $ZMAT deck. First, the symmetry matrix is quite large , so the number of NIJs needs to be increased. **Note: Line numbers listed are slightly different from the lines numbers in GAMESS source code.**

```
1841 C*MODULE ZMATRX  *DECK ZMATIN
1842        SUBROUTINE ZMATIN
1843        IMPLICIT DOUBLE PRECISION(A-H,O-Z)
1844        PARAMETER (MXATM=500)
1845        COMMON /FMCOM / X(1)
1846        COMMON /INFOA / NAT,ICH,MUL,NUM,NX,NE,NA,NB,ZAN(MXATM),C(3,MXATM)
1847 C
1848 C      ----- GROW FAST MEMORY FOR $ZMAT READING -----
1849 C
1850        NELS = 30*MAX(3*NAT-6,1)
1851 C
1852 C       NIJS = 6*3*NAT
1853 C
1854 c    JRS mod for DLC's
1855 c
1856        NIJS=100*6*3*NAT
1857 C
```

For other types of symmetry coordinates, the $ZMAT deck contains both the indices of the non-zero elements of the symmetry matrix as well as the non-zero values. For DLCs, all elements of the symmetry matrix are non-zero, so writing the indices of the whole matrix is a waste of space. Mike Schmidt has added a hidden option, dlc=.t., and modified ZMATRX:ZMTSYM read only the SIJs. My approach was to write 666,666 as the

only two elements for the IJs, and read the SIJs accordingly. Here's my code modifications

:

```
C*MODULE ZMATRX  *DECK ZMTSYM
      SUBROUTINE ZMTSYM(S,SIJ,IJS,IZMAT,IZMAT2,NZVAR,
     *                  N3NM6,NZMAT,NIJS,SYM)

c
c  DLC: don't enter all ijs in input file for full matrix
c
      if( (ijs(1,1).eq.666) .and. (ijs(2,1).eq.666)) then
        SYM=.TRUE.
        ictr=1
        do 600 i=1,nzvar*(3*nat-6)
          s(ictr)=sij(ictr)
          ictr=ictr+1
  600   continue
        goto 630
      endif
c
      DO 70 N = 1,NIJS
         I = IJS(1,N)
         J = IJS(2,N)
         SVAL = SIJ(  N)
C  ARE ALL VALUES BETWEEN 0-NZVAR?
         IF (      I) 120,70,30
   30    IF (NZVAR-I) 120,40,40
   40    IF (      J) 120,70,50
   50    IF (NZVAR-J) 120,60,60
   60    CONTINUE
         IJ = NZVAR*(J-1) + I
         S(IJ) = SVAL
         SYM = .TRUE.
   70 CONTINUE
c
  630 continue
c
```

D.4 Modifications to the iterative process to convert internals to cartesians

In 1993, Theresa Windus added an iterative scheme to convert optimization displacements in internal coordinates to updated Cartesian coordinates. In this iterative process, bond and torsion angles can switch from 180-δ to -180+δ. This means that the difference between the old coordinate value and the new value can get very large, from subtraction of a negative number. There are some checks on the value of a given change in coordinate based on the magnitude of the coordinate, i.e., if the value of the change is close to 2 π, the actual change is redefined as the difference between this value and 2 π. *This correction is actually wrong for symmetry coordinates.* Spectroscopic symmetry coordinates and Natural Internal Coordinates do not use many torsion angles, so their values are smaller than

the limits defined for this correction, so they do not trip this condition. DLCs include a large number of torsions, so their values can get large enough to trip this condition, which ends up producing wrong Cartesian coordinates, and the optimization soon diverges.

The right way to handle this is to invert the S matrix for the DLCs and track the iterative conversion process in PICs, then convert back to DLCs. The workaround I came up with is that when this condition is tripped, the iterative conversion process is aborted. This means that the conversion from internals to Cartesians isn't as good as it should be, but in limited testing this condition happened about once every 10 optimization cycles, so the optimization isn't affected too much.

```
C*MODULE STATPT  *DECK UPDISP
      SUBROUTINE UPDISP(DELCOR,NCVAL,NCOORD,DXMAXT,OUT,ITBMAT)

C    ITERATE AS IN PULAY AND COWORKERS, JACS, 101, 2550 (1979)
C    EXCEPT CHANGING THE B MATRIX AND ITS INVERSE IN EACH ITERATION
C
      DO 100 I = 1,ITBMAT
        CALL TFDS(DELCOR,NCVAL,NCOORD)
        CALL VADD(XX(LXCOR),1,DELCOR,1,XX(LXCOR),1,NCOORD)
        CALL DCOPY(NCOORD,XX(LXCOR),1,C,1)
        CALL BANDBI
        CALL DAREAD(IDAF,IODA,XX(LQNEW),NCVAL,INZMAT,0)
        CALL VSUB(XX(LQNEW),1,XX(LQ0),1,DELCOR,1,NCVAL)
c
c
C
C    CORRECT FOR DISPLACEMENTS THAT GO OVER 180 AND 360 DEGREES. (TLW)
C
c
C
c
c  This check screws up DLC's, as they are linear combinations of all
c  coordinates, including TORSIONS, and can have absolute values large
c  enough to  trigger this check
c
c  Actually, this check could screw up any symmetry coordinates, but most
c  normal symmetry coords don't include many torsions and so happen to miss
c  this check just by luck
c
c  Just zeroing out differences on those coordinates that were two large mixed
c  weird, finite displacements into all the Cartesians, which caused bad steps.
c  Now, if the difference is too large, we just skip the iterative procedure and
c  live with a larger error  in the coordinate conversion on those steps

c
      if (sym)  then
        do 500 j=1,ncval
           if (abs(delcor(j)).gt.(0.1d0)) then
              goto 101
           end if
  500   continue
```

```
4991          goto 51
4992        endif
4993 c
4994 c
4995 c
4996          DO 50 J = 1,NCVAL
4997             IF (ABS(DELCOR(J)).GT.(TWO*PI-ONE)) THEN
4998                IF (DELCOR(J).LT.ZERO) THEN
4999                   DELCOR(J) = DELCOR(J) + TWO*PI
5000                ELSE
5001                   DELCOR(J) = DELCOR(J) - TWO*PI
5002                END IF
5003             END IF
5004             IF (ABS(DELCOR(J)).GT.(PI-ONE)) THEN
5005                IF (DELCOR(J).LT.ZERO) THEN
5006                   DELCOR(J) = DELCOR(J) + PI
5007                ELSE
5008                   DELCOR(J) = DELCOR(J) - PI
5009                END IF
5010             END IF
5011    50    CONTINUE
5012 c
5013   51    continue
```

Putting a tolerance check in the decision to change the sign of a torsion angle also helps reduce the occurences of this problem.

```
1732 C*MODULE ZMATRX  *DECK TORS
1733        SUBROUTINE TORS(EQVAL,NOINT,I,J,K,L,C,B,NDIM)
1734 C

1823 c JRS DLC mod
1824 c
1825 c original code line
1826 c          IF(SENSE.LT.ZERO) EQVAL = -EQVAL
1827 c
1828 c trial modification
1829           IF ( (SENSE.LT.ZERO) .AND. (ABS(SENSE) .GT. TOL)) THEN
1830              EQVAL = -EQVAL
1831           END IF
```

D.5 delocal.f Source Code

```
C
C    23 SEP 96 PROGRAM TO SET UP DELOCALIZED COORDINATES AS PER BAKER'S
C              J CHEM PHYS PAPER
C
      PROGRAM DELOCAL
c
C      CONTAINS THE FOLLOWING SUBROUTINE
C
C      SUBROUTINE BONDTB                 MM2
C      SUBROUTINE THETA                  MM2
C      SUBROUTINE OMEGA                  MM2
C      SUBROUTINE HEAVY(NAT,ITYPE,ZMASS) SHOE  *** NOT USED ****
C      SUBROUTINE KSORT(NK,K,KK)         MM2
C      FUNCTION IPACK4(M,I,J,K,L)        MM2   (MAY NOT BE USED)
C      SUBROUTINE UNPACK4                MM2   (MAY NOT BE USED)
C
      IMPLICIT DOUBLE PRECISION(A-H,O-Z)
```

```
C
C
      COMMON/DLBERT/N,X(500),Y(500),Z(500),ITYPE(500),NAME(50),WT(50)
      COMMON/CONNECT/JJ(500),IAT(500,4),NCONN(40),ICONN(40,16),          M2 0013
     1             NATTCH,JATTCH(500),KATTCH(500)                        M2 0014

      COMMON/CYCLC/IBUTA(15),IBUT,NCBTN,NPROP                            M2 0019
      COMMON/BND/NBND,IR(124750),NBK(500,4),BK(350),BL(350),CSTR         M2 0020

      COMMON/THET/NTHETA,NONPL,IANG(650),KOUTP(50),ANAT(650),ACON(650), M2 0026
     1    KSBOPB(650),SBK(10),OPBK(100),SF                               M2 0027
      COMMON/OMEG/ NOMEGA,IOMG(1040),KTB(1040),NTC,TCON1(520),           M2 0028
     1    TCON2(520),TCON3(520)                                          M2 0029
      COMMON/ANOM/BNDP(50),ANGP(50),CORR,DCORR                           M2 0030

      INTEGER   ITYPE,NAME,JJ,IAT,NCONN,ICONN,JATTCH,KATTCH,             M2 0036
     1    IR,NBK                                                         M2 0037
C
C
      CHARACTER MT*10
      DATA MT/'          '/                                              M2 0068
C ------------------------------------------------------------------- M2 0069
C
C


      PARAMETER (MXATM=500,MXIZMAT=5000)
      PARAMETER (BHR2ANG=0.52917724924D+00)
C
      COMMON /INFOA / NAT,ICH,MUL,NUM,NX,NE,NA,NB,ZAN(MXATM),C(3,MXATM)
      COMMON /MASSES/ ZMASS(MXATM)
C
      CHARACTER CPD*30,HEADER*80
      CHARACTER ATNAME*4(MXATM),CUNITS*8
      DIMENSION IZMAT(MXIZMAT)
C
C     VARIABLES FOR BMAT AND GINVR SECTION
C
      PARAMETER (MX=500000)
      DIMENSION XT(3*MXATM),ZMAT(3*MXATM)
      DIMENSION XB(MX),XBINV(MX),XEVEC(MX),XG(MX),XRECPM(MX),
     # XEVAL(MX),XSCR(MX),XIA(MX),XGLIN(MX)
C ------------------------------------------------------------------- M2 0069
C                                                                        M2 0070
C   GET NAME OF INPUT FILE
C
C     UNIT=5 IS KEYBOARD ENTRY
C     UNIT=6 IS SCREEN OUTPUT
      IOUT=4                                                             M2 0057
      INP=3                                                              M2 0059
C
C     ----- DATA INPUT SECTION
C
      WRITE(6,*) '  '                                                    M2 0081
  140 WRITE(6,FMT='($,A)') ' INPUT FILE NAME = '                         M2 0082
      READ(5,150) CPD                                                    M2 0083
  150 FORMAT(A30)                                                        M2 0084
      OPEN(UNIT=INP,FILE=CPD,STATUS='OLD',ERR=160)                       M2 0085
      GO TO 170                                                          M2 0086
  160 WRITE(6,*) '  '                                                    M2 0087
      WRITE(6,*) ' FILE NOT FOUND ..... , REENTER.... '                  M2 0088
      WRITE(6,*) '  '                                                    M2 0089
      GO TO 140                                                          M2 0090
  170 CONTINUE
C
C                                                                        M2 0167
C
C  READ CONNECTED ATOM LISTS  ----------------------------------       M2 0168
```

```
C
      REWIND(INP)
      READ(INP,910) HEADER
      READ(INP,961) NAT
      READ(INP,961) NCON
      N=NAT
      NCOORD=3*NAT
C
  910 FORMAT(A80)
  960 FORMAT(24X,A8)
  961 FORMAT(12X,I3)
  962 FORMAT(22X,I3,2X,I3)
  963 FORMAT(24X,F10.5)
  964 FORMAT(20X,12I5)
C
      IF (NCON.EQ.0) GO TO 330                                          M2 0169
      DO 320 I=1,NCON                                                   M2 0170
      READ (INP,300) (ICONN(I,K),K=1,16)                                M2 0171
  300 FORMAT (16I5)                                                     M2 0172
      DO 310 K=1,16                                                     M2 0173
      IF (ICONN(I,K).EQ.0) GO TO 320                                    M2 0174
  310 NCONN(I)=NCONN(I)+1                                               M2 0175
  320 CONTINUE                                                          M2 0176
C
      READ(INP,961) NATTCH
C                                                                       M2 0177
C  READ ATTACHED ATOM LISTS  ----------------------------------         M2 0178
C
  330 IF (NATTCH.NE.0) READ(INP,300)(JATTCH(I),KATTCH(I),I=1,NATTCH)    M2 0179
C
C
C  READ COORDINATES AND ATOM TYPES  ---------------------------         M2 0180
C  THIS IS NOW GAMESS STYLE CARTESIANS
C
C
C    FLAG FOR UNITS BOHRS OR ANGSTROMS
C
      READ(INP,*) CUNITS
C
      DO 500 I=1,NAT
  500   READ(INP,*) ATNAME(I),ZAN(I),X(I),Y(I),Z(I)
C
C
c  500   READ(INP,970,END=505) ZAN(I),X(I),Y(I),Z(I)
C  970 FORMAT(20X,,F5.1,5X,F10.5,5X,F10.5,5X,F10.5)
C
C   MM2    WANTS X(*),Y(*), AND Z(*)
C   GAMESS WANTS C(3,*)
C
  505 CONTINUE
C
C
       IF(INDEX(CUNITS,'ANG')) THEN
         SF=(1.0D0/BHR2ANG)
       ELSE
         SF=1.0D0
       END IF
C
        DO 510 I=1,NAT
            C(1,I)=X(I)*SF
            C(2,I)=Y(I)*SF
            C(3,I)=Z(I)*SF
  510       ITYPE(I)=INT(ZAN(I))
C
C    ASSIGN MASSES BASED ON NUCLEAR CHARGE
C
C   ACTUALLY DON'T DO THIS IN BAKER'S PROCEDURE, CHANGE MADE IN GINDELOC
      CALL HEAVY(NAT,ITYPE,ZMASS)
```

```
C
C
      WRITE(*,900)
      DO 520 I=1,NAT
        WRITE(*,901) I,ATNAME(I),ZAN(I),ZMASS(I)
  520 CONTINUE
      WRITE(*,*) '     '
  900 FORMAT(5X,'ATOM',5X,'TYPE',5X,'CHARGE',5X,'MASS (AMU) ')
  901 FORMAT(5X,I3,7X,A4,3X,F6.2,6X,F8.4)
C
C
c 370 CONTINUE
C
C
C
C  PREPARE AND WRITE ATOMIC BOND TABLE  ------------
  610 CALL BONDTB
      NCPRN=NPROP
C
C
C  PARSE BOND TABLE INTO IZMAT SPECIFICATION  1,I,J, ETC
C
      NZVAR=0
      IZ=1
      DO 530 I=1,NAT
        DO 535 J=1,4
          IF ( (IAT(I,J) .NE. 0) .AND. (IAT(I,J) .GT. I))  THEN
            IZMAT(IZ)=1
            IZMAT(IZ+1)=I
            IZMAT(IZ+2)=IAT(I,J)
            IZ=IZ+3
            NZVAR=NZVAR+1
          END IF
  535   CONTINUE
  530 CONTINUE
      NBOND=NZVAR
C
C
c
C  --------------------
C                                                                M2 0262
C  SET UP BOND ANGLE LIST (IANG)        ------------             M2 0263
      CALL THETA                                                 M2 0264
c
C
C     I,J,K,L ARE THE INDICES IN THE IANG ARRAY
C       J-K-L DEFINE THE IN PLANE ANGLES, WHICH I WANT
C       K-I-K DEFIES THE MM2 OUT OF PLANE ANGLES, WHICH I DON'T
C
C
      DO 560 M=1,NTHETA
        CALL UNPACK4(IANG(M),I,J,K,L)
        IZMAT(IZ)=2
        IZMAT(IZ+1)=J
        IZMAT(IZ+2)=K
        IZMAT(IZ+3)=L
        IZ=IZ+4
  560 CONTINUE
C
      NZVAR=NZVAR+NTHETA
C                                                                M2 0265
C  SET UP DIHEDRAL ANGLE LIST (IOMG)    ------------             M2 0266
      IF(NCON.NE.0) CALL OMEGA                                   M2 0267
C
C
      DO 570 M=1,NOMEGA
        CALL UNPACK4(IOMG(M),I,J,K,L)
        IZMAT(IZ)=3
```

```
        IZMAT(IZ+1)=I
        IZMAT(IZ+2)=J
        IZMAT(IZ+3)=K
        IZMAT(IZ+4)=L
        IZ=IZ+5
  570 CONTINUE
        NZMAT=IZ
        NZVAR=NZVAR+NOMEGA

C
      WRITE(*,*) 'NUMBER OF BONDS                ',NBOND
      WRITE(*,*) 'NUMBER OF ANGLES               ',NTHETA
      WRITE(*,*) 'NUMBER OF TORSIONS             ',NOMEGA
      WRITE(*,*) 'TOTAL NUMBER OF PRIMITIVES     ',NZVAR
      WRITE(*,*) '    '
      WRITE(*,*) 'LENGTH OF IZMAT ARRAY          ',NZMAT
C
C
      WRITE(*,*) '    '
      WRITE(*,*) '                    IZMAT ARRAY'
      WRITE(*,*) '    '
      WRITE(*,970)
      NBND=NZVAR-NOMEGA-NTHETA
      ICTR=1
      DO 580 I=1,NZVAR
        IF (I .LE. NBND) THEN
          WRITE(*,971) IZMAT(ICTR),IZMAT(ICTR+1),IZMAT(ICTR+2)
          ICTR=ICTR+3
        END IF
        IF ( (I .GT. NBND) .AND. (I .LE. NBND+NTHETA) ) THEN
          WRITE(*,972) IZMAT(ICTR),IZMAT(ICTR+1),IZMAT(ICTR+2),
     *                 IZMAT(ICTR+3)
          ICTR=ICTR+4
        END IF
        IF (I .GT. NBND+NTHETA) THEN
          WRITE(*,973) IZMAT(ICTR),IZMAT(ICTR+1),IZMAT(ICTR+2),
     *                 IZMAT(ICTR+3),IZMAT(ICTR+4)
          ICTR=ICTR+5
        END IF
  580 CONTINUE
C
C
C  ------- CALCULATE B MATRIX
C
      NVAR=NZVAR
      CALL BMAT(XB,IZMAT,ZMAT,XSYM,XT,NZVAR,NVAR,NCOORD)
C
C
c     CALCULATE GINVR AND ANALYZE FOR ZERO EIGENVALUES
C
      CALL GINVR(XB,XBINV,XEVEC,XG,XRECPM,XEVAL,XSCR,XIA,XGLIN,
     *           NVAR,NCOORD,NAT,NZERO)
C
      CALL WRITZMT(XEVEC,IZMAT,NZVAR,NZERO,NBND,NTHETA,NOMEGA)
C
C  970 FORMAT(5X,'TYPE',8X,'I',9X,'J',9X,'K',9X,'L')
  970 FORMAT(5X,'IZMAT(1)=')
  971 FORMAT(5X,I4,',',2X,I4,',',2X,I4,',')
  972 FORMAT(5X,I4,',',2X,I4,',',2X,I4,',',2X,I4,',')
  973 FORMAT(5X,I4,',',2X,I4,',',2X,I4,',',2X,I4,',',2X,I4,',')
      WRITE(*,*) '     '

C
      END
C
C
C
C ******************************************************************
```

```
C
C                          SUBROUTINE WRITZMT
C
C ******************************************************************
C
      SUBROUTINE WRITZMT(EIGVEC,IZMAT,NZVAR,NZERO,NBND,NTHETA,
     # NOMEGA)
C
C    WRITES $ZMAT DECK IN GAMESS FORMAT
C
      IMPLICIT DOUBLE PRECISION(A-H,O-Z)
      DIMENSION EIGVEC(NZVAR,NZVAR),IZMAT(*)
C
      OPEN(UNIT=10,FILE='ZMAT',STATUS='NEW',ACCESS='SEQUENTIAL')
      REWIND(10)
      WRITE(10,900)
C
C    --------- WRITE IZMAT ARRAY
C
      NBND=NZVAR-NOMEGA-NTHETA
      ICTR=1
      DO 580 I=1,NZVAR
        IF (I .LE. NBND) THEN
          WRITE(10,911) IZMAT(ICTR),IZMAT(ICTR+1),IZMAT(ICTR+2)
          ICTR=ICTR+3
        END IF
        IF ( (I .GT. NBND) .AND. (I .LE. NBND+NTHETA) ) THEN
          WRITE(10,912) IZMAT(ICTR),IZMAT(ICTR+1),IZMAT(ICTR+2),
     #                IZMAT(ICTR+3)
          ICTR=ICTR+4
        END IF
        IF (I .GT. NBND+NTHETA) THEN
          WRITE(10,913) IZMAT(ICTR),IZMAT(ICTR+1),IZMAT(ICTR+2),
     #                IZMAT(ICTR+3),IZMAT(ICTR+4)
          ICTR=ICTR+5
        END IF
  580 CONTINUE
C
C    --------- WRITE IJS SPECIFICATION
c
c  26 mar 96 changed so I just write IJS(1)=666,666
c
C
      N3NM6=NZVAR-NZERO
      WRITE(10,920)
      write(10,*) '  666,666 '
c      DO 300 K=1,N3NM6
c         WRITE(10,921) (M,K, M=1,NZVAR)
c  300 CONTINUE
C
C    --------- WRITE SIJs (ROWS) OOPS !
C
C      WRITE(10,930)
C      DO 400 I=NZERO,NZVAR
C         WRITE(10,931) (EIGVEC(I,J),J=1,NZVAR)
C  400 CONTINUE
C
C    --------- WRITE SIJs (COLUMNS)
      WRITE(10,930)
      DO 400 I=NZERO+1,NZVAR
C      write(10,*) ' **** I **** ',I
         WRITE(10,931) (EIGVEC(J,I),J=1,NZVAR)
  400 CONTINUE
C
C
C
C
      WRITE(10,940)
```

```
      WRITE(10,950) NZVAR
      CLOSE(10)
C
C
C
  900 FORMAT(1X,'$ZMAT      IZMAT(1)=')
  911 FORMAT(5X,I4,',',2X,I4,',',2X,I4,',')
  912 FORMAT(5X,I4,',',2X,I4,',',2X,I4,',',2X,I4,',')
  913 FORMAT(5X,I4,',',2X,I4,',',2X,I4,',',2X,I4,',',2X,I4,',')
  920 FORMAT(1X,'IJS(1)=')
  921 FORMAT(7(I3,',',I3,',',2X))
  930 FORMAT(1X,'SIJ(1)=')
  931 FORMAT(8(F6.4,',  '))
  940 FORMAT(1X,'$END')
  950 FORMAT(1X,'$CONTRL NZVAR=',I4,' $END')
C
      RETURN
      END
C
C
C ******************************************************************
C
C                          SUBROUTINE BONDTB
C
C ******************************************************************
C
      SUBROUTINE BONDTB                                                 M2 0001
C  SETS UP IAT TABLE.                                                   M2 0002
C                                                                       M2 0003
      COMMON/TAPES/INP,IOUT                                             M2 0004
      COMMON/PARMS/IPRINT,INIT                                          M2 0005
C      COMMON/ATOMS/N,X(500),Y(500),Z(500),ITYPE(500),NAME(50),WT(50)   M2 0006
      COMMON/DLBERT/N,X(500),Y(500),Z(500),ITYPE(500),
     # NAME(50),WT(50)
      COMMON/CONNECT/JJ(500),IAT(500,4),NCONN(40),ICONN(40,16),         M2 0007
     1             NATTCH,JATTCH(500),KATTCH(500)                       M2 0008
      COMMON/CYCLC/IBUTA(15),IBUT,NCBTN,NPROP                           M2 0009
C
C
      INTEGER   ITYPE,NAME,JJ,IAT,NCONN,ICONN,JATTCH,KATTCH             M2 0010
      DIMENSION IATJ(4),IDUM(4)                                         M2 0011
      IBF(I,J,K,L)=1000000*I+10000*J+100*K+L                            M2 0012
C  IDUM IS HERE TO SATISFY THE DEMANDS OF SUBROUTINE KSORT.             M2 0013
      IDUM(1)=0                                                         M2 0014
C
       DO 170 J=1,N                                                     M2 0015
      L=0                                                               M2 0016
      DO 120 I=1,20                                                     M2 0017
      IF (NCONN(I).EQ.0)  GO TO 120                                     M2 0018
      II=NCONN(I)                                                       M2 0019
      DO 110 K=1,II                                                     M2 0020
      IF (ICONN(I,K).NE.J)  GO TO 110                                   M2 0021
      IF (K.EQ.1)  GO TO 100                                            M2 0022
      L=L+1                                                             M2 0023
      IATJ(L)=ICONN(I,K-1)                                              M2 0024
  100 IF (K.EQ.II)  GO TO 110                                           M2 0025
      L=L+1                                                             M2 0026
      IATJ(L)=ICONN(I,K+1)                                              M2 0027
  110 CONTINUE                                                          M2 0028
      IF (L.GE.4)  GO TO 150                                            M2 0029
  120 CONTINUE                                                          M2 0030
      DO 140 K=1,NATTCH                                                 M2 0031
      IF (JATTCH(K).NE.J)  GO TO 130                                    M2 0032
      L=L+1                                                             M2 0033
      IATJ(L)=KATTCH(K)                                                 M2 0034
      IF (L-4) 140,150,150                                              M2 0035
  130 IF (KATTCH(K).NE.J)  GO TO 140                                    M2 0036
      L=L+1                                                             M2 0037
```

```
      IATJ(L)=JATTCH(K)                                                 M2 0038
      IF (L.GE.4)  GO TO 150                                            M2 0039
  140 CONTINUE                                                          M2 0040
  150 JJ(J)=L                                                           M2 0041
      CALL KSORT(L,IATJ,IDUM)                                           M2 0042
      DO 160 I=1,L                                                      M2 0043
  160 IAT(J,I)=IATJ(I)                                                  M2 0044
  170 CONTINUE                                                          M2 0045
C  SEARCH CYCLOPROPANE AND CYCLOBUTANE RINGS                            M2 0046
      NCBTN=0                                                           M2 0047
      NPROP=0                                                           M2 0048
      IBUT=0                                                            M2 0049
      DO 180  I=1,10                                                    M2 0050
      IBUTA(I)=0                                                        M2 0051
  180 CONTINUE                                                          M2 0052
      DO 250 I=1,N                                                      M2 0053
      L1=JJ(I)                                                          M2 0054
      IF(L1.LE.1) GO TO 250                                             M2 0055
      DO 240 M1=1,L1                                                    M2 0056
      II=IAT(I,M1)                                                      M2 0057
      IF(I.GT.II) GO TO 240                                             M2 0058
      L2=JJ(II)                                                         M2 0059
      IF(L2.LE.1) GO TO 240                                             M2 0060
      DO 230 M2=1,L2                                                    M2 0061
      III=IAT(II,M2)                                                    M2 0062
      IF( I.EQ.III) GO TO 230                                           M2 0063
      L3=JJ(III)                                                        M2 0064
      IF(L3.LE.1) GO TO 230                                             M2 0065
      DO 220 M3=1,L3                                                    M2 0066
      IV=IAT(III,M3)                                                    M2 0067
      IF(IV.EQ.II) GO TO 220                                            M2 0068
      IF(I.EQ.IV .AND. II.LT.III) GO TO 190                             M2 0069
      GO TO 200                                                         M2 0070
  190 NPROP=NPROP+1                                                     M2 0071
      IBUT=1                                                            M2 0072
      GO TO 220                                                         M2 0073
  200 L4=JJ(IV)                                                         M2 0074
      IF(L4.LE.1) GO TO 220                                             M2 0075
      MIN=MINO(I,II,III,IV)                                             M2 0076
      IF(I.GT.MIN) GO TO 220                                            M2 0077
      DO 210 M4=1,L4                                                    M2 0078
      I5=IAT(IV,M4)                                                     M2 0079
      IF(I5.EQ.III) GO TO 210                                           M2 0080
      IF(JJ(I5).LE.1) GO TO 210                                         M2 0081
      IF(I.NE.I5) GO TO 210                                             M2 0082
      IF( II.GE.IV) GO TO 210                                           M2 0083
      NCBTN=NCBTN+1                                                     M2 0084
      IBUTA(NCBTN)=IBF(I,II,III,IV)                                     M2 0085
      IBUT=1                                                            M2 0086
  210 CONTINUE                                                          M2 0087
  220 CONTINUE                                                          M2 0088
  230 CONTINUE                                                          M2 0089
  240 CONTINUE                                                          M2 0090
  250 CONTINUE                                                          M2 0091
      IF(IBUT.EQ.0) RETURN                                              M2 0092
      WRITE(IOUT,260)                                                   M2 0093
  260 FORMAT(/6X,'THIS MOLECULE CONTAINS'/)                             M2 0094
      IF(NPROP.GT.0) WRITE(IOUT,270) NPROP                              M2 0095
  270 FORMAT(20X,I2,' 3-MEMBERED RING(S)')                              M2 0096
      IF(NCBTN.GT.0) WRITE(IOUT,280) NCBTN                              M2 0097
  280 FORMAT(20X,I2,' 4-MEMBERED RING(S)')                              M2 0098
      IF(IBUT.EQ.2) WRITE(IOUT,290) (IBUTA(J),J=1,NCBTN)                M2 0099
  290 FORMAT(/8X,'THE 4-MEMBED RINGS ARE :' /(18X,3(I8,3X)))            M2 0100
  300 RETURN                                                            M2 0101
      END                                                               M2 0102
C
C ***********************************************************************
C
```

```
C                          SUBROUTINE THETA
C
C ***********************************************************************
C
      SUBROUTINE THETA                                                  M2 0001
C  THIS SUBROUTINE COMPUTES THE NUMBER OF BOND ANGLES (NTHETA) AND SETS M2 0002
C  UP THE IANG ARRAY, WHERE IANG IS THE PACKED INTEGER IAIBICID.  IA,IB,M2 0003
C  IC, & ID ARE THE ATOM NUMBERS OF THE ANGLE A-B-C AND ID IS A THIRD   M2 0004
C  ATTACHED ATOM FOR OUT-OF-PLANE BENDING.  NONPL IS THE NUMBER OF ANGLEM2 0005
C  INVOLVED IN OUT-PL-BEND.                                             M2 0006
C                                                                       M2 0007
C
      COMMON/DLBERT/N,X(500),Y(500),Z(500),ITYPE(500),NAME(50),WT(50)
C
C      COMMON/ATOMS/N,X(500),Y(500),Z(500),ITYPE(500),NAME(50),WT(50)    M2 0008
      COMMON/CONNECT/JJ(500),IAT(500,4)                                 M2 0009
      COMMON/THET/NTHETA,NONPL,IANG(650),KOUTP(50)                      M2 0010
      INTEGER   ITYPE,NAME,JJ,IAT,MOUTP(50)                             M2 0011
C ---------------------------------------------------------------------M2 0012
C  OUT-OF-PLANE BENDING IF NON-ZERO                                     M2 0013
      DATA MOUTP/ 0, 2, 3, 0, 0,      0, 0, 0, 9, 0,                    M2 0014
     1            0, 0, 0, 0, 0,      0, 0, 0, 0, 0,                    M2 0015
     2            0, 0, 0, 0, 0,      0, 0, 0,29,30,                    M2 0016
     2            0, 0, 0, 0, 0,      0,37,38,39,40,                    M2 0017
     4           41, 0,43, 0, 0,     46, 0, 0, 0, 0/                    M2 0018
C ---------------------------------------------------------------------M2 0019
C     IPACK(I,J,K,L)=256*(256*(256*I+J)+K)+L                            M2 0020
C ---------------------------------------------------------------------M2 0021
      NELEMT=50                                                         M2 0022
      DO 100 I=1,NELEMT                                                 M2 0023
      IF(KOUTP(I).NE.0) GO TO 100                                       M2 0024
      KOUTP(I)=MOUTP(I)                                                 M2 0025
  100 CONTINUE                                                          M2 0026
C                                                                       M2 0027
      NTHETA=0                                                          M2 0028
      NONPL=0                                                           M2 0029
      DO 120 I=1,N                                                      M2 0030
      IA=IAT(I,1)                                                       M2 0031
      IB=IAT(I,2)                                                       M2 0032
      IC=IAT(I,3)                                                       M2 0033
      ID=IAT(I,4)                                                       M2 0034
      IT=ITYPE(I)                                                       M2 0035
C  IF KOUTP IS NOT ZERO,  SET IT=0 TO SIGNIFY THAT ALL X-I-Y            M2 0036
C  ANGLES WILL HAVE OUT-OF-PLANE BENDING.                               M2 0037
      IF(KOUTP(IT).NE.0 .AND. ID.EQ.0) IT=0                             M2 0038
      IF (IB.EQ.0) GO TO 120                                            M2 0039
      NTHETA=NTHETA+1                                                   M2 0040
      CALL IPACK4(IANG(NTHETA),IA,I,IB,0)
C   IF ALLENE LINKAGE (-2-4-2-) EXISTS, SET IANG NEGATIVE.              M2 0042
      IF(IT.NE.4 .OR. ITYPE(IA).NE.2 .OR. ITYPE(IB).NE.2) GO TO 110     M2 0043
      IANG(NTHETA)=-IANG(NTHETA)                                        M2 0044
C  IF ANGLE IS INVOLVED IN O-P-B, PUT THE THIRD ATOM ATTACHED TO I IN   M2 0045
C  IANG.                                                                M2 0046
  110 IF (IT.EQ.0) IANG(NTHETA)=IANG(NTHETA)+IC                         M2 0047
      IF (IC.EQ.0) GO TO 120                                            M2 0048
      NTHETA=NTHETA+1                                                   M2 0049
      CALL IPACK4(IANG(NTHETA),IA,I,IC,0)
C  CHECK FOR O-P-B                                                      M2 0051
      IF (IT.EQ.0) IANG(NTHETA)=IANG(NTHETA)+IB                         M2 0052
      NTHETA=NTHETA+1                                                   M2 0053
      CALL IPACK4(IANG(NTHETA),IB,I,IC,0)
C  CHECK FOR O-P-B                                                      M2 0055
      IF (IT.EQ.0) IANG(NTHETA)=IANG(NTHETA)+IA                         M2 0056
      IF (ID.EQ.0) GO TO 120                                            M2 0057
      NTHETA=NTHETA+1                                                   M2 0058
      IANG(NTHETA)=IANG(NTHETA-1)                                       M2 0059
      CALL IPACK4(IANG(NTHETA-1),IA,I,ID,0)
      CALL IPACK4(IANG(NTHETA+1),IB,I,ID,0)
```

```
      CALL IPACK4(IANG(NTHETA+2),IC,I,ID,0)
      NTHETA=NTHETA+2                                                   M2 0063
  120 CONTINUE                                                          M2 0064
  130 IF (NTHETA.EQ.0) GO TO 150                                        M2 0065
C  CONVERT THE IANG LIST (FOR ANGLE A-B-C) FROM ABCX TO XABC.           M2 0066
      DO 140 I=1,NTHETA                                                 M2 0067
      NCCC=0                                                            M2 0068
      IF(IANG(I).LT.0) NCCC=1                                           M2 0069
      CALL UNPACK4(IABS(IANG(I)),IA,IB,IC,ID)                            M2 0070
      IF (ID.NE.0) NONPL=NONPL+1                                        M2 0071
      CALL IPACK4(IANG(I),ID,IA,IB,IC)
      IF(NCCC.NE.0) IANG(I)=-IANG(I)                                    M2 0073
  140 CONTINUE                                                          M2 0074
  150 RETURN                                                            M2 0075
      END                                                               M2 0076
C
C ***********************************************************************
C
C                              SUBROUTINE OMEGA
C
C ***********************************************************************
C
      SUBROUTINE OMEGA                                                  M2 0001
C  COMPUTES THE NUMBER OF DIHEDRAL ANGLES (NOMEGA) AND THE NUMBERS OF   M2 0002
C  THE 4 ATOMS DEFINING THE ANGLE, IOMG IS PACKED AS THE INTEGER        M2 0003
C  IAIBICID AND FOR ALLENES, THE CENTRAL ATOM(C-SP) IS IGNORED, THEN    M2 0004
C  PACKED FOR SUBROUTINE KOMEGA.                                        M2 0005
C                                                                       M2 0006
      COMMON/THET/NTHETA,NONPL,IANG(650),KOUTP(50)                      M2 0007
      COMMON/OMEG/ NOMEGA,IOMG(1040),KTB(1040)                          M2 0008
C
c
C     IPACK(I,J,K,L)=256*(256*(256*I+J)+K)+L                            M2 0009
C                                                                       M2 0010
      NOMEGA=1                                                          M2 0011
      NN=NTHETA-1                                                       M2 0012
      DO 300 I=1,NN                                                     M2 0013
      CALL UNPACK4(IABS(IANG(I)),IDUM,IA,IB,IC)                         M2 0014
      ICCC=0                                                            M2 0015
      II=I+1                                                            M2 0016
      DO 290 J=II,NTHETA                                                M2 0017
      IF(IANG(J).LT.0) GO TO 290                                        M2 0018
      CALL UNPACK4(IABS(IANG(J)),IDUM,JA,JB,JC)                         M2 0019
      IF (IB.NE.JA) GO TO 130                                           M2 0020
      IF (IC.NE.JB) GO TO 110                                           M2 0021
C  OMEGA IA-IB-IC-JC  (IB=JA & IC=JB)                                   M2 0022
C  CHECK FOR THREEMEMBERED RING                                         M2 0023
      IF(IA.EQ.JC) GO TO 290                                            M2 0024
      IF(IANG(I).GT.0) GO TO 100                                        M2 0025
      ICCC=1                                                            M2 0026
      GO TO 180                                                         M2 0027
  100 IF (IA.LE.JC) CALL IPACK4(IOMG(NOMEGA),IA,IB,IC,JC)
      IF (IA.GT.JC) CALL IPACK4(IOMG(NOMEGA),JC,IC,IB,IA)
      GO TO 170                                                         M2 0030
  110 IF (IA.NE.JB) GO TO 290                                           M2 0031
C  OMEGA JC-IA-IB-IC  (IB=JA & IA=JB)                                   M2 0032
C  CHECK FOR THREEMEMBERED RING                                         M2 0033
      IF(JC.EQ.IC) GO TO 290                                            M2 0034
      IF(IANG(I).GT.0) GO TO 120                                        M2 0035
      ICCC=2                                                            M2 0036
      GO TO 180                                                         M2 0037
  120 IF (JC.LE.IC) CALL IPACK4(IOMG(NOMEGA),JC,IA,IB,IC)
      IF (JC.GT.IC) CALL IPACK4(IOMG(NOMEGA),IC,IB,IA,JC)
      GO TO 170                                                         M2 0040
  130 IF (IB.NE.JC) GO TO 290                                           M2 0041
      IF (IC.NE.JB) GO TO 150                                           M2 0042
C  OMEGA IA-IB-IC-JA  (IB=JC & IC=JB)                                   M2 0043
C  CHECK FOR THREEMEMBERED RING                                         M2 0044
```

```
      IF(IA.EQ.JA) GO TO 290                                            M2 0045
      IF(IANG(I).GT.0) GO TO 140                                        M2 0046
      ICCC=3                                                            M2 0047
      GO TO 180                                                         M2 0048
  140 IF (IA.LE.JA) CALL IPACK4(IOMG(NOMEGA),IA,IB,IC,JA)
      IF (IA.GT.JA) CALL IPACK4(IOMG(NOMEGA),JA,IC,IB,IA)
      GO TO 170                                                         M2 0051
  150 IF (IA.NE.JB) GO TO 290                                           M2 0052
C  OMEGA JA-IA-IB-IC  (IB=JC & IA=JB)                                   M2 0053
C  CHECK FOR THREEMEMBERED RING                                         M2 0054
      IF(JA.EQ.IC) GO TO 290                                            M2 0055
      IF(IANG(I).GT.0) GO TO 160                                        M2 0056
      ICCC=4                                                            M2 0057
      GO TO 180                                                         M2 0058
  160 IF (JA.LE.IC) CALL IPACK4(IOMG(NOMEGA),JA,IA,IB,IC)
      IF (JA.GT.IC) CALL IPACK4(IOMG(NOMEGA),IC,IB,IA,JA)
  170 KTB(NOMEGA)=0                                                     M2 0061
      NOMEGA=NOMEGA+1                                                   M2 0062
      GO TO 290                                                         M2 0063
C                                                                       M2 0064
C  FOR ALLENES X-IA=IB=IC-Y, SET IOMG NEGATIVE AND PACKED WITH          M2 0065
C  X-IA=IC-Y.                                                           M2 0066
  180 DO 280 K=1,NTHETA                                                 M2 0067
      CALL UNPACK4(IABS(IANG(K)),IDUM,KA,KB,KC)                          M2 0068
      GO TO (190,210,230,250),ICCC                                      M2 0069
      GO TO 280                                                         M2 0070
  190 IF(IA.NE.KB) GO TO 280                                            M2 0071
      IF(JA.NE.KA) GO TO 200                                            M2 0072
      IF (KC.LT.JC) CALL IPACK4(-IOMG(NOMEGA),KC,IA,IC,JC)
      IF (KC.GT.JC) CALL IPACK4(-IOMG(NOMEGA),JC,IC,IA,KC)
      GO TO 270                                                         M2 0075
  200 IF(JA.NE.KC) GO TO 280                                            M2 0076
      IF (KA.LT.JC) CALL IPACK4(-IOMG(NOMEGA),KA,IA,IC,JC)
      IF (KA.GT.JC) CALL IPACK4(-IOMG(NOMEGA),JC,IC,IA,KA)
      GO TO 270                                                         M2 0079
  210 IF(IC.NE.KB) GO TO 280                                            M2 0080
      IF(IB.NE.KA) GO TO 220                                            M2 0081
      IF (KC.LT.JC) CALL IPACK4(-IOMG(NOMEGA),KC,IC,IA,JC)
      IF (KC.GT.JC) CALL IPACK4(-IOMG(NOMEGA),JC,IA,IC,KC)
      GO TO 270                                                         M2 0084
  220 IF(IB.NE.KC) GO TO 280                                            M2 0085
      IF (KA.LT.JC) CALL IPACK4(-IOMG(NOMEGA),KA,IC,IA,JC)
      IF (KA.GT.JC) CALL IPACK4(-IOMG(NOMEGA),JC,IA,IC,KA)
      GO TO 270                                                         M2 0088
  230 IF(IA.NE.KB) GO TO 280                                            M2 0089
      IF(JC.NE.KA) GO TO 240                                            M2 0090
      IF (KC.LT.JA) CALL IPACK4(-IOMG(NOMEGA),KC,IA,IC,JA)
      IF (KC.GT.JA) CALL IPACK4(-IOMG(NOMEGA),JA,IC,IA,KC)
      GO TO 270                                                         M2 0093
  240 IF(JC.NE.KC) GO TO 280                                            M2 0094
      IF (KA.LT.JA) CALL IPACK4(-IOMG(NOMEGA),KA,IA,IC,JA)
      IF (KA.GT.JA) CALL IPACK4(-IOMG(NOMEGA),JA,IC,IA,KA)
      GO TO 270                                                         M2 0097
  250 IF(IC.NE.KB) GO TO 280                                            M2 0098
      IF(JC.NE.KA) GO TO 260                                            M2 0099
      IF (KC.LT.JA) CALL IPACK4(-IOMG(NOMEGA),KC,IC,IA,JA)
      IF (KC.GT.JA) CALL IPACK4(-IOMG(NOMEGA),JA,IC,IA,KC)
      GO TO 270                                                         M2 0102
  260 IF(JC.NE.KC) GO TO 280                                            M2 0103
      IF (KA.LT.JA) CALL IPACK4(-IOMG(NOMEGA),KA,IC,IA,JA)
      IF (KA.GT.JA) CALL IPACK4(-IOMG(NOMEGA),JA,IA,IC,KA)
  270 NOMEGA=NOMEGA+1                                                   M2 0106
  280 CONTINUE                                                          M2 0107
  290 CONTINUE                                                          M2 0108
  300 CONTINUE                                                          M2 0109
      NOMEGA=NOMEGA-1                                                   M2 0110
C  SORT THE IOMG AND KTB ARRAYS.                                        M2 0111
      IF (NOMEGA.GT.1) CALL KSORT(NOMEGA,IOMG,KTB)                      M2 0112
```

```
      RETURN                                                            M2 0113
      END                                                               M2 0114
C
C ******************************************************************
C
C                          SUBROUTINE HEAVY
C
C ******************************************************************
C
      SUBROUTINE HEAVY(NAT,ITYPE,ZMASS)
C
      IMPLICIT DOUBLE PRECISION(A-H,O-Z)
      DIMENSION ITYPE(*),ZMASS(*)
      DIMENSION AMS(106)
C
C    ASSIGN NUCLEAR MASSES BASED ON NUCLEAR CHARGE
C
C ------------------------------------------------------------------
C    THIS IS THE ATOMIC MASS TABLE FROM GAMESS VIBANL.SRC
C
      DATA (AMS(I),I=1,54)  /
     *   1.007825D+00,4.0026D+00,7.01600D+00,9.01218D+00,11.00931D+00,
     *   12.0D+00,14.00307D+00,15.99491D+00,18.99840D+00,19.99244D+00,
     *   22.9898D+00,23.98504D+00,26.98153D+00,27.97693D+00,
     *   30.97376D+00,31.97207D+00,34.96885D+00,39.948D+00,
     *   38.96371D+00,39.96259D+00,44.95592D+00,47.90D+00,50.9440D+00,
     *   51.9405D+00,54.9381D+00,55.9349D+00,58.9332D+00,57.9353D+00,
     *   62.9298D+00,63.9291D+00,68.9257D+00,73.9219D+00,74.9216D+00,
     *   79.9165D+00,78.9183D+00,83.9115D+00,
     *   84.9117D+00,87.9056D+00,89.9054D+00,89.9043D+00,92.9060D+00,
     *   97.9055D+00,97.0D+00,101.9037D+00,102.9048D+00,105.9032D+00,
     *   106.9041D+00,113.9036D+00,114.9041D+00,119.9022D+00,
     *   120.9038D+00,129.9067D+00,126.9044D+00,131.9042D+00/
      DATA (AMS(I),I=55,106)  /
     *   132.9054D+00,137.9052D+00,138.9063D+00,139.9054D+00,
     *   140.9076D+00,141.9077D+00,144.9127D+00,151.9197D+00,
     *   152.9212D+00,157.9241D+00,158.9253D+00,163.9292D+00,
     *   164.9303D+00,165.9303D+00,168.9342D+00,173.9389D+00,
     *   174.9408D+00,179.9465D+00,180.9480D+00,183.9509D+00,
     *   186.9557D+00,191.9615D+00,192.9629D+00,194.9648D+00,
     *   196.9665D+00,201.9706D+00,
     *   204.9744D+00,207.9766D+00,208.9804D+00,208.9824D+00,
     *   209.9871D+00,222.0176D+00,
     *   223.0197D+00,226.0254D+00,
     *   227.0278D+00,232.0381D+00,231.0359D+00,238.0508D+00,
     *   237.0482D+00,244.0642D+00,243.0614D+00,247.0703D+00,
     *   247.0703D+00,251.0796D+00,252.0829D+00,257.0751D+00,
     *   258.0986D+00,259.1009D+00,260.1053D+00,261.1087D+00,
     *   2*0.0D+00/
C ------------------------------------------------------------------
C
      DO 10 I=1,NAT
  10        ZMASS(I)=AMS(ITYPE(I))
C
C
      RETURN
      END
C
C ******************************************************************
C
C                          SUBROUTINE KSORT
C
C ******************************************************************
C
      SUBROUTINE KSORT(NK,K,KK)                                         M2 0001
C  SORTS THE K-ARRAY IN ASCENDING ORDER.  IF THE FIRST ELEMENT OF THE  M2 0002
C  KK-ARRAY IS NOT ZERO, IT IS SORTED ACCORDING TO K.  CALLED BY OMEGA M2 0003
      DIMENSION K(1),KK(1),KT(1040)                                     M2 0004
```

```
      INTEGER   N(1040),SIGN(1040)                                      M2 0005
C  TRANSFER K TO KT, THE TEMPORARY STORAGE ARRAY; SET ALL N=1.          M2 0006
      DO 100 I=1,NK                                                     M2 0007
      SIGN(I)=IABS(K(I))/K(I)                                           M2 0008
      KT(I)=K(I)*SIGN(I)                                                M2 0009
  100 N(I)=1                                                            M2 0010
C  CALCULATE THE RANK FOR EACH ENTRY IN KT                              M2 0011
      M=NK-1                                                            M2 0012
      DO 130 I=1,M                                                      M2 0013
      J=I+1                                                             M2 0014
      DO 130 L=J,NK                                                     M2 0015
      IF(KT(I).GT.KT(L)) GO TO 120                                      M2 0016
  110 N(L)=N(L)+1                                                       M2 0017
      GO TO 130                                                         M2 0018
  120 N(I)=N(I)+1                                                       M2 0019
  130 CONTINUE                                                          M2 0020
C  RESTORE THE K-ARRAY.  THE VALUE OF N FOR EACH ENTRY IN KT BECOMES THEM2 0021
C  SUBSCRIPT OF THIS ENTRY IN THE K-ARRAY.                              M2 0022
      DO 140 I=1,NK                                                     M2 0023
  140 K(N(I))=KT(I)*SIGN(I)                                             M2 0024
C  IF KK(1).NE.0, REARRANGE THIS ARRAY TO CORRESPOND TO K.              M2 0025
      IF (KK(1).EQ.0) GO TO 170                                         M2 0026
      DO 150 I=1,NK                                                     M2 0027
  150 KT(I)=KK(I)                                                       M2 0028
      DO 160 I=1,NK                                                     M2 0029
  160 KK(N(I))=KT(I)                                                    M2 0030
  170 RETURN                                                            M2 0031
      END
C
C ******************************************************************
C
C                          FUNCTION IPACK4
C
C ******************************************************************
C
      INTEGER FUNCTION IPACK4(M,I,J,K,L)
      M=215*(215*(215*I+J)+K)+L
      RETURN
      END
C
C ******************************************************************
C
C                          SUBROUTINE UNPACK
C
C ******************************************************************
C
      SUBROUTINE UNPACK4(M,I,J,K,L)                                     M2 0001
C     M = 215**3*I + 215**2*J + 215*K + L                               M2 0002
      LL=M/215                                                          M2 0003
      L=M-LL*215                                                        M2 0004
      KK=LL/215                                                         M2 0005
      K=LL-KK*215                                                       M2 0006
      I=KK/215                                                          M2 0007
      J=KK-I*215                                                        M2 0008
      RETURN                                                            M2 0009
      END                                                               M2 0010
```

Appendix E. Program Modifications for the IMMOM: GAMESS and MM3

E.1 Overview

The following is a compilation of the changes made to GAMESS and MM3 in order to perform a hybrid ab initio/MM geometry optimization. The following subroutines required source code modifications:

- GAMESS

Module gamess.S.f	Deck MAIN
Module inputa.S.f	Deck START
Module inputc.S.f	Deck MBLDR
Module statpt.S.f	Deck SIGINI
Module statpt.S.f	Deck SIGVAL

- MM3

	COMMON.PAR
Module mm3_aix.f	
Module mm31.S.f	SUBMM3
Module mm31.S.f	subroutine part1
Module mm31.S.f	subroutine part2
Module mm31.S.f	subroutine part3
Module mvib31.S.f	**subroutine fmin**
Module mvib31.S.f	**subroutine fmove**
Module mvib31.S.f	subroutine fd_rth
Module mvib31.S.f	subroutine fd_ebend
Module mvib31.S.f	subroutine fd_theta
Module mvib31.S.f	subroutine fd_opb1
Module mvib31.S.f	subroutine fd_opb2
Module mvib31.S.f	subroutine fd_opb3
Module mvib31.S.f	subroutine fd_ebbnd
Module mvib32.S.f	subroutine fd_vdwbd
Module mvib32.S.f	subroutine fd_vdwod
Module mvib32.S.f	subroutine fd_chgchg
Module mvib32.S.f	subroutine fd_dipole
Module mvib32.S.f	subroutine fd_chgdip
Module mvib32.S.f	subroutine fd_dipchg
Module mvib32.S.f	subroutine fd_etors
Module mvib32.S.f	subroutine fd_cosw

- NEW MODULES CREATED

  GHMM3.3.f

- Deconfliction of GAMESS-MM3 common and sub names

In addition, a large number of the MM3 subs had to have COMMON blocks renamed, as there were conflicts between named COMMON blocks in MM3 and subroutine names in GAMESS, and vice versa. In addition, GAMESS and MM3 had several subroutines

with the same names. In order to minimize the changes to GAMESS, the conflicting MM3 named COMMONs and subs were renamed.

E.2 GAMESS Source Code Modifications

NOTA BENE: All line numbers are approximate.

E.2.1 MAIN Module gamess.S.f. Not many modifications needed here. Be careful when using Hollerith variables. They can be tricky in comparison

```
263 C
264 C     ---- ADDITION 8 OCT 96 JRS
265       DATA HYBRID /8HHYBRID  /
266 C

449 C
450 C    ------ JRS NEW RUNTYP 8 OCT 96  -----
451 C        IF RUNTYP.EQ.'HYBRID  ', MIXED GAMESS MM3 OPTIMIZATION

475 C
476       IF(RUNTYP.EQ.HYBRID) CALL SIGX(.FALSE.)
477 C
```

E.2.2 Deck START Module Sinputa.S.f. Have to add RUNTYP=HYBRID when you read the $CONTRL card.

```
2165 C     ADDED 8 OCT 96
2166       DATA HYBRID /8HHYBRID  /
2167 C

2301       IF(RUNTYP.EQ.PROP)   OK=.TRUE.
2302 C   ----- NEW OPTION ADDED 8 OCT 96  JRS
2303 C
2304       IF(RUNTYP.EQ.HYBRID)   OK=.TRUE.
2305 C
2306       IF(.NOT.OK) THEN
2307          IF (MASWRK) WRITE(IW,9010) 'RUNTYP',RUNTYP
2308          NERR = NERR+1
2309       END IF
```

E.2.3 Deck MBLDR Module inputc.S.f. It makes more sense to use the Principal Axes that define the large molecule, the *ab initio* and molecular mechanics portions together, as the common reference frame for the calculation. GAMESS would normally convert to the PrinAxes frame of the *ab initio* piece, whose cartesian coordinates would then be inconsistent with the cartesian coordinates of the entire system shifted to its PrinAxes frame by MM3. The easy way around this problem is to diable the conversion to the PrinAxes frame in GAMESS for RUNTYP=HYBRID. *Another way around this is to use COORD=UNIQUE in $CONTRL card, which also bypasses the Principal Axis transformation* This conversion is accomplished in GAMESS module Sinputc.f Deck MBLDR.

```
 79 C
 80 C  ---- 8 OCT 96 JRS ADDED THE FOLLOWING COMMON AND DATA  ----
 81 C
 82       COMMON /RUNOPT/ RUNTYP,EXETYP,NEVALS
 83       DATA HYBRID /8HHYBRID  /
 84 C  ------------------------------------------------------------

162 C  8 OCT 96 JRS FOR RUNTYP=HYBRID, TRANSLATING THE COORDINATES TO THE
163 C    PRIN AXIS FRAME WILL CAUSE INCONSISTENCY WITH THE MM3 PART OF THE
164 C    CALCULATION
165       IF(RUNTYP.EQ.HYBRID) GOTO 333
166         CALL PRAXIS(CORD,AZNUC,NAT,MXATM,IXX,IYY,IZZ)
167         IF (MASWRK) WRITE(IW,9020) IXX,IYY,IZZ
168 C
169   333 CONTINUE
```

E.2.4 Deck SIGINI Module statpt.S.f. Modifications to SIGINI mainly involve intializing some parameters for the GAMESS optimization routine and calling ghmm2 to intialize the MM3 input and read in the variables needed for the linking process.

```
3926 C
3927       DATA HYBRID /8HHYBRID  /
3928 C

4021 C
4022          IF(RUNTYP.EQ.HYBRID) DXMAXT=0.1D+00
4023 C

4032 C
4033          IF(RUNTYP.EQ.HYBRID)  UPHESS=BFGS
4034 C

4076 C            ----- FOR RUNTYP=HYBRID, READ AND VERIFTY $MM3 DATA -----
4077 C
4078 C
4079 C  CALLING WITH 0 MEANS INITIALIZATION ONLY
4080 C
4081        IF(RUNTYP.EQ.HYBRID) CALL GHMM3(0)
```

E.2.5 Deck SIGVAL Module statpt.S.f. Modifications to SIGVAL were minor, mainly adding a call to ghmm2(1) for RUNTYP=HYBRID. I had to change the SUBROUTINE statement itself to resolve a conflict

- Line 4199: Subroutine Statement We need RUNTYP for optional call to ghmm2 for RUNTYP .EQ. HYBRID. Since the variable RUNTYP is contained in COMMON /RUNOPT/, which also contains EXETYP I had to change the subroutine statement to avoid an inconsistent common block compile time error. I.e., you can't pass a variable in a CALL if you also include the COMMON block in which that same variable resides in the same subroutine.

```
4194 C  13 JUL 96 JRS
4195 C  ORIGINAL CODE LINE
4196 C      SUBROUTINE SIGVAL(EXETYP,NCOORD,METHOD,NPRT)
4197 C ---NEW CODE LINE
4198 C
4199        SUBROUTINE SIGVAL(SHOEDM,NCOORD,METHOD,NPRT)

4235 C  13 JUL 96 JRS  COMMON/RUNOPT/ ADDED FOR HYBRID RUN OPTION
4236 C
4237        COMMON /RUNOPT/ RUNTYP,EXETYP,NEVALS
```

- Addition of MM3 Contribution to the GAMESS Gradient This call to ghmm2 drives an MM3 optimization of the entire hybrid system with the appropriate *ab initio* atoms restricted in MM3. The final gradient contributions to the *ab initio* internal coordinates (with the appropriate MM3 gradient contributions neglected) are added to the GAMESS gradient in internal coordinates. The Cartesian coordinates for the system, hence the *ab initio* piece, change as a result of the MM3 optimization. Therefore, new B and B Inverse matrices are calculated for the new *ab initio* coordinates before control is passed back to GAMESS. (New values of the internal coordinates are generated when the B matrix is calculated.)

```
4172 C  8 OCT 96 JRS
4173 C  NEED EXETYP AND RUNTYP, SO CALL EXETYP A SHOE DUMMY AND USE
4174 C  COMMON /RUNOPT/ TO PASS THE VALUES
4175 C
4176 C  ORIGINAL CODE LINE
4177 C      SUBROUTINE SIGVAL(EXETYP,NCOORD,METHOD,NPRT)
4178 C ---NEW CODE LINE
4179 C
4180        SUBROUTINE SIGVAL(SHOEDM,NCOORD,METHOD,NPRT)

4217 C
4218 C  8 OCT 96 JRS  COMMON/RUNOPT/ ADDED FOR HYBRID RUN OPTION
4219 C
4220        COMMON /RUNOPT/ RUNTYP,EXETYP,NEVALS
4221 C
4222        DATA HYBRID /8HHYBRID  /

4359 C      8 OCT 96 JRS
4360 C      FOR RUNTYP=HYBRID, CALL GHMM3  TO GET THE MM3 CONTRIBUTION TO THE
4361 C      ENERGY AND GRADIENT BEFORE RETURNING TO THE OPTIMIZATION
4362 C
4363 C    NOTA BENE: THE GRADIENT HERE IS THE CARTESIAN GRADIENT !!!!!!
4364 C
4365 C   THIS MEANS I HAVE TO USE THE NORMAL GAMESS ROUTINES TO CONVERT THIS
4366 C   GRADIENT TO A GRADIENT IN INTERNALS IN GHMM3 AS WELL AS CONVERTING THE
4367 C   MM3 CARTESIAN GRADIENT TO INTERNALS
4368 C
4369 C
4370        IF(RUNTYP.EQ.HYBRID) CALL GHMM3(1)
4371 C
```

E.3 MM3 Source Code Modifications

Most of the modified portions of the MM3 source code are prefaced by:

```
c  gam2mm
```

The modifications can be located by doing a grep on gam2mm.

E.3.1 COMMON.PAR. The default number of atoms that can be used in the "Full Matrix" optimization scheme, i.e., the technique that minimizes the gradient, is 120, too small for the bulk clusters considered in this work. In addition, because of the large number of internal coordinates that can be defined for large cage molecules, the number of angles and torions was also increased.

```
C          ((( MM3 )))
C --- ASSIGNMENT OF MAXIMUM NUMBERS
C --- MAXATOM=MAXIMUM ATOM NUMBER
C --- MAXTYPE=MAXIMUM NUMBER OF ATOM TYPE
      PARAMETER (MAXATOM=700,MAXTYPE=200)
C
C --- MAXVALC=MAXIMUM NUMBER OF VALENCE BOND
      PARAMETER (MAXCONN=150,MAXVALC=6)
      PARAMETER (MAXCYC4=54,MAXCYC5=20)
c
c ====================================
c  21 Apr 97 JRS bumped up maxtors
c
c      PARAMETER (MAXTORS=2800,MAXNTC=1750,MAXTOST=50)
      PARAMETER (MAXTORS=6000,MAXNTC=1750,MAXTOST=50)
c ====================================
C
C --- MAXPAIR=ATOM PAIRS IN THE SYSTEM
C            =MAXATOM*(MMAXATOM-1)/2
      PARAMETER (MAXBOND=840,MAXPAIR=244650)
      PARAMETER (MAXBCO=30,MXANOM=100)
C
C --- MAXIMUM NO OF PRIMARY AND SECONDARY ELECTROEGATIVITY PARAMETERS
      PARAMETER (MXPREL=120,MAXSEL=30)
C
C --- MAXVANG=NUMBER OF ANGLES ON MAXVALC BONDED ATOM
C            =MXVANG2/2
C
C --- MXVANG2=NUMBER OF ANGLE COMBINATION ON MAXVALC
C            =MAXVALC*(MAXVALC-1)
      PARAMETER (MAXANGL=1680,MAXVANG=15,MXVANG2=30)
C
C --- MAXV4=MAXIMUM NUMBER OF 4-CORRDINATION BOND ANGLE PARAMETERS
C --- MAXV5=MAXIMUM NUMBER OF 5-CORRDINATION BOND ANGLE PARAMETERS
C --- MAXV6=MAXIMUM NUMBER OF 6-CORRDINATION BOND ANGLE PARAMETERS
      PARAMETER (MAXVT4=100,MAXVT5=100,MAXVS5=100,MAXVT6=100)
C --- MAX NUMBER OF STRETCH-BENDING AND OUT-OF-PLN BENDING
      PARAMETER (MAXSTBN=25,MAXOUTP=120)
      PARAMETER (MAXHYBD=100,MAXCHG=200)
C --- MAXPATOM=MAXIMUM NUMBER OF PI-ATOM
      PARAMETER (MAXPATM=100,MAXPBND=140,MAXPTOR=560)
C --- MAXROT=HALF OF MAXATOM
C --- MAXDRIV=MAXIMUM NUMBER OF DIHEDRAL ANGLE FOR DRIVER
      PARAMETER (MAXROT=350,MAXDRIV=10)
C ------------------------------------------------------------------
c    The following PARAMETER statments are used in full matrix method
c    subroutines  (MVIB part)
c
c    MXFATOM = max number of atoms that full matrix method can handle.
c    MXVIB1  = MXFATOM * 3 + 6
c    MXVIB2  = MXVIB1 * (MXVIB1 + 1) / 2
c    MXVIB3  = MXVIB1 * 5
c    MXVIB4  = MXVIB1 - 10
c
```

```
c     eg. if the maximum number of MXFATOM is 120, then the other
c     parameters will be calculated as the following...
c
c     PARAMETER (MXVIB1=246,MXVIB2=30381,MXVIB3=1230,MXVIB4=236)
c
c ==============================
c 21 Apr 97 JRS bumped up MXFATOM
c
c      PARAMETER (MXFATOM = 120)
       PARAMETER (MXFATOM = 400)
c ==============================
       PARAMETER (MXVIB1 = MXFATOM * 3 + 6)
       PARAMETER (MXVIB2 = MXVIB1 * (MXVIB1 + 1) / 2)
       PARAMETER (MXVIB3 = MXVIB1 * 5)
       PARAMETER (MXVIB4 = MXVIB1 - 10)
```

E.3.2 Module mm3_aix.f . MM3 uses some system calls for timing, etc, that are not supported under AIX. This module contains a few functions to convert the more standard UNIX system calls to the AIX equivalents. For Sun UNIX, I wrote a module mm3_sun.f that uses the standard UNIX calls.*On an IBM SP2, you need to use mm3_aix*

E.3.3 Module mm31.S.f SUBMM3 .

```
C      PROGRAM MM3
      SUBROUTINE MM3(INPUT,IOUTPUT,IROAD)

C  gam2mm
C  I/O unit assignments consistent and deconflicter with GAMESS
      INP=INPUT
      IRD=INPUT
      IOUT=IOUTPUT
C
C   NEW Unit assignment for KONST.MM3 file
C
C   Will need to redo reading of KONST.MM3 file
C   Put KONST.MM3 in same location as executables
C
      IT12=32
      OPEN(UNIT=IT12,FILE='~/Bin/KONST.MM3',STATUS='OLD')
c      REWIND(IT12)
C
C   Lot's of stuff deleted as i don't need a lot of diferent options
C
C   MOVE CONTROLS THE OPTIMIZATION METHOD
C   MOVE=2 MEANs BLOCK FIRST, THEN FULL MATRIX MINIMIZATION
C   THEN FULL MATRIX MINIMIZATION
c   move=3 means full matrix from the get go
c
c   imove is in the file COMMON.PAR, read in at Link Time

c  gam2mm
C --- BEGIN SEQUENCE
C I ONLY WANT TO MAKE ONE CALCULATION, NOT KEEP LOOPING FOREVER
C
  800 CONTINUE
C
C  IROAD=0 READ MM3 PART OF INPUT FILE AND CHECK FOR ERRORS ONLY
C  IROAD=1 DO Optimization
```

```
C
      IF (IROAD.EQ.0) THEN
        CALL PART1
        WRITE(IOUT,*)'          NO ERRORS FOUND IN MM2 INPUT FILE '
c
c         write(iout,*)
c         write(iout,*) ' x  y  z in mm3 before we return '
c         do 667 jjj=1,n
c           write(iout,*) x(jjj),y(jjj),z(jjj)
c  667    continue
        RETURN
      ELSE IF (IROAD.EQ.1) THEN
        CALL PART2
        CALL PART3
      END IF
C
      WRITE(IOUT,810)
  810 FORMAT(/'    MM optimization of Region 4 Complete .....')
      RETURN
```

E.3.4 Module mm31.S.f subroutine part1 .

```
c  gam2mm
c        hard set tmax at an extremely large value
c        tmax entered im nimutes
c
      tmax=1440.
      TMAX=TMAX*60.

c
c  gam2mm
c    fmin and fmove modified to enable use of RESTRICTED atom motion
c
c
c      IF (MOVE.EQ.1.AND.NRSTR.NE.0) WRITE (IOUT,510)
c  510 FORMAT(10X,'THE MOTION OF SOME ATOMS IS RESTRICTED.')
c      IF (MOVE.GE.2.AND.NRSTR.NE.0) WRITE (IOUT,515)
c  515 FORMAT(10X,'THE RESTRICTED MOTION OPTION IS DISABLED.')
c
c
      write(iout,*)
      write(iout,511)
      write(iout,510)
  510 format(25X,' HYBRID OPTIMIZATION',/,15X,
     #  'RESTRICTED MOTION FOR FULL DIAGONAL METHOD ADDED')
      write(iout,511)
  511 format(15X,50('='))
c
c

c  gam2mm
c    Restricted motion for full matrix (MOVE=2,4) added
c
c  830 IF (MOVE.GE.2) GO TO 870
  830 continue

c gam2mm
c
      goto 960
      IF(NH.EQ.0) GO TO 960
      IF(NDRIVE.NE.0) GO TO 940
      HFORM=IABS(HFORM)+NH*10
      GO TO 960
C   WHEN DRIVER IS USED, IF HEAT PARAMETERS ARE READ IN, HEAT WILL NOT
C   BE CALCULATED.
  940 DO 950 K=1,NH
  950 READ(NRD,250) IDUM
```

```
762        HFORM=0
763 C
764 C  PRINT ENERGY EQUATIONS; CALC AND PRINT INITIAL ENERGY AND GEOMETRY.
765 C  GENERALLY, IF INIT=1 ENERGY IS PRINTED; IF INIT=0 IT"S OMITTED.  OVER
766 C  RIDING THIS IS IPRINT=2 (ALWAYS PRINT) AND IPRINT=1 (LIMIT VDW PRINT)
767 C  SET UP IPR SUCH THAT 0=NO PRINT, 1= PRINT BUT LIMIT VDW, 2=PRINT ALL.
768 C  IPRINT=5 ALLOWS TO PRINT BEND-BEND INTERACTION PAIRS.
769 c
770
771   960 IPR=2*INIT

938 c
939 c gamm3
940 c  we'll never have more that one data deck per file, so we always
941 c  return here
942 c      IF(INIT.EQ.0) GO TO 1290
943       RETURN
944 c
945 c
946 C
947 C --- NEW DATA DECK ==================================================
948
```

E.3.5 Module mm31.S.f subroutine part2 .

```
1063 c
1064 c gam2mm
1065 c
1066       move=2
1067 c

1195 c
1196 c  gam2mm skip this bit
1197 c
1198   goto 666
1199 C --- STORE NEW COORDINATES IN TAPE9 AND MOVE ON TO PART3 ------------- MM3 0164
1200 C      DO 210 I=1,N                                                      MM3 0165
1201 c      WRITE(IPN,200) X(I),Y(I),Z(I),CTYPE(I),ITYPE(I),I                 MM3 0166
1202 c  200 FORMAT(3F10.5,A2,I3,'(',I3,')')                                   MM3 0167
1203 c  210 CONTINUE                                                          MM3 0168
1204 c
1205   666 continue
1206 C
```

E.3.6 Module mm31.S.f subroutine part3 .

```
1403 c
1404 c  gam2mm: The next 75 lines or so are commented out.
1405 c          This is where the energy from EVERY interaction term is
1406 c          written to the output file. This part is skipped to reduce
1407 c          the size of the output file
1408 C      write(iout,570)
1409 C      call total
1410 c
1411 c          Notice the next 75 lines or so are commented out

1546 c gam2mm
1547 c
1548 c      write(iout,*)' Right before UNIT changes commented out'
1549 c     I had to change a file assignment from 12 to 32 in EHEAT
1550 c     to get this call to work
1551 c
1552       INP=NRD
1553 c      IF (HFORM.NE.0) CALL EHEAT
1554       INP=IRD
```

```
c

c
c  gam2mm Don't write MM3.TAPE9 file
c
      goto 999
C
C --------STORED IN TAPE9 ----------------------------------------
c  gam2mm
  999 continue
      RETURN
      END
```

E.3.7 Module mm31.S.f subroutine Davejr.

```
c  gam2mm This fixes problem with reassignment of IOUT somewhere in loop
c
      ioutgam=iout

c  gam2mm: Fix reassignment of Unit IOUT
c
      iout=ioutgam

c
c  gam2mm Disable MM3 time checking. Hard Set limit above
c
      IF(DELCPU.LT.CPULEFT ) GO TO 340
c
```

E.3.8 Module mvib31.S.f subroutine fmin . Changes to Maseras' version of fmin

```
C -- gam2mm  ---------- New COMMONS for merging with GAMESS ---------
C
      COMMON /FORCMM/ gradmm(750)
      COMMON /NREGNS/ NREGN1,NREGN2,NREGN3,NREGN4,NREGN5
      COMMON /IREGNS/ IREGN1(50),IREGN2(50),IREGN3(50),
     #                IREGN4(500),IREGN5(250)
      COMMON /MM2PAX/ XCOMM2,YCOMM2,ZCOMM2,XFPAM2(3,3)
c
      INTEGER NREGN1,NREGN2,NREGN3,NREGN4,NREGN5
      INTEGER IREGN1,IREGN2,IREGN3,IREGN4,IREGN5
      REAL*8 XCOMM2,YCOMM2,ZCOMM2,XFPAM2
C ------------------------------------------------------------

c
c  gam2mm  Disable time limit checking by setting tleft large
c
c   original code line
c     tleft      = tmax - cpusec
      tleft= 9999999.0
c

c  gam2mm
c  JRS I use a 1-d array for the vector
c
c       do 3010 ii= 1,natom
c        ii1= 1 + 3*(ii-1)
c        ii2= ii1 + 1
c        ii3= ii1 + 2
c        xg(ii)= ff(ii1)
c        yg(ii)= ff(ii2)
c        zg(ii)= ff(ii3)
c 3010   continue
c
      do 3010 ii=1,3*natom
        gradmm(ii)=ff(ii)
```

```
 561  3010 continue

 887 c gam2mm  JRS  Do this in interface module, not here
 888 C Prints gradient
 889 c       xgt= 0.
 890 c       ygt= 0.
 891 c       zgt= 0.
 892 c       write(iout,902)
 893 c  902 format(2x,'FINAL ATOMIC GRADIENT')
 894 c       do 908 ii= 1,natom
 895 c        xgt= xgt+xg(ii)
 896 c        ygt= ygt+yg(ii)
 897 c       zgt= zgt+zg(ii)
 898 c        write(iout,905) xg(ii),yg(ii),zg(ii)
 899 c  905  format(2x,3f20.10)
 900 c  908  continue
 901 c       write(iout,909) xgt,ygt,zgt
 902 c  909 format(2x,'SUM OF GRADIENTS PER COMPONENT',/,2x,3f20.10)
 903 c
 904 c
```

E.3.9 Module mvib31.S.f subroutine fd_estr .

```
 989 C ------------ New COMMONS for merging with GAMESS ------------
 990 C
 991        COMMON /FORCMM/ gradmm(750)
 992        COMMON /NREGNS/ NREGN1,NREGN2,NREGN3,NREGN4,NREGN5
 993        COMMON /IREGNS/ IREGN1(50),IREGN2(50),IREGN3(50),
 994       #                IREGN4(500),IREGN5(250)
 995        COMMON /MM2PAX/ XCOMM2,YCOMM2,ZCOMM2,XFPAM2(3,3)
 996 c
 997        INTEGER NREGN1,NREGN2,NREGN3,NREGN4,NREGN5
 998        INTEGER IREGN1,IREGN2,IREGN3,IREGN4,IREGN5
 999        REAL*8 XCOMM2,YCOMM2,ZCOMM2,XFPAM2
1000 C ------------------------------------------------------------

1016 c==================================================
1017 c  gam2mm Add term IFF imvd or ib in Region 4
1018 c
1019        do 800 igam=1,nregn4
1020           ikeep=iregn4(igam)
1021   800       if ((ikeep.eq.imvd) .or. (ikeep.eq.ib)) goto 810
1022 c
1023 c  Only get here when neither imvd nor ib in Region 4
1024         goto 10
1025 c
1026   810 continue

1087    10 continue
```

E.3.10 Module mvib31.S.f subroutine fmove .

E.3.11 Module mvib31.S.f subroutine fd_ebend .

```
1233 C ------------ New COMMONS for merging with GAMESS ------------
1234 C
1235        COMMON /FORCMM/ gradmm(750)
1236        COMMON /NREGNS/ NREGN1,NREGN2,NREGN3,NREGN4,NREGN5
1237        COMMON /IREGNS/ IREGN1(50),IREGN2(50),IREGN3(50),
1238       #                IREGN4(500),IREGN5(250)
1239        COMMON /MM2PAX/ XCOMM2,YCOMM2,ZCOMM2,XFPAM2(3,3)
1240 c
1241        INTEGER NREGN1,NREGN2,NREGN3,NREGN4,NREGN5
1242        INTEGER IREGN1,IREGN2,IREGN3,IREGN4,IREGN5
```

```
1243        REAL*8 XCOMM2,YCOMM2,ZCOMM2,XFPAM2
1244 C ------------------------------------------------------------

            TYPE 2 angles

1311 c  gam2mm: If ia,ib,ic,id NOT in Region 4, don't add derivative
1312 c
1313 c
1314        do 800 igam=1,nregn4
1315           ikeep=iregn4(igam)
1316   800       if ((ikeep.eq.ia) .or. (ikeep.eq.ib) .or. (ikeep.eq.ic) .or.
1317      #       (ikeep.eq.id)) goto 810
1318 c
1319 c  Only get here when none of ia,ib,ic,id is in Region 4
1320        goto 820
1321 c
1322   810 continue
1323 c
1324 c  Temporary Diagnostic
1325 c      write(iout,*) 'called fd_opb2 ',ia,ib,ic,id
1326 c ------------------------------------------------------------------
1327 c
1328         call fd_opb2 (i4,ia,ib,ic,id,const1,const,const2,imin)
1329         iopbc=1
1330        endif
1331       endif
1332 c
1333   820 continue

1338 c  gam2mm: If ib or imvd or ic NOT in Region 4, don't add derivative
1339 c
1340 c
1341        do 830 igam=1,nregn4
1342           ikeep=iregn4(igam)
1343   830       if ((ikeep.eq.ib) .or. (ikeep.eq.imvd) .or. (ikeep.eq.ic))
1344      #      goto 840
1345 c
1346 c  Only get here when neither ib,imvd, nor ic in Region 4
1347        goto 30
1348 c
1349   840 continue

1456 c      ---------------  end of stretch-bend derivatives  -------------
1457    30 continue
              TYPE 1 ANGLES

1585 c ------------------------------------------------------------------
1586 c  gam2mm: If ia,ib,ic,id NOT in Region 4, don't add derivative
1587 c
1588 c
1589        do 850 igam=1,nregn4
1590           ikeep=iregn4(igam)
1591   850       if ((ikeep.eq.ia) .or. (ikeep.eq.ib) .or. (ikeep.eq.ic) .or.
1592      #       (ikeep.eq.id)) goto 860
1593 c
1594 c  Only get here when none of ia,ib,ic,id is in Region 4
1595        goto 870
1596 c
1597   860 continue
1598 c
1599 c  Temporary Diagnostic
1600 c      write(iout,*) 'called fd_opb2 ',ia,ib,ic,id
1601 c ------------------------------------------------------------------
1602 c
1603 c
1604         call fd_opb1 (i4,ia,ib,ic,id,conout,const,const2,imin)
1605         iopbc=1
1606        endif
```

```
1607 c --------- when mp=1 (first angle) calculate derivates  -----------
1608 c --------- for in-plane ic-ia-id and out-plane ia-ib-ia -----------
1609 c
1610   870  continue

1622 c ----------------------------------------------------------------
1623 c  gam2mm: If ia,ib,ic,id NOT in Region 4, don't add derivative
1624 c
1625 c
1626       do 880 igam=1,nregn4
1627          ikeep=iregn4(igam)
1628   880      if ((ikeep.eq.ia) .or. (ikeep.eq.ib) .or. (ikeep.eq.ic) .or.
1629      #       (ikeep.eq.id)) goto 881
1630 c
1631 c  Only get here when none of ia,ib,ic,id is in Region 4
1632        goto 885
1633 c
1634   881 continue
1635 c
1636 c  Temporary Diagnostic
1637 c      write(iout,*) 'called fd_opb3 ',ia,ib,ic,id
1638 c
1639         call fd_opb3 (i4,ia,ib,ic,id,conout,conin,angin,imin)
1640        endif
1641       endif
1642 c
1643   885 continue
1644 c ------------------------------------------------------------------

1650 c  gam2mm: If ib or imvd or ic NOT in Region 4, don't add derivative
1651 c
1652 c
1653       do 890 igam=1,nregn4
1654          ikeep=iregn4(igam)
1655   890      if ((ikeep.eq.imvd) .or. (ikeep.eq.ia) .or. (ikeep.eq.ic))
1656      #     goto 891
1657 c
1658 c  Only get here when neither ib,imvd, nor ic in Region 4
1659        goto 270
1660 c
1661   891 continue

1761 c     ---------------  end of stretch-bend derivatives  -------------
1762   270 continue
```

E.3.12 Module mvib31.S.f subroutine fd_ebbnd .

```
5671 C ------------ New COMMONS for merging with GAMESS ------------
5672 C
5673       COMMON /FORCMM/ gradmm(750)
5674       COMMON /NREGNS/ NREGN1,NREGN2,NREGN3,NREGN4,NREGN5
5675       COMMON /IREGNS/ IREGN1(50),IREGN2(50),IREGN3(50),
5676      #                IREGN4(500),IREGN5(250)
5677       COMMON /MM2PAX/ XCOMM2,YCOMM2,ZCOMM2,XFPAM2(3,3)
5678 c
5679       INTEGER NREGN1,NREGN2,NREGN3,NREGN4,NREGN5
5680       INTEGER IREGN1,IREGN2,IREGN3,IREGN4,IREGN5
5681       REAL*8 XCOMM2,YCOMM2,ZCOMM2,XFPAM2
5682 C ------------------------------------------------------------

5685 c        type-1 bend-bend (two angles with common center atom)
5796 c     -------------------- calculate de/dx, etc ----------------------
5797 c
5798 c  gam2mm: If ia,ib(ie),ic,id,if NOT in Region 4, don't add derivative
5799 c
5800 c
5801       do 800 igam=1,nregn4
```

```
5802          ikeep=iregn4(igam)
5803          if ((ikeep.eq.ia) .or. (ikeep.eq.ib) .or. (ikeep.eq.ic).or.
5804      #   (ikeep.eq.id) .or. (ikeep.eq.ie) .or. (ikeep.eq.if)) goto 810
5805   800 continue
5806 c
5807 c  Only get here when ia,ib,ic,id,ie,if NOT in Region 4
5808        goto 80
5809 c
5810   810 continue
5811 c
5812 c  Temporary Diagnostic
5813 c      write(iout,*) 'fd_ebbnd  ia ib ic id ie if ',ia,ib,ic,id,ie,if
5814 c ------------------------------------------------------------------

5845    80   continue

5898 c     -------------------- calculate de/dx, etc ----------------------
5899 c
5900 c  gam2mm: If ia,ib(ie),ic,id,if NOT in Region 4, don't add derivative
5901 c
5902 c
5903       do 820 igam=1,nregn4
5904          ikeep=iregn4(igam)
5905          if ((ikeep.eq.ia) .or. (ikeep.eq.ib) .or. (ikeep.eq.ic).or.
5906      #   (ikeep.eq.id) .or. (ikeep.eq.ie) .or. (ikeep.eq.if)) goto 830
5907   820 continue
5908 c
5909 c  Only get here when ia,ib,ic,id,ie,if NOT in Region 4
5910        goto 140
5911 c
5912   830 continue

5947   140   continue
```

E.3.13 Module mvib32.S.f subroutine fd_vdwbd .

```
 72 C ------------ New COMMONS for merging with GAMESS ------------
 73 C
 74       COMMON /FORCMM/ gradmm(750)
 75       COMMON /NREGNS/ NREGN1,NREGN2,NREGN3,NREGN4,NREGN5
 76       COMMON /IREGNS/ IREGN1(50),IREGN2(50),IREGN3(50),
 77      #                IREGN4(500),IREGN5(250)
 78       COMMON /MM2PAX/ XCOMM2,YCOMM2,ZCOMM2,XFPAM2(3,3)
 79 c
 80       INTEGER NREGN1,NREGN2,NREGN3,NREGN4,NREGN5
 81       INTEGER IREGN1,IREGN2,IREGN3,IREGN4,IREGN5
 82       REAL*8 XCOMM2,YCOMM2,ZCOMM2,XFPAM2
 83 C ------------------------------------------------------------

132 c ---------------------------------------------------------
133 c  gam2mm    Add term  IFF one of atoms is in Region 4
134 C            or if both atoms are in Region 3
135 c
136       ir4yes=0
137       ir33yes=0
138       do 805 igam=1,nregn4
139          ikeep=iregn4(igam)
140   805    if ((ikeep.eq.i) .or. (ikeep.eq.k)) ir4yes=1
141 c
142       do 806 igam=1,nregn3
143          ikeep=iregn3(igam)
144   806    if (ikeep.eq.i)  ir33yes=1
145 c
146       if(ir33yes.eq.1) then
147         do 807 igam=1,nregn3
148           ikeep=iregn3(igam)
```

```
807     if (ikeep.eq.k)  ir33yes=2
      endif
c
      if ((ir4yes.eq.1) .or. (ir33yes.eq.2)) then
c        write(iout,*) ' fd_vdwbd   i   k   ',i,k
        goto 810
      else
        goto 300
      endif
810 continue
```

E.3.14 Module mvib32.S.f subroutine fd_vdwod .

```
C ------------ New COMMONS for merging with GAMESS ------------
C
      COMMON /FORCMM/ gradmm(750)
      COMMON /NREGNS/ NREGN1,NREGN2,NREGN3,NREGN4,NREGN5
      COMMON /IREGNS/ IREGN1(50),IREGN2(50),IREGN3(50),
     #                IREGN4(500),IREGN5(250)
      COMMON /MM2PAX/ XCOMM2,YCOMM2,ZCOMM2,XFPAM2(3,3)
c
      INTEGER NREGN1,NREGN2,NREGN3,NREGN4,NREGN5
      INTEGER IREGN1,IREGN2,IREGN3,IREGN4,IREGN5
      REAL*8 XCOMM2,YCOMM2,ZCOMM2,XFPAM2
C ------------------------------------------------------------
```

```
c ---------------------------------------------------------
c  gam2mm    Add term  IFF one of atoms is in Region 4
C            or if both atoms are in Region 3
c
      ir4yes=0
      ir33yes=0
      do 805 igam=1,nregn4
         ikeep=iregn4(igam)
805      if ((ikeep.eq.i) .or. (ikeep.eq.j)) ir4yes=1
c
      do 806 igam=1,nregn3
         ikeep=iregn3(igam)
806      if (ikeep.eq.i)  ir33yes=1
c
      if(ir33yes.eq.1) then
        do 807 igam=1,nregn3
          ikeep=iregn3(igam)
807       if (ikeep.eq.j)  ir33yes=2
      endif
c
      if ((ir4yes.eq.1) .or. (ir33yes.eq.2)) then
c Temporary Diagnostic
c        write(iout,*) ' fd_vdwod   i   j   ',i,j
        goto 810
      else
        goto 300
      endif
810 continue
```

E.3.15 Module mvib32.S.f subroutine fd_chgchg .

```
C ------------ New COMMONS for merging with GAMESS ------------
C
      COMMON /FORCMM/ gradmm(750)
      COMMON /NREGNS/ NREGN1,NREGN2,NREGN3,NREGN4,NREGN5
      COMMON /IREGNS/ IREGN1(50),IREGN2(50),IREGN3(50),
     #                IREGN4(500),IREGN5(250)
      COMMON /MM2PAX/ XCOMM2,YCOMM2,ZCOMM2,XFPAM2(3,3)
c
```

```
      INTEGER NREGN1,NREGN2,NREGN3,NREGN4,NREGN5
      INTEGER IREGN1,IREGN2,IREGN3,IREGN4,IREGN5
      REAL*8 XCOMM2,YCOMM2,ZCOMM2,XFPAM2
C ------------------------------------------------------------
```

```
c ------------------------------------------------------------
c  gam2mm    Add term  IFF one of atoms is in Region 4
C            or if both atoms are in Region 3
c
      ir4yes=0
      ir33yes=0
      do 805 igam=1,nregn4
         ikeep=iregn4(igam)
  805    if ((ikeep.eq.i) .or. (ikeep.eq.k)) ir4yes=1
c
      do 806 igam=1,nregn3
         ikeep=iregn3(igam)
  806    if (ikeep.eq.i)  ir33yes=1
c
      if(ir33yes.eq.1) then
        do 807 igam=1,nregn3
          ikeep=iregn3(igam)
  807     if (ikeep.eq.k)  ir33yes=2
      endif
c
      if ((ir4yes.eq.1) .or. (ir33yes.eq.2)) then
        write(iout,*) ' fd_chgchg   i   j   ',i,j
        goto 810
      else
        goto 300
      endif
c
  810 continue
c ------------------------------------------------------------
```

E.3.16 Module mvib32.S.f subroutine fd_dipole .

```
c-------------------------------------------------------------------c
c
C ------------ New COMMONS for merging with GAMESS ------------
C
      COMMON /FORCMM/ gradmm(750)
      COMMON /NREGNS/ NREGN1,NREGN2,NREGN3,NREGN4,NREGN5
      COMMON /IREGNS/ IREGN1(50),IREGN2(50),IREGN3(50),
     #                IREGN4(500),IREGN5(250)
      COMMON /MM2PAX/ XCOMM2,YCOMM2,ZCOMM2,XFPAM2(3,3)
c
      INTEGER NREGN1,NREGN2,NREGN3,NREGN4,NREGN5
      INTEGER IREGN1,IREGN2,IREGN3,IREGN4,IREGN5
      REAL*8 XCOMM2,YCOMM2,ZCOMM2,XFPAM2
C ------------------------------------------------------------
```

```
c ------------------------------------------------------------------
c  gam2mm: If one of i,j,imvd,idip NOT  in Region 4, skip
c
c
      do 800 igam=1,nregn4
         ikeep=iregn4(igam)
         if ((ikeep.eq.i) .or. (ikeep.eq.j) .or. (ikeep.eq.imvd) .or.
     #      (idip.eq.ikeep)) goto 810
  800 continue
c
c  Only get here when none of above are in Region 4
       goto 10
c
  810 continue
```

```
1596    10 continue
```

E.3.17 Module mvib32.S.f subroutine fd_chgdip .

```
1626 C ------------ New COMMONS for merging with GAMESS ------------
1627 C
1628       COMMON /FORCMM/ gradmm(750)
1629       COMMON /NREGNS/ NREGN1,NREGN2,NREGN3,NREGN4,NREGN5
1630       COMMON /IREGNS/ IREGN1(50),IREGN2(50),IREGN3(50),
1631      #                IREGN4(500),IREGN5(250)
1632       COMMON /MM2PAX/ XCOMM2,YCOMM2,ZCOMM2,XFPAM2(3,3)
1633 c
1634       INTEGER NREGN1,NREGN2,NREGN3,NREGN4,NREGN5
1635       INTEGER IREGN1,IREGN2,IREGN3,IREGN4,IREGN5
1636       REAL*8 XCOMM2,YCOMM2,ZCOMM2,XFPAM2
1637 C ------------------------------------------------------------

1667 c  gam2mm: If i,j, or imvd NOT in Region 4, don't add derivative
1668 c
1669 c
1670       do 800 igam=1,nregn4
1671          ikeep=iregn4(igam)
1672          if ((ikeep.eq.i) .or. (ikeep.eq.j) .or. (ikeep.eq.imvd))
1673      #     goto 810
1674   800 continue
1675 c
1676 c  Only get here when neither i,j, AND imvd NOT in Region 4
1677        goto 100
1678 c
1679   810 continue

1887   100  continue
```

E.3.18 Module mvib32.S.f subroutine fd_dipchg.

```
1916 C ------------ New COMMONS for merging with GAMESS ------------
1917 C
1918       COMMON /FORCMM/ gradmm(750)
1919       COMMON /NREGNS/ NREGN1,NREGN2,NREGN3,NREGN4,NREGN5
1920       COMMON /IREGNS/ IREGN1(50),IREGN2(50),IREGN3(50),
1921      #                IREGN4(500),IREGN5(250)
1922       COMMON /MM2PAX/ XCOMM2,YCOMM2,ZCOMM2,XFPAM2(3,3)
1923 c
1924       INTEGER NREGN1,NREGN2,NREGN3,NREGN4,NREGN5
1925       INTEGER IREGN1,IREGN2,IREGN3,IREGN4,IREGN5
1926       REAL*8 XCOMM2,YCOMM2,ZCOMM2,XFPAM2

1977 c ------------------------------------------------------------------
1978 c  gam2mm: If i,j, or imvd NOT in Region 4, don't add derivative
1979 c
1980 c
1981       do 800 igam=1,nregn4
1982          ikeep=iregn4(igam)
1983          if ((ikeep.eq.i) .or. (ikeep.eq.j) .or. (ikeep.eq.imvd))
1984      #     goto 810
1985   800 continue
1986 c
1987 c  Only get here when neither i,j, AND imvd NOT in Region 4
1988        goto 100
1989 c
1990   810 continue

2228   100  continue
```

E.3.19 Module mvib32.S.f subroutine fd_etors.

```
2271 C ------------ New COMMONS for merging with GAMESS ------------
2272 C
2273       COMMON /FORCMM/ gradmm(750)
2274       COMMON /NREGNS/ NREGN1,NREGN2,NREGN3,NREGN4,NREGN5
2275       COMMON /IREGNS/ IREGN1(50),IREGN2(50),IREGN3(50),
2276      #                IREGN4(500),IREGN5(250)
2277       COMMON /MM2PAX/ XCOMM2,YCOMM2,ZCOMM2,XFPAM2(3,3)
2278 c
2279       INTEGER NREGN1,NREGN2,NREGN3,NREGN4,NREGN5
2280       INTEGER IREGN1,IREGN2,IREGN3,IREGN4,IREGN5
2281       REAL*8 XCOMM2,YCOMM2,ZCOMM2,XFPAM2
2282 C ------------------------------------------------------------

2287 c                    type-1 torsion  imvd-n2-n3-n4

2536 c  gam2mm: If imvd,n2,n3, or n4 in Region 4, add term
2537 c
2538 c
2539       do 800 igam=1,nregn4
2540          ikeep=iregn4(igam)
2541          if ((ikeep.eq.imvd) .or. (ikeep.eq.n2) .or. (ikeep.eq.n3).or.
2542      #    (ikeep.eq.n4) ) goto 810
2543   800 continue
2544 c
2545 c  Only get here when none of imvd,n2,n3,n4 in Region 4
2546        goto 150
2547 c
2548   810 continue

2594   150    continue

2623 c                   type-2 torsion  n1-imvd-n3-n4

2873 c  gam2mm: If n1,imvd,n3, or n4 in Region 4, add term
2874 c
2875 c
2876       do 820 igam=1,nregn4
2877          ikeep=iregn4(igam)
2878          if ((ikeep.eq.n1) .or. (ikeep.eq.imvd) .or. (ikeep.eq.n3).or.
2879      #    (ikeep.eq.n4) ) goto 830
2880   820 continue
2881 c
2882 c  Only get here when none of imvd,n2,n3,n4 in Region 4
2883        goto 350
2884 c
2885   830 continue
2886 c
2954   350    continue
```

E.4 New Modules:ghmm2.f

This is the interface module between GAMESS and MM3

E.5 Resolution of GAMESS-MM3 Name Conflicts

```
RESOLUTION ON NAME CONFLICTS BETWEEN MM3 AND GAMESS

 - COMMON/ATOM/ USED BY BOTH

 - RENAMED MM3 COMMON BLOCK TO COMMON/ATMM3/

mm31.f:27:    COMMON/ATMM3/N,X(MAXATOM),Y(MAXATOM),Z(MAXATOM),ITYPE(MAXATOM),
mm31.f:350:   COMMON/ATMM3/N,X(MAXATOM),Y(MAXATOM),Z(MAXATOM),ITYPE(MAXATOM),
```

```
mm31.f:1123:  COMMON/ATMM3/N,X(MAXATOM),Y(MAXATOM),Z(MAXATOM),ITYPE(MAXATOM),
mm31.f:1290:  COMMON/ATMM3/N,X(MAXATOM),Y(MAXATOM),Z(MAXATOM),ITYPE(MAXATOM),
mm31.f:1695:  COMMON/ATMM3/N,X(MAXATOM),Y(MAXATOM),Z(MAXATOM),ITYPE(MAXATOM),
mm31.f:1730:  COMMON/ATMM3/N,X(MAXATOM),Y(MAXATOM),Z(MAXATOM),ITYPE(MAXATOM),
mm31.f:1839:  COMMON/ATMM3/N,X(MAXATOM),Y(MAXATOM),Z(MAXATOM),ITYPE(MAXATOM),
mm31.f:2000:  COMMON/ATMM3/N,X(MAXATOM),Y(MAXATOM),Z(MAXATOM),ITYPE(MAXATOM),
mm31.f:2053:  COMMON/ATMM3/N,X(MAXATOM),Y(MAXATOM),Z(MAXATOM),ITYPE(MAXATOM),
mm31.f:2211:  COMMON/ATMM3/N,X(MAXATOM),Y(MAXATOM),Z(MAXATOM),ITYPE(MAXATOM),
mm31.f:2258:  COMMON/ATMM3/N,X(MAXATOM),Y(MAXATOM),Z(MAXATOM),ITYPE(MAXATOM),
mm31.f:2277:  COMMON/ATMM3/NATOM,X(MAXATOM),Y(MAXATOM),Z(MAXATOM),
mm31.f:4286:  COMMON/ATMM3/NATOM,X(MAXATOM),Y(MAXATOM),Z(MAXATOM),
mm31.f:4429:  COMMON/ATMM3/N,X(MAXATOM),Y(MAXATOM),Z(MAXATOM),ITYPE(MAXATOM),
mm31.f:4640:  COMMON/ATMM3/N,X(MAXATOM),Y(MAXATOM),Z(MAXATOM),ITYPE(MAXATOM),
mm31.f:4709:  COMMON/ATMM3/N,X(MAXATOM),Y(MAXATOM),Z(MAXATOM),ITYPE(MAXATOM),
mm31.f:5330:  COMMON/ATMM3/N,X(MAXATOM),Y(MAXATOM),Z(MAXATOM),ITYPE(MAXATOM),
mm31.f:5382:  COMMON/ATMM3/N,X(MAXATOM),Y(MAXATOM),Z(MAXATOM),ITYPE(MAXATOM),
mm31.f:5495:  COMMON/ATMM3/NATOM,X(MAXATOM),Y(MAXATOM),Z(MAXATOM),
mm32.f:14:    COMMON/ATMM3/N,X(MAXATOM),Y(MAXATOM),Z(MAXATOM),ITYPE(MAXATOM),
mm32.f:300:   COMMON/ATMM3/N,X(MAXATOM),Y(MAXATOM),Z(MAXATOM),ITYPE(MAXATOM),
mm32.f:474:   COMMON/ATMM3/NATOM,X(MAXATOM),Y(MAXATOM),Z(MAXATOM),
mm32.f:550:   COMMON/ATMM3/N,X(MAXATOM),Y(MAXATOM),Z(MAXATOM),ITYPE(MAXATOM),
mm32.f:591:   COMMON/ATMM3/NATOM,X(MAXATOM),Y(MAXATOM),Z(MAXATOM),
mm32.f:1103:  COMMON/ATMM3/NATOM,X(MAXATOM),Y(MAXATOM),Z(MAXATOM),
mm32.f:1785:  COMMON/ATMM3/NATOM,X(MAXATOM),Y(MAXATOM),Z(MAXATOM),
mm32.f:2275:  COMMON/ATMM3/NATOM,X(MAXATOM),Y(MAXATOM),Z(MAXATOM),
mm32.f:2622:  COMMON/ATMM3/NATOM,X(MAXATOM),Y(MAXATOM),Z(MAXATOM),
mm32.f:3129:  COMMON/ATMM3/NTOTAL,X(MAXATOM),Y(MAXATOM),Z(MAXATOM),
mm32.f:3289:  COMMON/ATMM3/NTOTAL,X(MAXATOM),Y(MAXATOM),Z(MAXATOM),
mm32.f:3573:  COMMON/ATMM3/NTOTAL,X(MAXATOM),Y(MAXATOM),Z(MAXATOM),
mm32.f:3615:  COMMON/ATMM3/NTOTAL,X(MAXATOM),Y(MAXATOM),Z(MAXATOM),
mm32.f:3707:  COMMON/ATMM3/NTOTAL,X(MAXATOM),Y(MAXATOM),Z(MAXATOM),
mm32.f:4662:  COMMON/ATMM3/NTOTAL,X(MAXATOM),Y(MAXATOM),Z(MAXATOM),
mm33.f:14:    COMMON/ATMM3/N,X(MAXATOM),Y(MAXATOM),Z(MAXATOM),ITYPE(MAXATOM),
mm33.f:379:   COMMON/ATMM3/NATOM,X(MAXATOM),Y(MAXATOM),Z(MAXATOM),
mm33.f:444:   COMMON/ATMM3/NATOM,X(MAXATOM),Y(MAXATOM),Z(MAXATOM),
mm33.f:654:   COMMON/ATMM3/NATOM,X(MAXATOM),Y(MAXATOM),Z(MAXATOM),
mm33.f:994:   COMMON/ATMM3/N,X(MAXATOM),Y(MAXATOM),Z(MAXATOM),ITYPE(MAXATOM),
mm33.f:1326:  COMMON/ATMM3/N,X(MAXATOM),Y(MAXATOM),Z(MAXATOM),ITYPE(MAXATOM),
mm33.f:1421:  COMMON/ATMM3/N,X(MAXATOM),Y(MAXATOM),Z(MAXATOM),ITYPE(MAXATOM),
mm33.f:1532:  COMMON/ATMM3/N,X(MAXATOM),Y(MAXATOM),Z(MAXATOM),ITYPE(MAXATOM),
mm33.f:1639:  COMMON/ATMM3/N,X(MAXATOM),Y(MAXATOM),Z(MAXATOM),ITYPE(MAXATOM),
mm33.f:1772:  COMMON/ATMM3/N,X(MAXATOM),Y(MAXATOM),Z(MAXATOM),ITYPE(MAXATOM),
mm33.f:1939:  COMMON/ATMM3/N,X(MAXATOM),Y(MAXATOM),Z(MAXATOM),ITYPE(MAXATOM),
mm33.f:2212:  COMMON/ATMM3/NATOM,X(MAXATOM),Y(MAXATOM),Z(MAXATOM),
mm33.f:2366:  COMMON/ATMM3/N,X(MAXATOM),Y(MAXATOM),Z(MAXATOM),ITYPE(MAXATOM),
mm33.f:2555:  COMMON/ATMM3/NATOM,X(MAXATOM),Y(MAXATOM),Z(MAXATOM),
mm33.f:3152:  COMMON/ATMM3/N,X(MAXATOM),Y(MAXATOM),Z(MAXATOM),ITYPE(MAXATOM),
mm33.f:3378:  COMMON/ATMM3/NATOMS,X(MAXATOM),Y(MAXATOM),Z(MAXATOM),
mm33.f:3485:  COMMON/ATMM3/NATOMS,X(MAXATOM),Y(MAXATOM),Z(MAXATOM),
mm33.f:3586:  COMMON/ATMM3/NATOM,X(MAXATOM),Y(MAXATOM),Z(MAXATOM),
mm33.f:3670:  COMMON/ATMM3/NATOM,X(MAXATOM),Y(MAXATOM),Z(MAXATOM),
mm33.f:3722:  COMMON/ATMM3/N,X(MAXATOM),Y(MAXATOM),Z(MAXATOM),ITYPE(MAXATOM),
mm33.f:3881:  COMMON/ATMM3/N,X(MAXATOM),Y(MAXATOM),Z(MAXATOM),ITYPE(MAXATOM),
mm33.f:3908:  COMMON/ATMM3/NATOM,X(MAXATOM),Y(MAXATOM),Z(MAXATOM),
mm33.f:4012:  COMMON/ATMM3/N,X(MAXATOM),Y(MAXATOM),Z(MAXATOM),ITYPE(MAXATOM),
mm33.f:4652:  COMMON/ATMM3/N,X(MAXATOM),Y(MAXATOM),Z(MAXATOM),ITYPE(MAXATOM),
mm33.f:4693:  COMMON/ATMM3/N,X(MAXATOM),Y(MAXATOM),Z(MAXATOM),ITYPE(MAXATOM),
mm33.f:4717:  COMMON/ATMM3/N,X(MAXATOM),Y(MAXATOM),Z(MAXATOM),ITYPE(MAXATOM),
mm34.f:7:     COMMON/ATMM3/NATOM,X(MAXATOM),Y(MAXATOM),Z(MAXATOM),
mm34.f:171:   COMMON/ATMM3/N,X(MAXATOM),Y(MAXATOM),Z(MAXATOM),ITYPE(MAXATOM),
mm34.f:295:   COMMON/ATMM3/N,X(MAXATOM),Y(MAXATOM),Z(MAXATOM),ITYPE(MAXATOM),
mm34.f:401:   COMMON/ATMM3/N,X(MAXATOM),Y(MAXATOM),Z(MAXATOM),ITYPE(MAXATOM),
mm34.f:480:   COMMON/ATMM3/NATOM,X(MAXATOM),Y(MAXATOM),Z(MAXATOM),
mm34.f:665:   COMMON/ATMM3/N,X(MAXATOM),Y(MAXATOM),Z(MAXATOM),ITYPE(MAXATOM),
mm34.f:739:   COMMON/ATMM3/N,X(MAXATOM),Y(MAXATOM),Z(MAXATOM),ITYPE(MAXATOM),
mm34.f:840:   COMMON/ATMM3/N,X(MAXATOM),Y(MAXATOM),Z(MAXATOM),ITYPE(MAXATOM),
mm34.f:1107:  COMMON/ATMM3/N,X(MAXATOM),Y(MAXATOM),Z(MAXATOM),ITYPE(MAXATOM),
mm34.f:1258:  COMMON/ATMM3/N,X(MAXATOM),Y(MAXATOM),Z(MAXATOM),ITYPE(MAXATOM),
```

```
mm34.f:1402:  COMMON/ATMM3/N,X(MAXATOM),Y(MAXATOM),Z(MAXATOM),ITYPE(MAXATOM),
mm35.f:15:    COMMON/ATMM3/N,X(MAXATOM),Y(MAXATOM),Z(MAXATOM),ITYPE(MAXATOM),
mm35.f:1337:  COMMON/ATMM3/N,X(MAXATOM),Y(MAXATOM),Z(MAXATOM),ITYPE(MAXATOM),
mm35.f:2840:  COMMON/ATMM3/N,X(MAXATOM),Y(MAXATOM),Z(MAXATOM),ITYPE(MAXATOM),
mm35.f:2971:  COMMON/ATMM3/N,X(MAXATOM),Y(MAXATOM),Z(MAXATOM),ITYPE(MAXATOM),
mm35.f:2996:  COMMON/ATMM3/N,X(MAXATOM),Y(MAXATOM),Z(MAXATOM),ITYPE(MAXATOM),
mm36.f:22:    COMMON/ATMM3/N,X(MAXATOM),Y(MAXATOM),Z(MAXATOM),ITYPE(MAXATOM),
mm36.f:969:   COMMON/ATMM3/N,X(MAXATOM),Y(MAXATOM),Z(MAXATOM),ITYPE(MAXATOM),
mm36.f:1006:  COMMON/ATMM3/N,X(MAXATOM),Y(MAXATOM),Z(MAXATOM),ITYPE(MAXATOM),
mm36.f:2406:  COMMON/ATMM3/N,X(MAXATOM),Y(MAXATOM),Z(MAXATOM),ITYPE(MAXATOM),
mm36.f:2716:  COMMON/ATMM3/N,X(MAXATOM),Y(MAXATOM),Z(MAXATOM),ITYPE(MAXATOM),
mvib31.f:33:  COMMON/ATMM3/natom,x(maxatom),y(maxatom),z(maxatom),
mvib31.f:643: COMMON/ATMM3/natom,x(maxatom),y(maxatom),z(maxatom),
mvib31.f:796: COMMON/ATMM3/natom,x(maxatom),y(maxatom),z(maxatom),
mvib31.f:900: COMMON/ATMM3/natom,x(maxatom),y(maxatom),z(maxatom),
mvib31.f:1380:COMMON/ATMM3/natom,x(maxatom),y(maxatom),z(maxatom),
mvib31.f:1854:COMMON/ATMM3/natom,x(maxatom),y(maxatom),z(maxatom),
mvib31.f:3040:COMMON/ATMM3/natom,x(maxatom),y(maxatom),z(maxatom),
mvib31.f:4005:COMMON/ATMM3/natom,x(maxatom),y(maxatom),z(maxatom),
mvib31.f:5222:COMMON/ATMM3/natom,x(maxatom),y(maxatom),z(maxatom),
mvib32.f:14:  COMMON/ATMM3/natom,x(maxatom),y(maxatom),z(maxatom),
mvib32.f:303: COMMON/ATMM3/natom,x(maxatom),y(maxatom),z(maxatom),
mvib32.f:696: COMMON/ATMM3/natom,x(maxatom),y(maxatom),z(maxatom),
mvib32.f:817: COMMON/ATMM3/natom,x(maxatom),y(maxatom),z(maxatom),
mvib32.f:1407:COMMON/ATMM3/natom,x(maxatom),y(maxatom),z(maxatom),
mvib32.f:1663:COMMON/ATMM3/natom,x(maxatom),y(maxatom),z(maxatom),
mvib32.f:1974:COMMON/ATMM3/natom,x(maxatom),y(maxatom),z(maxatom),
mvib32.f:2679:COMMON/ATMM3/natom,x(maxatom),y(maxatom),z(maxatom),
mvib32.f:3358:COMMON/ATMM3/natom,x(maxatom),y(maxatom),z(maxatom),
mvib32.f:3641:COMMON/ATMM3/natom,x(maxatom),y(maxatom),z(maxatom),
mvib32.f:4096:COMMON/ATMM3/natom,x(maxatom),y(maxatom),z(maxatom),
mvib32.f:4936:COMMON/ATMM3/natom,x(maxatom),y(maxatom),z(maxatom),
mvib32.f:5486:COMMON/ATMM3/natom,x(maxatom),y(maxatom),z(maxatom),
mvib32.f:5627:COMMON/ATMM3/natom,x(maxatom),y(maxatom),z(maxatom),
mvib32.f:5785:COMMON/ATMM3/natom,x(maxatom),y(maxatom),z(maxatom),
mvib32.f:5972:COMMON/ATMM3/natom,x(maxatom),y(maxatom),z(maxatom),
mvib32.f:6202:COMMON/ATMM3/natom,x(maxatom),y(maxatom),z(maxatom),
mvib32.f:6264:COMMON/ATMM3/natom,x(maxatom),y(maxatom),z(maxatom),
mvib32.f:6327:COMMON/ATMM3/natom,x(maxatom),y(maxatom),z(maxatom),
mvib32.f:6481:COMMON/ATMM3/natom,x(maxatom),y(maxatom),z(maxatom),
mvib32.f:6893: COMMON/ATMM3/natom,x(maxatom),y(maxatom),z(maxatom),
-----------------------------------------------------------------------

  COMMON/TRANS/ USED BOTH BY GAMESS AND MM3

    - RENAMED MM3 COMMON BLOCK TO COMMON/TRMM3/

mm31.f:366:      COMMON/TRMM3/NROT,XI,YI,ZI,IFINDP
mm31.f:1130:      COMMON/TRMM3/NROT,XI,YI,ZI,IFINDP
mm31.f:1305:      COMMON/TRMM3/NROT,XI,YI,ZI,IFINDP
mm32.f:3133:      COMMON/TRMM3/NROT,XI,YI,ZI,IFINDP
mm32.f:3295:      COMMON/TRMM3/NROT,XI,YI,ZI,IFINDP
mm33.f:2370:      COMMON/TRMM3/NROT,XI,YI,ZI,IFINDP
mm33.f:2561:      COMMON/TRMM3/NROT,XI,YI,ZI,IFINDP
mm34.f:966:      COMMON/TRMM3/NROT,XI,YI,ZI,IFINDP

-----------------------------------------------------------------------

   COMMON     PICON USED IN GAMESS
   SUBROUTINE PICON USED IN MM3

      - RENAMED MM3 SUBROUTINE PICON TO PIMM3

mm31.f:862:      IF (NORB.NE.0) CALL PIMM3
mm31.f:1172:      CALL PIMM3
mm31.f:1206:         CALL PIMM3
mm31.f:1262:         CALL PIMM3
mm31.f:1453:      IF(NORB.NE.0) CALL PIMM3
```

```
mm34.f:731:       SUBROUTINE PIMM3
mm35.f:2320:C  PI-MODIFICATIONS IN PIMM3.
mm35.f:2378:C --- PI-MODIFICATIONS IN PIMM3.
mm35.f:2438:C --- PI-MODIFICATIONS IN PIMM3.
mm35.f:2500:C --- PI-MODIFICATIONS IN PIMM3 (5-MEMBERED RING).
-----------------------------------------------------------------------
```

SUBROUTINE ROTAT USED IN GAMESS
SUBROUTINE ROTAT ALSO USED IN MM3

- RENAMED MM3 SUBROUTINE TO ROMM3 (5 LETTERS LONG LIKE ORIGINAL)

```
mm34.f:340:       CALL ROMM3 (LIST,XR,YR,ZR,X,Y,Z)
mm34.f:1201:       SUBROUTINE ROMM3 (LIST,XR,YR,ZR,X,Y,Z)
-----------------------------------------------------------------------
```

SUBROUTINE ROTATE USED IN GAMESS
SUBROUTINE ROTATE ALSO USED IN MM3

- RENAMED MM3 SUBROUTINE TO ROTMM3

```
mm31.f:4827:       IF (ICODE.EQ.1) CALL ROTMM3(1,90.0,NROT)
mm31.f:4842:       IF (ICODE.EQ.1) CALL ROTMM3(1,-90.0,NROT)
mm31.f:4849:       IF (ICODE.EQ.1) CALL ROTMM3(1,180.0,NROT)
mm31.f:4871:       IF (ICODE.EQ.1) CALL ROTMM3(1,-180.0,NROT)
mm31.f:4892:       IF (ICODE.EQ.1) CALL ROTMM3(1,90.0,NROT)
mm31.f:4907:       IF (ICODE.EQ.1) CALL ROTMM3(1,-90.0,NROT)
mm31.f:4940:       IF (ICODE.EQ.1) CALL ROTMM3(1,90.0,NROT)
mm31.f:4947:       IF (ICODE.EQ.1) CALL ROTMM3(1,-90.0,NROT)
mm33.f:3319:       CALL ROTMM3(AXIS,ANGLE,NROT)
mm33.f:3867:       SUBROUTINE ROTMM3(AXIS,ANGLE,NROT)
-----------------------------------------------------------
```

Bibliography

1. M. Marciniak and J. Scofield. Private communication. 1996.
2. E. H. Nocollian and J. R. Brews. *MOS (Metal Oxide Semiconductor) Physics and Technology* . John Wiley and Sons, New York, 1982.
3. W. Lambert. Private communication.
4. F. Maseras and K. Morokuma. IMMOM: A new integrated ab initio + molecular mechanics geometry optimization scheme of equilibrium structures and transition states. *J. Comp. Chem.*, 16:1170, 1995.
5. M. J. Frisch, G. W. Trunks, H. B. Schlegel, P. M. W. Gill, B. G. Johnson, M. W. Wong, J. B. Foresman, M. A. Robb, M. Head-Gordon, E. S. Replogle, R. Gomperts, J. L. Andres, K. Raghavarchi, J. S. Binkley, C. Gonzalez, R. L. Martin, D. J. Fox, D. J. Defrees, J. Baker, J. J. P. Stewart, and J. A. Pople. *Gaussian92/DFT*. Gaussian Inc., Pittsburgh PA, 1993.
6. N. L. Allinger, L. Fanbing, and L. Yan. Mm3 refererence. *Molecular Mechanics: The MM3 Force Field for Alkenes*, 11:848, 1991.
7. A. Redondo, W. A. Goddard III, C. A. Swarts, and T. C. McGill. Oxidation of silicon surfaces. *J. Vac. Sci. Technol.*, 19:498, 1982.
8. C. J. Wu and E. A. Carter. Structures and adsorption energies for chemisorbed fluorine atoms on Si(100)-2x1. *Phys. Rev. B*, 45:9065, 1992.
9. M. W. Schmidt, K. K. Baldridge, J. A. Boatz, S. T. Elbert, M. S. Gordon, J. H. Jensen, S. Koseki, N. Matsunaga, K. A. Nguyen, S. J. Su, T. L. Windus, M. Dupuis, and J. A. Montgomery. General Atomic and Molecular Electronic Structure System. *J. Comp. Chem.*, 14:1347, 1993.
10. J Baker, A. Kessi, and B Delley. The generation and use of delocalized internal coordinates in geometry optimization. *J. Chem. Phys.*, 105:192, 1996.
11. C.S. Carmer, B Weiner, and M Frenklench. Molecular dynamics with combined quantum and empirical potentials: C_2H_2 adsorption on Si(100). *J. Chem. Phys.*, 99:1356, 1993.
12. M. Born and J. R. Oppenheimer. *Ann. Phys.Leipzig*, 84:457, 1927.
13. C. E. Dykstra. *Quantum Chemistry and Molecular Spectroscopy.* Prentice Hall, New Jersey, 1992.
14. F. Herman and S. Skillman. *Atomic Structure Calculations.* Prentice-Hill, New YOrk, 1962.
15. D. R. Hartree. *Proc. Cambridge Philos. Soc.*, 24:89, 1928.
16. V. Fock. *Z Physik*, 61:126, 1930.
17. J. C. Slater. *Phys. Rev.*, 36:57, 1930.
18. C. C. J. Roothaan. *Reviews of Modern Physics*, 23:69, 1951.
19. A. Szabo and N. S. Ostlund. *Modern Quantum Chemistry: Introduction to Advanced Electronic Structure Theory* . MacMillan, New York, 1982.

20. J. A. Pople and R. K. Nesbet. *J. Chem. Phys*, 52:431, 1954.

21. C. Edmiston and K. Ruedenberg. *Rev. Mod. Phys*, 35:457, 1963.

22. E. E. Anderson. *Modern Physics and Quantum Mechanics.* W. B. Saunders, Philadelphia, 1971.

23. S. F. Boys. *Proc. Roy. Soc London*, A200:542, 1950.

24. W. J. Hehre, R. F. Stewart, and J. A. Pople. Self-Consistent Molecular Orbitals Methods I: Use of Gaussian Expansions of Slater-Type Atomic Orbitals. *J. Chem. Phys.*, 51:2657, 1969.

25. T. Clark. *A Handbook of Computational Chemistry.* Wiley-Interscience, New York, 1985.

26. H. F. Schaeffer. *The Electronic Structure of Atoms and Molecules* . Addison Wesley, Reading Massachusetts, 1972.

27. P. O. Lowden. *Adv. Chem. Phys.*, 2:207, 1959.

28. P. O. Löwdin. Quantum theory of many-particle systems. I. Physical interpretation by means of density matrices, natural spin orbitals, and convergence problems in the method of configuration interaction. *Phys Rev.*, 97:1474, 1955.

29. C. F. Bender and E. R. Davidson. A natural orbital based energy calculation for helium hydride and lithium hydride. *J. Chem. Phys*, 70:2675, 1966.

30. W. A. Goddard, T. H. Dunning Jr., W. J. Hunt, and P. J. Hay. Generalized valence bond description of of bonding in low lying states of molecules. *Acc. Chem. Res.*, 6:368, 1973.

31. W. A. Goddard III and T. C. McGill. Study of surfaces and interfaces using quantum chemistry techniques. *J. Vac. Sci. Technol.*, 16:1308, 1979.

32. C. Cohen-Tannoudji, B. Du, and F. Laloe. *Quantum Mechanics.* Wiley-Interscience, New York, 1977.

33. C. Moller and M. S. Plesset. Note on an appoximation treatment for many electron systems. *Phys. Rev.*, 46:618, 1934.

34. S. Flüge. *Practical Quantum Mechanics.* Springer Verlag, Berlin, 1974.

35. J. M. Schulman and D. N. Kaufman. *J. Chem. Phys*, 53:477, 1970.

36. J. A. Pople, D. P. Santry, and G.A. Segal. Approximate Self-Consistent Molecular Orbital Theory I. Invariant Procedures. *J. Chem. Phys.*, 43:S129, 1965.

37. J. A. Pople, D. P. Santry, and G.A. Segal. Approximate Self-Consistent Molecular Orbital Theory II. Calculations with Complete Neglect of Differential Overlap. *J. Chem. Phys.*, 43:S136, 1965.

38. J. A. Pople, D. L. Beveridge, and P. A. Dobosh. Approximate Self Consistent Molecular Orbital Theory V. Intermediate Neglect of Differential Overlap . *J. Chem. Phys.*, 47:2026, 1967.

39. R. C. Bingham, M. J. S. Dewar, and D. H. Lo. Ground States of Molecules. XXV. MINDO/3. An Improved Version of the MINDO Semiempirical SCF-MO Method. *J. Am. Chem. Soc.*, 97:1285, 1975.

40. M. J. S. Dewar and W. Thiel. Ground States of Molecules 38. The MNDO Method. Approximations and Parameters. *J. Am. Chem. Soc.*, 99:4499, 1977.

41. M. J. S. Dewar, E. G. Zoebisch, E. F. Healy, and J. J. P. Stewart. AM1: A new general quantum mechanical molecular model. *J. A,. Chem. Soc.*, 107:3902, 1985.

42. J. J. P. Stewart. Optimization of parameters for semiempirical methods i. methods. *J. Comp. Chem.*, 10:209, 1989.

43. J. J. P. Stewart. *Reviews in Computational Chemistry.* VCH Publishers Inc, New York, 1990.

44. J. A. Pople and D. L. Beveridge. *Approximate Molecular Orbital Theory.* McGraw-Hill, New York, 1970.

45. P. M. Morse. *Phys. Rev.*, 34:57, 1929.

46. T. Schlick. *Optimization Methods in Computational Chemistry*, volume 3, page 1. VCH, New York, 1992.

47. F. H. Stillinger and T. A. Weber. Fluorination of the dimerized Si(100) surface studied by molecular-dynamics simulation. *Phys. Rev. Lett.*, 62:2144, 1989.

48. A. Nakano, R. K. Kalia, and P. Vashishta. *Phys. Rev. Lett.*, 75:3138, 1995.

49. R. G. Parr and W. Yang. *Density-Functional Theory of Atoms and Molecules* . Oxford University Press, New York, 1989.

50. L. H. Thomas. *Proc. Cambridge Phil. Soc.*, 23:542, 1927.

51. E. Fermi. *Z. Physik.*, 48:73, 1928.

52. P. Hohenberg and W. Kohn. *Phys. Rev.*, 136:B864, 1964.

53. W. Kohn and L. J. Sham. *Phys. Rev.*, 140:A1133, 1965.

54. M. Levy. Universal Variational Functionals of Electron Densities, First Order Density Matrices, and Natural Spin Orbitals and Solution of the ν-Representability Problem. *Proc. Nat. Acad. Sci. U.S.A.*, 76:6062, 1979.

55. E. Runge and E. K. U. Gross. Density-functional theory for time dependent system. *Phys. Rev. Lett*, 52:997, 1984.

56. P. A. M. Dirac. Note on exchange phenomena in the thomas atom. *Proc. Cambridge Phil. Soc.*, 26:376, 1930.

57. J. C. Slater. *The Self Consistent Field for Molecules and Solids.* McGraw-Hill, New York, 1974.

58. R. Car and M. Parrinello. Unified approach for molecular dynamics and density-functional theory. *Phys. Rev. Lett.*, 55:2471, 1985.

59. M. Challacombe and E. Schwegel. Linear scaling computation of the Fock matrix. *J. Chem. Phys.*, 106:5526, 1997.

60. E Schwegel and M Challacombe and M. Head-Gordon. Linear scaling computation of the Fock matrix II: Rigorous bounds on exahcnge integrals and incremental Fock build. *J. Chem. Phys*, 106:9708, 1997.

61. P Vashishta, A. Nakano, R. K. Kalia, and I. Ebso. Crack propagation and fracture in ceramic films: million atom molecular dynamics simulations on parallel computers. *Mater. Sci. Eng. B.*, B37:56, 1996.

62. J. Gao. In K. B. Lipkowitz and D. B. Boyd, editors, *Reviews in Computational Chemistry*, volume 7, page 119. VCH, 1995.

63. D. Bakowies and W. Thiel. Hybrid models for combined quantum mechanics and molecular mechanics approaches. *J. Phys. Chem.*, 100:10580, 1996.

64. M. Field and J. Gao. Report for the JOINT CECAM-NSF Planning Meeting on Hybrid Quantum and Classical Mechanical Methods for the Simulation of Biopolymers in Solution. *Int. J. of Comp. Chem.*, 60:1093, 1996.

65. U. Eichler, C. M. Kolmel, and J. Sauer. Combining ab initio techniques with analytical potential functions for structure predictions of large systems: Method and application to crystalline silica polymorphs. *J .Comp. Chem.*, 18:463, 1996.

66. J. Sauer. Molecular models in ab initio studies of solids and surfaces: From ionic crystals and semiconductors to catalysts. *Chem. Rev.*, 89:199, 1989.

67. U. C. Singh and P. A. Kollman. A combined ab initio quantum mechanical and molecular mechanical method for carrying out simulations on complex molecular systems. *J. Comp. Chem.*, 7:718, 1986.

68. M. J. Field, P. A. Bash, and M. Karplus. A combinedquantum mechanics and molecular mechanics potential for molecular dynamics simulations. *J. Comp. Chem.*, 11:700, 1990.

69. E.B. Wilson Jr, J. C. Decius, and P. C. Cross. *Molecular Vibrations: The Theory of Infrared and Raman Vibrational Spectra.* Dover, 1980.

70. P. Pulay, G. Fogarasi, F. Pang, and J. E. Boggs. Systematic ab initio gradient calculation of molecular geometries, force constants, and dipole moment derivatives. *J.A.C.S.*, 101:2550, 1979.

71. G. Fogarasi, X. Zhou, P. W. taylor, and P. Pulay. The calculation of ab initio molecular geometries: Efficient optimization by natural internal coordinates and empirical correction by offset forces. *J. Am. Chem. Soc.*, 114:8191, 1992.

72. P. Pulay and G. Fogarasi. Geometry optimization in redundant internal coordinates. *J. Chem. Phys*, 96:2856, 1992.

73. T. Matsubara, F. Maseras, N. Koga, and K. Morokuma. Application of the New "Integrated MO + MM" IMMOM Method to the Organometallic Reaction Pt(PR_3 + H_2 (R=H, Me, t-Bu, and Ph). *J. A. C. S.*, 100:2573, 1996.

74. N. W. Ashcroft and D. N. Mermin. *Solid State Physics.* W. B. Saunders, Philadelphia, 1976.

75. C. Kittel. *Introduction to Solid State Physics.* John Wiley and Sons, New York, 6 edition, 1986.

76. A. K. Rappe, T. A. Smedley, and W. A. Goddard III. The shape and hamiltonian consistent (shc) effective potentials. *J. Phys. Chem.*, 85:1662, 1981.

77. P. Kratzer, B. Hammer, and J. K. Norskov. Direct pathway for sticking/desorption of H_2 on Si(100). *Phys. Rev. B*, 51:13432, 1993.

78. A. Vittandi, A. Selloni, and M.Casarin. Energetics of atomic hydrogen diffusion on Si(100). *Surf. Sci. Lett.*, 289:L625, 1993.

79. D. Haneman. Surfaces of silicon. *Rep. Prog. Phys.*, 50:1045, 1987.

80. H. Neergaard and J. T. Yates. Surface chemistry of silicon. *Chem. Rev.*, 95:1589, 1995.

81. A. Redondo and W. A. Goddard III. Electronic correlation and the Si(100) surface: buckling vs nonbuckling. *J. Vac. Sci. Technol.*, 21:344, 1982.

82. S. Tang and A. J. Freeman. *Bull. Am. Phys. Soc.*, 36:344, 1991.

83. P. Nachtigall, K. D. Jordan, and K. C. Janda. Calculation of the si-h bond energies for the monohydride phase of Si(100). *J. Chem. Phys.*, 95:8652, 1991.

84. Z. Jing and J. L. Whitten. Ab initio studies of h chemisorption on Si(100). *Phys. Rev. B*, 46:9544, 1992.

85. T. H. Dunning Jr. and P. J. Hay. *Methods of Electronic Structure Theory*, volume 3. Plenum, New York, 1977.

86. Y. Wang, M. Shi, and J. W. Rabalais. Structures of the Si(100) surface in the clean (2x1), (2x1)-H monohydride, (1x1)-H dihydride, and c(4x4)-H phases. *Phys Rev B*, 48:1678, 1993.

87. Z. Jing and J. L. Whitten. Multiconfiguration self-consistent-field treatment of H_2 desorption from Si(100)-2x1h. *J. Chem. Phys.*, 102:3867, 1995.

88. J. A. Applebaum and D. R. Hamann. Theory of reconstruction induced subsurface strain-application to Si(100). *Surf. Sci.*, 74:21, 1978.

89. B. I. Craig and P. V. Smith. The surface structure of β SiC(100): the clean and monohydrid 2X1 phases. *Surf. Sci.*, 233:255, 1990.

90. J. E. Northrup. Structure of Si(100)H: Dependence on the H chemical potential. *Phys Rev B*, 44:1419, 1991.

91. Y. Wang, M. Shi, and J. W. Rabalais. Structures of hydrogen on the Si(100) surface in the (2x1)-H monohydride, (1x1)-H dihydride, and c(4x4)-H phases. *Phys Rev B*, 48:1689, 1993.

92. R. Felici, i. K. Robinson, C. Ottaviani, P Imperatori, P. Eng, and P. Perfetti. Room temperature si(001)-(2x1) reconstruction solved by X-ray diffraction. *Surf. Sci.*, 375:55, 1997.

93. R. M. Tromp, R. G. Smeenk, F. W. Saris, and D. J. Chadi. Ion beam crystallography of silicon surfaces II. Si(100)-(2x1). *Surf. Sci.*, 133:137, 1983.

94. N. Roberts and R. J. Needs. Total energy calculations of dimer reconstructions on the silicon (001) surface. *Surf Sci*, 236:112, 1990.

95. C. Yang, S. Y. Lee, and H. C. Kang. An embedded cluster study of dimer buckling on the Si(100) surface. *J. Chem. Phys.*, 107:3295, 1997.

96. K. Palmo, L.-O. Pietala, and S. Krimm. Treatment of Redundancies among Internal Coordinates in Optimizing Molecular Mechanics Force Constants. *J. Comp. Chem*, 13:1142, 1992.

97. J. W. Ponder. *Tinker: Software Tools for Molecular Design.* Washington University School of Medicine, St louis, MO, 1997.

98. J. H. Jensen and M. S. Gordon. Splicing I: Using mixed basis sets in ab initio calculations. *J. Comp. Chem.*, 4:421, 1991.

99. E. H. Teunissen and A. P. J. Jansen. Large basis sets and geometry optimizations in embedded cluster calculations. *Int. J. Quant. Chem.*, 54:73, 1995.

100. J. L. Whitten and T. A. Pakkanen. Chemisorption theory for metallic surfaces: Electron localization and the description of surface interactions. *Phys. Rev. B.*, 21:4357, 1980.

101. P. D. Madhaven and J. L. Whitten. *J. Chem. Phys*, 77:2673, 1982.

102. Z. Barandiaran and L. Seijo. The ab initio model potantial representation of the crystalline environment. theoretical study of the local distortion on NaCl:Cu^+. *J. Chem. Phys.*, 89:5739, 1988.

103. E. H. Teunissen, A P. J. Jansen, R. A. van Santen, R. Orlando, and R. Dovesi. Adsorption energies of NH_3 and NH_4^+ in zeolites corrected for the long-range electrostatic potential of the crystal. *J. Chem. Phys.*, 101:5865, 1994.

104. R. Dovesi, V. R. Saunders, and C. Roetti. *CRYSTAL92 User's Manual.*

105. G. Galli and M. Parinello. Large scale electronic structure calculations. *Phys. Rev. Lett.*, 69:3547, 1992.

106. S. Kruger and N. Rosch. The moderately-large-embedded-cluster method for metal surfaces; a density-functional study of atomic adsorption. *J. Phys.: Condens. Matter*, 6:8149, 1994.

107. C. Pisani, F. Cora, R. Nada, and R. Orlando. Hartree-Fock perturbed-cluster treatment of local defects in crystals: I. The EMBED program: general features. *Comp.Phys. Comm.*, 82:139, 1994.

108. W. J. Hehre. *Practical Strategies for Electronic Structure Calculations.* Wavefunction, Irvine CA, 1995.

109. R. S. Mulliken. Electronic population analysis on LCAO-MO molecular wave functions. i. *J.Chem. Phys.*, 23:1833, 1955.

110. J. P. Foster and F. Weinhold. Natural hybrid orbitals. *J A,. Chem. Soc.*, 102:7211, 1980.

111. L. E. Chirlian and M. M. Francl. Atomic charges derived from electrostatic potentials: A detailed study. *J. Comp. Chem.*, 8:894, 1987.

112. R. F. W. Bader. *Atoms in Molecules: A Quantum Theory.* Oxford University Press, Oxford, 1990.

113. W. J. Hehre, R. Ditchfield, R. F. Stewart, and J. A. Pople. Self-Consistent Molecular-Orbital Methods. IX An Extended Gaussian-Type Basis for Molecular Orbital Studies of Organic Molecules. *J. Chem. Phys.*, 52:2769, 1970.

114. C. K. Lutrus, T. Oshiro, D. E. Hagen, and S. H. Suck Sulk. Simulation of bulk silicon crystals and Si(111) surfaces with applications to study of fluorine coverage of the surfaces. *Phys. Rev. B*, 48:15086, 1993.

115. P.J.Hay and W.R.Wadt. *J.Chem.Phys.*, 82:270, 1985.

116. Wavemetrics, Inc, ake Oswego, OR. *IGOR User's Manual*, 1996.

117. R. Orlando, R. Dovesi, C. Roetti, and V. R. Saunders. Ab initio hartree fock calculations for periodic compounds: Applications to semiconductors. *J. Phys.: Condens. Matter*, 2:7769, 1990.

118. M. Sabisch, P. Kruger, A. Mazur, M. Rohfling, and J. Pollman. First-principles calculation of β-SiC(001) surfaces. *Phys. Rev. B*, 53:13121, 1996.

119. H. Morkoc, S. Strite, G. B. Gao, M. E. Lin, B. Sverdlov, and M. Burns. Large-band-gap SiC, iii-v gallium nitride, and ii-vi znse-based semiconductor device technologies. *J. Appl. Phys.*, 76:1363, 1994.

120. P. Kackell, J. Furthmuller, and F. Bechstedt. Ab initio calculations of the reconstructed (100) surfaces of cubic silicon carbide. *Surf. Sci.*, 104/105:45, 1995.

121. H. yan, A. P. Smith, and H. Jonsson. Atomic structure of β SiC(100) surfaces: an ab initio study. *Surf. Sci*, 330:265, 1995.

122. S. P. Mehandru and A. B. Anderson. Structures and energetics for polar and non-polar SiC surface relaxations. *Phys. Rev. B*, 42:9040, 1990.

123. J. M. Powers, A. Wander, M. A. van Hove, and G. A. Somorjai. Structural analysis of the β SiC(100)-(2X1) surface reconstruction by automated tensor LEED. *Surf. Sci. Lett*, 260:L7, 1992.

124. B. Wenzien, P. Kackell, and F. Bechstedt. Vacancy induced 2 X 2 reconstruction of the Si terminated 3C SiC(111) surface: ab initio calculations of the atomic and electronic structure. *Surf. Sci.*, 331-333:1105, 1995.

125. R. C. Weast, editor. *Handbook of Chemistry and Physics.* CRC Press, Boca Raton FL, 69 edition, 1988.

126. J. Scofield. Private communication. 1997.

127. B. Schubert, P. Avouris, and R. Hoffmann. A theoretical study of the intial stages of Si(111)-7x7 oxidation. I The molecular precursor. *J. Chem Phys*, 98:7593, 1993.

128. B Schubert, P. Avouris, and R. Hoffmann. A theoretical study of the initial stages of Si(111)-7x7 oxidation. II. The dissociated state and formation of SiO_4. *J. Chem . Phys.*, 98:7606, 1993.

129. H. G. Busmann, W. Zimmermann-Edling, and S. Lauer. Stability, reconstruction, and electronic properties of diamond (100) and (111) surfaces. *Phys Rev B*, 48:18189, 1993.

130. G. Kern, J. Hafner, and G. Kresse. Atomic and electronic structure of diamond (111) surfaces I. Reconstruction and hydrogen-induced de-reconstruction of the one dangling-bond surface. *Surf. Sci.*, 366:445, 1996.

131. G. Kern, J. Hafner, and G. Kresse. Atomic and electronic structure of diamond (111) surfaces II. (2x1) and ($\sqrt{3}x\sqrt{3}$) reconstructions of the clean and hydrogen covered three dangling-bond surfaces. *Surf. Sci.*, 366:464, 1996.

132. S. Wickramanayaka, Y. Nakaishi, and Y. Hatanaka. On the chemistry of a-SiO_2 deposition enhanced CVD. *App. Surf. Sci.*, 113/114:670, 1997.

Vita

Major James R. Shoemaker was born in Aurora, IL on 30 Aug 1963, growing up amongst the fragrant farms of northern Illinois on the outskirts of Chicago. He graduated from Marmion Military Academy in May 1981 and entered the University of Illinois at Urbana-Champaign in August of that year. He graduated in Dec 1984 with a B.S degree in Engineering Physics, received a commission in the U. S. Air Force in Jan 1985, and began his military service in the (then) Aero Propulsion Laboratory at Wright-Pattterson AFB as a research physicist in the Advanced Plasma Research Group. In Sep 89, he was reassigned to the Air Force Institute of Technology for post graduate studies in Nuclear Physics. He graduated with a M. S. degree in Mar 1991, having performed thesis work in computataional predictions of polymer strength. After completing his M.S, he was reassigned to HQ Air Force Technical Applications Center, Patrick AFB FL, where he worked supporting their mission of verification of nuclear treaty compliance. In June 1994, Major Shoemaker entered AFIT to begin doctoral studies in the field of computational chemical physics. In Sep 97, Major Shoemaker began a one year appointment as a Military Research Associate at Lawrence Livermore National Laboratory, Livermore CA.

Permanent address: 165 Estates St
Livermore, CA 94550

REPORT DOCUMENTATION PAGE

Form Approved
OMB No. 0704-0188

Public reporting burden for this collection of information is estimated to average 1 hour per response, including the time for reviewing instructions, searching existing data sources, gathering and maintaining the data needed, and completing and reviewing the collection of information. Send comments regarding this burden estimate or any other aspect of this collection of information, including suggestions for reducing this burden, to Washington Headquarters Services, Directorate for Information Operations and Reports, 1215 Jefferson Davis Highway, Suite 1204, Arlington, VA 22202-4302, and to the Office of Management and Budget, Paperwork Reduction Project (0704-0188), Washington, DC 20503.

1. AGENCY USE ONLY *(Leave blank)*

2. REPORT DATE

3. REPORT TYPE AND DATES COVERED

4. TITLE AND SUBTITLE
Hybrid Quantum and Molecular Mechanics Embedded Cluster Models for Chemistry on Silicon and Silicon Carbide Surfaces

5. FUNDING NUMBERS

6. AUTHOR(S)
James R Shoemaker, Major USAF

7. PERFORMING ORGANIZATION NAME(S) AND ADDRESS(ES)
AFIT/ENP
2950 P St
Wright-Patterson AFB, OH 45433

8. PERFORMING ORGANIZATION REPORT NUMBER
AFIT/DS/ENP/97-09

9. SPONSORING/MONITORING AGENCY NAME(S) AND ADDRESS(ES)
AFRL/MLPJ
Wright-Patterson AFB, OH 45433

10. SPONSORING/MONITORING AGENCY REPORT NUMBER

11. SUPPLEMENTARY NOTES

12a. DISTRIBUTION AVAILABILITY STATEMENT
Unlimited

12b. DISTRIBUTION CODE

13. ABSTRACT *(Maximum 200 words)*

Fabrication of silicon carbide (SiC) semiconductor devices are of interest for aerospace applications because of their high-temperature tolearnce. Growth of an insulating SiO2 layer on SiC is a poorly understood process, and sometimes produces interface defects that degrade device performance. Accurate theoretical models of surface chemistry, using quantum mechanics (QM), do not exist because of the huge computational cost of solving Schrodinger's equation for a molecular cluster large enough to represent a surface. Molecular mechanics (MM), which describes a molecule as a collection of atoms interacting through classical potentials, is a fast computational method, good at predicting molecular structure, but cannot accurately model chemical reactions.

A new hybrid QM/MM compuatational method for surface chemistry was developed and applied to silicon and SiC surfaces. The addition of MM steric constraints was shown to have a large effect on the energetics of O atom adsorption on SiC. Adsorption of O atoms on Si-terminated SiC(111) favors above surface sites, in contrast to Si(111), but favors subsurface adsorption on C-terminated SiC(111). This difference, and the energetics of C atom etching via CO2 desorption, can explain the observed poor performance of SiC devices in which insulating layers were grown on C-terminated surfaces.

14. SUBJECT TERMS
Surface chemistry, hybrid quantum/molecular mechanics calculations, silicon carbide

15. NUMBER OF PAGES
335

16. PRICE CODE

17. SECURITY CLASSIFICATION OF REPORT
Unclassified

18. SECURITY CLASSIFICATION OF THIS PAGE
Unclassified

19. SECURITY CLASSIFICATION OF ABSTRACT

20. LIMITATION OF ABSTRACT